The Role of Salt-Inducible Kinases in Maintaining and Regulating the Circadian Architecture

A thesis submitted for the degree of Doctor of Philosophy
at the University of Oxford

Trinity Term 2026

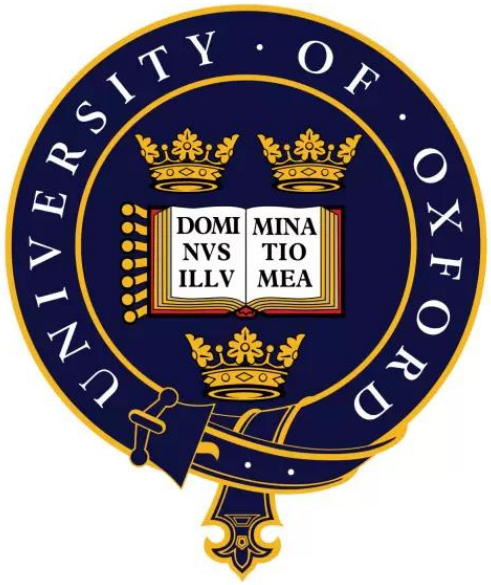

Yining Ru

St Edmund Hall

Department of Pharmacology
Word Count: 49,500

Table of Contents

Abstract

The behavioural rhythmicity of sleep can be effectively explained by the “Two Process Model”, where “Process S” characterizes the homeostatic drive for sleep (sleep pressure and sleep need) and “Process C” reflects the circadian clock. However, the dynamic molecular interactions of Process S and C remain a mystery. Recent studies highlight the role of kinases and phosphorylation of synaptic proteins as potential key drivers for sleep need. Salt-inducible kinases (SIKs) are AMP-activated protein kinases (AMPK) and consist of three members – SIK1, 2 and 3. Notably, previous studies have proposed that SIK1 phosphorylates CREB-regulated co-activators (CRTCs) and is involved in phase shifting and photoentrainment. SIK3 was shown to phosphorylate a hub of sleep-need index phosphoproteins (SNIPPs) related to sleep need and pressure. Therefore, SIKs are proposed as master regulators of both rhythmic transcriptional pathways and post-translational modification of sleep-associated proteins.

In this DPhil thesis, we investigated the isoform-specific roles, molecular substrates, and phosphorylation sites of SIKs in sleep and circadian regulation through behavioural, transcriptomics and phosphoproteomics approaches. We showed that all SIK isoforms are expressed in the suprachiasmatic nucleus (SCN), while only SIK2 and SIK3 are expressed in the cortical layers, which are associated with distinct circadian and sleep phenotypes that we characterized through wheel running and EEG/EMG recordings. We optimized the tissue-specific protein kinase assay linked phosphoproteomics (Pro-KALIP) method to detect the direct substrates of SIKs, which could be applied to substrate profiling for all applicable kinases. The direct substrates of SIKs proposed a network that facilitates synaptic transmission, calcium signaling, vesicle trafficking, and neuropeptide signaling. SIK3 phosphorylates synaptic proteins that overlapped with SNIPPs, supporting its function in sleep homeostasis. Furthermore, we identified and validated connexin-43 (CX43) S373 as a direct astrocytic phosphosite of SIK1 using *in vitro* assays. Isoform-dependent and overlapping molecular substrates were analyzed to delineate distinct roles and signaling pathways. This thesis proposes a phosphorylation-dependent signaling network mediated by SIKs and provides insights into understanding the molecular markers underlying the sleep-wake cycle.

Acknowledgements

To my supervisors and mentors, Dr Sridhar Vasudevan and Dr Aarti Jagannath, for providing invaluable support and advice throughout my DPhil. Thank you for providing me with a platform to gain the independence and confidence I have today. They gave me the courage and opened up the field for me to absorb, grow, and learn, which I am deeply grateful for. Sri's door is always open for scientific and life conversations. His excitement for science reminds me every day that research can be a passion and a lifetime. Aarti was always open to discussions and input whenever I needed them, and taught me the essential skills needed to set my career.

To the members of Sri's lab (past and present) for fostering such an encouraging environment. I would like to thank my wonderful postdocs, Dr Brooke Prakash and Dr Matthew Lloyd, for all the training and mentorship. To my fellow DPhils, Lucy Zhao and David Ni, thank you for the camaraderie, teamwork, and banter that carried me through the end. I am forever grateful for all the pub crawls, punting trips, Paul's lunches, lab t-shirts, and socials that made Pharmacology feel like home.

To the members of Aarti's lab, thank you for your support and generosity throughout my project. I'm grateful to Dr. Zeinab Wakaf for her guidance on experiments and for always being open to discussing the project's direction. I would like to thank Dr. Akanksha Bafna, Dr. Simon Guillot, Dr. Adam Campbell-Galland and Simona Di Pretoro for all the advice and support on new techniques, data analysis and career development. I will always remember the Kavli afternoon tea sessions!

I would like to thank all my friends in the department, at Teddy Hall and abroad for the wonderful memories and moral support.

To my partner and best friend, Kaito Namai. Thank you for being my person and my constant. You supported, reassured and held me through every step of the journey. I am deeply grateful for all the weekend and late-night trips to the lab, no matter how busy you were – the 20-minute walks back home are memories that I will cherish forever.

To my dearest family, to whom I dedicate this thesis. Firstly, I would like to thank my 爸爸 ('Dad') and 妈妈 ('Mom') for teaching me the definition of 'love', for showing me the world, and for supporting me wherever life takes me. I would also like to extend my gratitude to my grandparents - 亲娘，外公，外婆 – for giving me warmth on my annual visits. Your love for me has never wavered, even across 9000km. Thank you for always giving me the strength to become the best version of myself.

Statement of Contributions

This DPhil thesis represents work carried out by the candidate. Contributions from collaborators in the lab are outlined below.

EEG/EMG implantation, surgery, and recordings were performed with the assistance of Dr. Aarti Jagannath and Simona Di Pretoro. Sleep data processing was performed by Mikaella Ngo and Sarah Chamdawala in Chapter 4 and 5. SIK1 *in vivo* phosphoproteomics and SIK2 RNAseq sample preparation were performed by Dr Zeinab Wakaf in Chapter 3 and 5, respectively. LC-MS and raw data analysis for Pro-KALIP and *in vivo* phosphoproteomics were performed by Dr Otto Kauko at Turku Bioscience Centre, University of Turku.

Abbreviations

12:12	12 hour light/12 hour dark
ABC atlas	Allen Brain Cell Atlas
ACTH	adrenocorticotropic hormone
AD	Alzheimer's Disease
AMPA	α-Amino-3-hydroxy-5-methyl-4-isoxazolepropionic acid
AMPK	AMP-activated protein kinase
AVP	arginine vasopressin
BMAL1	basic helix-loop-helix ARNT-like protein 1
BP	Biological Processes
bZIP	basic leucine zipper
CACNA1	calcium voltage-gated channel subunit alpha 1
CAMK2A/B/D/G	Ca^{2+}/calmodulin-dependent protein kinase-II α/ β/ δ/ γ subunit
CAMKI/IV	Ca^{2+}/calmodulin-dependent protein kinase-I/IV
cAMP	cyclic adenosine monophosphate
CC	cellular component
CDK	cyclin-dependent kinase
CDK16	cyclin-dependent kinase 16
CLOCK	circadian locomotor output cycles kaput
CPM	counts per million
CRE	cAMP response element
CREB	cAMP response element binding protein
CRH	corticotropin-releasing hormone
CRTC1/2/3	CREB-regulated co-activator 1/2/3
CRY1/2	cryptochrome 1/2
CT	circadian time
CX43	connexin-43
DD	constant darkness
DEGs	differentially expressed genes
DG	dentate gyrus
DI	discrimination index
DMEM	Dulbecco’s Modified Eagle’s Medium
DPBS	Dulbecco's phosphate-buffered saline
DTT	dithiothreitol
EEG	electroencephalogram
EMG	electromyography
EOS	end of sleep
EOW	end of wake

ER	endoplasmic reticulum
ERK	extracellular signal-regulated kinase
F-12	Ham's F-12 Nutrient Mixture
FBS	fetal bovine serum
FDR	false discovery rate
FFT	Fast Fourier Transform
FSBA	5′-(4-fluorosulfonylbenzoyl) adenosine
GABA	gamma-aminobutyric acid
GCs	glucocorticoids
GO	gene ontology
GoF	gain of function
GRK3	G protein-coupled receptor kinase 3
GRP	gastrin-releasing peptide
HBSS	Hank's Balanced Salt Solution
HDAC4/5/9	histone deacetylase 4/5/9
HPA	hypothalamic-pituitary-aderenal
IS	interdaily stability
IV	intradaily variability
KEGG	Kyoto Encyclopedia of Genes and Genomes
KI	kinase-inactive knock-in
KO	knock-out
KSEA	kinase substrate enrichment analysis
LC-MS	liquid chromatography - mass spectrometry
LD	light-dark
LKB1	liver kinase B1
LL	constant light
Log2FC	Log2 fold change
LTD	long-term depression
LTP	long-term potentiation
MERFISH	multiplexed error-robust fluorescence in situ hybridization
MF	molecular function
MO25α	mouse protein-25 alpha
NOR	novel object recognition
NREM	non-rapid eye movement
OPN4	melanopsin
P/S	penicillin-streptomycin
PACAP	pituitary adenylate cyclase-activating polypeptide
PCA	principle component analysis
PER1/2/3	period 1/2/3
PKA	protein kinase A

PKCγ	protein kinase C gamma
PRC	phase response curve
Pro-KALIP	protein kinase assay linked phosphoproteomics
PTM	post-translational modification
PVH	paraventricular hypothalamus
PVN	paraventricular nucleus
REM	rapid eye movement
RGC	retinal ganglion cell
RHT	retinohypothalamic tract
SCN	suprachiasmatic nucleus
scRNAseq	single-cell RNAseq
SD	sleep deprivation
SEM	standard error of the mean
SHY	synatic homeostasis hypothesis
SIK1/2/3	salt-inducible kinases 1/2/3
Slp	*Sleepy* mutant
SNIPPs	sleep-need index phosphoproteins
SPVZ	subparaventricular zone
SRRM2	Serine/arginine repetitive matrix protein 2
STRADα	STE20-related kinase alpha
SWA	slow wave activity
SWS	slow wave sleep
SYN1	synapsin-1
Tim	timeless
TTFL	transcription-translation negative feedback loop
UBA	ubiquitin-associated domain
VIP	vasoactive intestinal peptide
WT	wildtype
ZT	zeitgeber time

Chapter 1: General Introduction

1.1 Circadian rhythms

1.1.1 Core circadian clock

Living organisms adapt to the environmental and solar cycles by coordinating internal circadian timings to the 24-hour day. Circadian clocks in our bodies are endogenous, self-sustaining oscillators that maintain the approximately 24-hour rhythm and behavior (Takahashi, 2017). Circadian rhythms were first discovered in plants in the early 1700s, when they were observed to preserve leaf movements in the absence of environmental photic cues. Researchers then examined the molecular mechanisms and introduced the transcription-translation negative-feedback loop (TTFL). Hardin et al showed that the *period (Per)* gene levels oscillate with circadian rhythms (Hardin et al., 1990) and that PER protein affects the oscillation of its own transcription (Hardin et al., 1992). The clock gene *timeless (Tim*) was later found to determine the timing of PER protein and promote the circadian rhythms of *Per* and *Tim* transcription (Sehgal et al., 1995).
The core of the circadian clock consists of activators circadian locomotor output cycles kaput (CLOCK) and basic helix-loop-helix ARNT-like protein 1 (BMAL1), which bind to regulatory E-boxes within the promoters of a set of rhythmic genes, including *period* (*Per1*, *Per2* and *Per3*) and *cryptochrome* (*Cry1* and *Cry2*) (Reppert & Weaver, 2002). During the light period, the CLOCK-BMAL1 complex is activated, facilitating transcription and translation of *Per* and *Cry* towards the onset of the dark period. During the dark period, PER and CRY proteins interact with each other and casein kinases to repress transcription by interacting with the CLOCK-BMAL1 complex in the nucleus.

This negative feedback loop coordinates the 24-hour oscillation and turnover (Horst et al., 1999; C. Lee et al., 2001; Shearman et al., 2000; Takahashi, 2017).

1.1.2 Suprachiasmatic nucleus (SCN) and Neurotransmission

The SCN in the hypothalamus was identified in the mammalian circadian system as the master pacemaker after the discovery of rhythm loss in the suprachiasmatic region in post-lesion rats, concluding that it is essential for maintaining rhythmicity (Moore & Eichler, 1972). Neural transplantation of the SCN, from fetal tissue, subsequently restored circadian rhythms in arrhythmic hamsters, confirming its role in determining both rhythmicity and period (Ralph et al., 1990).

Structurally, the SCN consists of two nuclei in the hypothalamus on each side of the third ventricle, sitting directly above the optic chiasm (Morrison & Ma, 2026). The SCN in mammals is composed of 20,000 neurons, widely characterized in rodents, and spontaneous firing activity confirmed that most SCN neurons contain individual circadian oscillators and robust firing patterns (Hastings et al., 2018; Honma et al., 1998, 2012). In addition, intracellular Ca^{2+} oscillations are independent of neuronal firing but depend on clock protein PER2 rhythms, modulating a cohesive SCN network (Noguchi et al., 2017). It was shown that aging affects SCN functions as aged hamsters and rats had reduced circadian amplitude and reduced expression of *Bmal1* and *Clock* (Davidson et al., 2008).

Studies have shown that neurotransmitters and neuropeptides make up a huge part of the SCN circadian system, including arginine vasopressin (AVP), vasoactive intestinal peptide (VIP), gamma-aminobutyric acid (GABA), dopamine, glutamate and acetylcholine (Reghunandanan, 2024; Reghunandanan & Reghunandanan, 2006; Rusak & Bina, 1990). Neuropeptides VIP and gastrin-releasing peptide (GRP) are located in the core of the SCN; whereas AVP-expressing cells are co-localized with GABA and predominate the shell subregion (Hastings et al., 2018). The core relays photic signals directly from the optic chiasm to oscillatory cells through the synchronizer VIP. The core also projects heavily to the shell, facilitating communication. VIP was shown to play key roles in maintaining circadian rhythmicity and phase shifts in response to photic signals (Reghunandanan & Reghunandanan, 2006). Moreover, researchers found that $VPAC_2$, the cognate receptor of VIP in the SCN, is crucial for temporal control and neuronal excitability. The deletion of $VPAC_2$ ($Vipr2^{-/-}$) impairs photic gating and entrainment (Wegner et al., 2024). AVP, making up a large part of the dorsomedial SCN, regulates circadian amplitude and firing rates by facilitating V1 receptors (Ono et al., 2021a). There is also extensive literature on the role of GABA, a major inhibitory neurotransmitter, in maintaining circadian oscillations and coupling within the SCN (Ono et al., 2021c). The SCN typically form synaptic connections and projects to neighboring hypothalamic and thalamic regions, including the subparaventricular zone (SPVZ), paraventricular hypothalamus (PVH) and dorsomedial hypothalamus (DMH) for sleep-wake regulation (Tsuno & Mieda, 2024). These regions are also innervated by VIP- and AVP-expressing SCN neurons. The efferent regions project to other regions for modulating sleep and arousal signals (Starnes et al., 2024).

For instance, it was shown that projections of GABAergic neurons in the DMH block the activity of sleep-promoting VLPO neurons, and glutamatergic DMH neurons activate wake-promoting neurons. These cascades activate monoaminergic pathways that project to the cortex (Scammell et al., 2017; Saper et al., 2005). Together, these demonstrate that neurotransmitters and neuropeptides complement each other to synchronize and coordinate the circadian system in the SCN (Fig. 1.1).

The circadian clock can synchronize endogenous biological rhythms in response to environmental external cues - “zeitgebers”. Light is the primary regulator that modulates circadian behavior and sleep-wake timing (Legates et al., 2014). Light projects information into the SCN from the retina through the retinohypothalamic tract (RHT) in intrinsically photosensitive retinal ganglion cells (ipRGCs) (Berson et al., 2002; Foster et al., 2020). The two main neurotransmitters involved in the RHT are glutamate and pituitary adenylate cyclase-activating polypeptide (PACAP) (Hannibal, 2002). The opsin expressed in these glutamate/PACAP-containing ipRGCs is melanopsin (OPN4), which is essential for photoentrainment; upon light-induced depolarisation, these cells release glutamate and PACAP into the SCN (Fig. 1.1). Researchers examined photic input in the SCN by conducting light-regulated transcriptomics in the SCN and identified upregulation of immediate early genes and clock genes such as *Per1*. *Opn4* is essential for circadian entrainment, and melanopsin-expressing retinal ganglion cells send projections to the SCN (Hughes et al., 2016; Lupi et al., 2008). By examining OPN4$^{-/-}$ mice, researchers discovered an attenuation of light-regulated genes in the SCN and response to light signals (Jagannath et al., 2013). Research has also shown that the

inhibition of glutamate blocks phase shifts to light and that PACAP modulates the response, suggesting the significance of both neurotransmitters in light signaling (Hannibal, 2002). In addition to photic cues, scheduled voluntary exercise (SVE) was shown to promote SCN synchrony and behavioural rhythms, without large alterations to gene expression (Hitrec et al., 2023; Hughes et al., 2021).

cAMP-response element binding protein (CREB) is a ubiquitous transcription factor that binds to cAMP response elements (CRE), target DNA sequences, and is found in many cellular promoters. Notably, the CREB/CRE transcriptional pathway was proposed to be important for SCN synchronicity and response to stimuli. It was suggested that CRE-driven transcription maintains an autonomous circadian oscillation in the SCN, which is activated by protein kinase A (PKA) phosphorylation of CREB at Serine (Ser) 133 (Obrietan et al., 1999). Subsequent work demonstrated nuclear accumulation of CRTC1 following light induction. Following photic stimulation, the release of glutamate and PACAP induces an increase in Ca^{2+} and cyclic adenosine monophosphate (cAMP) in the SCN. This triggers the translocation of CRTC1 to the nucleus, which is supported by studies showing nuclear accumulation of CRTC1 after light induction. This mediates CRTC1/CREB-mediated transcription of clock genes, such as the direct target *Per1* (Sakai et al., 2004). Though high levels of CRTC2 were detected in the SCN, CRTC2 expression was not regulated by the circadian clock or light signaling (Sakamoto et al., 2013a).

1.1.3 Peripheral Clocks

In addition to the SCN as a central clock in the brain, individual cells have independent circadian oscillators that are synchronized within the tissue. Peripheral clocks are influenced and entrained by various zeitgebers such as body temperature, hormone levels and feeding/fasting cycles. Research has shown that desynchronization of central and peripheral clocks could lead to diseases such as obesity, diabetes and cardiovascular diseases (Albrecht, 2012). While the SCN acts as a relay between the external light-dark (LD) cycle and the endogenous biological system, other zeitgebers' effects on peripheral systems are more direct (Hankins et al., 2008; Huang et al., 2023). For instance, restricted feeding and food availability would lead to phase shifts in the peripheral clock components, but keeping the central SCN clock unshifted, leading to misalignment (Mukherji et al., 2015). It is also reflected in the cardiovascular system. It is shown that the SCN regulates rhythms in heart rate and heart rate variability via the autonomic nervous system; however, contractibility and energy metabolism are regulated within the local cardiomyocyte clocks (Hayter et al., 2021). This suggests that the SCN and peripheral clocks work together to maintain coordination and whole-body synchronicity.

One key pathway through which the SCN maintains rhythms in peripheral tissues is the hypothalamic-pituitary-adrenal (HPA) axis, releasing glucocorticoids (GCs). The HPA acts as a stress response system to restore homeostasis, and GCs act as the end-effectors that regulate the biological activities of most major organs and tissues. The axis is centralized at the hypothalamic paraventricular nucleus (PVN), which releases

corticotropin-releasing hormone (CRH) and AVP. These, in turn, stimulate the adrenocorticotropic hormone (ACTH) and the production of GCs. The central CLOCK system in the SCN regulates the release of GCs in the adrenal glands by efferent connections to the PVN, aligning the circulation to photic cues (Ishida et al., 2005; Li & Androulakis, 2021; Nader et al., 2010).

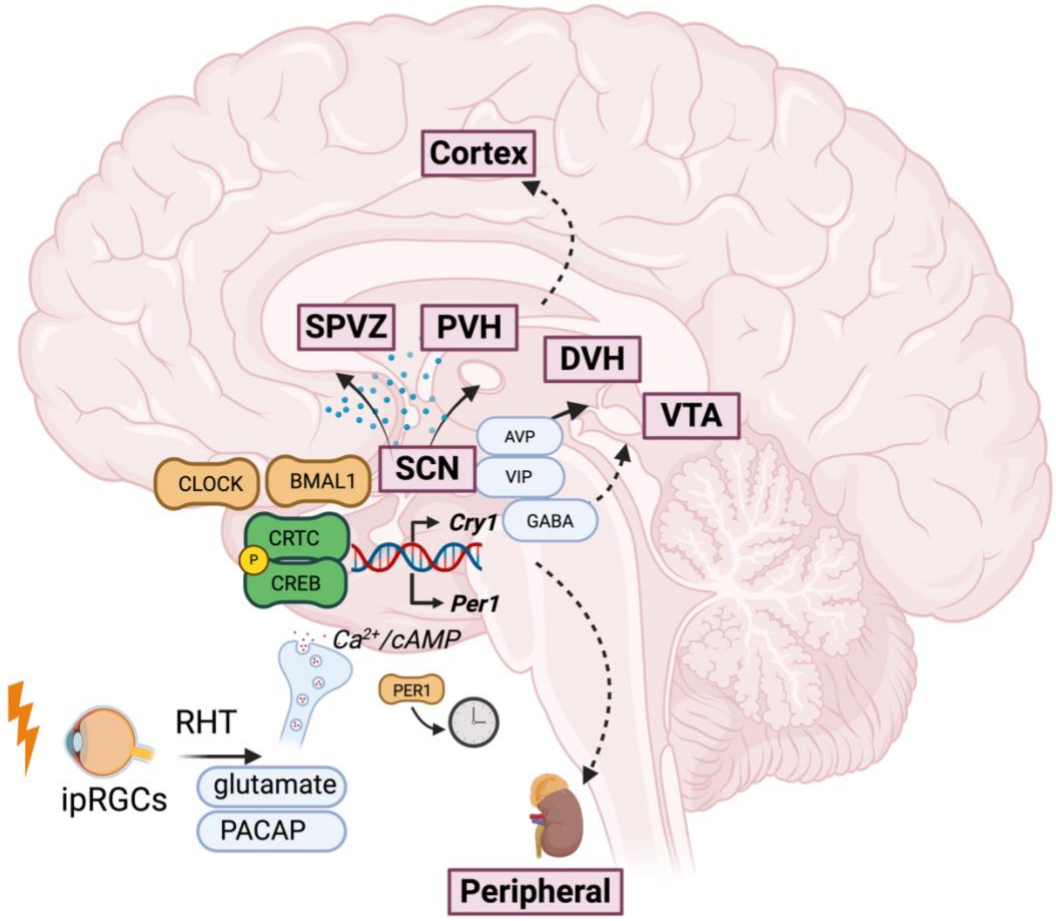

Fig. 1.1 Schematic diagram of the SCN network. The SCN receives input from the retina through the RHT in ipRGCs. Glutamate and PACAP induce the release of cAMP and Ca^{2+}, facilitating CREB-mediated transcription of clock genes and the 24hr rhythm. The SCN produces and projects neuropeptides and neurotransmitters. The SCN forms synaptic projections to neighboring regions such as SPVZ, PVH and DVH. Secondary and downstream projections include to the cortex and peripheral organs. The diagram is a simplified representation of the inputs and outputs of the SCN. Diagram created in Biorender.

1.1.4 Sleep

Sleep is an evolutionarily conserved behavior across species, though mammalian sleep duration could vary due to intrinsic sleep need levels or ecological trade-offs. The sleep-wake cycle is characterized by levels of brain arousal and multiple states. Wakefulness is generally defined as high arousal with voluntary engagement in response to internal and environmental cues. Sleep states, on the other hand, are associated with reduced responsiveness, changes in brain electrical activity patterns, reversibility and homeostatic regulation. The homeostatic response of sleep sustains the balance between sleep and wake, where deviations would be adjusted. It is showcased by rebound sleep after prolonged periods of wakefulness. During rapid eye movement (REM) sleep, functional brain connectivity remains high and rapid eye movement and high rates of respiration occur, associated with dreams. During non-rapid eye movement (NREM) sleep, cortical connectivity and propagation become weaker (Massimini et al., 2005), and it is characterized as the deepest stages of sleep (Joiner, 2016; Scammell et al., 2017).

A tool for measuring sleep is the electroencephalogram (EEG), placing electrodes to measure brain electrical activity, along with electromyography (EMG) to measure skeletal muscle tone (Campbell, 2009). Wake is associated with low amplitude, high frequency waves and muscle activity. NREM sleep dominates delta (0-4 Hz) waves and high amplitude signals marked as slow waves (Amzica & Steriade, 1998). Slow wave activity (SWA) or delta power is characterized as the index for sleep need (Achermann & Borbély, 2003; Scammell et al., 2017). However, as an invasive approach,

implantation of electrodes, anesthesia and post-surgery recovery may not be feasible on certain organisms and could impose risks of long-term damage. As a result, researchers and clinicians have adopted non-invasive alternatives, namely passive infrared (PIR) sensors, that capture movement and respiration rates (Bagci et al., 2025). In clinical settings, wearable and nearable devices are implemented to monitor sleep patterns in a home environment (Yoon et al., 2023).

Over the years, the neural mechanisms and circuitry of sleep-wake regulation are of great importance. Firing rates of neurons in different brain regions during wakefulness, NREM sleep and REM sleep are studied to characterize “sleep-wake active” neurons. The cerebral cortex was characterized in single-cell electrophysiological studies. Pyramidal neurons exhibited higher firing rates during sleep in primates (Evarts, 1964); the same applies to auditory cortical neurons in guinea pigs (Pena et al., 1999). It was shown that neurons in the brainstem and caudal hypothalamus direct innervate the cortex in parallel to promote arousal (Scammell et al., 2017). Cortical neuron firing has become a marker for sleep homeostasis. NREM sleep maintains short and synchronized firing with high frequency, reflected in SWA recordings. Following sustained sleep, cortical firing rates and frequencies decrease (Vyazovskiy et al., 2009). In addition, researchers showed that Layer 5 pyramidal neurons of the neocortex is crucial for initiation and propagation of slow waves (Krone et al., 2021). The firing patterns of primary motor cortex neurons (M1), essential for movement and neural plasticity, are also associated with sleep-wake states (Reid et al., 2026). The excitability of primary somatosensory neurons (S1) significantly enhanced following sleep

deprivation, proposing a marker of cortical responsiveness and sleep homeostasis (Gorgoni et al., 2014).

1.1.5 Clinical relevance of sleep and circadian rhythms

Sleep and circadian rhythm disruptions are linked to the risk and pathogenesis of various physiological conditions. Shift work percentage in the workforce has increased over the past decade and retirement age has also risen. Welton et al found that shift work is associated with thalamic and amygdala volume reduction, which leads to cognitive impairment (Welton et al., 2025). This is further supported by the study that there is an increasing brain age gap and apparent accelerated brain aging in young shift workers (Kim et al., 2025), which is related to the development of neurodegeneration. Lee et al showed in a meta-analysis that long-term shift work is correlated with risks of dementia development (Lee et al., 2023). These findings are underpinned by pre-clinical and molecular investigations. Researchers showed that Alzheimer's disease (AD) markers, amyloid β-peptide (Aβ) and pTau, accumulate, accompanied by increasing levels of corticosterone, following 6 hours of sleep deprivation (Lucey et al., 2017.; Rothman et al., 2013). It was also tested that interstitial fluid (ISF) levels are regulated by the sleep-wake cycle and that orexin receptor antagonists reduce the formation of Aβ plaques (Kang et al., 2009).

In addition, longitudinal studies on healthcare workers propose a link between sleep and circadian disturbances and the development of cancer. It was shown that health care shift workers have an increased risk for breast cancer, which is also positively

correlated with the duration in the occupation (Schernhammer et al., 2001). It also increases cardiovascular mortality (Wei et al., 2022). Similar studies have proposed that shift work also increases risks for lung cancer (Schernhammer et al., 2013), prostate cancer (Rivera-izquierdo et al., 2020) and bladder cancer (Haghayegh et al., 2023). Along with these disorders, due to irregular mealtimes and consumption of high-sugar food, there is also an observed increase in glucose and immune responses in shift workers (Yang et al., 2024). This is accompanied by a higher body mass index (BMI) and elevated blood pressure compared to day workers (Morikawa et al., 2007; Soltanzadeh et al., 2024). However, the molecular mechanisms and links remain a mystery.

There are increasing efforts to improve sleep and circadian disruptions, including melatonin (a sleep-promoting hormone synthesized by the pineal gland in response to darkness), light therapy, and the recently introduced dual-orexin receptor antagonists. However, as complications and confounding effects arise, further studies and trials would need to be carried out (Chakraborty et al., 2023; Gooley, 2008; Okawa et al., 1998; Tuft et al., 2023).

1.2 The Two Process Model

Borbély et al proposed the Two Process Model to effectively explain the rhythmicity and regulation of sleep. It connects the circadian and sleep homeostatic regulatory mechanisms. Process C is characterized by the circadian clock, which aligns our internal biological markers, such as core body temperature and melatonin levels, to the

environmental LD cycle. It maintains wake propensity throughout the day. Process S is measured by sleep need and pressure, which rise during wakefulness and drop during subjective night. SWA acts as the biomarker for Process S (Borbély, 1982, 2009). When Process S markers approach the lower boundary, wakefulness is triggered; when they reach the upper boundary, sleep onsets. The important interactions between the two processes occur at transition states between wake and sleep, when Process S reaches upper or lower thresholds (Deboer, 2018). Signals from both processes align to coordinate sleep-wake signaling, yet the molecular drivers remain a mystery. There is also evidence suggesting that Process S functions independently, through a non-SCN-dependent pathway. In SCN-lesion rats, only the circadian rhythms are disrupted, not homeostatic regulation (Tobler et al., 1983). Researchers also proposed the third process, Process W, which characterizes the sleepiness phase upon awakening, due to a “sleep inertia” effect (Åkerstedt & Folkard, 1995).

Continued efforts have focused on elucidating molecular markers regulating sleep homeostasis, including acetylcholine, dopamine, GABA and glutamate (Allada et al., 2017). Of these, adenosine was put forward as a strong contender as a key driver of sleep (Huang et al., 2024). Another hypothesis involves synaptic homeostatic regulation. It suggests that plastic processes result in an increase in synaptic strength during wakefulness in the cerebral cortex. Sleep facilitates the downscaling of synaptic strength to baseline for energy homeostasis, learning and memory (Cirelli & Tononi, 2019; Vyazovskiy et al., 2008; Vyazovskiy & Faraguna, 2014). Several studies have shown that NREM increases local synaptic strength and promotes dendrite formation,

which would depend on the input during wakefulness (Yang et al., 2014), though it is generally understood that sleep leads to downscaling for homeostasis. The molecular mechanisms linking synaptic function to sleep remain unclear.

1.3 Molecular regulation: phosphorylation in sleep and circadian regulation

Phosphorylation is arguably one of the best studied post-translational modifications (PTMs) of core clock components (Baker et al., 2009). With the advancement of quantitative mass spectrometry and computational methods, researchers have gained a comprehensive understanding of the role of post-transcriptional and post-translational mechanisms in sleep and circadian regulation. Koike et al conducted transcriptomics across 24 hours in the mouse liver and found that only 22% of mRNA transcripts of cycling genes were driven by transcription (Koike et al., 2012). Additionally, Robles et al supported this finding by demonstrating that approximately 6% of liver proteins cycle daily but not in tandem with their relative transcripts (Robles et al., 2014). These findings suggest that post-transcriptional mechanisms play key roles in the temporal control of liver metabolism. Moreover, in parallel in synaptic compartments, Noya et al found that 93% of the oscillating transcripts are exclusively rhythmic in synaptic compartments. They showed that synaptic transcripts anticipate dawn and dusk times, enriched for metabolic and synaptic transmission processes, respectively, emphasizing that the mRNA transcripts depend on a functional circadian clock. Importantly, the locally translated synaptic proteins are regulated by the sleep-wake cycle, as sleep

deprivation abolishes the daily cycles of proteins (Noya et al., 2019). These studies accentuate the post-transcriptional and post-translational regulation across various tissues.

Following these studies, Brüning et al conducted an *in vivo* quantitative phosphoproteomics study on forebrain synaptoneurosomes and found that 30% of 2000 phosphoproteins identified abundant ~24hr oscillations and that sleep deprivation abolished 98% of rhythmic phosphorylation. These changes in phosphorylation of key kinases involved in synaptic signaling are crucial for understanding sleep-wake mechanisms (Brüning et al., 2019a). This was further validated in the mouse liver phosphoproteome, where 25% out of 20,000 phosphosites oscillate daily in around 24h, including novel sites on key clock proteins. These proteins were also identified as downstream of key metabolic signalling cascades. Thus, this adds another layer of phosphorylation-dependent circadian regulation of physiological processes (Robles et al., 2017).

In addition to the aforementioned studies, recent findings have also identified phosphorylation as a key regulator of sleep. This places kinases as a plausible candidate capable of unifying sleep and circadian regulation (Ode & Ueda, 2020). For instance, researchers found that Ca^{2+}-dependent hyperpolarization is involved in slow-wave sleep and sleep duration. Tatsuki et al identified Ca^{2+}/calmodulin-dependent protein kinase II α/ β subunit (CAMK2A/B) as sleep-promoting kinases (Tatsuki et al., 2016). Genetic knockout studies have validated the finding, and specific

phosphorylation sites were identified as important for sleep regulation (Tone et al., 2022; Yang et al., 2025). In addition, extracellular signal-regulated kinase (ERK) activation increases sleep, suggesting that ERK phosphorylation modulates sleep amount and sleep-wake transition (Vanderheyden et al., 2013). It was further supported that pERK levels rise during wakefulness and are nearly threefold lower in NREM both *in vitro* and *in vivo* (Mikhail et al., 2017).

1.4 Salt-inducible kinases

1.4.1 Discovery of SIKs

The SIK family was first discovered in the adrenocortical tissues from high-salt diet-treated rats. SIKs are serine/threonine (Ser/Thr) kinases, part of the AMPK family, and consist of three members, SIK1/2/3 (Taub et al., 2010).

Literature has shown that *Sik1* mRNA, in addition to high levels in rat adrenal glands, is also expressed in the brain (cortex and hippocampus), testis, ovary, and cardiac tissue in mice (Feldman et al., 2000; Okamoto et al., 2004; Ruiz et al., 1994). Research has shown that *Sik1* mRNA levels increase after treatment with adrenocorticotropic hormone (ACTH) in rat adrenal glands and Y1 cells (Lin et al., 2001; Wang et al., 1999). Takemori et al also showed that SIK1 is phosphorylated by PKA at S577 during ACTH stimulation, resulting in cytoplasmic translocation. SIK1 is moved back into the nucleus following dephosphorylation. The nucleocytoplasmic shuttling of SIK1 is essential for ACTH signaling in adrenocortical cells (Takemori et al., 2002).

Two isoforms of the SIK family were later identified, namely SIK2 and SIK3. SIK2 is highly expressed in adipose tissues and is suggested to be involved in adipogenesis and insulin signaling (Horike et al., 2003; Katoh et al., 2004a), whereas the mRNA expression of SIK3 appears to be ubiquitous.

1.4.2 LKB1:STRADα:MO25α trimer regulation

Structurally, the SIK family has an N-terminal kinase domain, followed by a ubiquitin-associated domain (UBA) and a C-terminal tail. Phosphorylation of the threonine residues in the activation loop is essential for the catalytic activity of SIKs (T182 for SIK1, T175 for SIK2 and T163 for SIK3) (Darling & Cohen, 2021a). These sites are phosphorylated by the master kinase liver kinase B1 (LKB1) in mammalian cells, along with all the 13 AMP-activated protein kinases (AMPKs), established as an AMPK kinase (AMPKK) (Hawley et al., 2003; Lizcano et al., 2004).LKB1 acts as a tumor suppressor not only through inhibition of proliferation but also by exerting effects on cells' ability to respond to low cellular energy (Alessi et al., 2006). Furthermore, it acts in concert by directly binding to the STE20-related kinase (STRAD) and mouse protein-25 alpha (MO25) to activate SIKs. STRAD is an LKB1-specific substrate and binds to LKB1 via the catalytic domain, facilitating cytoplasmic localization (Baas et al., 2003a; Boudeau et al., 2003a), and the C-terminus of STRAD interacts with MO25 (Milburn et al., 2004). MO25 was initially identified as a gene expressed during the early cleavage stages of rat embryogenesis. The LKB1-STRAD complex creates new binding pockets for MO25, thereby stabilizing the complex (Boudeau et al., 2003b). In purified AMPK-related kinases, the kinase family on its own has very low basal levels, and the addition of

LKB1:STRAD:MO25 complex increases activity by 50- to 200-fold (Lizcano et al., 2004). In particular, the kinase activity of SIK1/2/3 is increased by around 20- to 50- fold in *E.coli*-purified kinases, starting from low basal activity. It is shown that LKB1 alone does not result in significant activation. The alpha subunits of STRAD and MO25 generate the greatest activation (Lizcano et al., 2004). It was validated *in vitro* that LKB1-deficient cell lines showed significantly lower AMPK activity compared to LKB1-expressing lines (Jaleel et al., 2006). The necessity of LKB1 for AMPK-kinase activity lies in the fact that the AMPK kinases are the only kinases in the human genome that possess a UBA domain. The UBA is required for AMPK-related phosphorylation and activity, though it does not act as a docking site for the LKB1 trimer (Jaleel et al., 2006).

In an isoform-specific manner, SIKs are also regulated by autophosphorylation feedback actions. S577, the PKA phosphorylation site, and S186 were identified as autophosphorylation sites of SIK1. Hashimoto et al showed that the autophosphorylation of S186 is a prerequisite for the LKB1-dependent activation at T182. Researchers also proposed that LKB1 phosphorylates SIK1 at T182 and initiates the autophosphorylation loop. Glycogen synthase kinase-3β (GSK-3β) recognizes the loop and, in turn, phosphorylates SIK1 at T182. This interaction is also present in SIK2 but not in SIK3 (Hashimoto et al., 2008), suggesting differential activity of LKB1 in activation cascades in SIK isoforms.

1.4.3 Regulators of SIKs

In addition to LKB1, it was shown that Ca^{2+}/calmodulin-dependent protein kinase kinases (CaMKKs) could phosphorylate T172 on AMPKs and the site is highly conserved in AMPK-related kinases, including SIKs (Hawley et al., 2005). However, it was shown that no SIKs were activated by CaMMKs in HeLa cells (Fogarty et al., 2010). It was supported by non-small cell lung cancer that SIK activity is mainly LKB1-dependent rather than CaMKK2 (Hollstein et al., 2019). Furthermore, Na^+, K^+-ATPase (NK) activity is essential for cell volume and composition. Sjostrom et al showed that SIK1, regulated by levels of salt intake, is associated with NK activity, while SIK2 and SIK3 isoforms are not. The phosphorylation of SIK1 at T322 by Ca^{2+}/calmodulin-dependent protein kinase (CaMK) results in the activation of NK α-subunit catalytic activity (Sjöström et al., 2007).

The SIK family is also in parallel regulated by cAMP-dependent PKA activity. The catalytic subunits of PKA (Cα and Cβ) are released when cAMP binds, activating phosphorylation of downstream targets. There are PKA phosphorylation sites on the C-terminal tail of SIKs (T457 and S577 for SIK1; S343, S358, T484 and S587 for SIK2; T469, S551 and S674 for SIK3). PKA enables SIKs to bind to 14-3-3 proteins in the cytoplasm, which reduces SIK substrate binding. SIKs restrict targets to the cytoplasm by inducing their association with 14-3-3, but upon cAMP stimulation and Ca^{2+} signals, PKA inactivates SIKs through phosphorylation, which allows CRTC's translocation to the nucleus, initiating CREB transcription (Sonntag et al., 2018). In parallel, PKA also phosphorylates CREB at S133, activating the CREB transcriptional pathway. Though

molecular pathways are understudied, it is generally understood that PKA deactivates SIKs.

1.4.4 Target of SIKs

Known downstream substrates of SIKs include CRTCs and histone deacetylases (HDACs), which regulate cellular signaling and metabolic pathways. The CREB-coactivator, CRTC, is typically translocated to the nucleus when dephosphorylated and upon dendritic synaptic inputs (Ch'Ng et al., 2012). When phosphorylated by SIKs, they bind to 14-3-3 proteins and are restricted in the cytoplasm. CRTCs have three isoforms (CRTC1, 2 and 3) and bind to the basic leucine zipper (bZIP) DNA-binding region of CREB (Conkright et al., 2003) and are essential for CREB-mediated transcription. Through the LKB1 axis, SIKs phosphorylate CRTCs and moves it back to the cytoplasm, which therefore act as repressors of CREB transcription (Katoh et al., 2006). This proposes a mechanism that is independent of S133 activation on CREB (Sakamoto et al., 2011, 2013b). PKA and CAMKI/IV, regulators of SIKs, also regulate the nuclear translocation of CRTC1, further validating the upstream and downstream cascades of SIKs (Nonaka et al., 2014). The system falls into place with the coincidence detection of two second messenger pathways - cAMP that activates PKA and Ca^{2+} that regulates calcium-dependent calcineurin. Calcineurin dephosphorylates CRTCs, and PKA deactivates SIK activity, resulting in nuclear translocation and CREB transcription (Screaton et al., 2004). In Drosophila, researchers showed that SIKs are responsible for inhibiting CRTC activity through phosphorylation, which contributes to lipid and energy homeostasis (Choi et al., 2011). SIKs' action on CRTCs is also implied in IL-10

production by macrophages and glucose metabolism (Clark et al., 2012; Koo et al., 2005).

The SIK-CREB axis is also implicated in neurophysiology. There is evidence showing that dendritic growth is regulated through calcium signalling via voltage-gated calcium channels (VGCCs) in cortical neurons. This is likely to be mediated by CaMKs, specifically CaMKIV, as maximal dendrite growth coincides with maximum CaMKIV levels. It is shown to be transcriptionally regulated by the prominent nuclear target of CaMKIV, CREB (Wong & Ghosh, 2002). There is increasing evidence that CREB is involved in memory formation, recognition, and fear using knockout mouse models. However, the role of CREB in plasticity appears to vary across brain regions (Sakamoto et al., 2011). These effects are strengthened by the coactivator CRTC1, involved in long-term memory formation and neural development, but are also shown to be region-specific (Nonaka et al., 2014; Saura & Cardinaux, 2017). It is shown that genetic overexpression of SIK2 in the hippocampus is associated with depressive behaviors, suggesting a kinase-substrate relationship in the pathogenesis of neurophysiology (Jiang et al., 2019b).

In addition, studies found that SIKs directly phosphorylate class IIa HDACs, which are similarly sequestered to the cytoplasm with CRTCs (Sonntag et al., 2018). They are crucial co-repressors of the myocyte enhancer factor 2 (MEF2) family, which plays significant roles in muscle development and the vascular system (Stewart et al., 2013; Walkinshaw et al., 2013) (Fig. 1.1).

1.4.5 Pharmacology of SIKs

As SIKs are involved in multiple levels of physiology (Jagannath et al., 2023), early efforts have yielded a handful of small-molecule SIK inhibitors. MRT67307, originally designed as an inhibitor of IkB kinase (IKK) – related kinase, was shown to inhibit SIK isoforms with similar potency to IKK-related kinases. Distinct from other AMPK kinases, SIKs embody a threonine residue at the 'gatekeeper' site, which creates an adjacent hydrophobic pocket that can be targeted by inhibitors (Clark et al., 2012; Darling & Cohen, 2021b). Further, KIN112 and HG-9-91-01 are potent inhibitors that target both the ATP-binding site and hydrophobic pocket of SIKs. In addition, ARN-3236 was introduced as a novel pan-SIK inhibitor that was tested in ovarian cancer cell lines and enhanced sensitivity to paclitaxel (Zhou et al., 2017a). In addition, recent early-phase clinical studies have begun targeting SIK2 and SIK3 in inflammatory disorders, with further ongoing efforts towards isoform-specific inhibitor development.

1.4.6 SIKs in sleep and circadian regulation

Existing literature supports that SIKs are involved in the regulation of circadian rhythms and sleep. *Sik1* expression was found to be upregulated post-nocturnal light pulse along with *Per1* (Jagannath et al., 2013). This is consistent with *Sik1* being a target of CRTC1/CREB transcriptional regulation in phase resetting in the SCN. *In vitro* assays demonstrated that SIK1 phosphorylates CRTC, leading to cytoplasmic translocation and limiting CREB-mediated transcription of clock genes, thereby attenuating phase shifting in the SCN. In *Sik1*-silenced mice, phase shifts and re-entrainment to light-dark (LD) cycle were significantly enhanced as a consequence of removing the inhibitory effect of

SIK1 on CRTC1/CREB signalling (Jagannath et al., 2013). This proposes that SIK1 acts as a buffering mechanism in response to photic input on the central clock, providing possibilities for jetlag and shift work.

Interestingly, a splice mutation in *Sik3*, named *Sleepy* mutant, exhibited significantly reduced total wake time and constitutive enhanced sleep need. SIK3 was further characterized as a sleep-promoting kinase involved in the sleep homeostatic regulation (Funato et al., 2016). Through whole-brain quantitative phosphoproteomics, researchers identified 80 synaptic sleep-need-index phosphoproteins (SNIPPs), strongly associated with sleep need and pressure (Wang et al., 2018). In addition, the SIK3-HDAC4 axis was established as a key regulator for circadian period in the SCN and sleep amount (Asano et al., 2023; Kim et al., 2022) (Fig. 1.1). Hayasaka et al further proposed that the extended circadian period in Sik3-deficient mice reflects altered phosphorylation of PER2 by SIK3 (Hayasaka et al., 2017). Together, these studies establish a role for SIKs in regulating the central circadian clock and sleep homeostasis.

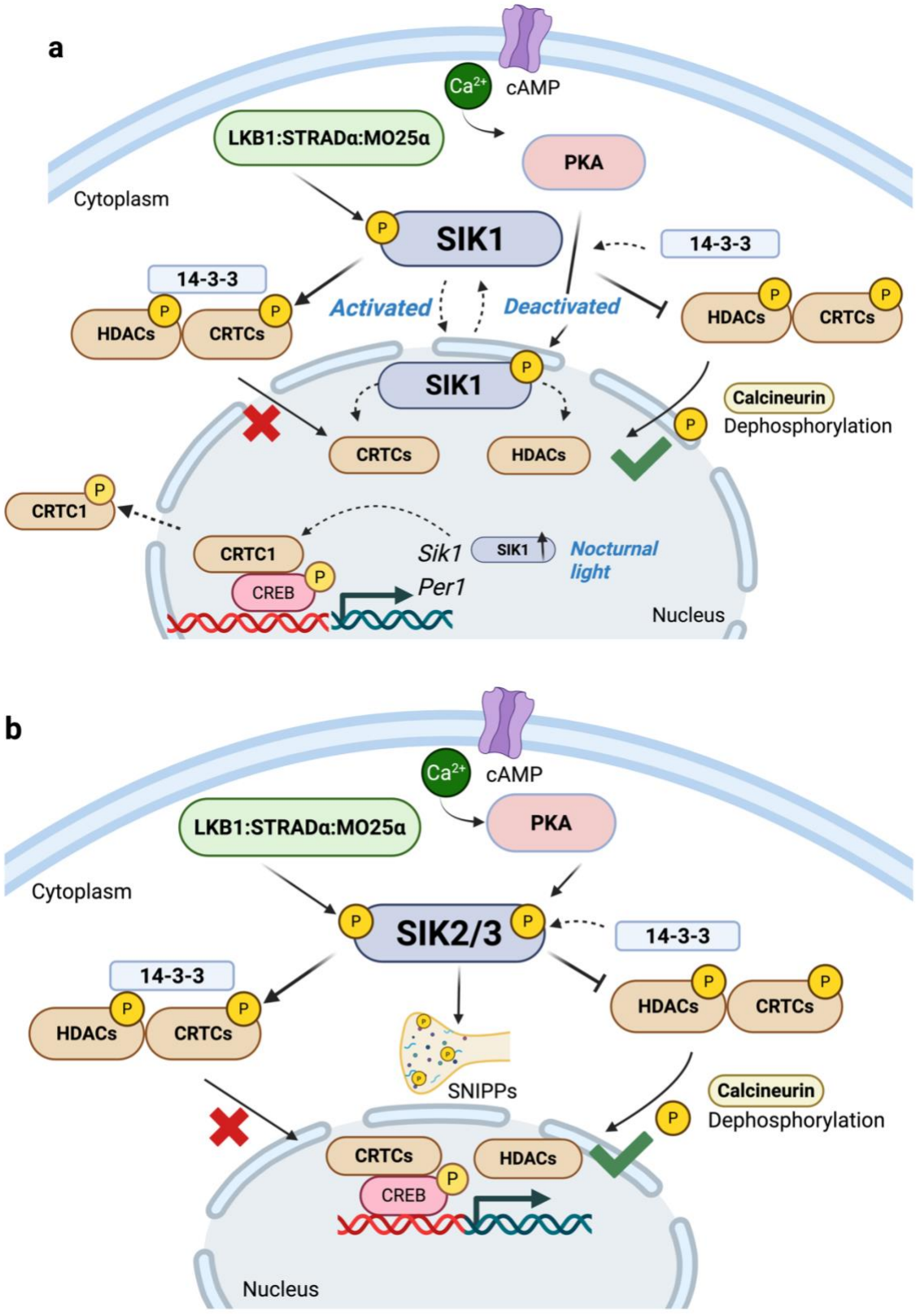
a
Ca2+
cAMP
LKB1:STRADα:MO25α
PKA
Cytoplasm
SIK1
14-3-3
14-3-3
HDACs
CRTCs
Activated
Deactivated
HDACs
CRTCs
SIK1
Calcineurin
Dephosphorylation
CRTCs
HDACs
CRTC1
CRTC1
Sik1
SIK1
Nocturnal light
CREB
Per1
Nucleus
b
Ca2+
cAMP
LKB1:STRADα:MO25α
PKA
Cytoplasm
SIK2/3
14-3-3
14-3-3
HDACs
CRTCs
HDACs
CRTCs
SNIPPs
Calcineurin
Dephosphorylation
CRTCs
HDACs
CREB
Nucleus

Fig. 1.2 **Regulation and targets of SIKs**. Schematic diagram of the regulation and targets of SIKs. LKB1:STRADα:MO25α trimer phosphorylates SIKs at respective sites on the activation loop of the kinase domains. SIKs phosphorylate their targets, CRTCs and HDACs, inhibiting their activity by facilitating binding to 14-3-3 protein and restricting nuclear translocation. PKA, on the other hand, upon cAMP stimulation, deactivates SIKs by phosphorylation and facilitates binding to 14-3-3. SIKs are unable to phosphorylate targets. CRTCs and HDACs are also coincidence detectors of calcium-mediated calcineurin that dephosphorylates them, moving them to the nucleus. Downstream transcription pathways are activated. (a) SIK1 is found in the nucleus when activated and sequestered to the cytoplasm when deactivated by PKA. SIK1 is involved in nucleocytoplasmic shuttling. SIK1 also forms a negative feedback loop during nocturnal light, regulating CRTC1-CREB-mediated transcription of clock genes and phase shifting. (b) SIK2 and SIK3 are mainly found in the cytoplasm. SIK3 phosphorylates a hub of synaptic proteins, SNIPPs. Diagram created in Biorender.

1.5 Experimental approaches

As the interest in SIKs and phosphorylation in sleep and circadian regulation arises, this thesis adopts various experimental models and methods to investigate and characterize the roles of SIKs.

1.5.1 SIK kinase-inactive knock-in (KI) model

As established in previous studies, SIKs possess key threonine sites in the activation loop that are phosphorylated by the LKB1 trimer for kinase activity. The mutation from threonine (Thr/T) and alanine (Ala/A) on corresponding sites results in inactivation of SIKs and other AMPKs (Lizcano et al., 2004). In this thesis, we adopted the SIK mouse line generated by Darling et al. The mutant line was generated by replacing the WT protein with a catalytically inactive mutant, by mutating the threonine residue to an alanine in the activation loop (SIK1-T182A, SIK2-T175A and SIK3-T163A). The kinase-inactive knock-in (KI) line for SIK1 and SIK3 did not show developmental and fertility

defects from WT animals. However, SIK3 KI lines showed slight defects in skeletal development, resulting in a smaller body size (Darling et al., 2017).

In the traditional knock-out lines, where a gene is deleted, the protein is not available to typical endogenous binding partners, which could severely disrupt protein interactions and compositions within the system. Previous literature has suggested that, though knockout strains are important tools for studying individual functions, they show defects in responses and that compensatory or redundancy mechanisms are activated (Kaufmann & Ladel, 1994; Nelson, 1997). The KI model maintains the scaffolding functions and the interactions between endogenous kinase complexes. It is a novel strategy to assess the therapeutic capabilities of the SIK family (Darling et al., 2017).

1.5.2 Kinase assay linked phosphoproteomics (KALIP)

Phosphorylation, a post-translational regulatory mechanism, is crucial for cellular functions and is implicated in disease pathways (Cohen, 2001). Liquid chromatography-mass spectrometry (LC-MS) – based proteomics and phosphoproteomics have arisen to identify and quantify protein-protein interaction and phosphorylation patterns (Aebersold & Mann, 2003; Mumby & Brekken, 2005). However, since proteomics and phosphoproteomics generate large datasets, motif and functional analysis are often performed to determine precise kinase relationships (Schwartz & Gygi, 2005). However, it is often difficult to distinguish direct substrates of a kinase from proteins phosphorylated by secondary kinases that are themselves activated downstream.

Xue et al developed kinase assay linked phosphoproteomics (KALIP) that integrates a highly sensitive *in vitro* kinase reaction and kinase-modulated *in vivo* phosphoproteomics. The *in vitro* kinase assay is performed either with peptides (Pep-KALIP) or proteins (Pro-KALIP). Pep-KALIP carries out the enzymatic digestion and phosphopeptide enrichment prior to the kinase reaction, while Pro-KALIP performs the kinase reaction with the undigested protein. The peptides or proteins undergo a dephosphorylation reaction with all the endogenous kinases inhibited, followed by a rephosphorylation reaction with the purified kinase of interest. It then goes through LC-MS to acquire a set of substrates. The dataset is overlapped with the kinase-modulated in vivo phosphoproteomics, such as knockout or inhibition of the kinase, to identify *bona fide* direct substrates (Xue et al., 2016) (Fig. 1.2). This method was applied to identify direct Syk substrates in B cells and breast cancer cells, validating and pinpointing specific signaling pathways. It provides a strategy for substrate specificity and kinase screening in various model systems (Xue et al., 2013).

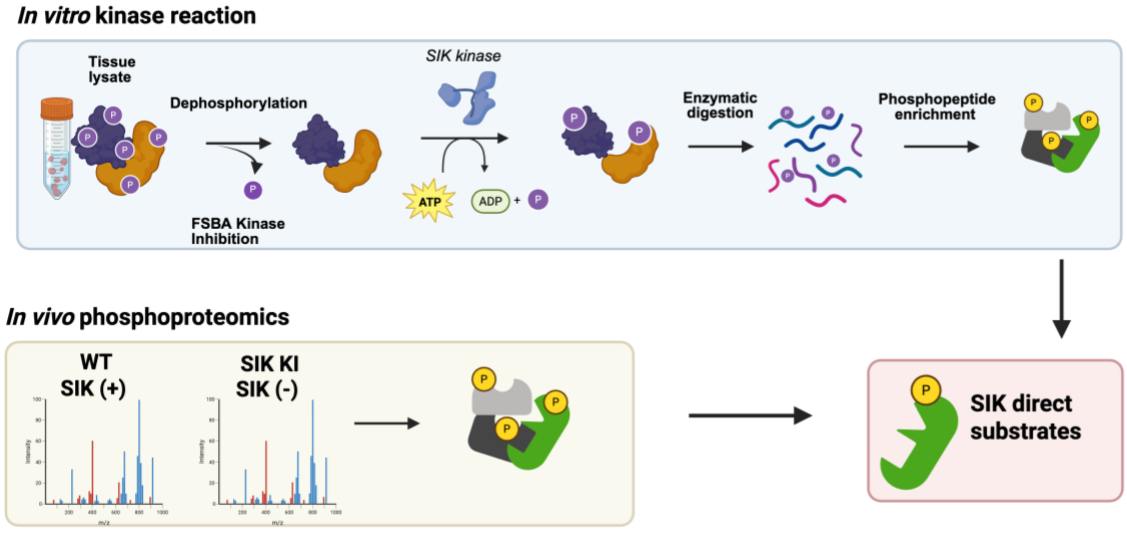

Fig. 1.3 **Workflow of Pro-KALIP.** Workflow of Pro-KALIP showing the in vitro kinase reaction component tissue lysate is dephosphorylated and endogenous kinases are irreversibly inhibited. Purified exogenous SIK kinases are added along with ATP to rephosphorylate the lysate. Samples undergo enzymatic digestion, phosphopeptide enrichment and LC-MS. The dataset is compared to an in vivo phosphoproteomics to obtain SIK direct substrates. Diagram created in Biorender.

1.6 Aims

Researchers have established the Two Process Model to explain the rhythmicity and regulation of sleep and its interaction with the central circadian clock, modulated by the SCN. One hypothesis links synaptic homeostasis, involving synaptic proteins, to sleep regulation, prompting research into phosphorylation and the roles of kinases. Existing research has introduced SIKs as being involved in both the transcriptional regulation of the circadian clock and the post-translational modification of synaptic proteins. However, the molecular substrates, mechanisms and functional distinctions between the three isoforms remain poorly understood. This thesis aims to establish the role of SIKs in sleep and circadian regulation by identifying direct molecular mechanisms and signalling pathways.

This thesis investigates the roles of individual SIK isoforms in circadian and sleep regulation, with each chapter dedicated to a specific isoform. The molecular pathways and substrates identified are integrated in the General Discussion (Chapter 6) to elucidate shared and isoform-specific mechanisms within interconnected signalling networks. Together, the findings provide a comprehensive molecular framework for understanding how SIKs collectively and differentially contribute to the Two Process model. These are achieved through the following three approaches:

Research Aim (1): Direct substrates of SIK1

In Chapter 3, building on the established light-inducible phenotype of SIK1, we aim to identify its direct molecular substrates and phosphorylation sites. We aim to optimize

and apply tissue-specific protein kinase assay linked phosphoproteomics (Pro-KALIP). Candidate substrates will be validated by *in vitro* cell-based functional assays.

Research Aim (2): Characterization of SIK3

In Chapter 4, we aim to define the role of SIK3 in sleep and circadian regulation using SIK3 KI animals. We aim to conduct circadian characterizations by analyzing wheel-running activity. We will perform cortex-specific mRNA-seq and Pro-KALIP to identify SIK3-dependent transcriptional and phosphorylation patterns.

Research Aim (3): Characterization of SIK2

In Chapter 5, we aim to characterize the role of SIK2 in sleep and circadian regulation using SIK2 KI animals. Wheel-running activity and EEG/EMG recordings will be analyzed and quantified as measurements for circadian and sleep behavior, respectively. Tissue-specific mRNA-seq, phosphoproteomics and Pro-KALIP will be performed to identify direct molecular substrates of SIK2. Exploratory cognitive and memory tests will be conducted for further phenotyping.

REFERENCES

Achermann, P., & Borbély, A. A. (2003). MATHEMATICAL MODELS OF SLEEP REGULATION. In *Frontiers in Bioscience* (Vol. 8).

Aebersold, R., & Mann, M. (2003). Mass spectrometry-based proteomics. *Nature*, *422*(6928), 198–207. https://doi.org/10.1038/nature01511

Åkerstedt, T., & Folkard, S. (1995). Validation of the S and C Components of the Three-Process Model of Alertness Regulation. *Sleep*, *18*(1), 1–6. https://doi.org/10.1093/sleep/18.1.1

Albrecht, U. (2012). Timing to Perfection: The Biology of Central and Peripheral Circadian Clocks. In *Neuron* (Vol. 74, Number 2, pp. 246–260). https://doi.org/10.1016/j.neuron.2012.04.006

Alessi, D. R., Sakamoto, K., & Bayascas, J. R. (2006). LKB1-Dependent Signaling Pathways. *Annual Review of Biochemistry*, *75*(1), 137–163. https://doi.org/10.1146/annurev.biochem.75.103004.142702

Allada, R., Cirelli, C., & Sehgal, A. (2017). Molecular mechanisms of sleep homeostasis in flies and mammals. *Cold Spring Harbor Perspectives in Biology*, *9*(8). https://doi.org/10.1101/cshperspect.a027730

Amzica, F., & Steriade, M. (1998). *Electrophysiological correlates of sleep delta waves 1*.

Asano, F., Kim, S. J., Fujiyama, T., Miyoshi, C., Hotta-Hirashima, N., Asama, N., Iwasaki, K., Kakizaki, M., Mizuno, S., Mieda, M., Sugiyama, F., Takahashi, S., Shi, S., Hirano, A., Funato, H., & Yanagisawa, M. (2023). SIK3–HDAC4 in the suprachiasmatic nucleus regulates the timing of arousal at the dark onset and circadian period in mice. *Proceedings of the National Academy of Sciences of the United States of America*, *120*(11). https://doi.org/10.1073/pnas.2218209120

Baas, A. F., Boudeau, J., Sapkota, G. P., Smit, L., Medema, R., Morrice, N. A., Alessi, D. R., & Clevers, H. C. (2003). Activation of the tumour suppressor kinase LKB1 by the STE20-like pseudokinase STRAD. *EMBO Journal*, *22*(12), 3062–3072. https://doi.org/10.1093/emboj/cdg292

Bağcı, M. F., Nguyen, T., & Öztürk, Y. (2025). Respiration Rate Monitoring During Sleep using an Ambient PIR Sensor Array. *2025 47th Annual International Conference of the IEEE Engineering in Medicine and Biology Society (EMBC)*, 1–5. https://doi.org/10.1109/EMBC58623.2025.11253519

Baker, C. L., Kettenbach, A. N., Loros, J. J., Gerber, S. A., & Dunlap, J. C. (2009). Quantitative Proteomics Reveals a Dynamic Interactome and Phase-Specific Phosphorylation in the Neurospora Circadian Clock. *Molecular Cell*, *34*(3), 354–363. https://doi.org/10.1016/j.molcel.2009.04.023

Berson, D. M., Dunn, F. A., & Takao, M. (2002). Phototransduction by Retinal Ganglion Cells That Set the Circadian Clock. *Science*, *295*(5557), 1070–1073. https://doi.org/10.1126/science.1067262

Borbély, A. A. (1982). A two process model of sleep regulation. *Human Neurobiology*, *1*(3), 195–204.

Borbély, A. A. (2009). Refining sleep homeostasis in the two-process model: Editorial. In *Journal of Sleep Research* (Vol. 18, Number 1, pp. 1–2). https://doi.org/10.1111/j.1365-2869.2009.00750.x

Boudeau, J., Baas, A. F., Deak, M., Morrice, N. A., Kieloch, A., Schutkowski, M., Prescott, A. R., Clevers, H. C., & Alessi, D. R. (2003a). MO25α/β interact with STRADα/β enhancing their ability to bind, activate and localize LKB1 in the cytoplasm. *EMBO Journal*, *22*(19), 5102–5114. https://doi.org/10.1093/emboj/cdg490

Boudeau, J., Baas, A. F., Deak, M., Morrice, N. A., Kieloch, A., Schutkowski, M., Prescott, A. R., Clevers, H. C., & Alessi, D. R. (2003b). MO25α/β interact with STRADα/β enhancing their ability to bind, activate and localize LKB1 in the cytoplasm. *EMBO Journal*, *22*(19), 5102–5114. https://doi.org/10.1093/emboj/cdg490

Brüning, F., Noya, S. B., Bange, T., Koutsouli, S., Rudolph, J. D., Tyagarajan, S. K., Cox, J., Mann, M., Brown, S. A., & Robles, M. S. (2019). Sleep-wake cycles drive daily dynamics of synaptic phosphorylation. *Science*, *366*(6462). https://doi.org/10.1126/science.aav3617

Campbell, I. G. (2009). EEG recording and analysis for sleep research. In *Current Protocols in Neuroscience* (Number SUPPL.49). Blackwell Publishing Inc. https://doi.org/10.1002/0471142301.ns1002s49

Chakraborty, D. S., Choudhury, S., & Lahiry, S. (2023). Daridorexant, a Recently Approved Dual Orexin Receptor Antagonists (DORA) in Treatment of Insomnia. In *Sleep Science* (Vol. 16, Number 2, pp. 256–264). Brazilian Association of Sleep and Latin American Federation of Sleep Societies. https://doi.org/10.1055/s-0043-1770805

Ch'Ng, T. H., Uzgil, B., Lin, P., Avliyakulov, N. K., O'Dell, T. J., & Martin, K. C. (2012). Activity-dependent transport of the transcriptional coactivator CRTC1 from synapse to nucleus. *Cell*, *150*(1), 207–221. https://doi.org/10.1016/j.cell.2012.05.027

Choi, S., Kim, W., & Chung, J. (2011). Drosophila salt-inducible kinase (SIK) regulates starvation resistance through cAMP-response element-binding protein (CREB)-regulated transcription coactivator (CRTC). *Journal of Biological Chemistry*, *286*(4), 2658–2664. https://doi.org/10.1074/jbc.C110.119222

Cirelli, C., & Tononi, G. (2019). Linking the need to sleep with synaptic function. In *Science* (Vol. 366, Number 6462, pp. 189–190). American Association for the Advancement of Science. https://doi.org/10.1126/science.aay5304

Clark, K., MacKenzie, K. F., Petkevicius, K., Kristariyanto, Y., Zhang, J., Choi, H. G., Peggie, M., Plater, L., Pedrioli, P. G. A., McIver, E., Gray, N. S., Arthur, J. S. C., & Cohen, P. (2012). Phosphorylation of CRTC3 by the salt-inducible kinases controls the interconversion of classically activated and regulatory macrophages. *Proceedings of the National Academy of Sciences of the United States of America*, *109*(42), 16986–16991. https://doi.org/10.1073/pnas.1215450109

Cohen, P. (2001). The role of protein phosphorylation in human health and disease: Delivered on June 30th 2001 at the FEBS meeting in Lisbon. *European Journal of Biochemistry*, *268*(19), 5001–5010. https://doi.org/10.1046/j.0014-2956.2001.02473.x

Conkright, M. D., Canettieri, G., Screaton, R., Guzman, E., Miraglia, L., Hogenesch, J. B., & Montminy, M. (2003). TORCs: Transducers of Regulated CREB Activity Additional regulatory contributions by the CREB bZIP The Salk Institute for Biological Studies CREB protein in certain cells, for example, represses cellular gene expression via a bZIP-dependent mecha-10010 North Torrey Pines Road. In *Molecular Cell* (Vol. 12). http://www.molecule.org/cgi/

Darling, N. J., & Cohen, P. (2021a). Nuts and bolts of the salt-inducible kinases (SIKs). In *Biochemical Journal* (Vol. 478, Number 7, pp. 1377–1397). Portland Press Ltd. https://doi.org/10.1042/BCJ20200502

Darling, N. J., & Cohen, P. (2021b). Nuts and bolts of the salt-inducible kinases (SIKs). In *Biochemical Journal* (Vol. 478, Number 7, pp. 1377–1397). Portland Press Ltd. https://doi.org/10.1042/BCJ20200502

Darling, N. J., Toth, R., Arthur, J. S. C., & Clark, K. (2017). Inhibition of SIK2 and SIK3 during differentiation enhances the anti-inflammatory phenotype of macrophages. *Biochemical Journal*, *474*(4), 521–537. https://doi.org/10.1042/BCJ20160646

Davidson, A. J., Yamazaki, S., Arble, D. M., Menaker, M., & Block, G. D. (2008). Resetting of central and peripheral circadian oscillators in aged rats. *Neurobiology of Aging*, *29*(3), 471–477. https://doi.org/10.1016/j.neurobiolaging.2006.10.018

Deboer, T. (2018). Sleep homeostasis and the circadian clock: Do the circadian pacemaker and the sleep homeostat influence each other's functioning? In *Neurobiology of Sleep and Circadian Rhythms* (Vol. 5, pp. 68–77). Elsevier Inc. https://doi.org/10.1016/j.nbscr.2018.02.003

Evarts, E. V. (1964). TEMPORAL PATTERNS OF DISCHARGE OF PYRAMIDAL TRACT NEURONS DURING SLEEP AND WAKING IN THE MONKEY. *Journal of Neurophysiology*, *27*(2), 152–171. https://doi.org/10.1152/jn.1964.27.2.152

Feldman, J. D., Vician, L., Crispino, M., Hoe, W., Baudry, M., & Herschman, H. R. (2000). The salt-inducible kinase, SIK, is induced by depolarization in brain. *Journal of Neurochemistry*, *74*(6), 2227–2238. https://doi.org/10.1046/j.1471-4159.2000.0742227.x

Fogarty, S., Hawley, S. A., Green, K. A., Saner, N., Mustard, K. J., & Hardie, D. G. (2010). Calmodulin-dependent protein kinase kinase-β activates AMPK without forming a stable complex: Synergistic effects of Ca2+ and AMP. *Biochemical Journal*, *426*(1), 109–118. https://doi.org/10.1042/BJ20091372

Foster, R. G., Hughes, S., & Peirson, S. N. (2020). Circadian photoentrainment in mice and humans. In *Biology* (Vol. 9, Number 7, pp. 1–45). MDPI AG. https://doi.org/10.3390/biology9070180

Funato, H., Miyoshi, C., Fujiyama, T., Kanda, T., Sato, M., Wang, Z., Ma, J., Nakane, S., Tomita, J., Ikkyu, A., Kakizaki, M., Hotta-Hirashima, N., Kanno, S., Komiya, H., Asano, F., Honda, T., Kim, S. J., Harano, K., Muramoto, H., … Yanagisawa, M. (2016). Forward-genetics analysis of sleep in randomly mutagenized mice. *Nature*, *539*(7629), 378–383. https://doi.org/10.1038/nature20142

Gooley, J. J. (2008). Treatment of circadian rhythm sleep disorders with light. *Annals of the Academy of Medicine, Singapore*, *37*(8), 669–676.

Gorgoni, M., Ferlazzo, F., Moroni, F., D'Atri, A., Donarelli, S., Fanelli, S., Gizzi Torriglia, I., Lauri, G., Ferrara, M., Marzano, C., Rossini, P. M., Bramanti, P., & De Gennaro, L. (2014). Sleep Deprivation Affects Somatosensory Cortex Excitability as Tested Through Median Nerve Stimulation. *Brain Stimulation*, *7*(5), 732–739. https://doi.org/10.1016/j.brs.2014.04.006

Haghayegh, S., Liu, Y., Zhang, Y., Strohmaier, S., Papantoniou, K., Markt, S., Giovannucci, E., & Schernhammer, E. (2023). Rotating Night Shift Work and Bladder Cancer Risk in Women: Results of Two Prospective Cohort Studies. *International Journal of Environmental Research and Public Health*, *20*(3). https://doi.org/10.3390/ijerph20032202

Hankins, M. W., Peirson, S. N., & Foster, R. G. (2008). Melanopsin: an exciting photopigment. In *Trends in Neurosciences* (Vol. 31, Number 1, pp. 27–36). https://doi.org/10.1016/j.tins.2007.11.002

Hannibal, J. (2002). Neurotransmitters of the retino-hypothalamic tract. In *Cell and Tissue Research* (Vol. 309, Number 1, pp. 73–88). https://doi.org/10.1007/s00441-002-0574-3

Hardin, P. E., Hallt, J. C., & Rosbash, M. (1990). *Feedback of the Drosophila period gene product on circadian cycling of its messenger RNA levels*.

Hardin, P. E., Hallt, J. C., & Rosbash, M. (1992). Circadian oscillations in period gene mRNA levels are transcriptionally regulated (circadlan rhythms/transciptional control/Drosophila). In *Neurobiology* (Vol. 89). https://www.pnas.org

Hashimoto, Y. K., Satoh, T., Okamoto, M., & Takemori, H. (2008). Importance of autophosphorylation at Ser186 in the a-loop of salt inducible kinase 1 for its sustained kinase activity. *Journal of Cellular Biochemistry*, *104*(5), 1724–1739. https://doi.org/10.1002/jcb.21737

Hastings, M. H., Maywood, E. S., & Brancaccio, M. (2018). Generation of circadian rhythms in the suprachiasmatic nucleus. In *Nature Reviews Neuroscience* (Vol. 19, Number 8, pp. 453–469). Nature Publishing Group. https://doi.org/10.1038/s41583-018-0026-z

Hawley, S. A., Boudeau, J., Reid, J. L., Mustard, K. J., Udd, L., Mäkelä, T. P., Alessi, D. R., & Hardie, G. (2003). *Complexes between the LKB1 tumor suppressor, STRAD / and MO25 / are upstream kinases in the AMP-activated protein kinase cascade*. http://jbiol.com/content/2/4/28

Hawley, S. A., Pan, D. A., Mustard, K. J., Ross, L., Bain, J., Edelman, A. M., Frenguelli, B. G., & Hardie, D. G. (2005). Calmodulin-dependent protein kinase kinase-β is an alternative upstream kinase for AMP-activated protein kinase. *Cell Metabolism*, *2*(1), 9–19. https://doi.org/10.1016/j.cmet.2005.05.009

Hayasaka, N., Hirano, A., Miyoshi, Y., Tokuda, I. T., Yoshitane, H., Matsuda, J., & Fukada, Y. (2017). Salt-inducible kinase 3 regulates the mammalian circadian clock by destabilizing PER2 protein. *ELife*, *6*. https://doi.org/10.7554/eLife.24779

Hayter, E. A., Wehrens, S. M. T., Van Dongen, H. P. A., Stangherlin, A., Gaddameedhi, S., Crooks, E., Barron, N. J., Venetucci, L. A., Neill, J. S. O., Brown, T. M., Skene, D. J., Trafford, A. W., & Bechtold, D. A. (2021). Distinct circadian mechanisms govern cardiac rhythms and susceptibility to arrhythmia. *Nature Communications*, *12*(1). https://doi.org/10.1038/s41467-021-22788-8

Hitrec, T., Petit, C., Cryer, E., Muir, C., Tal, N., Fustin, J. M., Hughes, A. T. L., & Piggins, H. D. (2023). Timed exercise stabilizes behavioural rhythms but not molecular programs in the brain's suprachiasmatic clock. *IScience*, *26*(2). https://doi.org/10.1016/j.isci.2023.106002

Hollstein, P. E., Eichner, L. J., Brun, S. N., Kamireddy, A., Svensson, R. U., Vera, L. I., Ross, D. S., Rymoff, T. J., Hutchins, A., Galvez, H. M., Williams, A. E., Shokhirev, M. N., Screaton, R. A., Berdeaux, R., & Shaw, R. J. (2019). The AMPK-related kinases SIK1 and SIK3 mediate key tumor-suppressive effects of LKB1 in NSCLC. *Cancer Discovery*, *9*(11), 1606–1627. https://doi.org/10.1158/2159-8290.CD-18-1261

Honma, S., Ono, D., Suzuki, Y., Inagaki, N., Yoshikawa, T., Nakamura, W., & Honma, K. I. (2012). Suprachiasmatic nucleus: Cellular clocks and networks. In *Progress in Brain Research* (Vol. 199, pp. 129–141). Elsevier B.V. https://doi.org/10.1016/B978-0-444-59427-3.00029-0

Honma, S., Shirakawa, T., Katsuno, Y., Namihira, M., & Honma, K.-I. (1998). Circadian periods of single suprachiasmatic neurons in rats. In *Neuroscience Letters* (Vol. 250).
Horike, N., Takemori, H., Katoh, Y., Doi, J., Min, L., Asano, T., Sun, X. J., Yamamoto, H., Kasayama, S., Muraoka, M., Nonaka, Y., & Okamoto, M. (2003). Adipose-specific expression, phosphorylation of Ser794 in insulin receptor substrate-1, and activation in diabetic animals of salt-inducible kinase-2. *Journal of Biological Chemistry*, *278*(20), 18440–18447. https://doi.org/10.1074/jbc.M211770200
Horst, G. T. J. van der, Muijtjens, M., Kobayashi, K., Takano, R., Kanno, S., Takao, M., Wit, J. de, Verkerk, A., Eker, A. P. M., Leenen, D. van, Buijs, R., Bootsma, D., Hoeijmakers, J. H. J., & Yasui, A. (1999). Mammalian Cry1 and Cry2 are essential for maintenance of circadian rhythms. *Nature*, *398*(6728), 627–630. https://doi.org/10.1038/19323
Huang, L., Zhu, W., Li, N., Zhang, B., Dai, W., Li, S., & Xu, H. (2024). Functions and mechanisms of adenosine and its receptors in sleep regulation. In *Sleep Medicine* (Vol. 115, pp. 210–217). Elsevier B.V. https://doi.org/10.1016/j.sleep.2024.02.012
Huang, Y., Zhang, Y., & Braun, R. (2023). A minimal model of peripheral clocks reveals differential circadian re-entrainment in aging. *Chaos*, *33*(9). https://doi.org/10.1063/5.0157524
Hughes, A. T. L., Samuels, R. E., Baño-Otálora, B., Belle, M. D. C., Wegner, S., Guilding, C., Northeast, R. C., Loudon, A. S. I., Gigg, J., & Piggins, H. D. (2021). Timed daily exercise remodels circadian rhythms in mice. *Communications Biology*, *4*(1). https://doi.org/10.1038/s42003-021-02239-2
Hughes, S., Jagannath, A., Rodgers, J., Hankins, M. W., Peirson, S. N., & Foster, R. G. (2016). Signalling by melanopsin (OPN4) expressing photosensitive retinal ganglion cells. *Eye (London, England)*, *30*(2), 247–254. https://doi.org/10.1038/eye.2015.264
Ishida, A., Mutoh, T., Ueyama, T., Bando, H., Masubuchi, S., Nakahara, D., Tsujimoto, G., & Okamura, H. (2005). Light activates the adrenal gland: Timing of gene expression and glucocorticoid release. *Cell Metabolism*, *2*(5), 297–307. https://doi.org/10.1016/j.cmet.2005.09.009
Jagannath, A., Butler, R., Godinho, S. I. H., Couch, Y., Brown, L. A., Vasudevan, S. R., Flanagan, K. C., Anthony, D., Churchill, G. C., Wood, M. J. A., Steiner, G., Ebeling, M., Hossbach, M., Wettstein, J. G., Duffield, G. E., Gatti, S., Hankins, M. W., Foster, R. G., & Peirson, S. N. (2013). The CRTC1-SIK1 pathway regulates entrainment of the circadian clock. *Cell*, *154*(5). https://doi.org/10.1016/j.cell.2013.08.004
Jagannath, A., Taylor, L., Ru, Y., Wakaf, Z., Akpobaro, K., Vasudevan, S., & Foster, R. G. (2023). THE MULTIPLE ROLES OF SALT-INDUCIBLE KINASES IN REGULATING PHYSIOLOGY. In *Physiological Reviews* (Vol. 103, Number 3, pp. 2231–2269). American Physiological Society. https://doi.org/10.1152/physrev.00023.2022
Jaleel, M., Villa, F., Deak, M., Toth, R., Prescott, A. R., Van Aalten, D. M. F., & Alessi, D. R. (2006). The ubiquitin-associated domain of AMPK-related kinases regulates conformation and LKB1-mediated phosphorylation and activation. *Biochemical Journal*, *394*(3), 545–555. https://doi.org/10.1042/BJ20051844
Jiang, B., Wang, H., Wang, J.-L., Wang, Y.-J., Zhu, Q., Wang, C.-N., Song, L., Gao, T.-T., Wang, Y., Meng, G.-L., Wu, F., Ling, Y., Zhang, W., & Li, J.-X. (2019). Hippocampal Salt-Inducible Kinase 2 Plays a Role in Depression via the CREB-Regulated Transcription Coactivator 1–cAMP Response Element Binding–Brain-Derived

Neurotrophic Factor Pathway. *Biological Psychiatry*, *85*(8), 650–666. https://doi.org/10.1016/j.biopsych.2018.10.004
Joiner, W. J. (2016). Unraveling the Evolutionary Determinants of Sleep. In *Current Biology* (Vol. 26, Number 20, pp. R1073–R1087). Cell Press. https://doi.org/10.1016/j.cub.2016.08.068
Kang, J. E., Lim, M. M., Bateman, R. J., Lee, J. J., Smyth, L. P., Cirrito, J. R., Fujiki, N., Nishino, S., & Holtzman, D. M. (2009). Amyloid-β dynamics are regulated by orexin and the sleep-wake cycle. *Science*, *326*(5955), 1005–1007. https://doi.org/10.1126/science.1180962
Katoh, Y., Takemori, H., Horike, N., Doi, J., Muraoka, M., Min, L., & Okamoto, M. (2004). Salt-inducible kinase (SIK) isoforms: Their involvement in steroidogenesis and adipogenesis. *Molecular and Cellular Endocrinology*, *217*(1–2), 109–112. https://doi.org/10.1016/j.mce.2003.10.016
Katoh, Y., Takemori, H., Lin, X. Z., Tamura, M., Muraoka, M., Satoh, T., Tsuchiya, Y., Min, L., Doi, J., Miyauchi, A., Witters, L. A., Nakamura, H., & Okamoto, M. (2006). Silencing the constitutive active transcription factor CREB by the LKB1-SIK signaling cascade. *FEBS Journal*, *273*(12), 2730–2748. https://doi.org/10.1111/j.1742-4658.2006.05291.x
Kaufmann, S. H. E., & Ladel, C. H. (1994). Application of knockout mice to the experimental analysis of infections with bacteria and protozoa. *Trends in Microbiology*, *2*(7), 235–242. https://doi.org/10.1016/0966-842X(94)90628-9
Kilduff, T. S., Cauli, B., & Gerashchenko, D. (2011). Activation of cortical interneurons during sleep: an anatomical link to homeostatic sleep regulation? *Trends in Neurosciences*, *34*(1), 10–19. https://doi.org/10.1016/j.tins.2010.09.005
Kim, S. J., Hotta-Hirashima, N., Asano, F., Kitazono, T., Iwasaki, K., Nakata, S., Komiya, H., Asama, N., Matsuoka, T., Fujiyama, T., Ikkyu, A., Kakizaki, M., Kanno, S., Choi, J., Kumar, D., Tsukamoto, T., Elhosainy, A., Mizuno, S., Miyazaki, S., … Funato, H. (2022). Kinase signalling in excitatory neurons regulates sleep quantity and depth. *Nature*, *612*(7940), 512–518. https://doi.org/10.1038/s41586-022-05450-1
Kim, Y., Choi, J. Y., Petrovskiy, E., & Lee, W. (2025). Association between shift work and brain age gap: a neuroimaging study using MRI-based brain age prediction algorithms. *Frontiers in Aging Neuroscience*, *17*. https://doi.org/10.3389/fnagi.2025.1650497
Koike, N., Yoo, S.-H., Huang, H.-C., Kumar, V., Lee, C., Kim, T.-K., & Takahashi, J. S. (2012). Transcriptional Architecture and Chromatin Landscape of the Core Circadian Clock in Mammals. *Science*. https://www.science.org
Koo, S. H., Flechner, L., Qi, L., Zhang, X., Screaton, R. A., Jeffries, S., Hedrick, S., Xu, W., Boussouar, F., Brindle, P., Takemori, H., & Montminy, M. (2005). The CREB coactivator TORC2 is a key regulator of fasting glucose metabolism. *Nature*, *437*(7062), 1109–1114. https://doi.org/10.1038/nature03967
Lee, C., Etchegaray, J.-P., Cagampang, F. R. A., Loudon, A. S. I., & Reppert, S. M. (2001). Posttranslational Mechanisms Regulate the Mammalian Circadian Clock. *Cell*, *107*(7), 855–867. https://doi.org/10.1016/S0092-8674(01)00610-9
Lee, K.-W., Yang, C.-C., Chen, C.-H., Hung, C.-H., & Chuang, H.-Y. (2023). Shift work is significantly and positively associated with dementia: A meta-analysis study. *Frontiers in Public Health*, *11*, 998464. https://doi.org/10.3389/fpubh.2023.998464

Legates, T. A., Fernandez, D. C., & Hattar, S. (2014). Light as a central modulator of circadian rhythms, sleep and affect. In *Nature Reviews Neuroscience* (Vol. 15, Number 7, pp. 443–454). Nature Publishing Group. https://doi.org/10.1038/nrn3743

Li, Y., & Androulakis, I. P. (2021). Light entrainment of the SCN circadian clock and implications for personalized alterations of corticosterone rhythms in shift work and jet lag. *Scientific Reports*, *11*(1). https://doi.org/10.1038/s41598-021-97019-7

Lin, X.-Z., Takemori, H., Katoh, Y., Doi, J., Horike, N., Makino, A., Nonaka, Y., & Okamoto, M. (2001). *Salt-Inducible Kinase Is Involved in the ACTH/ cAMP-Dependent Protein Kinase Signaling in Y1 Mouse Adrenocortical Tumor Cells*. https://academic.oup.com/mend/article/15/8/1264/2748004

Lizcano, J. M., Göransson, O., Toth, R., Deak, M., Morrice, N. A., Boudeau, J., Hawley, S. A., Udd, L., Mäkelä, T. P., Hardie, D. G., & Alessi, D. R. (2004). LKB1 is a master kinase that activates 13 kinases of the AMPK subfamily, including MARK/PAR-1. *EMBO Journal*, *23*(4), 833–843. https://doi.org/10.1038/sj.emboj.7600110

Lucey, B. P., Hicks, T. J., McLeland, J. S., Toedebusch, C. D., Boyd, J., Elbert, D. L., Patterson, B. W., Baty, J., Morris, J. C., Ovod, V., Mawuenyega, K. G., & Bateman, R. J. (n.d.). *Effect of Sleep on Overnight Cerebrospinal Fluid Amyloid b Kinetics Subjects and Methods Participants and Sleep Interventions*. https://doi.org/10.1002/ana

Lupi, D., Oster, H., Thompson, S., & Foster, R. G. (2008). The acute light-induction of sleep is mediated by OPN4-based photoreception. *Nature Neuroscience*, *11*(9), 1068–1073. https://doi.org/10.1038/nn.2179

Massimini, M., Ferrarelli, F., Huber, R., Esser, S. K., Singh, H., & Tononi, G. (2005). Breakdown of Cortical Effective Connectivity During Sleep. *Science*, *309*(5744), 2228–2232. https://doi.org/10.1126/science.1117256

Mikhail, C., Vaucher, A., Jimenez, S., & Tafti, M. (2017). ERK signaling pathway regulates sleep duration through activity-induced gene expression during wakefulness. *Science Signaling*, *10*(463). https://doi.org/10.1126/scisignal.aai9219

Milburn, C. C., Boudeau, J., Deak, M., Alessi, D. R., & van Aalten, D. M. F. (2004). Crystal structure of MO25α in complex with the C terminus of the pseudo kinase STE20-related adaptor. *Nature Structural & Molecular Biology*, *11*(2), 193–200. https://doi.org/10.1038/nsmb716

Moore, R. Y., & Eichler, V. B. (1972). Loss of a circadian adrenal corticosterone rhythm following suprachiasmatic lesions in the rat. *Brain Research*, *42*(1), 201–206. https://doi.org/10.1016/0006-8993(72)90054-6

Morikawa, Y., Nakagawa, H., Miura, K., Soyama, Y., Ishizaki, M., Kido, T., Naruse, Y., Suwazono, Y., & Nogawa, K. (2007). Effect of shift work on body mass index and metabolic parameters. *Scandinavian Journal of Work, Environment and Health*, *33*(1), 45–50. https://doi.org/10.5271/sjweh.1063

Morrison, E. H., & Ma, M. A. (2026). *Neuroanatomy, Nucleus Suprachiasmatic.* . StatPearls Publishing.

Mukherji, A., Kobiita, A., Damara, M., Misra, N., Meziane, H., Champy, M. F., & Chambon, P. (2015). Shifting eating to the circadian rest phase misaligns the peripheral clocks with the master SCN clock and leads to a metabolic syndrome. *Proceedings of the National Academy of Sciences of the United States of America*, *112*(48), E6691–E6698. https://doi.org/10.1073/pnas.1519807112

Mumby, M., & Brekken, D. (2005). Phosphoproteomics: New insights into cellular signaling. *Genome Biology*, *6*(9), 230. https://doi.org/10.1186/gb-2005-6-9-230
Nader, N., Chrousos, G. P., & Kino, T. (2010). Interactions of the circadian CLOCK system and the HPA axis. In *Trends in Endocrinology and Metabolism* (Vol. 21, Number 5, pp. 277–286). https://doi.org/10.1016/j.tem.2009.12.011
Nelson, R. J. (1997). The Use of Genetic '"Knockout"' Mice in Behavioural Endocrinology Research The genetic instructions for each individual are con. In *Hormones and Behavior* (Vol. 31). Article No. HB971381.
Noguchi, T., Leise, T. L., Kingsbury, N. J., Diemer, T., Wang, L. L., Henson, M. A., & Welsh, D. K. (2017). Calcium circadian rhythmicity in the suprachiasmatic nucleus: Cell autonomy and network modulation. *ENeuro*, *4*(4). https://doi.org/10.1523/ENEURO.0160-17.2017
Nonaka, M., Kim, R., Fukushima, H., Sasaki, K., Suzuki, K., Okamura, M., Ishii, Y., Kawashima, T., Kamijo, S., Takemoto-Kimura, S., Okuno, H., Kida, S., & Bito, H. (2014). Region-Specific Activation of CRTC1-CREB Signaling Mediates Long-Term Fear Memory. *Neuron*, *84*(1), 92–106. https://doi.org/10.1016/j.neuron.2014.08.049
Noya, S. B., Colameo, D., Brüning, F., Spinnler, A., Mircsof, D., Opitz, L., Mann, M., Tyagarajan, S. K., Robles, M. S., & Brown, S. A. (2019). The forebrain synaptic transcriptome is organized by clocks but its proteome is driven by sleep. *Science*, *366*(6462). https://doi.org/10.1126/science.aav2642
Obrietan, K., Impey, S., Smith, D., Athos, J., & Storm, D. R. (1999). *Circadian Regulation of cAMP Response Element-mediated Gene Expression in the Suprachiasmatic Nuclei**. http://www.jbc.org
Ode, K. L., & Ueda, H. R. (2020). Phosphorylation Hypothesis of Sleep. In *Frontiers in Psychology* (Vol. 11). Frontiers Media S.A. https://doi.org/10.3389/fpsyg.2020.575328
Okamoto, M., Takemori, H., & Katoh, Y. (2004). Salt-inducible kinase in steroidogenesis and adipogenesis. In *Trends in Endocrinology and Metabolism* (Vol. 15, Number 1, pp. 21–26). Elsevier Inc. https://doi.org/10.1016/j.tem.2003.11.002
Okawa, M., Uchiyama, M., Ozaki, S., Shibui, K., Kamei, Y., Hayakawa, T., & Urata, J. (1998). Melatonin treatment for circadian rhythm sleep disorders. *Psychiatry and Clinical Neurosciences*, *52*(2), 259–260. https://doi.org/10.1111/j.1440-1819.1998.tb01063.x
Ono, D., Honma, K. I., & Honma, S. (2021a). Roles of Neuropeptides, VIP and AVP, in the Mammalian Central Circadian Clock. In *Frontiers in Neuroscience* (Vol. 15). Frontiers Media S.A. https://doi.org/10.3389/fnins.2021.650154
Ono, D., Honma, K. ichi, & Honma, S. (2021b). GABAergic mechanisms in the suprachiasmatic nucleus that influence circadian rhythm. In *Journal of Neurochemistry* (Vol. 157, Number 1, pp. 31–41). Blackwell Publishing Ltd. https://doi.org/10.1111/jnc.15012
Peña, J. L., Pérez-Perera, L., Bouvier, M., & Velluti, R. A. (1999). Sleep and wakefulness modulation of the neuronal firing in the auditory cortex of the guinea pig. *Brain Research*, *816*(2), 463–470. https://doi.org/10.1016/S0006-8993(98)01194-9
Ralph, M. R., Foster, R. G., Davis, F. C., & Menaker, M. (1990). Transplanted Suprachiasmatic Nucleus Determines Circadian Period. *Science*, *247*(4945), 975–978. https://doi.org/10.1126/science.2305266

Reid, M. R., Sattler, N. J., & Dooley, J. C. (2026). Motor cortex activity during sleep and wake movements sharpens across development but continues to lag the red nucleus. *Scientific Reports*, *16*(1), 12872. https://doi.org/10.1038/s41598-026-41754-2

Reghunandanan, V. (2024). Functional interactions between neurotransmitters and neuropeptides in regulating suprachiasmatic nucleus function and circadian rhythms. *Exploration of Neuroscience*, *3*(5), 434–477. https://doi.org/10.37349/en.2024.00059

Reghunandanan, V., & Reghunandanan, R. (2006). Neurotransmitters of the suprachiasmatic nuclei. In *Journal of Circadian Rhythms* (Vol. 4). https://doi.org/10.1186/1740-3391-4-2

Reppert, S. M., & Weaver, D. R. (2002). *Coordination of circadian timing in mammals*. www.nature.com/nature

Rivera-izquierdo, M., Martínez-ruiz, V., Castillo-ruiz, E. M., Manzaneda-navío, M., Pérez-gómez, B., & Jiménez-moleón, J. J. (2020). Shift work and prostate cancer: An updated systematic review and meta-analysis. In *International Journal of Environmental Research and Public Health* (Vol. 17, Number 4). MDPI AG. https://doi.org/10.3390/ijerph17041345

Robles, M. S., Cox, J., & Mann, M. (2014). In-Vivo Quantitative Proteomics Reveals a Key Contribution of Post-Transcriptional Mechanisms to the Circadian Regulation of Liver Metabolism. *PLoS Genetics*, *10*(1). https://doi.org/10.1371/journal.pgen.1004047

Robles, M. S., Humphrey, S. J., & Mann, M. (2017). Phosphorylation Is a Central Mechanism for Circadian Control of Metabolism and Physiology. *Cell Metabolism*, *25*(1), 118–127. https://doi.org/10.1016/j.cmet.2016.10.004

Rothman, S. M., Herdener, N., Frankola, K. A., Mughal, M. R., & Mattson, M. P. (2013). Chronic mild sleep restriction accentuates contextual memory impairments, and accumulations of cortical Aβ and pTau in a mouse model of Alzheimer's disease. *Brain Research*, *1529*, 200–208. https://doi.org/10.1016/j.brainres.2013.07.010

Ruiz, J. C., Conlon, F. L., & Robertson, E. J. (1994). Identification of novel protein kinases expressed in the myocardium of the developing mouse heart. In *Mechanisms of Development* (Vol. 48).

Rusak, B., & Bina, K. G. (1990). Neurotransmitters in the Mammalian Circadian System. *Annual Review of Neuroscience*, *13*(1), 387–401. https://doi.org/10.1146/annurev.ne.13.030190.002131

Sakai, T., Tamura, T., Kitamoto, T., & Kidokoro, Y. (2004). *A clock gene, period, plays a key role in long-term memory formation in Drosophila* (Vol. 101). https://www.pnas.org

Sakamoto, K., Karelina, K., & Obrietan, K. (2011). CREB: A multifaceted regulator of neuronal plasticity and protection. In *Journal of Neurochemistry* (Vol. 116, Number 1, pp. 1–9). https://doi.org/10.1111/j.1471-4159.2010.07080.x

Sakamoto, K., Norona, F. E., Alzate-Correa, D., Scarberry, D., Hoyt, K. R., & Obrietan, K. (2013a). Clock and light regulation of the CREB coactivator CRTC1 in the suprachiasmatic circadian clock. *Journal of Neuroscience*, *33*(21), 9021–9027. https://doi.org/10.1523/JNEUROSCI.4202-12.2013

Sakamoto, K., Norona, F. E., Alzate-Correa, D., Scarberry, D., Hoyt, K. R., & Obrietan, K. (2013b). Clock and light regulation of the CREB coactivator CRTC1 in the suprachiasmatic circadian clock. *Journal of Neuroscience*, *33*(21), 9021–9027. https://doi.org/10.1523/JNEUROSCI.4202-12.2013

Saura, C. A., & Cardinaux, J. R. (2017). Emerging Roles of CREB-Regulated Transcription Coactivators in Brain Physiology and Pathology. In *Trends in Neurosciences* (Vol. 40, Number 12, pp. 720–733). Elsevier Ltd. https://doi.org/10.1016/j.tins.2017.10.002

Scammell, T. E., Arrigoni, E., & Lipton, J. O. (2017). Neural Circuitry of Wakefulness and Sleep. In *Neuron* (Vol. 93, Number 4, pp. 747–765). Cell Press. https://doi.org/10.1016/j.neuron.2017.01.014

Schernhammer, E. S., Feskanich, D., Liang, G., & Han, J. (2013). Rotating night-shiftwork and lung cancer risk among female nurses in the United States. *American Journal of Epidemiology*, *178*(9), 1434–1441. https://doi.org/10.1093/aje/kwt155

Schernhammer, E. S., Laden, F., Speizer, F. E., Willett, W. C., Hunter, D. J., Kawachi, I., & Colditz, G. A. (2001). Rotating night shifts and risk of breast cancer in women participating in the nurses' health study. *Journal of the National Cancer Institute*, *93*(20), 1563–1568. https://doi.org/10.1093/jnci/93.20.1563

Schwartz, D., & Gygi, S. P. (2005). An iterative statistical approach to the identification of protein phosphorylation motifs from large-scale data sets. *Nature Biotechnology*, *23*(11), 1391–1398. https://doi.org/10.1038/nbt1146

Screaton, R. A., Conkright, M. D., Katoh, Y., Best, J. L., Canettieri, G., Jeffries, S., Guzman, E., Niessen, S., Yates, J. R., Takemori, H., Okamoto, M., & Montminy, M. (2004). The CREB Coactivator TORC2 Functions as a Calcium- and cAMP-Sensitive Coincidence Detector. *Cell*, *119*(1), 61–74. https://doi.org/10.1016/j.cell.2004.09.015

Sehgal, A., Rothenfluh-Hilfiker, A., Hunter-Ensor, M., Chen, Y., Myers, M. P., & Young, M. W. (1995). Rhythmic Expression of *timeless* : A Basis for Promoting Circadian Cycles in *period* Gene Autoregulation. *Science*, *270*(5237), 808–810. https://doi.org/10.1126/science.270.5237.808

Shearman, L. P., Sriram, S., Weaver, D. R., Maywood, E. S., Chaves, I., Zheng, B., Kume, K., Lee, C. C., van der, G. T. J., Horst, Hastings, M. H., & Reppert, S. M. (2000). Interacting Molecular Loops in the Mammalian Circadian Clock. *Science*, *288*(5468), 1013–1019. https://doi.org/10.1126/science.288.5468.1013

Sjö Strö, M., Stenströ, K., Eneling, K., Zwiller, J., Katz, A. I., Takemori, H., & Bertorello, A. M. (2007). *SIK1 is part of a cell sodium-sensing network that regulates active sodium transport through a calcium-dependent process*. www.pnas.org/cgi/content/full/

Soltanzadeh, A., Eyvazlou, M., Mohammad-ghasemi, M., Sadeghi-Yarandi, M., Rahimkhani, M., Ghasemi, N., Bonyadi, M., & Sadeghi-Yarandi, M. (2024). Investigating the relationship between shift work schedule and blood and metabolic parameters: a 10-years retrospective cohort study. *Scientific Reports*, *14*(1). https://doi.org/10.1038/s41598-024-68378-8

Sonntag, T., Vaughan, J. M., & Montminy, M. (2018). 14-3-3 proteins mediate inhibitory effects of cAMP on salt-inducible kinases (SIKs). In *FEBS Journal* (Vol. 285, Number 3, pp. 467–480). Blackwell Publishing Ltd. https://doi.org/10.1111/febs.14351

Stewart, R., Akhmedov, D., Robb, C., Leiter, C., & Berdeaux, R. (2013). Regulation of SIK1 abundance and stability is critical for myogenesis. *Proceedings of the National Academy of Sciences*, *110*(1), 117–122. https://doi.org/10.1073/pnas.1212676110

Takahashi, J. S. (2017). Transcriptional architecture of the mammalian circadian clock. In *Nature Reviews Genetics* (Vol. 18, Number 3, pp. 164–179). Nature Publishing Group. https://doi.org/10.1038/nrg.2016.150

Takemori, H., Katoh, Y., Horike, N., Doi, J., & Okamoto, M. (2002). ACTH-induced nucleocytoplasmic translocation of salt-inducible kinase: Implication in the protein kinase A-activated gene transcription in mouse adrenocortical tumor cells. *Journal of Biological Chemistry*, *277*(44), 42334–42343. https://doi.org/10.1074/jbc.M204602200

Tatsuki, F., Sunagawa, G. A. A., Shi, S., Susaki, E. A. A., Yukinaga, H., Perrin, D., Sumiyama, K., Ukai-Tadenuma, M., Fujishima, H., Ohno, R. ichiro, Tone, D., Ode, K. L. L., Matsumoto, K., & Ueda, H. R. R. (2016). Involvement of Ca2+-Dependent Hyperpolarization in Sleep Duration in Mammals. *Neuron*, *90*(1), 70–85. https://doi.org/10.1016/j.neuron.2016.02.032

Taub, M., Springate, J. E., & Cutuli, F. (2010). Targeting of renal proximal tubule Na,K-ATPase by salt-inducible kinase. In *Biochemical and Biophysical Research Communications* (Vol. 393, Number 3, pp. 339–344). https://doi.org/10.1016/j.bbrc.2010.02.037

Tobler, I., Borbély, A. A., & Groos, G. (1983). The effect of sleep deprivation on sleep in rats with suprachiasmatic lesions. *Neuroscience Letters*, *42*(1), 49–54. https://doi.org/10.1016/0304-3940(83)90420-2

Tone, D., Ode, K. L., Zhang, Q., Fujishima, H., Yamada, R. G., Nagashima, Y., Matsumoto, K., Wen, Z., Yoshida, S. Y., Mitani, T. T., Arisato, Y., Ohno, R. I., Ukai-Tadenuma, M., Garçon, J. Y., Kaneko, M., Shi, S., Ukai, H., Miyamichi, K., Okada, T., … Ueda, H. R. (2022). Distinct phosphorylation states of mammalian CaMKIIβ control the induction and maintenance of sleep. *PLoS Biology*, *20*(10). https://doi.org/10.1371/journal.pbio.3001813

Tsuno, Y., & Mieda, M. (2024). Circadian rhythm mechanism in the suprachiasmatic nucleus and its relation to the olfactory system. In *Frontiers in Neural Circuits* (Vol. 18). Frontiers Media SA. https://doi.org/10.3389/fncir.2024.1385908

Tuft, C., Matar, E., Schrire, Z. M., Grunstein, R. R., Yee, B. J., & Hoyos, C. M. (2023). Current Insights into the Risks of Using Melatonin as a Treatment for Sleep Disorders in Older Adults. In *Clinical Interventions in Aging* (Vol. 18, pp. 49–59). Dove Medical Press Ltd. https://doi.org/10.2147/CIA.S361519

Vanderheyden, W. M., Gerstner, J. R., Tanenhaus, A., Yin, J. C., & Shaw, P. J. (2013). ERK phosphorylation regulates sleep and plasticity in Drosophila. *PLoS ONE*, *8*(11). https://doi.org/10.1371/journal.pone.0081554

Vyazovskiy, V. V., Cirelli, C., Pfister-Genskow, M., Faraguna, U., & Tononi, G. (2008). Molecular and electrophysiological evidence for net synaptic potentiation in wake and depression in sleep. *Nature Neuroscience*, *11*(2), 200–208. https://doi.org/10.1038/nn2035

Vyazovskiy, V. V., & Faraguna, U. (2014). *Sleep and Synaptic Homeostasis* (pp. 91–121). https://doi.org/10.1007/7854_2014_301

Vyazovskiy, V. V., Olcese, U., Lazimy, Y. M., Faraguna, U., Esser, S. K., Williams, J. C., Cirelli, C., & Tononi, G. (2009). Cortical Firing and Sleep Homeostasis. *Neuron*, *63*(6), 865–878. https://doi.org/10.1016/j.neuron.2009.08.024

Walkinshaw, D. R., Weist, R., Kim, G. W., You, L., Xiao, L., Nie, J., Li, C. S., Zhao, S., Xu, M., & Yang, X. J. (2013). The tumor suppressor kinase LKB1 activates the downstream kinases SIK2 and SIK3 to stimulate nuclear export of class IIa histone deacetylases. *Journal of Biological Chemistry*, *288*(13), 9345–9362. https://doi.org/10.1074/jbc.M113.456996

Wang, Z., Ma, J., Miyoshi, C., Li, Y., Sato, M., Ogawa, Y., Lou, T., Ma, C., Gao, X., Lee, C., Fujiyama, T., Yang, X., Zhou, S., Hotta-Hirashima, N., Klewe-Nebenius, D., Ikkyu, A., Kakizaki, M., Kanno, S., Cao, L., … Liu, Q. (2018). Quantitative phosphoproteomic analysis of the molecular substrates of sleep need. *Nature*, *558*(7710), 435–439. https://doi.org/10.1038/s41586-018-0218-8

Wang, Z.-N., Takemori, H., Halder, S. K., Nonaka, Y., & Okamoto, M. (n.d.). *Cloning of a novel kinase (SIK) of the SNF1/AMPK family from high salt diet-treated rat adrenal 1*.

Wegner, S., Belle, M. D. C., Chang, P. S., Hughes, A. T. L., Conibear, A. E., Muir, C., Samuels, R. E., & Piggins, H. D. (2024). Loss of neuropeptide signalling alters temporal expression of mouse suprachiasmatic neuronal state and excitability. *European Journal of Neuroscience*, *60*(11), 6617–6633. https://doi.org/10.1111/ejn.16590

Welton, T., Teo, T. W. J., Saffari, S. E., Chan, L. L., & Tan, E. K. (2025). Shift work is associated with selective brain volume loss: a longitudinal study. *NeuroImage*, *324*. https://doi.org/10.1016/j.neuroimage.2025.121619

Wong, R. O. L., & Ghosh, A. (2002). Activity-dependent regulation of dendritic growth and patterning. *Nature Reviews Neuroscience*, *3*(10), 803–812. https://doi.org/10.1038/nrn941

Xue, L., Geahlen, R. L., & Andy Tao, W. (2013). Identification of direct tyrosine kinase substrates based on protein kinase assay-linked phosphoproteomics. *Molecular and Cellular Proteomics*, *12*(10), 2969–2980. https://doi.org/10.1074/mcp.O113.027722

Xue, L., Wang, W.-H., Iliuk, A., Hu, L., Galan, J. A., Yu, S., Hans, M., Geahlen, R. L., & Tao, W. A. (n.d.). *Sensitive kinase assay linked with phosphoproteomics for identifying direct kinase substrates*. https://doi.org/10.1073/pnas.1119418109/-/DCSupplemental

Yang, G., Lai, C. S. W., Cichon, J., Ma, L., Li, W., & Gan, W.-B. (2014). Sleep promotes branch-specific formation of dendritic spines after learning. *Science*, *344*(6188), 1173–1178. https://doi.org/10.1126/science.1249098

Yang, L., Gan, Y.-H., He, X.-Y., Deng, Y.-T., Zhang, W., You, J., Kuo, K., Zhang, Y.-R., Huang, S.-Y., Wu, B.-S., Guo, Y., Zhang, Y., Dong, Q., Feng, J.-F., Cheng, W., & Yu, J.-T. (2024). Shift work effects on incident neuropsychiatric disorders and shift work tolerance. *Journal of Affective Disorders*, *362*, 323–333. https://doi.org/10.1016/j.jad.2024.07.003

Yang, W., Shi, J., Li, C., Yang, J., Yu, J., Huang, J., & Rao, Y. (2025). Calcium/calmodulin-dependent protein kinase II α and β differentially regulate mammalian sleep. *Communications Biology*, *8*(1). https://doi.org/10.1038/s42003-024-07449-y

Yoon, H., & Choi, S. H. (2023). Technologies for sleep monitoring at home: wearables and nearables. *Biomedical Engineering Letters*, *13*(3), 313–327. https://doi.org/10.1007/s13534-023-0305-8

Zhou, J., Alfraidi, A., Zhang, S., Santiago-O'Farrill, J. M., Reddy, V. K. Y., Alsaadi, A., Ahmed, A. A., Yang, H., Liu, J., Mao, W., Wang, Y., Takemori, H., Vankayalapati, H., Lu, Z., & Bast, R. C. (2017). A novel compound ARN-3236 inhibits salt-inducible kinase 2 and sensitizes ovarian cancer cell lines and xenografts to paclitaxel. *Clinical Cancer Research*, *23*(8), 1945–1954. https://doi.org/10.1158/1078-0432.CCR-16-1562

Chapter 2: Materials and Methods

2.1 General Methods

2.1.1 Cell Culture

Cell and tissue culture techniques were carried out in Class II Biosafety Cabinets (BioMAT 2) under sterile conditions. All equipment was cleaned with 70% ethanol and high-level surface disinfectant (Chemgene). Cells were maintained in tissue culture (TC)-treated 25cm^2, 75cm^2, or 175cm^2 flasks (Greiner) at 37 °C and 5% CO2 in a multi-gas incubator (Panasonic). Transfections and luminescence assays were performed in clear-bottom 96-well and 384-well plates (Greiner).

HEK293 cells (ATCC), isolated from the kidney of a human embryo, were cultured in Dulbecco's Modified Eagle Medium (DMEM), high glucose (Gibco), with 10% Fetal Bovine Serum (FBS, Sigma) and 1% Penicillin/Streptomycin (P/S, Sigma). C6 cells (ATCC), glial cell line isolated from the brain of a rat with Glioma, were cultured in Ham's F-12 Nutrient Mixture (F-12, Gibco) with 10% FBS and 1% P/S. Cells were maintained at passage 3-30.

Once cells reached 80-90% confluency, cells were washed with Dulbecco's phosphate-buffered saline (DPBS), no calcium, no magnesium (Gibco) and lifted with TrypLe Express (Gibco). Cell pellets were diluted in DMEM or F-12. Cell counting was performed with Countess Automated Cell Counter (Invitrogen), supplemented with Trypan Blue and counting chamber slides. Cells were lastly either passaged or seeded for experiments.

2.1.2 Single-cell RNAseq analysis

Single-cell RNAseq (scRNAseq) analysis of SIKs was performed and adapted from Allen Brain Cell Atlas (Brain Knowledge Platform, Allen Institute). The dataset combines single-cell RNA-sequencing (scRNA-seq) of around 7 million cells and a spatial transcriptomic dataset of around 4.3 million cells using multiplexed error-robust fluorescence in situ hybridization (MERFISH) (Yao et al., 2023; M. Zhang et al., 2023). Gene expression of SIKs was adapted from the "MERFISH-C57BL6J-638850 with Imputed Genes + Reconstructed Coordinates" dataset in the coronal grid. Colour gradient corresponds to Log2(Counts per Million (CPM) +1), where the darkest regions have the highest CPM. Coronal slices containing the regions of interest were selected for visual representation. Cell type analysis was performed using the "10x scRNAseq whole brain", "Neurons", and "Non-Neuronal Cells" datasets.

2.1.3 Animals

Sik1$^{tm1.1Arte}$, Sik2$^{tm1.1Arte}$ and Sik3$^{tm1.1Arte}$ mouse models were generated as previously described (Darling et al., 2017). In these animal models, wild-type C57BL/6 mice were introduced via homologous recombination threonine-to-alanine mutations of LKB1 sites T182, T175 and T163 of *Sik1*, *Sik2* and *Sik3*, respectively. The models are described as kinase-inactive knock-in (KI) mice. Wildtype (WT) animals were age-matched controls in the same colony and both sexes were used. All procedures were performed following the UK Home Office Animals (Scientific Procedures) Act 1986 and the University of Oxford's Policy on the Use of Animals in Scientific Research (PPL 70/6382, PPL

8092CED3), as approved by the local Animal Care and Ethical Review committee (ACER).

2.1.4 Circadian wheel-running activity

SIK KI and WT animals were singly-housed with *ad libitum* access to food and water. Running wheels were placed inside the cages for animals to access. Circadian wheel-running activity was monitored under a 12-hour light/12-hour dark cycle (100 lux, 12:12 LD). Circadian cabinets with full ventilation, LED lighting, temperature and humidity sensors were used (Phenome Technologies, USA). Activity was recorded using the ClockLab data collection software (Actimetrics, USA) across multiple chambers simultaneously. ClockLab Chamber Control was used to continuously monitor light, humidity and temperature levels in the chambers.

2.1.5 Circadian wheel-running analysis

Recording of circadian activity was visualized and analyzed using ClockLab Analysis v.6 (Actimetrics, USA) on actograms across a 24-hour period. The height of the black activity bars is the number of wheel revolutions pulled into 1-minute bins. The actograms were plotted using a normalized scale where each day of the recording was scaled individually. Zero activity and the largest activity during the day were determined as minimum and maximum values for normalization. Light levels and LD cycle adjustments were overlaid with wheel-running activity on actograms. The onsets were detected automatically by the software first and adjusted manually for accuracy. Chi-

squared periodograms were plotted, and circadian period and amplitude measures were extracted. The activity profile was plotted as the average of activity across the selected period for non-parametric circadian rhythm analysis (NPRCA) such as interdaily stability (IS) and intradaily variability (IV). For activity analysis (bouts and counts), the measure was set to “Bouts”. Bouts were counted if they passed a threshold of 1 count/minute over 10 minutes. Bouts per minute, number of counts and counts per bout were exported for further analysis. For phase shifting, least-squares fitting was performed from the onsets of activity and extrapolated for five to seven days before (“Fit 1”) and after (“Fit 2”) the LD cycle shift. Phase shift is calculated as the difference between the two fits on the day selected, multiplied by 24 and divided by Tau.

2.1.6 EEG and EMG electrode implantation

To continuously monitor sleep/wake states, custom electroencephalogram (EEG) and electromyography (EMG) headmounts were implanted. Briefly, surgical procedures were conducted under aseptic conditions and isoflurane anaesthesia (2-3% for induction, 1-2% for maintenance), with animals head-fixed in a stereotactic frame (David Kopf Instruments, California). Analgesic was administered immediately before the start of surgery (Metacam 1–2 mg/kg s.c. and Vetergesic 0.08 mg/kg s.c.). Screw electrodes, mounted to an 8-pin surface mount connector (8415-SM, Pinnacle Technology Inc, Kansas), were implanted in the frontal (motor area, anteroposterior +2 mm, mediolateral 2 mm) and occipital (visual area, V1, anteroposterior −3.5 to −4 mm, mediolateral 2.5 mm) cortical areas and a reference electrode was implanted above the cerebellum. Two stainless-steel wires were implanted on each side of the nuchal muscle to record EMG

and the entire headmount was then fixed to the skull using RelyX Unicem 2 dental cement (3M, Bracknell, UK). Following surgery animals were provided with thermal support, administered saline (0.1 mL/20 g s.c.), and then closely monitored, with analgesia provided if necessary (Metacam 1-2 mg/kg orally), during a 2-week recovery period. For sleep state recording, animals were individually housed in custom clear plexiglass cages (20.3 × 32 × 35 cm) kept in ventilated, sound-attenuated Faraday chambers (Campden Instruments, Loughborough, UK), under a 12:12 LD cycle (100 lux) with ad libitum access to food and water.

2.1.7 Sleep processing and analysis

EEG and EMG acquired using the Multi-channel Neurophysiology Recording System (Tucker-Davis Technologies, Alachua, FL). The EEG and EMG signals were filtered between 0.1 and 100 Hz, amplified using a PZ5 NeuroDigitizer preamplifier (Tucker-Davis Technologies) and then collected at a sampling rate of 256.9 Hz. The EEG and EMG data were then resampled offline at 256 Hz, converted to .txt files using custom Matlab scripts and then converted to European data format (EDF) using Neurotraces software. Vigilance states were then assigned by manual inspection of consecutive 4 second epochs using the Sleepsign software (Kissei Comtec Co., Nagano, Japan). Vigilance states were classified as wake (low amplitude, high frequency EEG with associated EMG signal), non-rapid eye movement sleep (NREM – high amplitude, low frequency EEG signal with slow waves present) or REM sleep (low amplitude, high frequency theta EEG signal). Brief awakenings were defined as wake periods lasting only 4 epochs or less. Epochs that contained artefactual signals (resulting from

contamination by eating, drinking, or gross movement) were scored as such so that they could be excluded from the appropriate analyses. EEG power spectra were then produced using a Fast Fourier Transform routine for all 4-second epochs, with a 0.25-Hz resolution. Delta power (SWA) is calculated as the average spectral power between 0.5-4 Hz of all NREM epochs in the desired time bin and expressed as a percentage of the average spectral power between 0.5-4 Hz of all NREM epochs over the entire baseline day. Delta energy was calculated as the total delta spectral power summed across all NREM epochs within each bin. Additionally, the power spectrum from 0.5-30 Hz from NREM epochs was visualized.

2.1.8 Tissue collection

SIK KI and WT animals were housed under 12:12 LD and allowed to entrain fully. Tissue collection was performed at specified time points depending on individual experiments. Animals were sacrificed by cervical dislocation, and eyes were removed immediately to ensure intact slices. Whole brains were removed from the animals and placed into a brain matrix (1mm coronal, Kent Scientific). Two single-edge razor blades (VWR International) were positioned at Bregma -0.1mm and -1.10mm, 1mm caudal from each other. SCN punches were taken from the 1mm thick brain slice using a dermal punch (1.5mm, Miltex by Kai). Cortex punches were taken from the same 1mm slice to keep consistency. Brain punches were flash frozen on dry ice and stored at -80 °C for downstream processing.

2.1.9 SDS-PAGE gel electrophoresis and Immunoblot

20µg of protein sample was added to 1x Protein Sample Loading Buffer (LICORbio™), 1X β-mercaptoethanol and ddH_2O to make up 25µl of mixture in each PCR tube for each sample. Samples were denatured in a SimpliAmp Thermal Cycler (Fisher Scientific) at 95°C for 5 minutes. Denatured samples were loaded in Invitrogen Mini Gel Tank onto Novex Tris-Glycine Mini Protein Gels, 10-20%, 1mm (ThermoFisher Scientific). The tanks were filled with 1X Novex Tris-Glycine SDS Running Buffer (10X, ThermoFisher Scientific). The ladder used was PageRuler Plus Prestained Protein Ladder (10 – 250kDa). Gels were run for 25 minutes at 225V.

Gels were transferred onto 0.2µm PVDF membranes stacked in transfer filter stacks using a Trans-Blot Turbo Transfer System (Bio-Rad Laboratories) for 7 minutes at 25V (1.3A). The membranes were equilibrated with methanol until translucent before transfer. Membrane was incubated in Revert 520 Total Protein Stain for 5 minutes and washed with Revert Wash Solution three times (LICORbio™). The membrane was imaged on the Odyssey® Imager at 520nm. Revert Destaining Solution was used to destain the membrane before blocking and immunoblotting.

Membranes were incubated with Intercept TBS Blocking Buffer for 1 hour at room temperature with gentle shaking to block non-specific binding sites (LICORbio™). Primary and secondary antibodies were diluted in 50% (v/v) Blocking Buffer and 50% (v/v) TBST containing 0.3% Tween 20. Membranes were washed in between antibody incubations for 5 minutes, 3 times with TBST and gentle shaking. Membranes were

stored in TBS and imaged at respective wavelengths by Odyssey® Imager (LICORbio™). Analysis and quantification were performed with Empiria Studio software (LICORbio™).

2.1.10 Pro-KALIP Sample Preparation

For Pro-KALIP SCN and cortex punches, WT animals were used, and there was no specific time point for tissue collection.

1mg of SCN (equivalent to 20-25 SCN punches) and cortex brain tissue were lysed by adding 1mL of Urea lysis buffer (700mM Urea, 200mM Thiourea, 1mM DTT in 50mM Tris-HCl pH 7.5) and homogenized using a Dounce homogenizer (Sigma Aldrich, UK). Lysed tissue was centrifuged at 13,000 x g for 20 mins at 4°C. Protein concentration of clarified lysate was determined by a BCA protein assay kit (Thermo Fisher Scientific, Loughborough, UK). Clarified lysate was resuspended in 200µl of dephosphorylation complex containing 1x phosphatase buffer, thermosensitive phosphatase units at a ratio of 1 unit per 10µg of protein (rAPid Alkaline Phosphatase, Roche, UK) and 1x protease inhibitor (Roche, UK). The complex was incubated at 37°C overnight. The phosphatase was deactivated by heating to 75°C for 5 mins. Endogenous kinases were inhibited by treating dephosphorylated proteins with 1 mM 5′-(4-fluorosulfonylbenzoyl) adenosine (FSBA) with 10 % DMSO in Tris–HCl, pH 7.5 at 30 °C for 1h to mitigate any residual activity. Excess FSBA was removed by centrifugal filtration units (Amicon Ultra 30K device, Merck Millipore).

Filtered lysate was incubated with kinase buffer containing 5mM $MgCl_2$, 3mM ATP, 60nM SIK1 kinase, 0.5 µg/µl LKB1: STRADα: MO25α complex, 1x Halt Protease and Phosphatase Inhibitor Cocktail, and 50mM Tris-HCl pH7.5. Kinase buffer volume depended on the desired substrate concentration. The mixture was incubated at 30°C for 30 – 40 minutes. The reaction was quenched by 1% acetic acid to a pH<3 and kept at -80°C.

Another dephosphorylation and kinase reaction was prepared for the LKB1: STRADα: MO25α complex only control run. Small aliquots of lysate, dephosphorylation lysate and kinase reaction mixture were kept to run a Phospho-AMPK Substrate Motif immunoblot for validation.

Sample preparation for LC-MS was performed at Turku Bioscience Centre, University of Turku, by our collaborator, Dr. Otto Kauko. Samples were resuspended in 8M Urea in 100mM Tris-HCl, pH 8.0. Samples were sonicated with Bioruptor Plus with high power mode for 10 cycles (30 seconds ON, 30 seconds OFF) and reduced with 10mM D, L-dithiothreitol (DTT), and alkylated with 40 mM iodoacetamide. Urea concentration was diluted with 50mM Tris-HCl pH 8.0 to less than 1.6M. Samples were digested with sequencing-grade trypsin (5µg/sample; Promega) overnight. Samples were desalted with a Sep-Pak tC18 96-well plate (Waters). After drying, 5% was taken from each sample for total protein analysis and the rest underwent phosphopeptide enrichment using the High-Select Fe-NTA Phosphopeptide Enrichment Kit (ThermoFisher Scientific).

2.1.11 LC-MS Method and Raw Data Analysis

LC-MS and initial raw data processing were performed at Turku Bioscience Center as described above. The following processing protocol was provided by Dr. Otto Kauko. LC-MS was performed on a nanoflow HPLC system (Easy-nLC1200, Thermo Fisher Scientific) coupled to an Orbitrap Exploris 480 mass spectrometer (Thermo Fisher Scientific, Bremen, Germany) equipped with a FAIMS interface with compensation voltages of -40V and -60V. Peptides were first loaded on a trapping column and subsequently separated inline on a 15 cm C18 column (75 µm x 15 cm, ReproSil-Pur 3 µm 120 Å C18-AQ, Dr. Maisch HPLC GmbH, Ammerbuch-Entringen, Germany). The mobile phase consisted of water with 0.1% formic acid (solvent A) and acetonitrile/water (80:20 (v/v)) with 0.1% formic acid (solvent B). A 120 min gradient was used to elute peptides (in 62 min from 5 % to 21% min solvent B, in 48 min from 21% to 36% solvent B, and in 5 min from 36 to 100% solvent B followed by a 5 min wash stage with solvent B).

Samples were analyzed by Data Independent Acquisition (DIA) LC-MS method. Data was acquired automatically using Thermo Xcalibur 4.6 software (Thermo Fisher Scientific). Data was analyzed by Spectronaut software (Biognosys; version 19.2). The DirectDIA approach was used for protein identification and MaxLFQ was used to perform label-free quantifications. Local normalization was used, as described previously (Callister et al., 2006).

2.1.12 Kinase motif analysis

Initial screening of the Pro-KALIP phosphoproteomics was performed using PhosphoSitePlus v6.8.2 (Cell Signaling Technology). SIK kinase motif prediction was performed using The Kinase Library that integrates the newly characterized substrate specificities from the human Serine/Threonine (Ser/Thr) kinome (Johnson et al., 2023). Using FASTA sequences, motif conservation was detected and the mouse orthologs were mapped. Each phosphorylation site identified from the Pro-KALIP phosphoproteomics was put through the Kinase Prediction tool to identify the likely kinases responsible for the particular phosphorylation site using a developed open-source Python package (Phosphosite Plus v6.8.2). The kinases were ranked by percentile scores and raw motif compatibility. A SIK motif percentile score of 80% was used as a screening cut-off value for phosphorylation sites. Motif sequence logo was generated by WebLogo from FASTA sequences.

The Site Table tool was used to look at the total number of references for the identified substrate and phosphorylation site. High-throughput references (HTP) are the number of records in which the phosphorylation or modification sites are identified using proteomic discovery mass spectrometry. They were used to identify key upstream regulators. Low-throughput references (LTP) are the number of records in which the site was determined using other methods. They were used to identify downstream targets, pathways and functions.

2.1.13 Functional analysis and protein-protein interaction

Functional analysis was performed using g:GOSt of g:Profiler. From the input target gene lists, it provides data on functional evidence such as biological pathways, regulatory motifs and protein-protein interactions. The tool performs Fisher's one-tailed test to find over-represented pathways in the given list. The Gene Ontology (GO) was used to investigate functional relationships (Raudvere et al., 2019). Protein-protein interaction network and pathway enrichment were performed using STRING. The data originates from different sources, including automated text mining of the scientific literature, computational interaction predictions, and conserved genomic databases (Szklarczyk et al., 2023).

2.1.14 Data analysis and Statistics

Data visualization and statistical analysis were conducted on GraphPad Prism (Version 10.2.0 (335)) and RStudio (Version 2024.12.1+563). All data points are Mean ± SEM unless stated otherwise. Chi-squared test, t-tests and ANOVA analysis were used as post-hoc tests. p-value < 0.05 is considered statistically significant unless stated otherwise. The exact test used is mentioned in the corresponding figure legends. Transcriptomics and phosphoproteomics analysis including R packages and statistical cutoffs are stated in the chapter methods below.

2.2 Chapter 3 Methods

2.2.1 Antibodies

Phospho-AMPK Substrate Motif [LXRXX(pS/pT) MultiMab® Rabbit mAb (Cell Signaling #5759) at 1:1000.

Antibodies for the LKB1: STRADα: MO25α complex were acquired from MRC PPU Reagents and Services. GST-LKB1 Polyclonal (#S957A, mouse) at 1µg/mL, GST-STRAD alpha Polyclonal (#S535B, sheep) at 0.1ug/ml, GST-MO25 alpha Polyclonal (#S898A, sheep) at 1µg/mL overnight at 4°C.

Secondary antibodies used were: IRDye® 680RD Donkey anti-Rabbit (926-68073, Li-Cor), IRDye® 800CW Goat anti-Mouse (926-32210, Li-Cor) at 1:20,000 for 1 hour at room temperature and Alex Fluor™ 680 Donkey anti-Sheep IgG (H+L) Cross-Adsorbed Secondary Antibody (A-21102, Invitrogen) at 1:2000 for 1 hour at room temperature.

Revert™ 520 Total Protein Stain (926-10016, Li-Cor) was used for normalization control and quantification, providing improved accuracy over housekeeping protein.

2.2.2 Plasmid Concentration

Plasmid	**Concentration (µg/µl)**	**A260/A280**
GST-LKB1	0.973	1.9

FLAG-STRADα	2.35	1.9
Myc-MO25α	1.704	1.9
pcDNA3.2-Cx43-HA	0.279	1.9
pDEST/hCx43-EGFP-N1	0.940	1.89
pcDNA3.2-GJA1-S373A	3.884	1.92
SIK1-HA	2.014	1.93

2.2.3 Bacterial Transformation

The DNA constructs encoding wild-type GST-LKB1 in the pEBG2T vector (DU6182), FLAG-STRADα (DU2026) and Myc-MO25α (DU6173) in the pCMV vector were acquired from the MRC Protein Phosphorylation and Ubiquitylation Unit at the University of Dundee. 60-80ng of GST-tagged LKB1, FLAG-tagged STRADα, and Myc-tagged MO25α cDNA clones were added to NEB Stable Competent *E.coli* cells (C3040H, New England Biolabs) for high-efficiency transformation. The mixture was placed on ice for 30 minutes and heat-shocked at 42°C for 30 seconds. The mixture was then put on ice for another 5 minutes. 950ul of Stable Outgrowth Medium (S.O.C.) (Melford) was added to the mixture and was incubated at 37°C, 225rpm for 1 hour. For outgrowth, 1ml of the mixture was added to 10ml of Luria Broth (LB) Base (Invitrogen, U.K.) with 125µg/ml of ampicillin and inoculated at 37°C, 225rpm for 6-8 hours. 1ml of the outgrowth culture was then added to 100ml of LB broth with 125µg/ml of ampicillin and inoculated at 37°C, 225rpm for 12-16 hours to acquire a large batch for purification.

2.2.4 Plasmid Purification and Concentration

The overnight culture was pelleted by centrifugation at 3000 x g for 20 minutes at 4°C. Plasmids were purified using NucleoBond Xtra Midi EF and concentrated with NucleoBond Finalizers (Macherey-Nagel). The cell pellet was resuspended in 8ml of Resuspension Buffer (RES-EF) and lysed with 8ml of Lysis Buffer (LYS-EF). The mixture was neutralized with Neutralization Buffer (NEU-EF) and loaded into the equilibrated NucleoBond Xtra Column Filter. The column was washed three times with Filter Wash Buffer (FIL-EF), Wash Buffer (ENDO-EF) and Wash Buffer (WASH-EF), respectively. The plasmid DNA was eluted with 5ml of Elution Buffer (ELU-EF).

For additional desalting and concentration, 0.7 volumes of isopropanol were added to the 5ml eluate. The mixture was loaded into a 30ml syringe, attached with a NucleoBond Finalizer. The Finalizer was washed with endotoxin-free 70% ethanol and dried by pressing air through the Finalizer for over 10 times. The Finalizer was reattached to 1ml syringe and an appropriate amount of Redissolving Buffer TE-EF was added for elution. The eluate was loaded back into the syringe for a complete elution. Plasmid concentration and integrity were measured using a NanoDrop Spectrophotometer (Thermo Scientific).

2.2.5 Expression of LKB1: STRADα: MO25α complex in HEK293 cells using Calcium Phosphate Method

HEK293T cells were seeded to a confluency of 70-80% when ready for transfection. Media was changed to warmed DMEM + FBS – PenStrep media. T175 flasks of HEK293T cells were transiently transfected using the calcium phosphate method. The transfection complex is composed of 8.4µg of purified GST-tagged LKB1, FLAG-tagged STRADα, and Myc-tagged MO25α constructs each, 126µL of 2M $CaCl_2$, and H_2O to make up a total volume of 900µL. A 1:1 volume of HEPES was added to the complex on the vortex at mid speed. The full content was added drop by drop to pre-warmed flasks with HEK293T cells. Cells were incubated for 6-12 hours post-transfection and incubated with DMEM+FBS+PenStrep media for another 24- 36 hours at 37 °C.

2.2.6 Affinity purification of LKB1: STRADα: MO25α complex

The complex was affinity-purified using a modified version of the method previously described in Boudeau et al (Boudeau et al., 2003a). Cells were lysed in 1ml of ice-cold lysis buffer 36 hours post-transfection (50mM Tris/HCl pH 7.5, 1 mM EGTA, 1mM EDTA, 1% (w/v) Triton-X 100, 1mM sodium orthovanadate, 50mM sodium fluoride, 5mM sodium pyrophosphate, 0.27M sucrose, 0.1% (v/v) 2-mercaptoethanol and proteinase inhibitor cocktail). Cell lysates were centrifuged at 14,000 x g for 10 min at 4°C. To equilibrate the resin, 3-5mL of Glutathione agarose (Pierce Glutathione Agarose, Thermo Scientific, #16100) was centrifuged for 2 minutes at 700 x g and supernatant was discarded. 1 – 2 resin-bed volumes of wash buffer (50mM Tris/HCl pH 7.5, 1 mM

EGTA, 1mM EDTA, 1% (w/v) Triton-X 100, 1mM sodium orthovanadate, 50mM sodium fluoride, 5mM sodium pyrophosphate, 0.27M sucrose, 0.1% (v/v) 2-mercaptoethanol and proteinase inhibitor cocktail + 150mM NaCl) were added to resuspend the resin. The resin was centrifuged for 2 minutes at 700 x g and the supernatant was discarded. Clarified cell lysate (equivalent to ~40 million cells) was added to equilibrated resin and mixed on a shaker for 60 minutes at room temperature or at 4°C overnight. The mixture was centrifuged at 700 x g for 2 minutes, and the supernatant was discarded. The resin was washed with 5 resin-bed volumes of wash buffer and centrifuged at 700 x g for 2 minutes. The wash step was repeated up to four times. The GST-tagged trimer was eluted using 250- 500µL of elution buffer (50mM Tris/HCl pH 7.5, 10mM reduced glutathione, 1mM EGTA, 0.1% 2-mercaptoethanol, proteinase inhibitor cocktail, 0.05% Tween-20, adjusted to pH 8.0). The resin was centrifuged at 700 x g for 2 minutes and the elution step was repeated two times. The supernatant after each elution was saved in separate tubes. For immunoblotting analysis, affinity-purified trimer concentration was determined using Pierce BCA protein assay kit (Thermo Scientific #23225). The purified trimer was subsequently visualized on an immunoblot using respective antibodies.

2.2.7 Kinase Glo Luminescence Assay

SIK kinase activity was measured by Kinase-Glo Max Luminescence Kinase Assay (Promega, UK) using a 384-well plate. Final reaction volume was 20µl per well, a 1:1 ratio of reaction mixture and Kinase-Glo Reagent.

1µl of substrate, either AMARA peptide (#HY-P1576, MedChemExpress) or dephosphorylated brain sample, was added to each well. DMSO was used for solvent-only control wells. The reaction mixture contained 2.5x the optimal concentration of SIK1 kinase (#PV6445, Thermo Fisher Scientific) and 1x kinase reaction buffer (5mM $MgCl_2$ in 50mM Tris-HCl pH 7.5). The ATP mixture contained 2x the desired concentration of ATP (#R0441, Thermo Fisher Scientific) in 1x kinase reaction buffer. 1µg of purified LKB1: STRADα: MO25α complex was added to the designated wells. Kinase-Glo Reagent was added to each well after incubating for the optimal amount of time. The plate was mixed at room temperature on a shaker, and end-point luminescence was recorded using a standard plate reader. Kinase activity was measured as a unit of 1/Luminescence (RLU) and reported as technical replicates for each condition tested.

Conditions for the reaction were optimized with a series of Kinase Glo Assay. Optimal substrate and kinase concentrations were determined by performing twofold serial dilutions of dephosphorylated brain lysate and SIK kinase, respectively. Optimal kinase reaction time was determined using the linear range of the ATP-ADP luminescence curve over time.

SIK1 kinase concentration and volume were calculated using the formulae provided in the LanthaScreen Eu Kinase Binding Assay for SIK1 (Life Technologies). SIK1 Stock concentration used was 0.1mg/ml and the molecular weight is 60900 g/mol.

$$Stock\ kinase\ concentration\ (nM)$$

$$= \frac{stock\ concentration\ (mg/ml) * \ 1\ x\ 10^9\ (nmol/mol)}{Kinase\ molecular\ weight\ (g/mol)}$$

$$Kinase\ Volume\ (\mu L)\ = \frac{Total\ reaction\ volume\ (\mu L)\ *\ Final\ kinase\ concentration\ (nM)}{Stock\ kinase\ concentration\ (nM)}$$

2.2.8 Bacterial Stab Culture – Connexin-43 (CX43)

Bacterial stabs used for plasmid purification were as follows: pDEST/hCx43-EGFP-N1(Addgene #40907), pcDNA3.2-Cx43-HA (Addgene #49851), pcDNA3.2-GJA1-S373A (Addgene #52879). LB agar plates were acquired with appropriate antibiotics from the Department of Biochemistry, University of Oxford. A sterile pipette tip was used to transfer the bacteria from the stab culture and gently spread them over the appropriate selection plate. The plates were incubated at 37°C overnight. Single colonies were picked out and inoculated in 5mL of LB broth (Invitrogen, U.K.) at 37°C for 6-8 hours in a shaking incubator. For a larger culture, a 1:100 culture to LB Broth ratio was used. The large bacterial culture was incubated at 37°C overnight. Plasmids were purified using the methods in 2.2.4.

2.2.9 Viafect Transfections

C6 rat glioma cells were grown in T25 or T75 flasks to 75-80% confluent on the day of transfection. The media was switched to Ham's F12 Nutrient Mix without antibiotics 1 hour before transfection. Cells were digested and counted before plating. Reverse transfection was performed, where cells were plated with the transfection reagents at

the same time. For a 96-well plate, 100ng of total DNA per 10µl of serum-free medium, Optimem (Thermo Fisher, UK). Viafect Transfection Reagent (Promega, UK) was added at a 1:6 ratio of DNA to reagent. The transfection mixture was incubated for 15 minutes at room temperature. 10µl of transfection mixture was added to each well. 20,000 C6 cells were diluted in 100µl of Ham's F12 Nutrient Mix and added to each well. Control wells were transfected with GFP plasmids to monitor efficiency.

2.2.10 Extracellular ATP measurements

1-3 days post-transfection, GFP expression was checked using a fluorescence microscope to evaluate transfection efficiency. The wells were washed twice and replaced with 100µl of Hanks' Balanced Salt Solution (HBSS) (Ca^{2+}, Mg^{2+} free, no phenol red) (#14175095, ThermoFisher Scientific) with and without the determined concentration of Calcium Ionophore A23187 (C7522, Sigma Aldrich, UK) without disturbing the cells during the process. Cells were incubated at 37°C for 5 minutes. Media from all wells were transferred to a fresh 96-well plate and centrifuged briefly to avoid cell debris. A 1:1 ratio of extracellular media to ATPlite substrate solution (ATPlite 1step Luminescence Assay System, Revvity) was added to a 384-well plate. 20µl was used for these particular experiments. End-point luminescence was measured on a standard plate reader (BMG Optima).

2.2.11 Calcium Signalling Assay

GFP expression was checked one day post-transfection using a fluorescence microscope. Culture media was aspirated, and cells were washed twice with 200µl Hank's Balanced Salt Solution (HBSS) containing calcium (HBSS-Ca^{2+}). 100µl of assay buffer (4uM Fluo-4-AM (Life Technologies), 0.02% Pluronic F127) was added to each well. Cells were incubated at room temperature for 1h for dye loading. Cells were then incubated at 37°C for 30 mins for the intracellular esterase reaction. Assays buffer was aspirated and washed twice with HBSS-Ca^{2+}. Fresh 90µl of HBSS-Ca^{2+} was added to each well, and cells were incubated for 15 mins at room temperature to equilibrate.

Baseline fluorescence was measured on a plate reader (BMG Optima). The plate was measured bottom with a 485/520 excitation to emission filter. Baseline was recorded for 15-20 cycles per well (3s per cycle) and followed by the addition of 10µl of Calcium Ionophore A23187 (C7522, Sigma Aldrich, UK) or DMSO. Fluorescence was recorded for an additional 20-30 cycles to allow full visualization of the response curve. The final concentration of DMSO per well was 0.1% (v/v).

2.2.12 Cell Viability Assay

PrestoBlue HS Cell Viability Assay (Thermo Fisher, UK) was used to assess C6 cell viability after transfections. PrestoBlue HS was diluted 1:10 in Ham's F12 Nutrient Mix. Cells were incubated with 1x reagent for 10 minutes at 37°C. Wells with no cells were used as controls, and cell viability was normalized to untransfected control wells. Bottom-read luminescence was measured on a standard plate reader (BMG Optima).

PrestoBlue HS reagent was washed out from cells and subsequent assays were performed.

2.2.13 Time-Lapse Dye Uptake Assay

C6 rat glioma cells were grown and transfected with Viafect™ in 24-well plates. Prior to the assay, cells were washed twice with HBSS ($Ca^{2+,}$ Mg^{2+} free) and incubated with fresh HBSS during the assay. The plate was mounted on the stage of EVOS™ FL Auto 2 with EVOS™ Onstage Incubator and 4X objective. Cells were incubated with 5μM of DAPI Nucleic Acid Stain (1mg/ml, #62248, ThermoFisher Scientific) in HBSS media and imaged immediately. Time-lapse images were taken every 30 seconds, 5 minutes in total. Wells were imaged one at a time. Thresholds were kept consistent for all images. Background subtraction and fluorescent cell counting were performed and analyzed using ImageJ.

2.3 Chapter 4 Methods

2.3.1 Circadian wheel-running activity

SIK3 KI and WT animals (n=10-14 each) were singly housed with *ad libitum* access to food and water and a running wheel attached. Circadian wheel-running activity was monitored under 12 hour light/12 hour dark cycle (100 lux, 12:12 LD), constant darkness (DD) or constant light (100 lux, LL). White LED lights were used in the coffins as the light source. Activity was recorded using ClockLab (Actimetrics, USA). For each

condition, 7-10 days were recorded. Analysis was conducted on a stable window (roughly the middle 5 days) to ensure no carry-over circadian effects from the previous condition.

2.3.2 LD cycle advance protocol

SIK3 KI and WT animals (n=10-14 each) were singly housed and circadian activity was monitored under a 12:12 LD cycle (100 lux). The animals were allowed to entrain to the LD cycle. After stable entrainment, the light phase was advanced for six hours. Circadian wheel-running activity was monitored during re-entrainment until the animals were aligned with the new LD cycle. For analysis, onsets were allocated automatically by ClockLab Analysis 6 and adjusted manually. Phase differences were measured every other day from the LD cycle shift.

2.3.3 Light pulses and phase shifting

SIK3 KI and WT animals (n=10-14 each) were singly housed and circadian activity was monitored under a 12:12 LD cycle (100 lux). After stable entrainment to the LD cycle, animals were released into DD for 3-5 days. Subsequently, animals were exposed to 30-minute light pulses (30 lux), timed to cover all the CTs across the 24-hour period, plotting a photic phase response curve (PRC). A total of six light pulses were set and 7 days were left in between them. Per convention, phase delays are plotted as negative and phase advances as positive. The phase angles for the days prior to and after the light pulses were measured, and the differences were calculated. To observe

behavioural masking, the activity counts 30 minutes before and during the 30-minute light pulses were recorded. The photic PRC was plotted with 2nd order smoothing with three neighbors on each side.

2.3.4 Ultradian (T7) light-dark cycle

SIK3 KI and WT animals were singly housed and circadian activity was monitored. Animals were subjected to a 5-day ultradian cycle, which entails a 3.5-hour lights-on, 3.5-hour lights-off cycle (100 lux). The animals were released into DD after the T7 cycle to observe entrainment.

2.3.5 25hr entrainment and light advance

SIK3 KI and WT animals were singly housed and circadian activity was monitored under a 25-hour LD cycle (100 lux), which entails 12.5 hours lights-on, 12.5 hours lights-off. After stable entrainment to the non-24 hr LD cycle, the light phase was advanced by 6.25 hours. Circadian wheel-running activity was monitored during re-entrainment until they were aligned with the new LD cycle. The animals were released into DD afterward.

Light protocol	Light schedule	Duration
Entrainment	7am ON; 7pm OFF	10 days
6 hr light advance	12am ON; 12pm OFF	10 days
DD		1 weeks
Light pulses (every week; 6 times total)		7 weeks
25 hr entrainment		10 days
6.25 hr shift (light advance)		1 weeks
DD		1 week
3.5 hr LD	T7 cycle	5 days
DD		5 days
LL	100 lux	1 week
DD		Tissue collection

Table 2.3.1 **Light schedule for SIK3 circadian characterization.** Longitudinal study on the same cohort of mice for roughly 5-6 months.

2.3.6 Sleep recording and analysis

EEG/EMG recordings were performed according to 2.1.6 as previously described. Processing and analysis of sleep-wake states were as 2.1.7. For 6 hours of sleep deprivation (SD), animals were kept awake between ZT0 and ZT6 by introducing novel objects (n=2).

2.3.7 RNA extraction

Cortex samples were collected from WT and SIK3 KI animals at the end of light phase (ZT10) and the end of dark phase (ZT22) (n=3-4 each genotype and timepoint). Samples were disrupted in TRIzol (ThermoFisher Scientific) using a handheld homogenizer. RNA was separated from DNA with chloroform and centrifuged at

13000xg for 15 minutes at 4 °C. RNA extraction was performed using RNAeasy Mini Kit (#74104, Qiagen). Briefly, the upper colorless aqueous phase was added to gDNA eliminator columns and centrifuged at 13000 x g for 2 minutes. The samples were precipitated 70% ethanol and loaded into RNAeasy spin columns. Samples were washed with Buffer RW1 and RPE with centrifugation steps in between, and finally eluted with 40ul of RNase-free water.

RNA was quantified with the Qubit™ RNA BR (Broad-Range) Assay Kit (ThermoFisher Scientific). Sample RNA quality was assessed using Agilent RNA ScreenTape Assay (Agilent Technologies). RNA samples were mixed with RNA Sample Buffer and loaded into the Agilent 4200 TapeStation, along with RNA Ladder. RNA Integrity Number (RIN) was obtained from the assay. RNA purity (A260/230 ratio) was determined with NanoDrop Spectrophotometer (ThermoFisher Scientific).

2.3.8 BRB-sequencing library preparation and Sequencing

Following RNA extractions, Bulk RNA barcoding and sequencing (BRB-seq) preparation was performed. BRB-seq uses highly optimized barcoded oligo(dT) primers and unique molecular identifiers (UMIs) that tag RNA samples during first-strand synthesis (Alpern et al., 2019). This allows cDNA samples from individual experimental groups to be pooled into one tube for library preparation. The Merurius™ BRB-seq Library Preparation 96 kit (#10814, Alithea Genomics) was used. Briefly, purified and diluted RNA samples were mixed and reconstituted with dried oligo-dT in the 96-well plate provided. Samples were reverse transcribed in a thermocycler with Master Mix

containing FSB and FSE reagents. cDNA samples are then pooled and purified with SPRI AMPure Beads (#A63881, Beckman Coulter) on a magnetic stand. The purified cDNA pool was incubated in EXB and EXO reagents for free primer digestion. Followed by double-strand synthesis with SSB and SSE reagents, sample was purified again with SPRI beads and resuspended in water. cDNA quantification was performed with Qubit™ dsDNA High Sensitivity (HS) Assay Kit (ThermoFisher Scientific). Full-length cDNA sample was tagmented and purified with SPRI beads and resuspended in water. A real-time PCR reaction was performed using pre-amplified cDNA samples to determine the optimal number of cycles for amplification. The 5' terminal fragments were amplified using Unique Dual Indexing (UDL) adaptor primers after 9 cycles of amplification. Indexed cDNA library was cleaned up with SPRI beads and resuspended in water. Final quantification and fragment analysis were performed using Qubit™ dsDNA HS Assay Kit and High Sensitivity DNA Kit for 2100 Bioanalyzer (Agilent Technologies). The library was sequenced on NovaSeq X Plus series, loaded at 100pM, by Novogene (UK) Company Limited. Sequenced data was demultiplexed by Alithea Genomics.

2.3.9 SIK3 RNAseq data analysis

Prior to differential gene analysis, genes with a raw expression level of less than 50 counts were excluded. Differential gene expression analysis was conducted with the R package DESeq2. Principal Component Analysis (PCA) was performed and plotted to check for batch effects and distribution between sample conditions. Outliers were excluded from analysis. Mean intensity dispersion was fitted using glmGamPoi,

calculated using a local median regression. Volcano plots of differential gene expression were generated using EnhancedVolcano. Log2 Fold Change and p-adjusted value cutoff thresholds were set at 0.5 and 0.05, respectively, and considered statistically significant per convention. An explorative method was adopted to observe biological trends where few targets passed the cutoff and unadjusted p-value of 0.05 was used. Functional enrichment and protein-protein interaction analysis were performed using the list of significant genes.

2.4 Chapter 5 Methods

2.4.1 Circadian wheel-running activity

SIK2 KI and WT animals (n=6-14 each) were singly housed with *ad libitum* access to food and water and a running wheel attached. Circadian wheel-running activity was monitored under 12 hour light/12 hour dark cycle (100 lux, 12:12 LD), constant darkness (DD) or constant light (100 lux, LL). White LED lights were used in the circadian coffins as the light source. Activity was recorded using ClockLab (Actimetrics, USA) (Table 2.4.1).

2.4.2 LD cycle advance protocol

SIK2 KI and WT animals (n=6-14 each) were singly housed and circadian activity was monitored under a 12:12 LD cycle (100 lux). The animals were allowed to entrain to the light dark cycle. After stable entrainment, the light phase was advanced for 6 hours. Circadian wheel-running activity was monitored during re-entrainment until they were

aligned with the new LD cycle. With the repeated light advance protocol, the light phase was advanced for 6 hours again after realignment. The animals were released into DD afterward. For analysis, onsets were allocated automatically by ClockLab Analysis 6 and adjusted manually. Phase was calculated as the time of activity onset minus the time of dark onset. Phase differences were calculated by subtracting the phase from 6 (light advance shift) (Table 2.4.1).

2.4.3 Light pulses and phase shifting

SIK2 KI and WT animals (n=6 each) were singly housed and circadian activity was monitored under a 12:12 LD cycle (100 lux). After stable entrainment to the LD, animals were released into DD for 3-5 days. Subsequently, animals were exposed to two 30-minute light pulses (30 lux), timed at CT14 and CT22, leaving 3-5 days in between. The phase angles for the days prior to and after the light pulses were measured, and the differences were calculated. As per convention, phase advance has a negative phase difference, and phase delay has a positive phase difference. The activity counts 30 minutes before and during the light pulses were recorded to observe masking effects (Table 2.4.1).

2.4.4 Ultradian (T7) light-dark cycle

SIK2 KI and WT animals (n=6 each) were singly housed and circadian activity was monitored. Animals were subjected to a 7-day ultradian cycle, which entails a 3.5-hour lights-on, 3.5-hour lights-off cycle (Table 2.4.1).

Light schedule	Light protocol	Duration
7AM-7PM ON/OFF	Entrainment	2 weeks
1AM-1PM ON/OFF	6 hr light advance	10 days
7PM-7AM ON/OFF	6 hr light advance	10 days
DD	DD	10 days
0.5hr at 8AM	CT14	
DD	DD	1 week
0.5hr at 2PM	CT22	
DD	DD	1 week
LL	LL	1 week
3.5 hr LD	T7 cycle	1 week
DD changed after midnight	DD	

Table 2.4.1 **Light schedule for SIK2 circadian characterization.** Longitudinal study on the same cohort of mice for roughly 3-4 months.

2.4.5 SIK2 RNAseq data analysis

SCN and cortex punches were collected from WT and SIK2 KI animals 3 hours after the onset of the dark phase (ZT3) (n=4 each). RNA extractions and BRB-seq library preparation were performed by Dr. Zeinab Wakaf.

Prior to differential gene analysis, genes with a raw expression level of less than 50 counts were excluded. Differential gene expression analysis was conducted with the R package DESeq2. Principle Component Analysis (PCA) was performed and plotted to check for batch effects and distribution between sample conditions. Mean intensity dispersion was fitted using glmGamPoi, calculated using a local median regression. Volcano plots of differential gene expression were generated using EnhancedVolcano. Log2 Fold Change and p-adjusted value cutoff thresholds were set at 0.5 and 0.05,

respectively, and considered statistically significant. Functional enrichment and protein-protein interaction analysis were performed using the list of significant genes.

2.4.6 Phosphoproteomics sample pre-processing

1mm^3 SCN and cortex punches (described in General Methods section) from each animal were collected from WT and SIK2 KI animals at the end of light phase (ZT10) and the end of dark phase (ZT22) (n=16 each genotype and timepoint). Four punches were pulled into one tube as one “n” for optimal detection. Samples were solubilized in Lysis Buffer (2% SDS, 50mM HEPES pH8.5) containing 100nM of okadaic acid using a KIMBLE® Dounce tissue grinder set (2mL, DWK Life Sciences). Samples were sonicated in Bioruptor and protein concentrations were quantified using a Pierce micro BCA™ protein assay kit (Thermo Scientific #23235).

Samples were extracted using the SP3 extraction method. Proteins were reduced (10mM TCEP) and alkylated (50mM CAA). SpeedBeads magnetic carboxylate modified particles (GE65152105050250, Merck) were prepared to 50ug/ul and activated by acetonitrile (MeCN). Proteins were incubated in activated beads and washed with 80% ethanol and 100% MeCN on a DynaMag-2 magnetic rack. Peptides were digested (Trypsin 1:25, LysC 1:25 in 50mM HEPES pH 8.5) overnight at room temperature. Peptides were eluted with 2% DMSO and acidified with 20% formic acid to reach a final pH of 3. Samples were then stored in -80 and sent off for TMT labeling, TiO2 phosphopeptide enrichment, peptide desalting, HPLC fractionation, and LC-MS.

1mg of SCN and cortex punches from an extra batch of C57/BL6 animals were pooled and processed as the carrier proteome for peptide detection depth and quantification.

2.4.7 Phosphoproteomics analysis

Consistent with default parameters, shared features and all features attributed to contaminants and reverse hits were removed prior to analysis. Normalization and processing were conducted using MSstats and raw data file was adjusted to fit the format on RStudio. Fragmented phosphopeptides were collapsed and summed into one row. The phosphoproteome was first processed and normalized to the global median across all samples. Summarization was performed using Tukey's Median Polish (TMP). The missing values were replaced with "NA" as unknown. The proteome datasets were similarly processed and normalized. The phosphoproteome was then normalized to the proteomics after processing by subtracting the log intensities. Comparisons between genotypes and timepoints were conducted using Limma (linear model). The fit applies the empirical Bayes variance. P-value adjustment used the Benjamini-Hochberg method. Volcano plots of differential phosphorylation changes were generated using EnhancedVolcano. Log2 Fold Change (FC) and p-adjusted value cutoff thresholds were set at 0.5 and 0.05, respectively, and considered statistically significant per convention.

2.4.8 Kinase-Substrate Enrichment Analysis (KSEA)

KSEA was performed on PhosphositePlus Kinase Prediction. It integrates all identified Ser/Thr kinases and predicts upstream kinases responsible for phosphorylation sites in

the dataset. It ranks kinases by motif percentile and compatibility. The kinases were then filtered by percentile, and 90% cutoff was used. Top predicted upstream kinases were plotted and visualized using KinMap (Eid et al., 2017)

2.4.9 Novel Object Recognition (NOR) test

SIK2 KI and WT animals were singly housed with *ad libitum* access to food and water under 12:12 LD cycle (100 lux) (n=13-14 each). Mice were handled every day for a week before the experiment. A 20cmx20cm arena was used. An external video camera was used to record the experiment. Experiment was performed at ZT3 (light phase).

During habituation, animals were placed in the middle of the open, empty arena. They were allowed for free exploration of the arena for 5 minutes and placed back into their home cages. Habituation was repeated for three days with one session per day at ZT3. Training (T1) was performed with two identical objects in opposite quadrants of the arena. Animals were allowed for free exploration for 10 minutes. Testing (T2) was performed 24 hours after T1, one object used in T1 was replaced with a novel object. Animals were allowed for free exploration for 10 minutes. T1 and T2 were repeated one more time with a new set of objects. Objects and positions in the arena were counterbalanced and cleaned with 70% (v/v) ethanol between animals. Experiments were conducted in a closed chamber with even 30lux lighting and noise canceling.

Total exploration time was manually scored. Exploration was defined as pointing the nose at the objects at a distance of less than 2cm. Facing the other way, sitting on the

object or climbing on top without actively exploring the object were not counted as exploratory behavior. The scorer was blinded with regard to animal ID, genotype and sex. The discrimination index was the percentage of the difference between the exploration time of the novel and familiar object over total exploration time combined and was calculated as follows:

$$Discrimination\ index\ (\%) = \frac{Novel\ (s) - Familiar\ (s)}{Novel\ (s) - Familiar\ (s)}$$

2.4.10 Y-maze Short-term Spatial Memory Test

SIK2 KI and WT animals were singly housed with *ad libitum* access to food and water under a 12:12 LD cycle (100 lux) (n=6 each). Mice were handled every day for a week before the experiment. An external video camera was used to record the experiment. The experiment was performed at ZT3 (light phase).

A solid plastic arena with three arms (30cm long, 7cm wide and 20cm high arms) was placed on the floor. Arms were labeled as “starting”, “other” and “novel”. All three arms were counterbalanced and randomized between animals. For the exposure phase, the “novel” arm was blocked with a yellow block. Animals were placed in the “starting” arm and allowed to explore the “starting” and “other” arms for 5 minutes. During the test phase, the block was removed and the animals were allowed to explore all three arms. The whole process was recorded. The Y-maze arena and block were cleaned with 70% (v/v) ethanol between animals.

Time spent in each arm and total distance traveled were tracked and analyzed using AnimalTA. Missing values were checked and corrected manually.

REFERENCES

Alpern, D., Gardeux, V., Russeil, J., Mangeat, B., Meireles-Filho, A. C. A., Breysse, R., Hacker, D., & Deplancke, B. (2019). BRB-seq: ultra-affordable high-throughput transcriptomics enabled by bulk RNA barcoding and sequencing. *Genome Biology*, *20*(1), 71. https://doi.org/10.1186/s13059-019-1671-x

Boudeau, J., Baas, A. F., Deak, M., Morrice, N. A., Kieloch, A., Schutkowski, M., Prescott, A. R., Clevers, H. C., & Alessi, D. R. (2003). MO25α/β interact with STRADα/β enhancing their ability to bind, activate and localize LKB1 in the cytoplasm. *EMBO Journal*, *22*(19), 5102–5114. https://doi.org/10.1093/emboj/cdg490

Callister, S. J., || R. C. B., Adkins, J. N., Johnson, E. T., Qian, W., Webb-Robertson, B.-J. M., Smith, R. D., & Lipton, M. S. (2006). *Normalization Approaches for Removing Systematic Biases Associated with Mass Spectrometry and Label-Free Proteomics*.

Darling, N. J., Toth, R., Arthur, J. S. C., & Clark, K. (2017). Inhibition of SIK2 and SIK3 during differentiation enhances the anti-inflammatory phenotype of macrophages. *Biochemical Journal*, *474*(4), 521–537. https://doi.org/10.1042/BCJ20160646

Eid, S., Turk, S., Volkamer, A., Rippmann, F., & Fulle, S. (2017). KinMap: a web-based tool for interactive navigation through human kinome data. *BMC Bioinformatics*, *18*(1), 16. https://doi.org/10.1186/s12859-016-1433-7

Johnson, J. L., Yaron, T. M., Huntsman, E. M., Kerelsky, A., Song, J., Regev, A., Lin, T. Y., Liberatore, K., Cizin, D. M., Cohen, B. M., Vasan, N., Ma, Y., Krismer, K., Robles, J. T., van de Kooij, B., van Vlimmeren, A. E., Andrée-Busch, N., Käufer, N. F., Dorovkov, M. V., … Cantley, L. C. (2023). An atlas of substrate specificities for the human serine/threonine kinome. *Nature*, *613*(7945), 759–766. https://doi.org/10.1038/s41586-022-05575-3

Raudvere, U., Kolberg, L., Kuzmin, I., Arak, T., Adler, P., Peterson, H., & Vilo, J. (2019). G:Profiler: A web server for functional enrichment analysis and conversions of gene lists (2019 update). *Nucleic Acids Research*, *47*(W1), W191–W198. https://doi.org/10.1093/nar/gkz369

Szklarczyk, D., Kirsch, R., Koutrouli, M., Nastou, K., Mehryary, F., Hachilif, R., Gable, A. L., Fang, T., Doncheva, N. T., Pyysalo, S., Bork, P., Jensen, L. J., & von Mering, C. (2023). The STRING database in 2023: protein–protein association networks and functional enrichment analyses for any sequenced genome of interest. *Nucleic Acids Research*, *51*(D1), D638–D646. https://doi.org/10.1093/nar/gkac1000

Yao, Z., van Velthoven, C. T. J., Kunst, M., Zhang, M., McMillen, D., Lee, C., Jung, W., Goldy, J., Abdelhak, A., Aitken, M., Baker, K., Baker, P., Barkan, E., Bertagnolli, D., Bhandiwad, A., Bielstein, C., Bishwakarma, P., Campos, J., Carey, D., … Zeng, H. (2023). A high-resolution transcriptomic and spatial atlas of cell types in the whole mouse brain. *Nature*, *624*(7991), 317–332. https://doi.org/10.1038/s41586-023-06812-z

Zhang, M., Pan, X., Jung, W., Halpern, A. R., Eichhorn, S. W., Lei, Z., Cohen, L., Smith, K. A., Tasic, B., Yao, Z., Zeng, H., & Zhuang, X. (2023). Molecularly defined and spatially resolved cell atlas of the whole mouse brain. *Nature*, *624*(7991), 343–354. https://doi.org/10.1038/s41586-023-06808-9

Chapter 3: Direct substrate identification and functional characterization of SIK1 in the SCN

This chapter contains work that is also presented in a manuscript currently under review (see Appendix 1). Overlapping sections were modified and adapted to this thesis. Section 3.1 summarizes partial key findings of the manuscript, which serve as the background of this chapter.

3.1 Introduction

Existing literature has shown that CRTCs are validated downstream targets of SIKs whose phosphorylation of CRTCs inhibits nuclear translocation and represses CREB-mediated transcription (Katoh et al., 2006). As CREB-mediated transcription drives key clock gene expression, regulating circadian timing and photic entrainment, the SIK-CRTC cascade has also been investigated in the context of the circadian clock (Jagannath et al., 2013; Sakai et al., 2004; Sakamoto et al., 2013b). Light-regulated transcriptomics following a nocturnal light pulse identified the upregulation of *Sik1*, along with *Per1* (Jagannath et al., 2013), supporting a role for SIK1 in attenuating clock resetting and photic re-entrainment through phosphorylation of CRTC1 in the SCN. Consistent with this, *Sik1* knockdown produces rapid re-entrainment and large phase shifts to a new LD cycle.

As *Sik1* is induced upon the induction of nocturnal light, it is implied as an important component in circadian gating. It refers to a mechanism where the circadian clock gates processes and responses to signals depending on a temporal pattern including entrainment and responses to zeitgebers. The light-inducible nature of SIK1 therefore

positions it as a key component of circadian gating, opening up opportunities for jetlag and shift work (Paajanen et al., 2025; Zhang et al., 2022).

3.1.1 SIK1 circadian and sleep implications

Circadian wheel running assays and EEG/EMG sleep recordings were used to characterize the behavioural phenotypic changes in Sik1 T182A knock-in (KI), a model of loss-of-function SIK1. No significant changes in core clock parameters such as circadian period or amplitude were observed under constant conditions, indicating that SIK1 is not involved in the maintenance of core circadian rhythms. However, under atypical nocturnal light such as light advance, jetlag paradigms and discrete photic stimulations (light pulses), SIK1 KI animals showed rapid entrainment and early arousal, reflecting enhanced circadian plasticity of the circadian clock. The behaviour was also shown to persist after release into darkness, confirming true entrainment rather than masking effects. These findings align with the inducible nature of SIK1 that is isoform-specific, establishing SIK1's unique role in entrainment in the SCN ((Wakaf et al., 2026); Appendix 1).

Sleep phenotypes mirrored the circadian entrainment phenotype. Following the 6hr advance of the LD cycle, SIK1 KI showed wakefulness earlier in the dark phase, consistent with accelerated arousal timing. Process S was intact, as homeostatic sleep pressure and slow wave activity remained unchanged following both the LD shift and sleep deprivation. These results demonstrate that SIK1 selectively regulates Process C and circadian entrainment while leaving Process S intact (Wakaf et al., 2026).

3.1.2 SIK1 transcriptomics and brain phosphoproteome

These findings from circadian and sleep characterizations were further explored through mRNAseq and tissue-specific quantitative *in vivo* phosphoproteomics to delineate SIK1-dependent differential gene expression and phosphorylation changes. Transcriptomics after the 6hr LD shift between WT and SIK1 KI animals showed no changes in core clock genes such as *Per1* and *Clock*, but changes in calcium-related genes and *Avp* were observed, suggesting a role in neurotransmission and calcium signalling. Similarly, the phosphoproteomics in WT and SIK1 KI SCN after shift proposed multiple key phosphoproteins such as PKCγ and PAK1. Functional analysis showed enrichment in calcium signalling processes, namely CACNA1I and CAMK2A/B/D/G. Our recent manuscript proposed and validated a neuronal cascade with PKCγ, connecting pre- and post-synaptic phosphosites, shaping Ca^{2+} oscillations in the synaptic terminals. The post-translational networks of SIK1 maintain SCN stability and response to changing light conditions, which is reflected in the circadian and sleep entrainment phenotypes. It was proposed that the post-translational regulation of circadian arousal timing preceded transcriptional changes (Wakaf et al., 2026).

Previous research has shown that phosphorylation of synaptic proteins increases following sleep deprivation, proposing a set of substrates that are driven by sleep homeostasis (Process S) (Brüning et al., 2019). Quantitative phosphoproteomics in cortex tissue using SIK1 KI animals revealed substrates that are circadian-regulated (Process C). The overlapping phosphoproteins are characterized as universal “wake

substrates". Elevated levels of CAMK2A supported increased excitatory activity in the cortex in SIK1 KI following 6hr shift but were shown to be an indirect effect from the SCN, forming a SCN-cortex network ((Wakaf et al., 2026); Appendix 1). The tissue-specific omics dataset expands SIK1's signalling mechanisms, in addition to previously validated CRTCs and HDACs.

3.1.3 Aims

Given the existing body of evidence, SIK1 was implicated in both transcriptional regulation and post-translational modification of synaptic proteins. Defining the direct molecular substrates, signalling pathways, and phosphorylation sites of SIK1 is essential to mechanistically account for the circadian and sleep phenotypes observed. We aim to optimise protein kinase assay linked phosphoproteomics (Pro-KALIP) for SCN brain tissue to identify direct substrates of SIK1, addressing the central challenge of distinguishing direct kinase targets from proteins phosphorylated by secondary, downstream kinases. The optimised Pro-KALIP dataset will complement the *in vivo* quantitative phosphoproteomics to elucidate direct molecular targets and phosphorylation sites underlying the rapid entrainment and light-inducible nature of SIK1. Selected candidates will be validated through in vitro cell-based functional assays to clarify SIK1's role in circadian regulation and identify potential pharmacological targets.

3.2 Results

3.2.1 Single-cell RNAseq (scRNAseq) explores the distribution of *Sik1* in the brain and cell types

Given the evidence on the light-induced and rapid entrainment phenotype of *Sik1*, we consulted a publicly available spatial transcriptomics dataset, Allen Brain Atlas MERFISH (Yao et al., 2023), to investigate *Sik1* gene localization and expression in various cell types. From 1x coronal slices of the brain, *Sik1* has the highest gene expression and is predominantly expressed in the SCN, followed by the thalamus (Fig. 3.1a). Gene expression level, measured by log2 (Counts Per Million (CPM) +1), of *Sik1* in the SCN is around 90 to 120 counts per million. Out of 3.74 million cells imputed, 1200 cells were marked in the SCN, taking up only 0.03% of the total cell population. This is reflected in a lower scale bar in the high *Sik1* CPM range, showing a small proportion of *Sik1*-rich cells across the brain. Within the SCN, *Sik1* is most abundant in hypothalamic GABAergic (HY-GABA) cells (Fig. 3.1b). There is very little expression in other regions of the brain, namely the cortex and hippocampus, having an average *Sik1* expression of 0.5 to 1 CPM (Fig. 3.1a). In these regions, *Sik1* is mainly expressed in glutamatergic neurons (Fig. 3.1c).

Overall, *Sik1* is expressed mostly in vascular cells, which are present widely across brain regions that form the blood-brain barrier and facilitate nutrient delivery. The enrichment of *Sik1* in the SCN shows the significance of its role in regulating the circadian core clock and Process C.

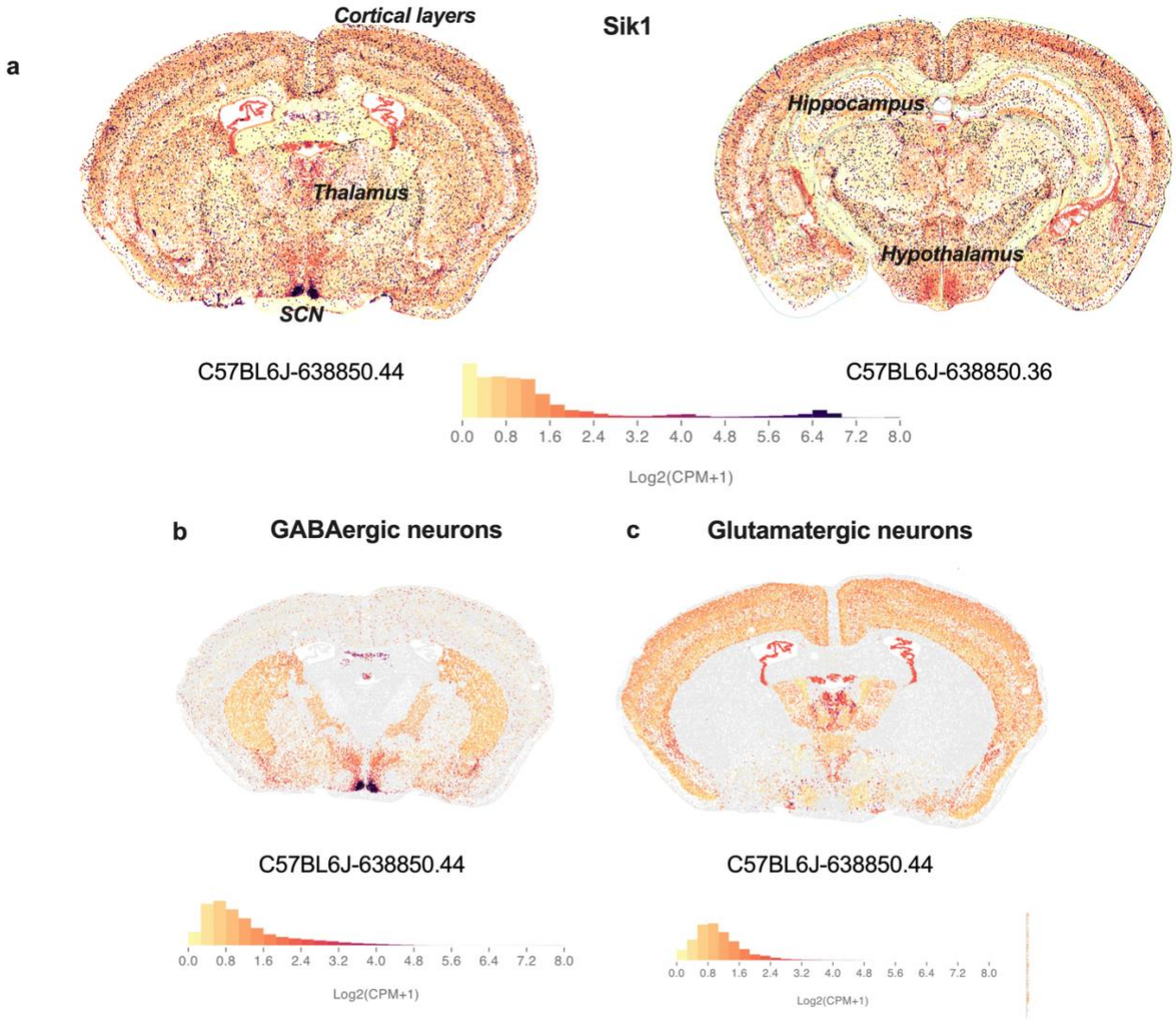

Fig 3.1 ***Sik1* gene expression in different brain regions and cell types.** Spatial transcriptomics of Sik1 from Allen Brain Atlas MERFISH C57BL6J-638850 with Imputed Genes + Reconstructed Coordinates (Yao et al., 2023).**(a)** Coronal slices containing the SCN (left) (C57BL6J-638850.44) and hippocampus (right) (C57BL6J-638850.36) were selected. Spatial transcriptomics Allen Brain Atlas MERFISH coronal slices containing the SCN (C57BL6J-638850.44) of *Sik1* expression overlapping with 10x scRNAseq UMAP plot of **(b)** GABAergic neurons and **(c)** glutamatergic neurons. Gene expression measured by Log2(Counts Per Million (CPM) + 1) scale, corresponding to the darkness of bars. The height of scale bars represents the proportion of cells with that level of expression.

3.2.2 Optimization of Pro-KALIP conditions

To effectively explain and understand the behavioural phenotype of SIK1, we used Pro-KALIP to identify the direct substrates and phosphorylation sites of SIK1. Following the spatial transcriptomics showing localization of *Sik1* in the SCN, we chose to focus on identifying direct substrates in the SCN. We collected and pooled 1mm^3 punches from C57BL6 WT animals, which roughly resulted in 1mg of protein. As described previously, Pro-KALIP consists of an *in vitro* assay that dephosphorylates the protein sample and rephosphorylates it by incubating with a purified exogenous SIK kinase, followed by Liquid-Chromatography Mass Spectrometry (LC-MS) (Xue et al., 2013). The hub of substrates is compared to the *in vivo* brain phosphoproteome conducted with WT and SIK KI animals.

Previously, the *in vitro* assay component of Pro-KALIP was optimized for cell lysate and small-scale experiments, so a major focus of this DPhil was the development of the region-specific Pro-KALIP. The first step was to determine optimal assay conditions for SIK1 in brain tissue. As SCN samples were limited, we used the cortex tissue of WT animals and AMARA peptide to optimize kinase assay conditions. AMARA peptide is a validated minimal substrate for SIK and AMPK, used to measure kinase activity (Shan et al., 2016). Conditions for the rephosphorylation kinase reaction, such as SIK1 kinase concentration and reaction time, were optimized. All *in vitro* optimization experiments and SIK1 kinase activity quantification were performed using Kinase Glo Luminescent Assay (Promega, UK). Substrates were incubated with SIK1 kinase and ATP for the rephosphorylation reaction. The remaining ATP in the reaction that wasn't converted to

ADP was used as a substrate by the luciferase to catalyse mono-oxygenation of beetle luciferin, which produces one photon of light per turnover. The luminescence readings were therefore inversely proportional to SIK1 kinase activity (1/Luminescence) as arbitrary units of kinase activity. Optimal SIK1 kinase concentration was determined by carrying out a serial dilution of purified SIK1 kinase, keeping the kinase reaction time constant at 30 minutes. Taking the linear range of the kinase titration curve, SIK1 is optimal between 10nM and 40nM. The concentrations lower than 10nM resulted in non-linear kinase activity (Fig. 3.2a). For accurate quantitative analysis, values in the linear range of the curve were included and fitted (Somberg et al., 2003). Optimal kinase reaction time was determined by incubating the AMARA peptide with SIK1 kinase for different lengths of time, keeping kinase concentration constant at 20nM. By varying the kinase reaction time from 5 to 40 minutes, the highest kinase activity occurred at 30 minutes and plateaued after (Fig. 3.2b). Due to limited replicates and large error bars, these conditions, optimized using *in vitro* assays and the AMARA peptide, were taken with caution. These assays set the premise for the large-scale SIK1 KALIP assay with SCN tissue.

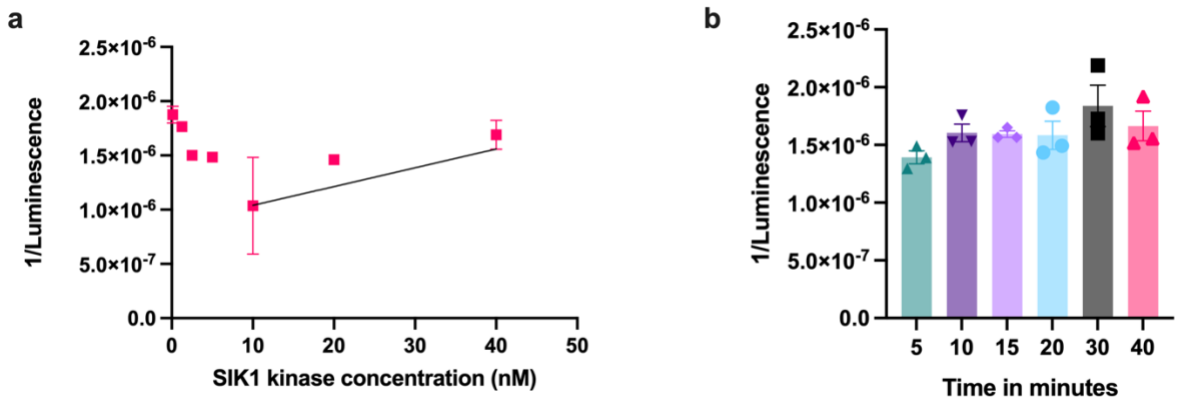

Fig 3.2 **Determining optimal SIK1 kinase concentration and reaction time.** *In vitro* Kinase Glo Luminescence assay using AMARA peptide as substrate in 384-well plates. (a) SIK1 kinase titration curve with two-fold serial dilution of SIK1 kinase from 0.125nM to 40nM at 30 minutes of reaction time. Linear range fitted with simple linear regression. (b) Kinase reaction time varying from 5 to 40 minutes of incubation time at 30 °C with constant SIK1 kinase concentration at 20nM. SIK1 kinase activity measured as 1/Luminescence (inverse). n=2-3

To avoid impurities, the composition of the urea lysis buffer was also tested *in vitro*. Varying concentrations of urea, 500mM to 900mM, were added in separate wells along with SIK1 kinase to test the effect on kinase activity. We showed that the addition of urea does not have a significant effect on SIK1 kinase activity compared to no urea control, indicating a safe use of urea buffer for tissue lysis (Supp. Fig. 3.1).

3.2.3 LKB1-STRADα-MO25α trimer increases SIK1 kinase activity

The SIK subfamily, part of the AMPK family, is activated by an upstream master kinase, LKB1. LKB1 forms a trimer with STRADα and MO25α and activates SIK1 activity 20- to 30-fold in *E.coli*-purified kinase (Lizcano et al., 2004). As the basal kinase level is low and the trimer is an essential activator, we chose to carry out the Pro-KALIP rephosphorylation reaction by adding purified LKB1 trimer along with SIK1 kinase. cDNA constructs of LKB1, STRADα and MO25α were obtained from the MRC Protein

Phosphorylation and Ubiquitylation (MRC PPU) Unit. They were transformed, purified, and validated on a DNA gel at corresponding bands for pEBG2T LKB1, FLAG STRADα and Myc MO25α at 7800bp, 5500bp and 4400bp, respectively (Fig. 3.3a). The plasmids were subsequently transfected into HEK293 cells with GFP control flasks to check for transfection efficiency (Fig. 3.3b). The trimer was affinity-purified with Glutathione Sepharose beads and validated using immunoblot. GST-LKB1, GST-STRADα and GST-MO25α were observed on the immunoblot at 40kDa, 50kDa and 40kDa, respectively (Fig. 3.3c, Supp. Fig. 3.2).

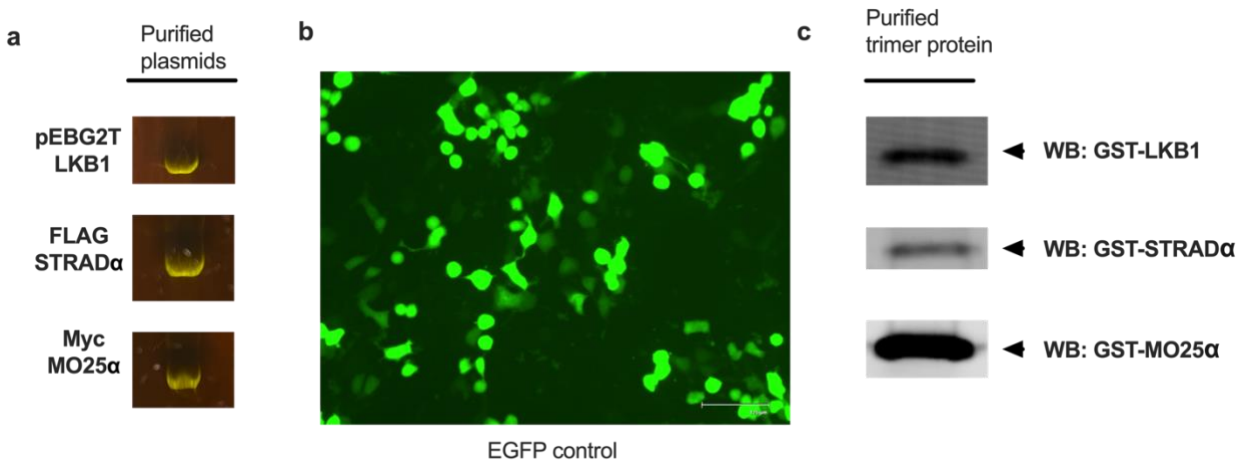

Fig 3.3 **Construction and purification of LKB1:STRADα:MO25α trimer.** pEBG2T LKB1, FLAG STRADα and Myc MO25α cDNA constructs were transformed into competent cells and grown in overnight bacterial cultures. (a) Plasmids were purified and validated on a DNA gel showing single bands for pEBG2T LKB1, FLAG STRADα and Myc MO25α at 7800bp, 5500bp and 4400bp, respectively. (b) Representative GFP expression in control HEK293T in T75 flasks parallel to trimer transfections (scale bar = 125μm). (c) Immunoblot of affinity-purified trimer showing individual single bands for GST-LKB1, GST-STRADα and GST-MO25α at 40kDa, 50kDa and 40kDa, respectively.

We then verified the effect of the LKB1 trimer on SIK1 kinase activity under the conditions of the rephosphorylation reaction. Firstly, the trimer was tested with the Kinase Glo Luminescence assay with AMARA peptide, carried out with the conditions optimized previously. Baseline SIK1 kinase, measured by inverse luminescence, was $1.44*10^{-7}$. With the addition of the LKB1 trimer, SIK1 kinase activity increased to $4.83*10^{-7}$, which validates the activating effect of the trimer on SIK1 kinase activity (Fig. 3.4a). To understand the interaction of the LKB1 trimer, it was incubated with and without SIK1 kinase in the absence of peptide. LKB1 is active only when the LKBtide peptide substrate is present (Zeqiraj et al., 2009), so the remaining kinase activity without LKB1-specific substrate presence was identified as autophosphorylation. With the binding of STRADα, LKB1 autophosphorylation is strongly enhanced at T336 and T363. Literature has also shown that increasing AMPK kinase activity augments LKB1 autophosphorylation (Baas et al., 2003b; Shaw, 2009). Our results showed significant levels of LKB1 autophosphorylation compared to baseline SIK1 kinase activity. Levels were similar between LKB1 trimer alone and the addition of SIK1 kinase (Fig. 3.4b). These results suggest that SIK1 and the LKB1:STRADα:MO25α trimer have an interdependent regulatory mechanism.

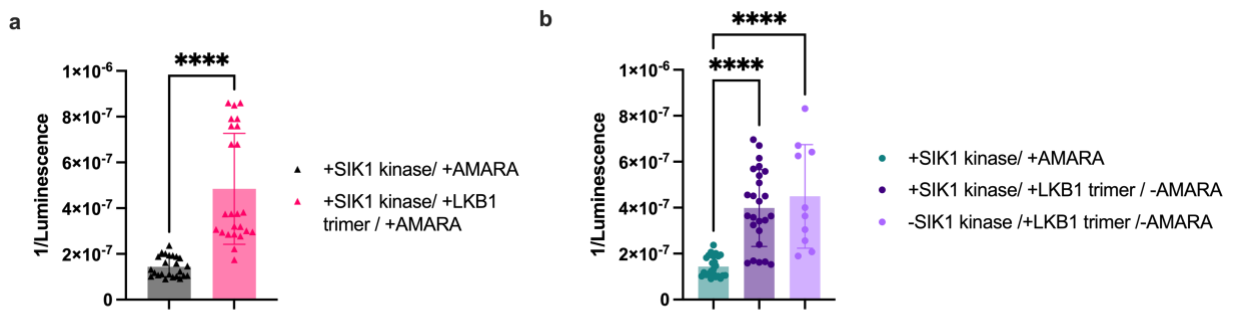

Fig 3.4 **The effect of LKB1:STRADα:MO25α trimer on SIK1 activity** *In vitro* Kinase Glo Luminescence assay using AMARA peptide as substrate in 384-well plates. (a) Kinase activity measured under conditions with or without LKB1:STRADα:MO25α trimer complex. Data tested against normality (Shapiro-Wilk test). Mann-Whitney non-parametric test used. **** $p<0.0001$. (b) Kinase activity measured under conditions with varying combinations of SIK1 kinase, LKB1:STRADα:MO25α trimer complex and AMARA peptide substrate. Ordinary one-way ANOVA. Tukey's multiple comparison test. **** $p<0.0001$. Kinase activity is the inverse of luminescence (1/Luminescence). n=10-24.

We then validated the effects of the LKB1 trimer on SIK1 activity using cortex tissue as substrate. Due to the complex kinase network present in brain tissue, an extra step was added to the protocol. 1mM of FSBA was incubated with the brain lysate after dephosphorylation to irreversibly inhibit all endogenous kinases present in the brain tissue. This ensures that the only kinases present in the sample are SIK1 and LKB1. We validated using the Kinase Glo Luminescent assay that SIK1 kinase activity was not affected by FSBA treatment. Similar to the results with AMARA peptide, the addition of the LKB1 trimer increases SIK1 kinase activity from $2.19*10^{-7}$ to $5.48*10^{-7}$ – around 2-3-fold (Fig. 3.5a).

Prior to phosphopeptide enrichment and LC-MS, tissue lysis, dephosphorylation and resphosphorylation kinase reactions were visualized on a pAMPK substrate motif immunoblot, a measure of the SIK1 substrates detected. Compared to the lysate lane,

the dephosphorylated sample lane appeared to have significantly fewer substrates detected. Remaining faint bands indicated potential incomplete dephosphorylation. A qualitative trend towards increased band intensity was observed with increasing concentrations of LKB1 trimer – 1x to 3x – during rephosphorylation (Fig. 3.5b).

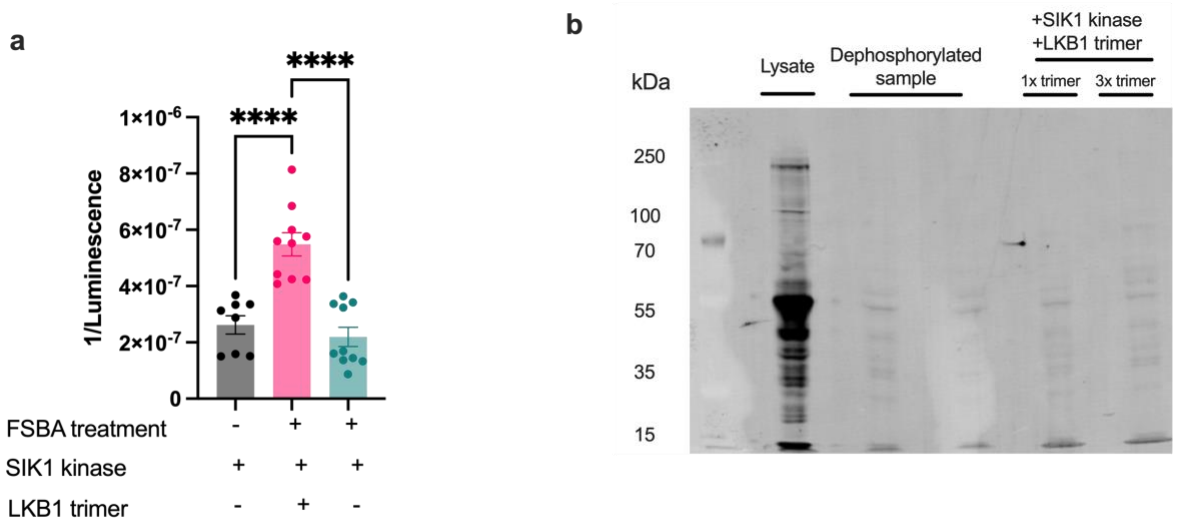

Fig.3.5 **The effect of LKB1:STRADα:MO25α trimer on SIK1 activity in brain tissue.** (a) *In vitro* Kinase Glo Luminescence assay using dephosphorylated brain sample as substrate in 384-well plates. Dephosphorylated brain samples were either directly used for kinase reaction or treated with 1mM of FBSA for 1hour beforehand. Kinase activity with or without the LKB1:STRADα:MO25α trimer complex was measured. Kinase activity is the inverse of luminescence (1/Luminescence). n=8-10. p>0.05, **** p<0.0001, Ordinary one-way ANOVA, Tukey's multiple comparison test. (b) Immunoblot of pAMPK substrate motif with lanes showing lysate, dephosphorylated brain sample, kinase reaction with SIK1 kinase and 1x and 3x LKB1:STRADα:MO25α trimer complex. PageRuler Plus Prestained Ladder was used. ns

3.2.4 Analysis of SIK1 KALIP dataset in the SCN

From SIK1 KALIP in the SCN, we detected 2808 phosphopeptides from LC-MS, which mapped to 1105 unique phosphoproteins and 2135 unique phosphosites (Supp. Table 3.1). Since this is an SIK1-targeted assay, we checked if the dataset is enriched for the SIK1 motif. We performed a contingency test with an integrated dataset on PhosphoSitePlus that incorporates a meta dataset that detected all 89784 Serine/Threonine (Ser/Thr) sites (Johnson et al., 2023) as the background. The dataset ranks all the mouse ortholog sites and maps them to the 303 Serine/Threonine kinases by percentile, showing how likely the site is phosphorylated by the kinase. We set the percentile cutoff at 80% as a site with the SIK1 signature. Out of the 2135 unique phosphosites, 506 phosphosites were above the 80% cutoff, included as SIK1 sites. Using a chi-squared test, the SIK1 SCN KALIP dataset showed enrichment of SIK1 ($p=0.0003$). The effect size of 1.204 also showed that there is an increasing odds of highly predicted SIK1 sites in the SIK1 KALIP dataset compared to the background meta dataset (Fig. 3.6a). As the LKB1 trimer was added in the kinase reaction for optimal substrate detection, we performed the contingency test for the LKB1 motif. 184 phosphosites were detected as LKB1 motif, and the odds ratio was 0.2746 ($p<0.0001$), showing that the LKB1 motif was significantly depleted (Fig. 3.6b). The same contingency tests were performed for two other kinases, cyclin-dependent kinase 16 (CDK16) and G-protein-coupled receptor kinase 3 (GRK3), part of the CMGC and AGC kinase families, respectively. Out of 2135 unique phosphosites, 293 phosphosites were CDK16 motif and 79 phosphosites were GRK3 motif. The odds ratios were below 1, 0.5696 for CDK16 and 0.1503 for GRK3 ($p<0.0001$), showing that these kinases were

also depleted in the SIK1 SCN dataset (Fig. 3.6c-d). These results confirmed that the SIK1 SCN dataset was significantly enriched for SIK1 sites and not other kinases.

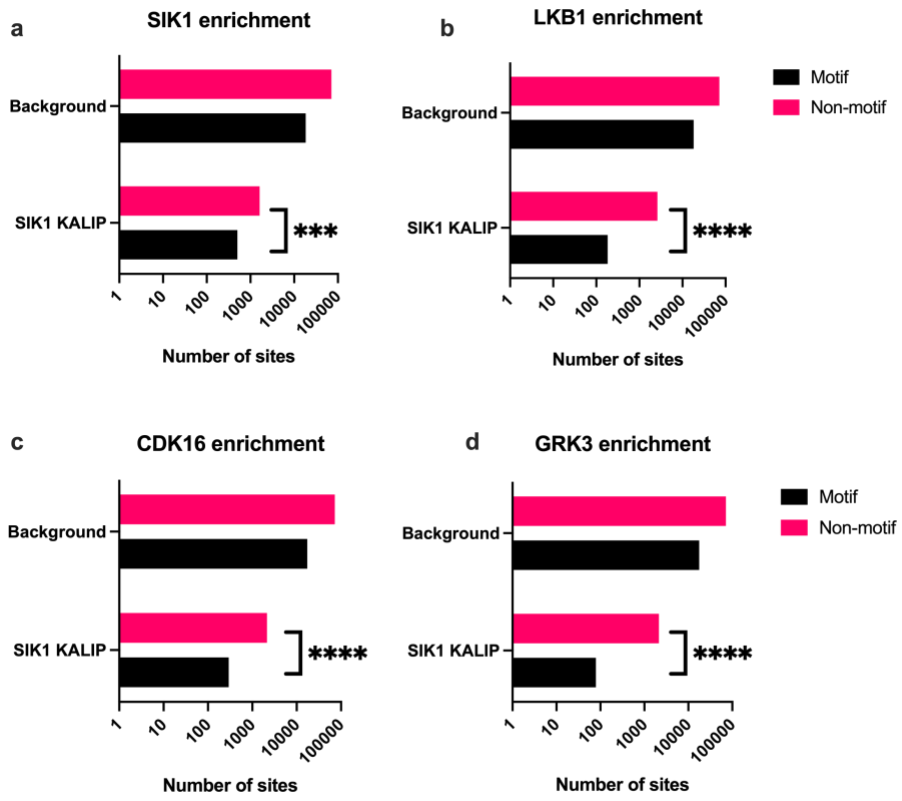

Fig. 3.6 **Motif enrichment analysis of the SIK1 KALIP SCN dataset.** Motif enrichment analysis using Johnson et al as background signal for (a) SIK1, (b) LKB1, (c) CDK16, and (d) GRK3. “Motif” was defined as a site that has a motif percentile of over 80%. Number of sites was plotted for both the background and SIK1 KALIP SCN dataset comparing number of “motif” and “non-motif” sites. *** p <0.001, **** p<0.0001, Chi-squared test, Two-sided p-value.

Johnson et al obtained phosphorylation-site motifs from positional scanning peptide array (PSPA) analysis for all 303 Ser/Thr kinases. Site percentiles were allocated by residue favourability at each position (Johnson et al., 2023). The FASTA sequences of the phosphosites from the SIK1 SCN KALIP dataset generated a motif sequence logo by WebLogo (Crooks et al). The SIK1 KALIP logo was compared to the SIK1 motif atlas (Fig. 3.7a). The zero-position showed that the dataset was composed of serine-dominant sites, which matched the serine-specificity of SIK1. Dominant residues in the SIK1 KALIP dataset at positions -3 and -4. -5 and +4 were strongly favoured by SIK1, namely the arginine (R) residues with an electrically charged side chain. We also observed a blend of the LKB1 motif, expected with the addition of the LKB1 trimer. Dominant residues at positions +2 and +3 were strongly favoured by LKB1 kinase, namely a proline (P) residue with a non-polar hydrophobic side chain. Other positions showed residues more favourable for other kinases dominantly from the CAMK family, this shows that the dataset is enriched for multiple kinases but had the highest compatibility with the SIK1 motif (Fig. 3.7b-c).

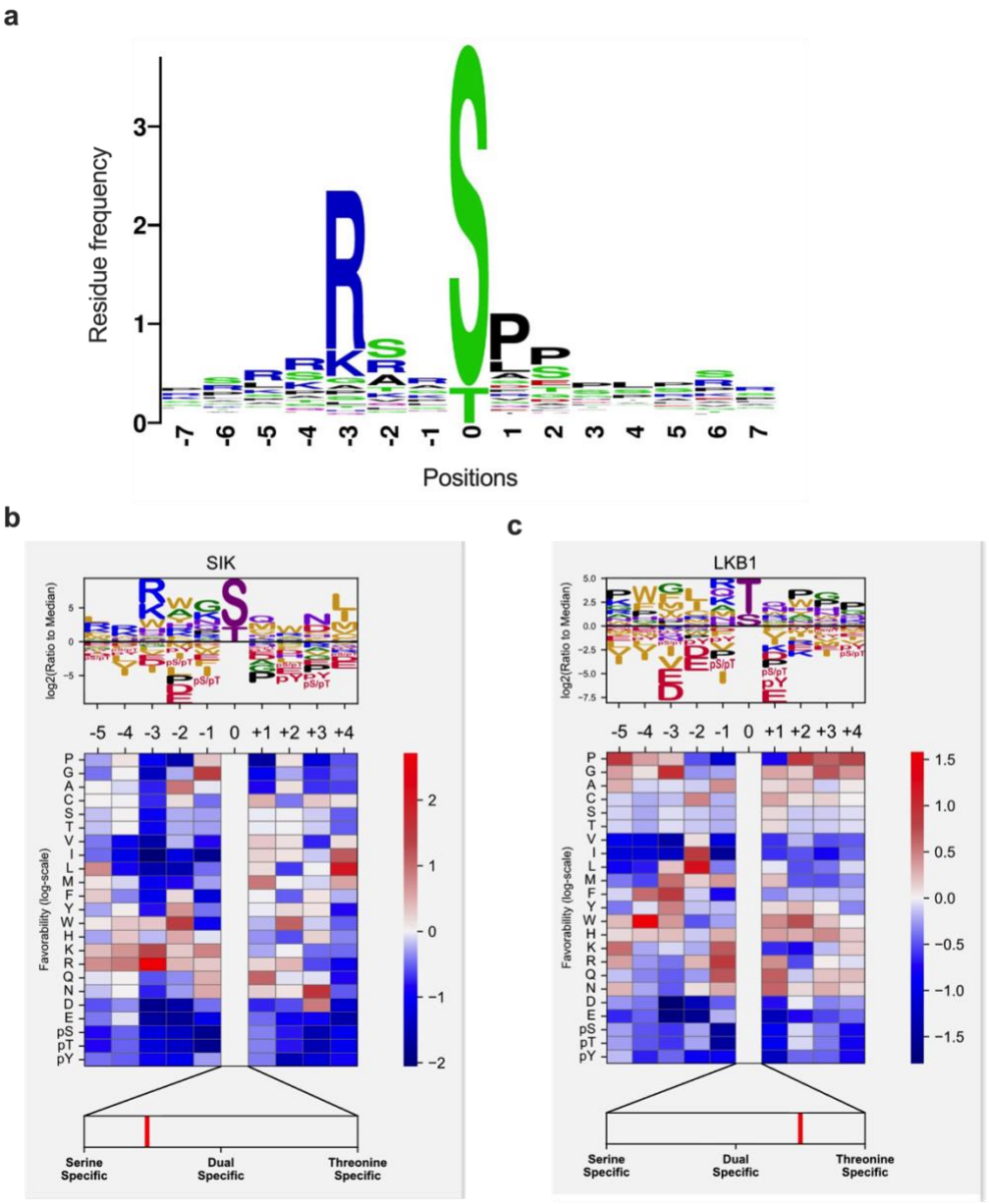

Fig. 3.7 **SIK1 and LKB1 motif sequences.** (a) Sequence motif logos generated using FASTA sequences on WebLogo for SIK1 SCN KALIP dataset (Crooks et al., 2004). Residue positions on the x-axis. Residue size and height representing the probability of it appearing at the particular position in the dataset. (b) SIK1 and (c) LKB1 motif sequences from PhosphoSite. Org. Favourability for each residue at corresponding positions is indicated with the heatmap and scale.

For downstream functional analysis, we have chosen to include the phosphosites that have an SIK1 motif percentile of over 80%. We filtered to a total of 638 phosphopeptides, which mapped to 506 unique phosphosites and 388 unique phosphoproteins. Phosphosites with only an LKB1 motif were excluded. Using the list of 388 phosphoproteins, we conducted a series of functional analyses to understand which processes and components are enriched (Supp. Table 3.1). Gene Ontology (GO) Biological Processes (BP) showed that the dataset is enriched for "neurogenesis" and "neuron development", including proteins such as BRAF, BRSK1 and SYNGAP1. These proteins also interact with processes and pathways involved in synaptic, postsynaptic regulation and synaptic plasticity. In addition, "cell junction" and "regulation of cellular component organization" were also top GO:BP terms (CACNA1B, CX43). These proteins are also involved in the maintenance of location in cells, such as ion-transport channels and gap junctions, indicating a role of SIK1 in intercellular communication in the SCN (Fig. 3.8a). These findings correspond to the enrichment of Cellular Components (GO:CC), which also showed enrichment in synaptic components, dendrites and neuronal cell body (ABLIM1, ARFGAP1) (Fig. 3.8b). Molecular function (GO:MF) terms showed enrichment in protein kinase binding and protein serine/threonine kinase activity (PRKD1, HDAC4), indicating that the substrates are involved in complex downstream kinase networks. GTPase regulator activity and lipid binding activity were significant terms including proteins such as ARFGAP1, ARHGEF6/7 and RASGRF1 sites were detected. CAMK2G, CAMKK2 and UBR4, categorized into calmodulin binding and involved in calcium regulation (Fig. 3.8c). Key KEGG pathways include tight junction, synaptic vesicle and mTOR signalling (BRAF,

CLIP1). These pathway analysis results of SIK1 KALIP showed that SIK1 is involved in multiple synaptic signalling pathways, intercellular communication and maintaining a cohesive kinase network in the SCN.

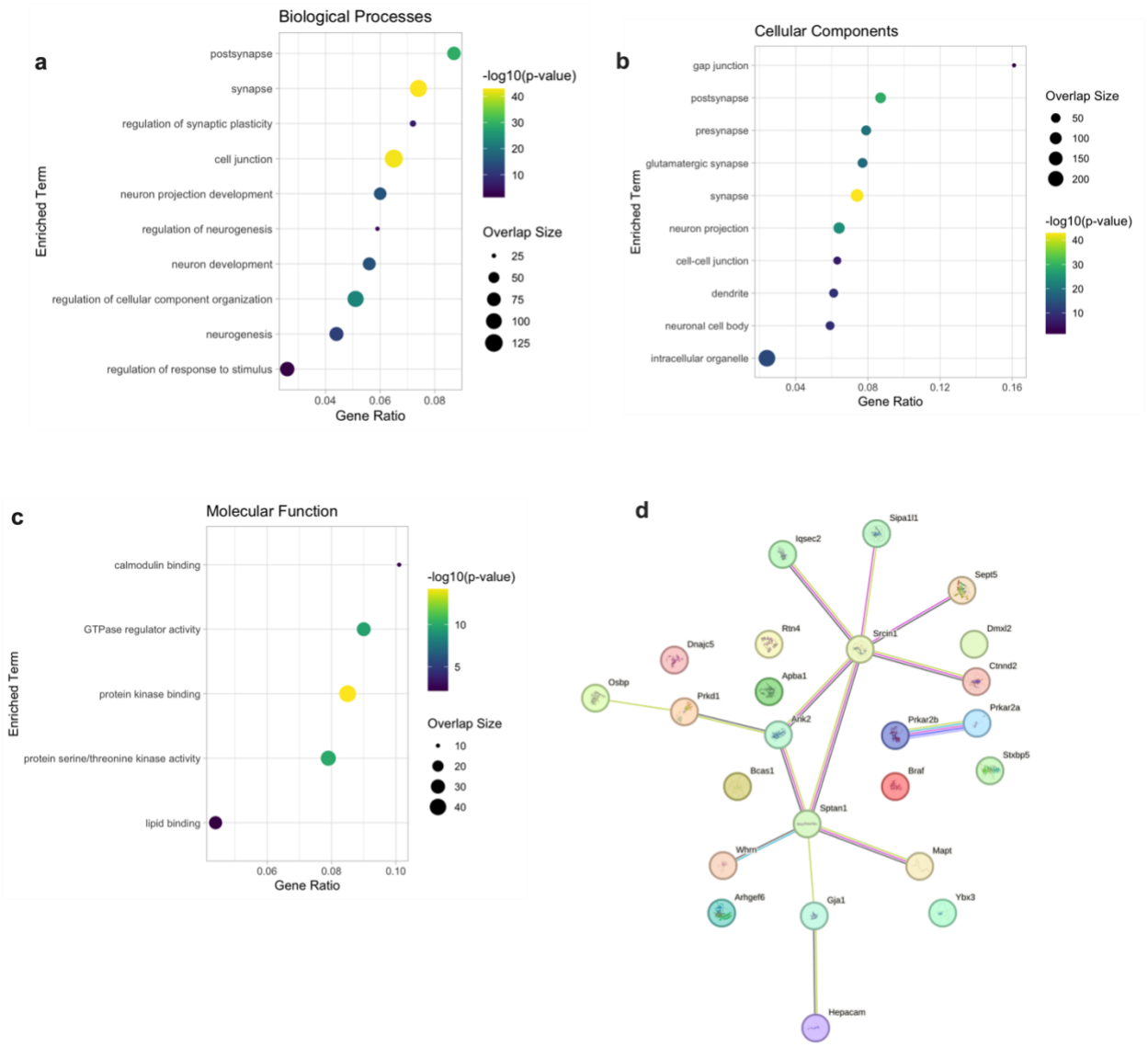

Fig. 3.8 **Gene Ontology (GO) and STRING protein-protein interaction analysis of SIK1 SCN KALIP substrates.** GO functional analysis of detected substrates in SIK1 SCN KALIP dataset. Top and selected GO (a) Biological Processes (BP), (b) Cellular Components (CC), and (c) Molecular Function (MF) terms were listed. -log10(p-value) and overlap size were calculated and programmed in R Studio. STRING protein-protein interaction of detected substrates in SIK1 SCN KALIP dataset, showing (d) synapse. Connecting lines show interaction between proteins.

3.2.5 Direct substrates of SIK1 in the SCN

As SIK1 is light-induced, the *in vivo* phosphoproteome was obtained by collecting SCN samples from WT and SIK1 KI mice exposed to a shifted LD cycle previously by Dr. Zeinab Wakaf (Wakaf et al., 2026). Samples were collected 2 hours into the onset of dark phase on the day of the shift, where the WT animals were asleep and the SIK1 KI animals were awake. Quantitative phosphoproteome detected a total of 7225 phosphosites that mapped to 2886 unique phosphoproteins. Differential analysis identified 29 phosphosites that were significantly changing between WT and SIK1 KI animals after LD cycle shift (padj<0.1) (Supp. Table 3.1). These proteins were shown to be associated with synaptic plasticity and calcium signaling, which overlapped with the pathways we identified in the *in vitro* Pro-KALIP assay. To eliminate false positives and impurities in the *in vitro* assay, we overlapped the 388 phosphoproteins detected in SIK1 KALIP with the *in vivo* SCN phosphoproteome in WT and SIK1 KI animals. We narrowed down to a total of 170 phosphoproteins that were direct substrates of SIK1 with a SIK1 signature (Fig. 3.9a), of which STRIP1 S335, DMXL2, and SRRM1 were statistically significant in the *in vivo* phosphoproteomics (Supp. Table 3.1). Several of these proteins overlapped with datasets associated with sleep need and pressure. Wang et al proposed a list of 80 proteins, sleep need index phosphoproteins (SNIPPs), that correlated with increased sleep need (Wang et al., 2018). 5 of these SNIPPs overlapped with the direct substrates of SIK1, including SRCIN1, CASKIN1, all involved in synaptic function and pathways (Fig. 3.9b). In addition, Bruning et al found synaptic proteins that maintain rhythmicity under sleep deprivation, relating to sleep pressure. 2

of these proteins overlapped with our dataset, PLCH2 and RTN4, involved in Ca^{2+} signaling and synapse formation (Brüning et al., 2019) (Fig. 3.9c).

We performed a STRING functional enrichment analysis to explore the predicted protein-protein interactions of the 170 direct substrates of SIK1. The two prominent hubs of interactions were “synapse” and “cell junction”. In the synaptic protein hub, SRCIN1 was in the center connecting to IQSEC2 and CTNND2, proteins also relating to synaptic plasticity. PRKAR2B and PRKAR2A were also part of the PKA network that are shown to be involved in sleep regulation (Ueda et al 2024). In addition, cell-cell communication and channel protein interactions were identified, notably KCNJ10 and CX43. These proteins create a network in synapse stabilization and cell matrix adhesion (Fig. 3.8d).

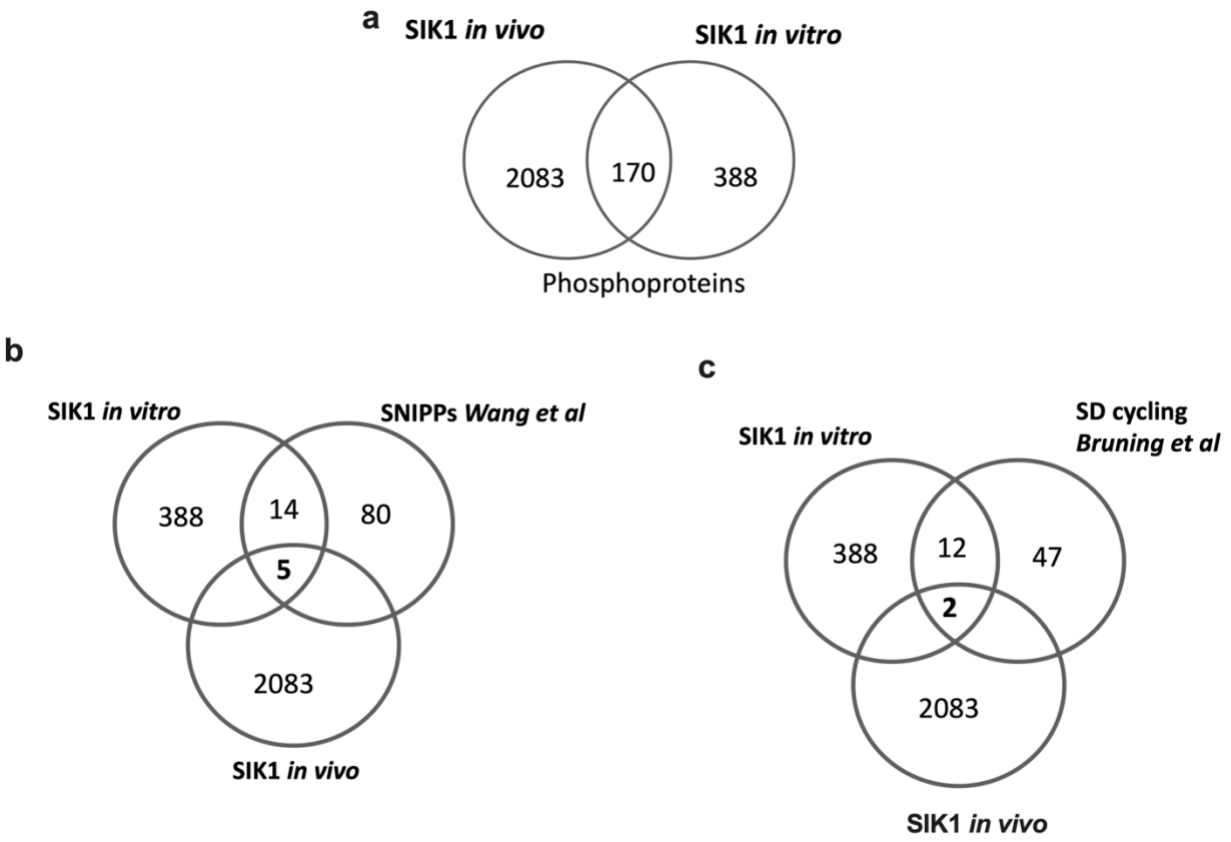

Fig. 3.9 **Overlaps with the SIK1 *in vivo* phosphoproteome and other key datasets.** Venn diagrams of overlapping phosphoproteins between SIK1 *in vitro* KALIP assay and (a) SIK1 in vivo phosphoproteome, (b) SIK1 *in vivo* phosphoproteome and SNIPPs (Wang et al., 2018) and (c) SIK1 *in vivo* phosphoproteome and cycling phosphoproteins (Brüning et al., 2019b).

By ranking the list of 170 substrates by SIK1 motif percentile, p-value from the in vivo phosphoproteome and Pro-KALIP raw signal intensities, we summarized the key substrates (Table 3.1). Of which, Striatin-interacting protein 1 (STRIP1) regulates cell morphology and cytoskeletal organization. Being part of the core STRIPAK complex, essential for PP2A subunits (Hwang & Pallas, 2014), STRIP1 is shown to control daytime CLOCK dephosphorylation in *Drosophila* (Andreazza et al., 2015). Serine/arginine repetitive matrix protein 2 (SRRM2) helps to regulate alternate splicing and the organization of nuclear speckles. The SRRM2 S1068 phosphosite that we

detected is observed to be hyperphosphorylated in the brains of Alzheimer's Disease (AD) mouse models at early onset stages and is known to be an early marker for AD as it affects RNA splicing of synaptic genes (Tanaka et al., 2018). Gap junction alpha-1 (GJA1) or Connexin-43 (CX43) is also essential for intercellular communication and astrocytic coupling (Reppert & Weaver, 2002; Martin-Marques et al., 2019; Li et al., 1996; Cooper et al., 2026). Other key proteins include Reticulon-4 (RTN4) and Sodium/potassium/calcium exchanger 2 (NCKX2), involved in the structure of endoplasmic reticulum (ER) (Jozsef et al., 2014) and temperature-compensated Ca^{2+} signalling (Kon et al., 2021)(Table 3.1). The normalized KALIP signal with LKB1 trimer excluded was plotted against the log-transformed signal to show that phosphosites with high intensity were SIK1-specific signals. Together, we found that SIK1 is involved in regulating synaptic function in the SCN through direct phosphorylation (Fig. 3.10b).

Protein names		Positions	Letter	Functions/Pathways
Striatin-interacting protein 1	STRP1	335	S	Cell morphology and cytoskeletal organization
SRC kinase signaling inhibitor 1	SRCN1	1054	S	Protein kinase binding; SNAP-25/SRCIN1 pathway
Gap junction alpha-1 protein (GJA1) (Connexin 43)	CXA1	373	S	Cell communication, actin stabilization
Reticulon-4	RTN4	165	S	ER regulation and inhibition of neurite outgrowth in the CNS
SWI/SNF complex subunit	SMARCC2	302	S	Chromatin remodeling, Ras-PI3K, AKT pathway
Serine/arginine repetitive matrix protein 2	SRRM2	1068	S	Alternative splicing, nuclear speckles
Ankyrin-2	ANK2	3786	S	Localization; membrane stabilization of ion transporters and channels
IQ motif and SEC7 domain-containing protein 2	IQSEC2	1148	S	Guanyl-nucleotide exchange factor activity; chemical synaptic transmission
Serine/threonine-protein kinase D1	KPCD1	203	S	Downstream of PKC; MAPK8/JNK1 and Ras signaling
Septin-5	SEPT5	13	T	Filament forming cytoskeletal GTPase
Signal-induced proliferation-associated 1-like protein-1	SI1L1	1564	S	Ras signaling; GTPase activity
Caskin-1	CASKIN1	1268	T	Scaffolding protein
Oxysterol-binding protein 1	OSBP1	238	S	Lipid transporter between the Golgi complex and ER membranes
DnaJ homolog subfamily C member 5	DNAJC5	10	S	Co-chaperone for SNAP-25; exocytosis; presynaptic function
1-phosphoatidylinositol 4,5-bisophate phosphodiesterase eta-2	PLCH2	987	S	Second messenger molecules (DAG and IP3); calcium-sensitive
Rabphilin-3A	RP3A	271	S	Regulates the release of neurotransmitters at synapses

Table 3.1 **List of selected direct substrates of SIK1.** Selected direct substrates of SIK1 were listed in a table with protein full name, protein name, phosphorylated residue, phosphorylated position and summarized functions and pathways. Direct substrates were not organized in any particular order of significance.

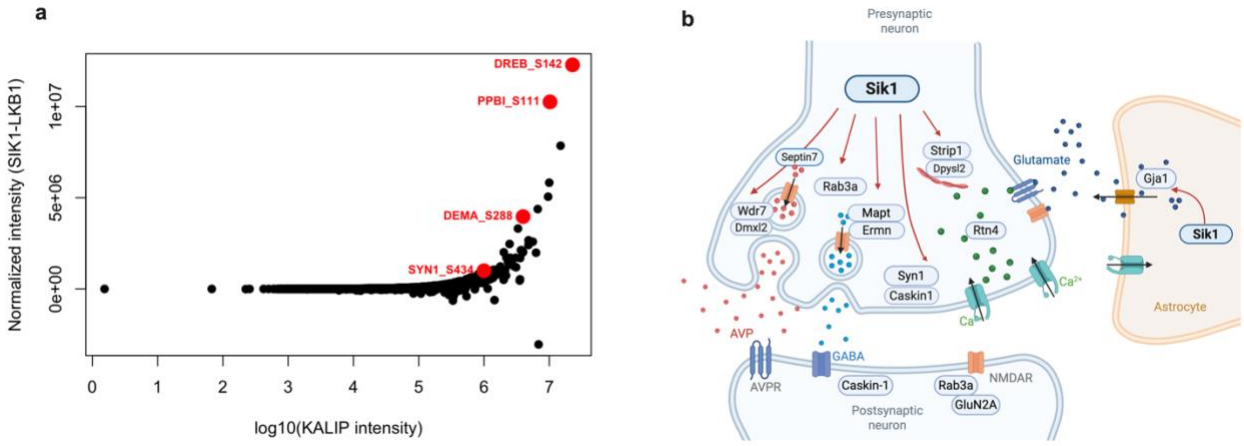

Fig. 3.10 **Pro-KALIP signals and proposed schematic diagram** (a) Pro-KALIP raw intensity differences in quantity of phosphorylated peptides between the sample treated with SIK1+LKB1 trimer versus LKB1 trimer alone in the SCN, plotted against the log10-transformed intensity of peptides detected in SIK1 + LKB1 trimer. Each point represents an individual phosphosite; selected differential phosphosites are highlighted in red. (b) Schematic diagram of SIK1-mediated substrates regulating synaptic function validated through Pro-KALIP.

3.2.6 SIK1 phosphorylates CX43 at S373 and modulates hemichannel opening

As CX43 S373 was detected as a top hit in the SIK1 KALIP dataset, we chose to investigate the direct functional effect of SIK1 on the site.

CX43, along with 12 other connexin protein subunits, form hemichannels that facilitate ion transport in the extracellular space, including ATP and glutamate (De Vuyst et al., 2009). Two hemichannels form a gap junction that facilitates intercellular communication such as the transport of Ca^{2+} and cAMP. Research has shown that extracellular ATP release is directly linked to hemichannel opening (Kang et al., 2008), as there is an efflux of ATP and other ions through CX43 hemichannels. It is also shown that hemichannels respond to different stimuli, including intracellular Ca^{2+} and glutamate changes (De Vuyst et al., 2009).

We aimed to investigate the role of SIK1 on CX43 and in particular, how it affects hemichannel function and regulation. CX43 S373 detected in the *in vivo* phosphoproteome had a log2FC of –0.53 (SIK1 KI/WT), showing that there was higher expression in the WT animals compared to SIK1 KI animals. The SIK1 KALIP dataset also resulted in a positive signal with purified exogenous SIK1 kinase added. Therefore, we predicted that SIK1 activates the phosphorylation of CX43 at site S373.
To effectively explore the SIK1-CX43 relationship, we developed an *in vitro* reporter assay using C6 glioma cells. Though it does not embody the complex network and

rhythmicity of the SCN, it provides direct biophysical outputs in response to intracellular Ca^{2+} changes. C6 glioma cells have low expression levels of endogenous CX43, and CX43 was overexpressed to isolate the effect from other connexins. Extracellular ATP release was used as a functional marker for hemichannel opening using an ATP sensor, where luminescence is directly proportional to extracellular ATP concentration in the cell lysate. Calcium ionophore-induced intracellular Ca^{2+} changes were used as stimuli for hemichannel opening. In C6 glioma cells transfected with CX43-WT, at varying concentrations of ionomycin (1μM to 5μM), it was shown that the largest extracellular ATP release occurred between 2.5μM and 3μM (Supp. figure 3.3). The dose response curve was shown in a bell shape, with decreasing ATP release at high concentrations, indicating saturation or assay capacity limit.

We first explored C6 glioma cells under baseline and CX43-transfected conditions. We showed that there was no Ca^{2+}- induced extracellular ATP release under baseline (untransfected) conditions. As C6 cells express low endogenous levels of CX43, there was no functional CX43 protein subunits present in the cells to facilitate extracellular communication. Luminescence (RLU) was measured as extracellular ATP concentration and signals were normalized to baseline bars as a percentage (%). 100% corresponds to the average of baseline bars (De Vuyst et al., 2009). When overexpressed with CX43-WT, Ca^{2+}-induced extracellular ATP release was increased by 83% at 2.5μM of ionomycin, which validates the significant role of CX43 and intracellular Ca^{2+} as a stimulus (Fig. 3.11a). We next investigated the relationship between SIK1 and CX43 by co-transfecting C6 glioma cells with CX43-WT and SIK1-WT. As we predicted, SIK1 has

an activating effect on CX43, so we reduced the ionomycin concentration to 2μM to avoid saturation of ATP release. We showed that Ca^{2+}-induced extracellular ATP release and hemichannel opening were significantly higher in SIK1 WT co-expressed cells than CX43 alone (38% more) (Fig. 3.11b).

We next explored the role of the site S373 on hemichannel opening by mutating the serine residue to the non-phosphorylatable form, alanine (A). Ca^{2+}-induced extracellular ATP release was abolished when C6 cells were transfected with CX43-S373A (Fig. 3.11c). We then co-transfected C6 cells with SIK1 WT and CX43-S373A, and we observed that the Ca^{2+}-induced extracellular ATP release effect was similarly abolished (Fig. 3.11d). Power analysis revealed that all conditions had a large effect size and reach statistical power of over 90%. These results indicated that the site S373 is an important activating site for CX43 hemichannel opening, and SIK1 modulates hemichannel opening and functions of CX43 through phosphorylation at site S373.

In the calcium signalling assay in CX43-transfected C6 glioma cells, we observed a significant increase in intracellular Ca^{2+} levels with increasing concentration of ionomycin (2μM to 50μM) (Supp. Fig. 3.4). These results gave us confidence that the changes in extracellular ATP release were SIK1 and CX43-phosphorylation dependent. Changes were also not due to cell death, confirmed with the cell viability assay (Supp. Fig. 3.5).

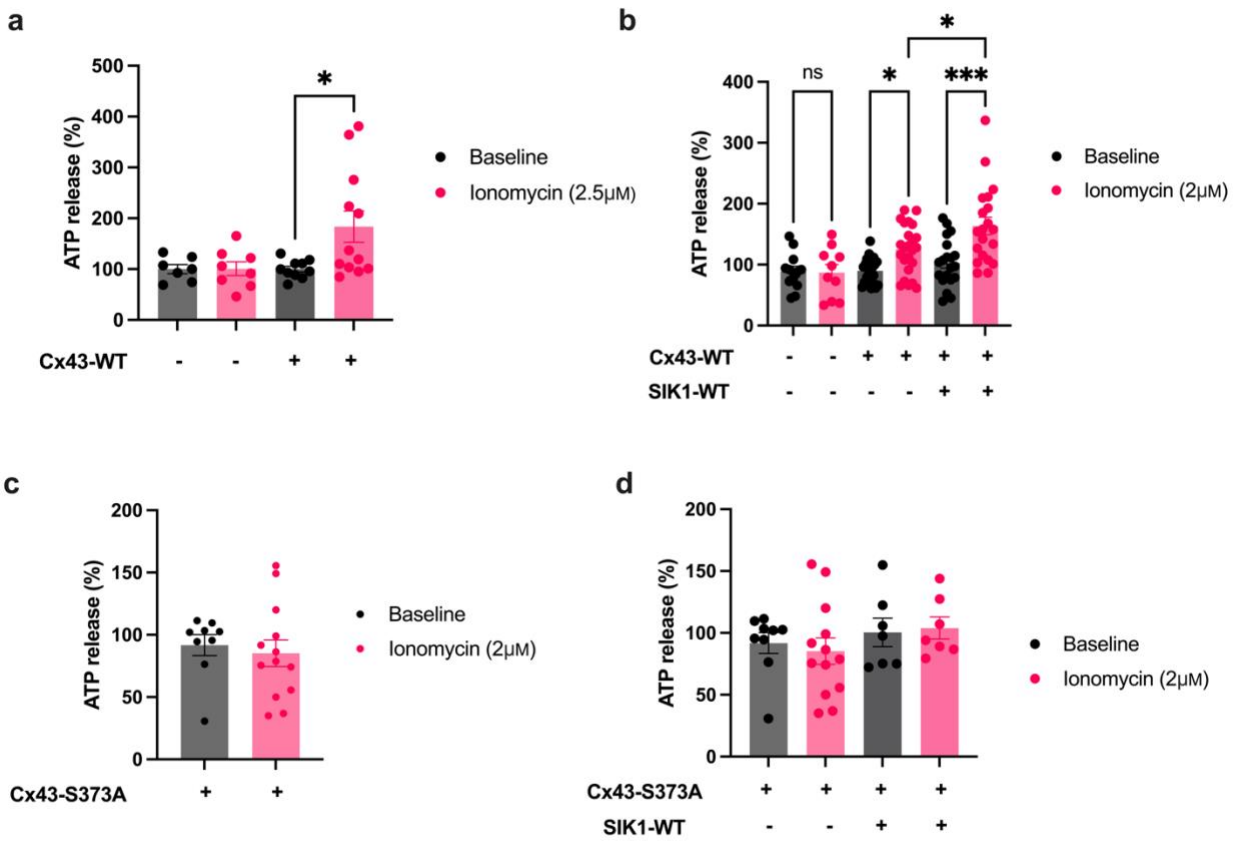

Fig 3.11 **The effect of SIK1 on Cx43 hemichannel opening.** Extracellular ATP measurement using ATPGlo Sensor Luminescence assay. (a) Extracellular ATP release (%) measured in WT and CX43-WT transfected C6 glioma cells. (b) Extracellular ATP release (%) measured in WT, CX43-WT and SIK1-WT co-transfected C6 glioma cells. (c) Extracellular ATP release (%) measured in WT and CX43-S373A transfected C6 glioma cells. (d) Extracellular ATP release (%) measured in CX43-S373A and SIK1-WT co-transfected C6 glioma cells. Alterations in intracellular calcium levels with calcium ionophore (ionomycin). Luminescence readings were taken 5 minutes after ionomycin addition. n=15-20. (a)(c) Unpaired t-test. (b)(d) One-way ANOVA with Tukey's multiple comparisons test. *p < 0.05, ** p<0.01, *** p< 0.001, **** p<0.0001.

3.2.7 SIK1 adjusts the permeability of Cx43 hemichannels

To further understand how SIK1 regulates CX43 hemichannel functions, we performed a DAPI dye uptake assay to investigate the permeability of hemichannels in C6 glioma cells. We transfected C6 glioma cells with CX43 and CX43 S373A and captured fluorescence images before and after the addition of 5μM of DAPI. The T0 representative image captured the baseline signal with no DAPI addition (Fig. 3.12a), which was consistent across all conditions. T1 images were acquired 30 seconds after the addition of DAPI, showing the level of DAPI dye uptake into C6 cells (Fig. 3.12b). At T1, significantly more cells had DAPI fluorescent dye in C6-CX43 cells, whereas untransfected C6-WT cells had minimal visible DAPI. C6 cells transfected with S373A, though significantly higher than untransfected cells, the difference to C6-CX43 cells was visually indistinguishable (Fig. 3.12a-b).

The fluorescent signals were counted, normalized to the background and the total area. C6 glioma cells transfected with CX43-WT had a significantly higher number of DAPI fluorescent cells (701.4) than untransfected cells (18.5). CX43-WT cells were also higher than CX43-S373A (511.7) but not statistically significant (Fig. 3.12c). The difference between CX43-WT and CX43-S373A did not reach statistical significance. Therefore, these data should be treated as preliminary. A larger and adequately powered experiment is required to draw reliable conclusions.

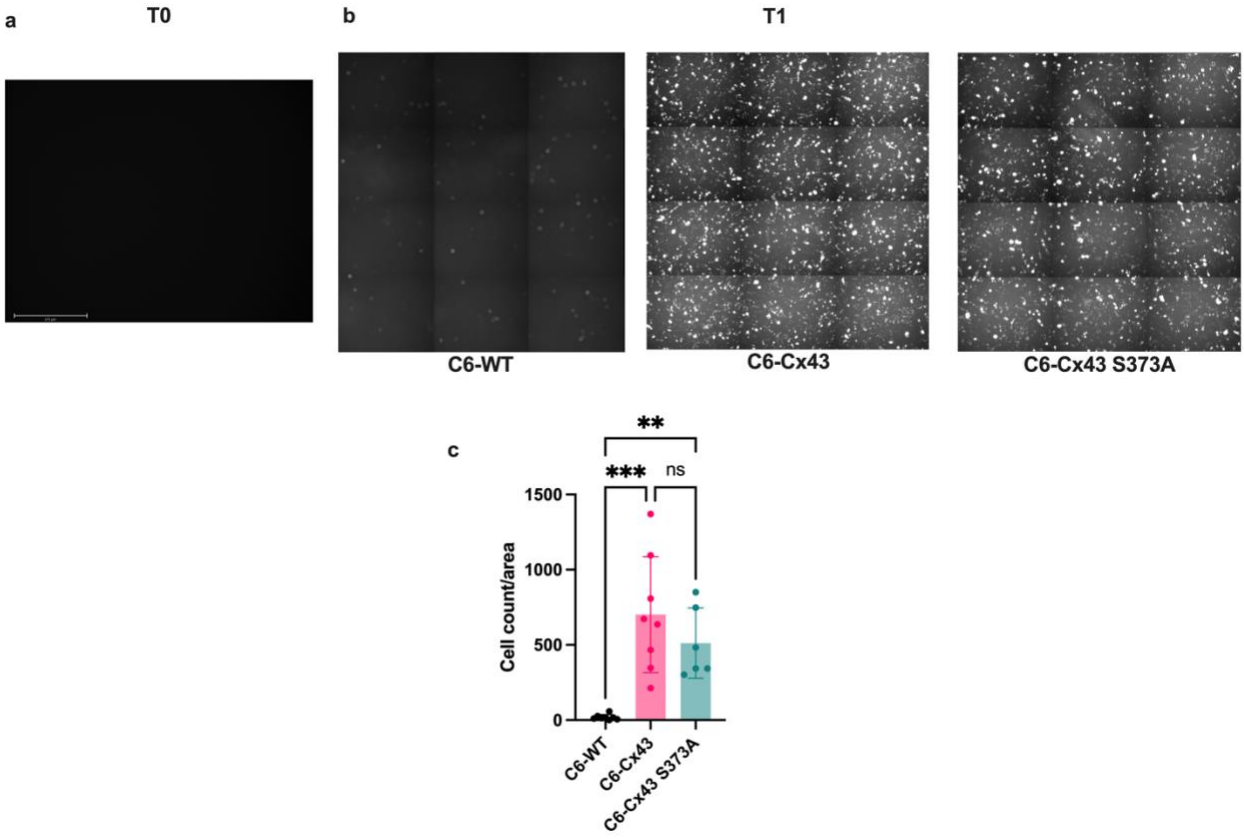

Fig. 3.12 **Uptake of DAPI dye in C6 glioma cells.** (a) Representative fluorescence image of DAPI dye uptake in C6 glioma cells at T0 before DAPI addition. No differences in fluorescence observed between untransfected and CX43-transfected cells. (b) Representative fluorescence images of DAPI dye uptake in WT, CX43 transfected and CX43 S373A transfected C6 glioma cells taken 30 seconds after DAPI addition (T1). (d) Cell count plots of C6 glioma cells with DAPI fluorescence signal at T1. Quantification with ImageJ and normalized to image area and background. Scale bar = 275µm. Ordinary one-way ANOVA with Tukey's multiple comparisons test. ** $p<0.01$ *** $p<0.001$. Mean ± SEM, n=5-7.

3.3 Discussion

3.3.1 Implications of Pro-KALIP

By utilizing the Allen Brain Atlas MERFISH and 10x scRNAseq datasets, we confirmed Sik1's gene expression in different brain regions and cell types (Yao et al., 2023). We showed that *Sik1* is mainly expressed in the SCN region and has low expression in other regions such as the cortex and hippocampus. As the SCN region occupies 0.03% of cells in the brain, total *Sik1* expression is also lower. Overlapping with the 10x scRNAseq dataset, we showed that *Sik1* in the SCN region is expressed dominantly in GABAergic neurons. All SCN neurons are comprised of the inhibitory neurotransmitter, GABA. It was shown that GABA facilitates SCN dorsal and ventral coupling and mediates circadian oscillations and firing rhythms (Ono et al., 2021d). These findings showed that *Sik1* is essential for SCN-specific regulation, consistent with the prominent circadian entrainment phenotype and Process C regulation.

As previous Pro-KALIP methods were developed in cell lysate, we optimized and tailored the protocol to large-scale brain tissue lysate. SIK1 kinase concentration and kinase reaction time were determined using *in vitro* assays. We confirmed the effect of LKB1:STRADα:MO25α trimer on the activation of SIK1 kinase activity using both *in vitro*, AMARA, and *in vivo*, dephosphorylated brain lysate, substrates. The trimer complex is a triad of kinase-substrate interaction. The subunit MO25α interacts solely with STRADα/β, and STRADα, as a substrate of LKB1, binds through the catalytic domain, resulting in a stable trimer interaction (Boudeau et al., 2003b).

Autophosphorylation of LKB1 is greatly enhanced by binding with STRADα to increase catalytic activity. Our results also showed significant autophosphorylation of LKB1 as it forms a trimer with STRADα and MO25α, compared to baseline control conditions. We have also validated that autophosphorylation of LKB1 is high in the presence of SIK1, an AMPK kinase. These showed that in addition to being an upstream master kinase, LKB1 also has an interdependent relationship with SIK1 activity.

Out of 2135 unique phosphosites detected from SIK1 KALIP in the SCN, we verified significant enrichment for the SIK1 motif, while kinases in other families were significantly depleted. We confirmed that the dataset was enriched with serine-specific phosphosites and detected residues that are favourable to SIK1. In addition, we also detected residues that are favourable to LKB1 at a few positions in the sequence motif. The motif contingency test for LKB1 showed significant depletion. These findings showed that SIK1 KALIP had a blend of SIK1 and LKB1 motifs, but with the highest compatibility and enrichment of SIK1 sites. The interdependent relationship between SIK1 and LKB1 in the context of the SIK1 KALIP assay also generated a hub of unique LKB1 direct substrates and sites with both SIK1 and LKB1 motifs, in addition to SIK1 direct substrates. As a result, we prepared an LKB1 trimer-only sample as a background signal for analysis, and LKB1-specific substrates were excluded for downstream processing. As we observed incomplete dephosphorylation and impurities in Pro-KALIP preparation, we subsequently overlapped the list of SIK1-specific substrates with the *in vivo* brain phosphoproteome, which gave us 170 direct substrates of SIK1.

The optimized Pro-KALIP assay improved the feasibility of using brain tissues as substrates to detect direct substrates of kinases and provides a complete dataset to explore downstream effects and signalling of SIK1. It enables efficient and specific substrate profiling in brain tissues for all applicable kinases in diverse contexts.

3.3.2 Proposed signalling pathways of direct substrates of SIK1

Functional analysis from the GO profiler and STRING protein-protein interaction of the direct substrates of SIK1 showed distinct pathways and processes. Enrichment of presynaptic and postsynaptic pathways was identified, mapping to a significant hub of synaptic interactions involved in synapse maintenance and neurotransmitter release. For instance, Synapsin-1 (SYN1) is important for synaptic vesicle formation, specifically the site detected S605 that is shown to be involved in actin polymerization (Chhabra et al., 2025). ITSN2 (forms clathrin-coated vesicles), DMXL2 and WDR7 are active in the synaptic vesicle and play a role in endocytosis. Specifically, a deficiency in ANK2 is repeatedly detected in autism spectrum disorder and neurodevelopmental disorders (Yoon & Penzes, 2025). In parallel, we detected an enrichment for synaptic scaffolding proteins localized in the postsynaptic terminals. SHANK3 is shown to be a key autism risk gene and maintains cortical functional connectivity (Pagani et al., 2019). CASKIN-1, co-localizing with SYN1 and PSD-95 in the synapse, is implicated in neural functions. CASKIN1-KO animals showed low memory retention, anxiety-like behaviour and a wide range of phenotypes (Katano et al., 2018). Rabphilin-3A (RPH3A) also plays an important role in long-term potentiation, specifically interacting with GluN2A and stabilizing NMDA and AMPA receptors in the post-synapse (Ferrari et al., 2022; Stanic

et al., 2015). In the pre-synapse, it is associated with synaptic vesicles and neurotransmitter release processes (Shirataki et al., 1994). CTNND2 is involved in postnatal synapse maturation and maintenance in adulthood. The loss of CTNND2 is also coupled with synaptic deterioration of SYNGAP1 (Assendorp et al., 2024).
In addition, key channel proteins were identified. For instance, SCN2A encodes the sodium channel protein NaV1.2, which is involved in neuronal communication and the initiation of action potentials. KCNJ10 and KCNAB2 encode Kir4.1 and voltage-gated potassium channels, respectively, important for electrical coupling and excitability. KCNJ10 and CX43 (GJA1) are heavily enriched in glial cells, facilitating cell-cell communication and junction. CACNB1 is part of the calcium channel beta subunit family.

Exploring potential mechanisms, a large group of these synaptic proteins were enriched and expressed in the glutamatergic synapses and calmodulin binding. With the light-inducible phenotype of SIK1, the prominent presence of proteins such as SYNGAP and SHANK3 in the glutamatergic terminals reinforces downstream processing from the light input (Foster et al 2020). Calcium channel proteins (CACNB1) and Ca^{2+} regulating proteins (RASGRF2, DCLK1, PLCH2) are implicated in the calcium responses to light input, reflected in the phenotype of SIK1.

Furthermore, SIK1 acts as a master kinase that coordinates other major kinases, forming an interconnected network to regulate and maintain synchronized synaptic function and calcium dynamics in the SCN through direct phosphorylation. Ser/Thr protein kinase D2 (PRKD2), which acts downstream of PKC and is part of the

MAPK/ERK signalling pathway, and BRAF, a component of the RAS/MAPK pathway (Wang et al., 2020), were also detected as direct substrates of SIK1. Although PKCγ was not detected in the Pro-KALIP assay, our recent study demonstrated and validated that SIK1 regulates Ca^{2+}-dependent PKC activity. In addition, KSEA analysis identified PKCγ as an upstream regulator of SIK1 substrates such as SYN1 and MAPT (Appendix 1). Linking back to sleep and circadian context, we detected a few phosphoproteins and sites that were previously shown in the literature. Using SIK1 SCN Pro-KALIP, we detected the PKA subunit, PRKAR2B, which the knockout line was shown to have a significant reduction in sleep duration and exhibit stabilized wakefulness (Park et al., 2020; Wang et al., 2024a).

In addition, we overlapped the list of direct substrates of SIK1 with other key datasets that are associated with sleep need and synaptic homeostasis. We identified five substrates overlapping with SNIPPs, SIPA1L1, IQSEC2, SRCIN1, CASKIN1 and PITPNM2. SRCIN1 is a SNAP-25 interacting protein located in the pre- and post-glutamatergic synapses. It is heavily implied in schizophrenia, and the *blind-drunk* (Bdr) model is widely used for the purpose. It is shown that these mice exhibit fragmented activity rhythms and disturbed sleep patterns (Oliver et al., 2012). Similarly, IQSEC2 mutations are associated with autism and epilepsy. It additionally promotes the exchange of GDP for GTP on ARFs, specifically ARF6, connecting synaptic trafficking and neuronal proteins (Brant et al., 2021). SIPA1L1 KO mice also exhibit significant behavioural abnormalities and increased anxiety (Matsuura et al., 2022). These

identified targets of SIK1 point to synaptic function, further supporting the link between synaptic homeostasis and sleep need (Brüning et al., 2019b).

3.3.3 SIK1 and CX43 relationship

We chose to investigate the relationship between SIK1 and our top hit CX43, specifically the site S373. In our *in vivo* brain phosphoproteome, we observed an increase of CX43 S373 phosphorylation in WT animals compared to SIK1 KI animals, showing that SIK1 activates phosphorylation. Cx43, along with 12 other connexin (CX) protein subunits, makes up hemichannels and gap junctions for extracellular and intercellular communication between two neighbouring cells. CX43 also couples astrocytes extensively, allowing passage of small ions up to a molecular weight of 1000 such as Ca^{2+}, cAMP, etc. CX43, unlike its other connexin counterparts, is expressed in both astrocyte gap junctions and ependymocyte junctions, which matches the expression of Sik1 in ependymal astrocytes (Rash et al., 2001). Researchers have shown that CX43 is a substrate of Akt kinase downstream of the PI3K/AKT pathway. The site S373 is also shown to be phosphorylated by Akt and is associated with increasing gap junction size and CX43 hemichannel-dependent membrane permeabilization (Salas et al., 2015). *In vitro* CX43 S373 phosphorylation is also required for ATP release to the extracellular medium (De Vuyst et al., 2009). Kang et al indicated that hemichannel opening is directly linked to extracellular ATP release. There are also key implications that CX43 hemichannel opening responds to various stimuli, notably intracellular Ca^{2+} changes (Kang et al., 2008).

As CX43 plays a key role in hemichannels and gap junctions, we aimed to investigate the effect of SIK1 on CX43 function in cell-cell communication. Using calcium ionophore (ionomycin) as a stimulus, we found that co-expression of Cx43 and SIK1 WT in C6 glioma cells activated Ca^{2+}-induced hemichannel opening more than Cx43 alone. This showed that SIK1 facilitates and activates hemichannel opening. Mutating the site S373 to a non-phosphorylatable alanine (A) abolishes the augmentation, marking S373 as an activating site for hemichannel opening. Co-expression of SIK1 WT and the mutated site Cx43 S373A in C6 glioma cells also abolished the effect, showing that SIK1 modulates Ca2+ induced hemichannel opening through phosphorylating the activating site S373. Cx43, as the most abundant connexin expressed by astrocytes in the brain, exhibits different permeabilities towards ions and dyes (Sáez et al., 2018). As SIK1 modulates extracellular ATP release, facilitating hemichannel opening, we conducted a complementary DAPI dye uptake experiment to investigate how SIK1 modulates the permeability to cationic dyes. The comparison between Cx43-WT (701.4 DAPI-positive cells) and Cx43-S373A (511.7) did not reach statistical significance (n=5-7), and no conclusion can be drawn regarding the role of S373 in cationic dye permeability. The finding that untransfected C6 cells showed minimal DAPI entry relative to Cx43-transfected cells is consistent with published evidence that Cx43 expression is required for hemichannel function and serves as a positive control for the assay. The DAPI data are therefore preliminary; whether S373 phosphorylation influences hemichannel ionic selectivity requires a larger, adequately powered experiment. Other dyes such as 5(6)-carboxyfluorescein and fura-2 could also be explored in the future. It was previously shown that larger molecular size is correlated with lower levels of uptake (Li et al., 1996).

As various neuronal targets of SIK1 were well-characterized and validated, these findings provided a novel astrocytic target of SIK1.

The interplay between neurons and astrocytes in the TTFL was discussed extensively in previous research. In Cry1/2-null mice, Brancaccio et al showed expression of Cry1:EGFP in astrocytes solely generated stable Per2:Luc oscillations, supporting the self-sustaining astrocytic TTFL. The inhibition of CX43 by TAT-Gap19, a mimetic peptide, significantly reduced amplitude and period lengthening of Per2:Luc oscillations in SCN slices, in addition to the release of gliotransmitters ATP and glutamate (Brancaccio et al., 2017, 2019). It was shown that glutamate is a key mediator of astrocytic circadian time-keeping.

Research has suggested that gap junctions play an important role in electrical coupling and the synchronization of individual circadian clocks (Rash et al., 2007). Previous research has also proposed the role of connexins in regulating the sleep-wake cycle in animal models. Ali et al has shown that under constant light (LL), double knockout (DKO) mice of CX30 and CX43 could compensate for the dampening of nocturnal activity and maintain consistent levels. Re-entrainment after a 6hr phase delay was slightly influenced in the DKO animals. There were no significant differences in core clock parameters such as period lengths or amplitude (Ali et al., 2019). These findings align with the SIK1 KI circadian phenotype that we observed with regulation in re-entrainment to light and Process C. CX43 cKO GFAP mice also exhibited excessive sleepiness and fragmented wakefulness during the nocturnal active phase. It is shown that orexin-

producing neurons in the lateral hypothalamic area (LHA) have reduced excitability in these mice (Clasadonte et al., 2017).

Our recent study conducted single-cell sequencing using SIK1 KI and WT SCN samples to explore cell-type changes. We observed large transcriptional differences in astrocytes, which sets the basis that the changes could be facilitated through CX43 as a direct substrate of SIK1 (Appendix 1; (Wakaf et al., 2026). Though the role of CX43 in entrainment and circadian regulation requires further investigation, these findings support that SIK1 network spans across cell types.

Our results propose a pathway in which SIK1 phosphorylates CX43 and facilitates Ca^{2+} induced hemichannel opening and gap junction activity, coupling with neuronal Ca^{2+} networks in the SCN. These imply that SIK1 regulates Ca^{2+} dynamics and neuron-astrocyte communication through phosphorylation of downstream direct substrates. CX43 S373 did not pass the statistical threshold of FDR<0.1 in the *in vivo* phosphoproteome (Wakaf et al., 2026); however, the validation in this chapter provides biological relevance that overrides statistical analysis. These findings reflect the inherent noise and heterogeneity of quantitative *in vivo* phosphoproteomics, particularly when sampling a small-scale complex tissue like the SCN. Pro-KALIP serves as a discovery-enabling tool that identifies direct substrates that may be overlooked as “false negatives” in *in vivo* phosphoproteomics studies. Functional validation would be required to confirm *bona fide* kinase-substrate relationships for the remaining SIK1 substrates.

Though the C6 glioma cell line does not fully represent the complex topological features and circadian rhythmicity of the SCN, it provides an isolated, simple reporter assay that allows close examination of CX43 and site S373. Previous studies showed that extracellular ATP accumulation fluctuates rhythmically (Svobodova et al., 2018), generated by SCN astrocytes. They position extracellular ATP fluctuations as an output signal of the SCN and cellular oscillations (Womac et al., 2009). This model establishes a screening system that visualizes the SIK1-CX43 kinase-substrate relationship. Future studies will include cultured astrocytes and organotypic SCN slices using CX43 S373 phosphomutants. Circadian and sleep phenotypes could be explored using CX43 S373 mutant mouse models.

3.3. Conclusions

With the growing body of evidence on the intriguing role of Sik1 in both the transcriptional regulation of circadian rhythms and post-translational modification of synaptic proteins, this chapter aimed to investigate the direct substrates of SIK1. From literature, we gathered the light-inducible phenotype of SIK1. It was shown that Sik1 is involved in the CRTC1-CREB-mediated transcription of clock genes. This was reflected in our SIK1 KI animal model, where after a 6hr light advance, they showed rapid entrainment. Our in vivo brain phosphoproteome with WT and SIK1 KI animal SCN samples after the LD shift showed differential phosphorylation in synaptic proteins, overlapping with phosphoproteins associated with sleep pressure and need (Wang et al 2018, Bruning et al 2021). We aimed to optimize and use Pro-KALIP assay to detect the

direct substrates and phosphorylation sites of SIK1. From the 170 direct substrates of SIK1, we concluded that SIK1 modulates synaptic transmission and Ca^{2+} dynamics through direct phosphorylation. We subsequently validated the modulating effects of SIK1 on CX43 and the site S373 on Ca^{2+}-induced hemichannel opening. These findings suggested a role of CX43 in maintaining neuron-astrocyte communication and SCN Ca^{2+} network. As a whole, this dataset and results provide a platform to understand and elucidate SIK1's complex role in maintaining SCN synchrony and behavioural outcomes through direct post-translational mechanisms.

REFERENCES

Ali, A. A. H., Stahr, A., Ingenwerth, M., Theis, M., Steinhäuser, C., & Von Gall, C. (2019). Connexin30 and Connexin43 show a time-of-day dependent expression in the mouse suprachiasmatic nucleus and modulate rhythmic locomotor activity in the context of chronodisruption. *Cell Communication and Signaling*, *17*(1). https://doi.org/10.1186/s12964-019-0370-2

Andreazza, S., Bouleau, S., Martin, B., Lamouroux, A., Ponien, P., Papin, C., Chélot, E., Jacquet, E., & Rouyer, F. (2015). Daytime CLOCK Dephosphorylation Is Controlled by STRIPAK Complexes in Drosophila. *Cell Reports*, *11*(8), 1266–1279. https://doi.org/10.1016/j.celrep.2015.04.033

Assendorp, N., Fossati, M., Libé-Philippot, B., Christopoulou, E., Depp, M., Rapone, R., Dingli, F., Loew, D., Vanderhaeghen, P., & Charrier, C. (2024). CTNND2 moderates the pace of synaptic maturation and links human evolution to synaptic neoteny. *Cell Reports*, *43*(10). https://doi.org/10.1016/j.celrep.2024.114797

Baas, A. F., Boudeau, J., Sapkota, G. P., Smit, L., Medema, R., Morrice, N. A., Alessi, D. R., & Clevers, H. C. (2003). Activation of the tumour suppressor kinase LKB1 by the STE20-like pseudokinase STRAD. *EMBO Journal*, *22*(12), 3062–3072. https://doi.org/10.1093/emboj/cdg292

Boudeau, J., Baas, A. F., Deak, M., Morrice, N. A., Kieloch, A., Schutkowski, M., Prescott, A. R., Clevers, H. C., & Alessi, D. R. (2003). MO25α/β interact with STRADα/β enhancing their ability to bind, activate and localize LKB1 in the cytoplasm. *EMBO Journal*, *22*(19), 5102–5114. https://doi.org/10.1093/emboj/cdg490

Brancaccio, M., Edwards, M. D., Patton, A. P., Smyllie, N. J., Chesham, J. E., Maywood, E. S., & Hastings, M. H. (2019). Cell-autonomous clock of astrocytes drives circadian behavior in mammals. *Science*, *363*(6423), 187–192. https://doi.org/10.1126/science.aat4104

Brancaccio, M., Patton, A. P., Chesham, J. E., Maywood, E. S., & Hastings, M. H. (2017). Astrocytes Control Circadian Timekeeping in the Suprachiasmatic Nucleus via Glutamatergic Signaling. *Neuron*, *93*(6), 1420-1435.e5. https://doi.org/10.1016/j.neuron.2017.02.030

Brant, B., Stern, T., Shekhidem, H. A., Mizrahi, L., Rosh, I., Stern, Y., Ofer, P., Asleh, A., Umanah, G. K. E., Jada, R., Levy, N. S., Levy, A. P., & Stern, S. (2021). IQSEC2 mutation associated with epilepsy, intellectual disability, and autism results in hyperexcitability of patient-derived neurons and deficient synaptic transmission. *Molecular Psychiatry*, *26*(12), 7498–7508. https://doi.org/10.1038/s41380-021-01281-0

Brüning, F., Noya, S. B., Bange, T., Koutsouli, S., Rudolph, J. D., Tyagarajan, S. K., Cox, J., Mann, M., Brown, S. A., & Robles, M. S. (2019). Sleep-wake cycles drive daily dynamics of synaptic phosphorylation. *Science*, *366*(6462). https://doi.org/10.1126/science.aav3617

Chhabra, A., Hoffmann, C., Aguilar Pérez, G., Korobeinikov, A. A., Rentsch, J., Hümpfer, N., Kokwaro, L., Gnidovec, L., Petrović, A., Wallace, J. N., Tromm, J. V., Román-Vendrell, C., Johnson, E. C., Ranković, B., Perego, E., Volpi, T., Fernández-Busnadiego, R., Köster, S., Rizzoli, S. O., … Milovanović, D. (2025). Condensates of synaptic vesicles and synapsin-1 mediate actin sequestering and polymerization. *EMBO Journal*, *44*(18), 5112–5148. https://doi.org/10.1038/s44318-025-00516-y

Clasadonte, J., Scemes, E., Wang, Z., Boison, D., & Haydon, P. G. (2017). Connexin 43-Mediated Astroglial Metabolic Networks Contribute to the Regulation of the Sleep-Wake Cycle. *Neuron*, *95*(6), 1365-1380.e5. https://doi.org/10.1016/j.neuron.2017.08.022

Cooper, M. L., Selles, M. C., Cammer, M., Redd, C., Gildea, H. K., Sall, J., Chiurri, K. E., Cheung, P., Wheeler, D. G., Saab, A. S., Liddelow, S. A., & Chao, M. V. (2026). Astrocytes connect specific brain regions through plastic networks. *Nature*. https://doi.org/10.1038/s41586-026-10426-6

Crooks, G. E., Hon, G., Chandonia, J. M., & Brenner, S. E. (2004). WebLogo: A sequence logo generator. *Genome Research*, *14*(6), 1188–1190. https://doi.org/10.1101/gr.849004

De Vuyst, E., Wang, N., Decrock, E., De Bock, M., Vinken, M., Van Moorhem, M., Lai, C., Culot, M., Rogiers, V., Cecchelli, R., Naus, C. C., Evans, W. H., & Leybaert, L. (2009). Ca2+ regulation of connexin 43 hemichannels in C6 glioma and glial cells. *Cell Calcium*, *46*(3), 176–187. https://doi.org/10.1016/j.ceca.2009.07.002

Ferrari, E., Scheggia, D., Zianni, E., Italia, M., Brumana, M., Palazzolo, L., Parravicini, C., Pilotto, A., Padovani, A., Marcello, E., Eberini, I., Calabresi, P., Diluca, M., & Gardoni, F. (2022). Rabphilin-3A as a novel target to reverse α-synuclein-induced synaptic loss in Parkinson's disease. *Pharmacological Research*, *183*. https://doi.org/10.1016/j.phrs.2022.106375

Hwang, J., & Pallas, D. C. (2014). STRIPAK complexes: Structure, biological function, and involvement in human diseases. In *International Journal of Biochemistry and Cell Biology* (Vol. 47, Number 1, pp. 118–148). https://doi.org/10.1016/j.biocel.2013.11.021

Jagannath, A., Butler, R., Godinho, S. I. H., Couch, Y., Brown, L. A., Vasudevan, S. R., Flanagan, K. C., Anthony, D., Churchill, G. C., Wood, M. J. A., Steiner, G., Ebeling, M., Hossbach, M., Wettstein, J. G., Duffield, G. E., Gatti, S., Hankins, M. W., Foster, R. G., & Peirson, S. N. (2013). The CRTC1-SIK1 pathway regulates entrainment of the circadian clock. *Cell*, *154*(5). https://doi.org/10.1016/j.cell.2013.08.004

Johnson, J. L., Yaron, T. M., Huntsman, E. M., Kerelsky, A., Song, J., Regev, A., Lin, T. Y., Liberatore, K., Cizin, D. M., Cohen, B. M., Vasan, N., Ma, Y., Krismer, K., Robles, J. T., van de Kooij, B., van Vlimmeren, A. E., Andrée-Busch, N., Käufer, N. F., Dorovkov, M. V., … Cantley, L. C. (2023). An atlas of substrate specificities for the human serine/threonine kinome. *Nature*, *613*(7945), 759–766. https://doi.org/10.1038/s41586-022-05575-3

Jozsef, L., Tashiro, K., Kuo, A., Park, E. J., Skoura, A., Albinsson, S., Rivera-Molina, F., Harrison, K. D., Iwakiri, Y., Toomre, D., & Sessa, W. C. (2014). Reticulon 4 Is Necessary for Endoplasmic Reticulum Tubulation, STIM1-Orai1 Coupling, and Store-operated Calcium Entry. *Journal of Biological Chemistry*, *289*(13), 9380–9395. https://doi.org/10.1074/jbc.M114.548602

Kang, J., Kang, N., Lovatt, D., Torres, A., Zhao, Z., Lin, J., & Nedergaard, M. (2008). Connexin 43 hemichannels are permeable to ATP. *Journal of Neuroscience*, *28*(18), 4702–4711. https://doi.org/10.1523/JNEUROSCI.5048-07.2008

Katano, T., Takao, K., Abe, M., Yamazaki, M., Watanabe, M., Miyakawa, T., Sakimura, K., & Ito, S. (2018). Distribution of Caskin1 protein and phenotypic characterization of its knockout mice using a comprehensive behavioural test battery. *Molecular Brain*, *11*(1). https://doi.org/10.1186/s13041-018-0407-2

Katoh, Y., Takemori, H., Lin, X. Z., Tamura, M., Muraoka, M., Satoh, T., Tsuchiya, Y., Min, L., Doi, J., Miyauchi, A., Witters, L. A., Nakamura, H., & Okamoto, M. (2006). Silencing the constitutive active transcription factor CREB by the LKB1-SIK signaling cascade. *FEBS Journal*, *273*(12), 2730–2748. https://doi.org/10.1111/j.1742-4658.2006.05291.x

Kon, N., Wang, H., Kato, Y. S., Uemoto, K., Kawamoto, N., Kawasaki, K., Enoki, R., Kurosawa, G., Nakane, T., Sugiyama, Y., Tagashira, H., Endo, M., Iwasaki, H., Iwamoto, T., Kume, K., & Fukada, Y. (2021). Na+/Ca2+ exchanger mediates cold Ca2+ signaling conserved for temperature-compensated circadian rhythms. *Science Advances*, *7*(18). https://doi.org/10.1126/sciadv.abe8132

Li, H., Liu, T. F., Lazrak, A., Peracchia, C., Goldberg, G. S., Lampe, P. D., & Johnson, R. G. (1996). Properties and regulation of gap junctional hemichannels in the plasma membranes of cultured cells. *The Journal of Cell Biology*, *134*(4), 1019–1030. https://doi.org/10.1083/jcb.134.4.1019

Lizcano, J. M., Göransson, O., Toth, R., Deak, M., Morrice, N. A., Boudeau, J., Hawley, S. A., Udd, L., Mäkelä, T. P., Hardie, D. G., & Alessi, D. R. (2004). LKB1 is a master kinase that activates 13 kinases of the AMPK subfamily, including MARK/PAR-1. *EMBO Journal*, *23*(4), 833–843. https://doi.org/10.1038/sj.emboj.7600110

Martins-Marques, T., Ribeiro-Rodrigues, T., Batista-Almeida, D., Aasen, T., Kwak, B. R., & Girao, H. (2019). Biological Functions of Connexin43 Beyond Intercellular Communication. *Trends in Cell Biology*, *29*(10), 835–847. https://doi.org/10.1016/j.tcb.2019.07.001

Matsuura, K., Kobayashi, S., Konno, K., Yamasaki, M., Horiuchi, T., Senda, T., Hayashi, T., Satoh, K., Arima-Yoshida, F., Iwasaki, K., Negishi, L., Yasui-Shimizu, N., Kohu, K., Kawahara, S., Kirino, Y., Nakamura, T., Watanabe, M., Yamamoto, T., Manabe, T., & Akiyama, T. (2022). SIPA1L1/SPAR1 Interacts with the Neurabin Family of Proteins and is Involved in GPCR Signaling. *Journal of Neuroscience*, *42*(12), 2448–2473. https://doi.org/10.1523/JNEUROSCI.0569-21.2022

Oliver, P. L., Sobczyk, M. V., Maywood, E. S., Edwards, B., Lee, S., Livieratos, A., Oster, H., Butler, R., Godinho, S. I. H., Wulff, K., Peirson, S. N., Fisher, S. P., Chesham, J. E., Smith, J. W., Hastings, M. H., Davies, K. E., & Foster, R. G. (2012). Disrupted circadian rhythms in a mouse model of schizophrenia. *Current Biology*, *22*(4), 314–319. https://doi.org/10.1016/j.cub.2011.12.051

Ono, D., Honma, K. ichi, & Honma, S. (2021). GABAergic mechanisms in the suprachiasmatic nucleus that influence circadian rhythm. In *Journal of Neurochemistry* (Vol. 157, Number 1, pp. 31–41). Blackwell Publishing Ltd. https://doi.org/10.1111/jnc.15012

Paajanen, P., Kimmey, J. M., & Dodd, A. N. (2025). Circadian gating: concepts, processes, and opportunities. *Philosophical Transactions of the Royal Society B: Biological Sciences*, *380*(1918). https://doi.org/10.1098/rstb.2023.0346

Pagani, M., Bertero, A., Liska, A., Galbusera, A., Sabbioni, M., Barsotti, N., Colenbier, N., Marinazzo, D., Scattoni, M. L., Pasqualetti, M., & Gozzi, A. (2019). Deletion of autism risk gene shank3 disrupts prefrontal connectivity. *Journal of Neuroscience*, *39*(27), 5299–5310. https://doi.org/10.1523/JNEUROSCI.2529-18.2019

Park, M., Miyoshi, C., Fujiyama, T., Kakizaki, M., Ikkyu, A., Honda, T., Choi, J., Asano, F., Mizuno, S., Takahashi, S., Yanagisawa, M., & Funato, H. (2020). Loss of the conserved

PKA sites of SIK1 and SIK2 increases sleep need. *Scientific Reports*, *10*(1). https://doi.org/10.1038/s41598-020-65647-0
Rash, J. E., Olson, C. O., Pouliot, W. A., Davidson, K. G. V, Yasumura, T., Furman, C. S., Royer, S., Kamasawa, N., Nagy, J. I., & Dudek, F. E. (2007). Connexin36 vs. Connexin32, “Miniature” Neuronal Gap Junctions, and Limited Electrotonic Coupling in Rodent Suprachiasmatic Nucleus. In *Neuroscience* (Vol. 149, Number 2).
Rash, J. E., Yasumura, T., Davidson, K. G. V, Furman, C. S., Dudek, F. E., Nagy, J. I., & Rash, J. E. (2001). Identification of Cells Expressing Cx43, Cx30, Cx26, Cx32 and Cx36 in Gap Junctions of Rat Brain and Spinal Cord. In *Cell Commun Adhes* (Vol. 8).
Reppert, S. M., & Weaver, D. R. (2002). *Coordination of circadian timing in mammals*. www.nature.com/nature
Sáez, J. C., Contreras-Duarte, S., Gómez, G. I., Labra, V. C., Santibañez, C. A., Gajardo-Gómez, R., Avendaño, B. C., Díaz, E. F., Montero, T. D., Velarde, V., & Orellana, J. A. (2018). Connexin 43 Hemichannel Activity Promoted by Pro-Inflammatory Cytokines and High Glucose Alters Endothelial Cell Function. *Frontiers in Immunology*, *9*, 1899. https://doi.org/10.3389/fimmu.2018.01899
Sakai, T., Tamura, T., Kitamoto, T., & Kidokoro, Y. (2004). *A clock gene, period, plays a key role in long-term memory formation in Drosophila* (Vol. 101). https://www.pnas.org
Sakamoto, K., Norona, F. E., Alzate-Correa, D., Scarberry, D., Hoyt, K. R., & Obrietan, K. (2013). Clock and light regulation of the CREB coactivator CRTC1 in the suprachiasmatic circadian clock. *Journal of Neuroscience*, *33*(21), 9021–9027. https://doi.org/10.1523/JNEUROSCI.4202-12.2013
Salas, D., Puebla, C., Lampe, P. D., Lavandero, S., & Sáez, J. C. (2015). Role of Akt and Ca2+ on cell permeabilization via connexin43 hemichannels induced by metabolic inhibition. *Biochimica et Biophysica Acta (BBA) - Molecular Basis of Disease*, *1852*(7), 1268–1277. https://doi.org/10.1016/j.bbadis.2015.03.004
Shan, T., Xiong, Y., Zhang, P., Li, Z., Jiang, Q., Bi, P., Yue, F., Yang, G., Wang, Y., Liu, X., & Kuang, S. (2016). Lkb1 controls brown adipose tissue growth and thermogenesis by regulating the intracellular localization of CRTC3. *Nature Communications*, *7*(1), 12205. https://doi.org/10.1038/ncomms12205
Shaw, R. J. (2009). Tumor suppression by LKB1: SIK-ness prevents metastasis. In *Science Signaling* (Vol. 2, Number 86). https://doi.org/10.1126/scisignal.286pe55
Shirataki, H., Yamamoto, T., Hagi, S., Miura, H., Oishi, H., Jin-no, Y., Senbonmatsu, T., & Takai, Y. (1994). Rabphilin-3A is associated with synaptic vesicles through a vesicle protein in a manner independent of Rab3A. *Journal of Biological Chemistry*, *269*(52), 32717–32720. https://doi.org/10.1016/s0021-9258(20)30049-1
Stanic, J., Carta, M., Eberini, I., Pelucchi, S., Marcello, E., Genazzani, A. A., Racca, C., Mulle, C., Di Luca, M., & Gardoni, F. (2015). Rabphilin 3A retains NMDA receptors at synaptic sites through interaction with GluN2A/PSD-95 complex. *Nature Communications*, *6*. https://doi.org/10.1038/ncomms10181
SOMBERG, R., PFERDEHIRT, B., & KUPCHO, K. (2003). *KINASE-GLO™ LUMINESCENT KINASE ASSAY: DETECT VIRTUALLY ANY KINASE*.
Svobodova, I., Bhattaracharya, A., Ivetic, M., Bendova, Z., & Zemkova, H. (2018). Circadian ATP Release in Organotypic Cultures of the Rat Suprachiasmatic Nucleus Is Dependent on P2X7 and P2Y Receptors. *Frontiers in Pharmacology*, *9*. https://doi.org/10.3389/fphar.2018.00192

Tanaka, H., Kondo, K., Chen, X., Homma, H., Tagawa, K., Kerever, A., Aoki, S., Saito, T., Saido, T., Muramatsu, S. ichi, Fujita, K., & Okazawa, H. (2018). The intellectual disability gene PQBP1 rescues Alzheimer's disease pathology. *Molecular Psychiatry*, *23*(10), 2090–2110. https://doi.org/10.1038/s41380-018-0253-8

Wakaf, Z., Ru, Y., Taylor, L., Ferrari, M., Dang, Q., Li, S., Hasan, S., Clark, K., Cohen, P., Vyazovskiy, V., Kauko, O., Brancaccio, M., Vasudevan, S., & Foster, R. (2026). *A SIK1-led presynaptic phosphorylation network gates the circadian control of sleep-wake timing*.

Wang, X. L., Yuan, K., Zhang, W., Li, S. X., Gao, G. F., & Lu, L. (2020). Regulation of Circadian Genes by the MAPK Pathway: Implications for Rapid Antidepressant Action. In *Neuroscience Bulletin* (Vol. 36, Number 1, pp. 66–76). Springer. https://doi.org/10.1007/s12264-019-00358-9

Wang, Y., Cao, S., Tone, D., Fujishima, H., Yamada, R. G., Ohno, R. I., Shi, S., Matsuzawa, K., Yada, S., Kaneko, M., Sakamoto, H., Onishi, T., Ukai-Tadenuma, M., Ukai, H., Hanashima, C., Hirose, K., Kiyonari, H., Sumiyama, K., Ode, K. L., & Ueda, H. R. (2024). Postsynaptic competition between calcineurin and PKA regulates mammalian sleep–wake cycles. *Nature*, *636*(8042), 412–421. https://doi.org/10.1038/s41586-024-08132-2

Wang, Z., Ma, J., Miyoshi, C., Li, Y., Sato, M., Ogawa, Y., Lou, T., Ma, C., Gao, X., Lee, C., Fujiyama, T., Yang, X., Zhou, S., Hotta-Hirashima, N., Klewe-Nebenius, D., Ikkyu, A., Kakizaki, M., Kanno, S., Cao, L., … Liu, Q. (2018). Quantitative phosphoproteomic analysis of the molecular substrates of sleep need. *Nature*, *558*(7710), 435–439. https://doi.org/10.1038/s41586-018-0218-8

Womac, A. D., Burkeen, J. F., Neuendorff, N., Earnest, D. J., & Zoran, M. J. (2009). Circadian rhythms of extracellular ATP accumulation in suprachiasmatic nucleus cells and cultured astrocytes. *European Journal of Neuroscience*, *30*(5), 869–876. https://doi.org/10.1111/j.1460-9568.2009.06874.x

Xue, L., Geahlen, R. L., & Andy Tao, W. (2013). Identification of direct tyrosine kinase substrates based on protein kinase assay-linked phosphoproteomics. *Molecular and Cellular Proteomics*, *12*(10), 2969–2980. https://doi.org/10.1074/mcp.O113.027722

Yao, Z., van Velthoven, C. T. J., Kunst, M., Zhang, M., McMillen, D., Lee, C., Jung, W., Goldy, J., Abdelhak, A., Aitken, M., Baker, K., Baker, P., Barkan, E., Bertagnolli, D., Bhandiwad, A., Bielstein, C., Bishwakarma, P., Campos, J., Carey, D., … Zeng, H. (2023). A high-resolution transcriptomic and spatial atlas of cell types in the whole mouse brain. *Nature*, *624*(7991), 317–332. https://doi.org/10.1038/s41586-023-06812-z

Yoon, S., & Penzes, P. (2025). Roles of ANK2/ankyrin-B in neurodevelopmental disorders: Isoform functions and implications for autism spectrum disorder and epilepsy. In *Current Opinion in Neurobiology* (Vol. 90). Elsevier Ltd. https://doi.org/10.1016/j.conb.2024.102938

Zeqiraj, E., Filippi, B. M., Deak, M., Alessi, D. R., & Van Aalten, D. M. F. (2009). Structure of the LKB1-STRAD-MO25 complex reveals an allosteric mechanism of kinase activation. *Science*, *326*(5960), 1707–1711. https://doi.org/10.1126/science.1178377

Zhang, Z.-B., Sinha, J., Bahrami-Nejad, Z., & Teruel, M. N. (2022). The circadian clock mediates daily bursts of cell differentiation by periodically restricting cell-differentiation commitment. *Proceedings of the National Academy of Sciences*, *119*(33). https://doi.org/10.1073/pnas.2204470119

Chapter 4: Characterization of the role of SIK3

4.1 Introduction

4.1.1 SIK3 circadian and sleep regulation

In recent years, SIK3 was implicated in many diverse roles on various levels of physiology. Contrary to the tissue-specific expression of *Sik1* and *Sik2*, *Sik3* was shown to have ubiquitous expression (Katoh et al., 2004b). Researchers explored the circadian regulation of SIK3. It was first characterized when exploring metabolic phenotypes of Sik3 knock-out (KO) mice (Sik3 $^{-/-}$) (Hayasaka et al., 2017; Uebi et al., 2012). It was shown that the oxygen consumption rhythm was significantly phase-delayed by 6 hours in Sik3-deficient mice compared to WT, along with other physiological rhythms. Through in situ hybridization, researchers found that *Sik3* is expressed in the SCN, though mRNA expression is not circadian-dependent. It is shown that SIK3-deficient mice displayed a significant phase-delay phenotype, along with defects in light-input pathways and delayed re-entrainment. Through *in vitro* studies, they showed that SIK3 phosphorylates and destabilizes PER2 protein. The accumulation of PER2 in SIK3-deficient mice potentially contributes to the observed weaker and less stable circadian rhythmicity (Hayasaka et al., 2017). In addition, researchers examined SIK3's role in various neuron populations in the SCN. Namely, *Sik3* deficiency (Sik3^{flox}) in GABAergic and NMS-positive neurons exhibited a longer circadian period and delayed activity onset in the dark phase, whereas Sik3 deficiency in AVP-positive neurons had normal arousal (Asano et al., 2023). These results highlight SIK3's circadian regulation in different neuronal populations in the SCN, influencing core parameters and synchrony. It was proposed that the circadian phenotype and arousal regulation could be explained through the SIK3-HDAC axis (Asano et al., 2023; Walkinshaw et al., 2013). The LKB1-

SIK3-HDAC axis was extensively explored in sleep regulation. Genetic and transcriptomic studies show that HDAC4 interacts with CREB and regulates NREM sleep amount in the posterior hypothalamus (Zhou et al., 2022). Kim et al further supported the study and identified that the phosphorylation of HDAC4 S245 by SIK3 increases NREM sleep (Kim et al., 2022).

Interestingly, by inducing randomized point mutations, Funato et al identified a mutant pedigree, named *Sleepy (Slp)* mutant, which showed extensive prolonged sleep need. Whole genome sequencing of the mutant mice showed a heterozygous single nucleotide substitution for intron 13 of the Sik3 gene, resulting in a gain-of-function (GoF) mutation (Funato et al., 2016). The increased sleep need was shown to be solely caused by the SIK3 splice mutation. Heterozygous Sleepy mutant ($Sik3^{Slp/+}$) showed reduced wakefulness and increased total NREM sleep, which is also more pronounced in homozygous $Sik3^{Slp/Slp}$. Slow wave activity (SWA) and baseline activity increased after 6hr of sleep deprivation, validating an inherently higher sleep need. Therefore, SIK3 was characterized as an important molecular marker for sleep need. A few key phosphorylation sites were identified. Researchers observed a hyperphosphorylation of SIK3 T163 *in vivo* following sleep deprivation when sleep need is elevated. T163 is the murine LKB1 activation loop site that is associated with SIK3 kinase activity (Katoh et al., 2006). A hypophosphorylation in SIK3 Ser551 was also detected, which was validated as a critical PKA site that abolishes 14-3-3 binding (Honda et al., 2018). As a result, the single amino acid alterations at the site S551 from serine (S) to alanine (A) or aspartate (D) reproduce the hypersomnia phenotype of *Slp* mutant (Honda et al., 2018).

4.1.2 SIK3 *Slp* gene phosphoproteome

Hoping to decipher the signaling pathways, researchers conducted whole-brain *in vivo* quantitative phosphoproteomics analysis of sleep-deprived and *Slp* animal models. By comparing the two models, researchers aimed to decipher how arousal interacts with sleep and the molecular explanation of sleep homeostasis. Similar to sleep deprivation, Sik3 *Slp* had global hyperphosphorylation of proteins. Researchers, by overlapping the significant phosphorylation changes in both sleep-deprived and *Slp* brains, identified 80 sleep need index phosphoproteins (SNIPPs). Over 86% of the SNIPPs identified are synaptic proteins and 15% of them are associated with sleep phenotypes. They also exhibit time-dependent cumulative phosphorylation (Wang et al., 2018).

Though a few sites were validated and suggested as molecular pathways for SIK3 regulation of circadian and sleep, namely CRTCs, HDACs and PKA sites, the rise of large-scale quantitative analytical methods suggests more SIK3-dependent pathways that are yet to be discovered.

4.1.3 SIK3 regulation

In addition to sleep and circadian regulation, SIK3 is implicated extensively in metabolic and developmental pathways. Sasagawa et al proposed that SIK3-deficient mice had bone abnormalities and dwarfism due to impaired chondrocyte hypertrophy. HDAC4, as a negative regulator of chondrocyte hypertrophy, binds directly to SIK3 (Vega et al., 2004), which leads to the downstream developmental impairments (Sasagawa et al., 2012). In addition, the SIK3-HDAC4 axis is proposed a novel therapeutic for

neurogenerative diseases as HDAC4 facilitates genes and pathways related to synaptic plasticity (Dai et al., 2024). During early developmental stages, Sik3 is expressed in outer hair cells in the cochlea and spiral ganglion cells, which suggests its role in the maintenance of auditory function (Wolber et al., 2014).

SIK3, as a key energy regulator, is induced in the murine liver following the consumption of a high-fat, -sucrose, and -cholesterol diet, which introduces its study in the context of energy metabolism. Researchers observed a lipodystrophic phenotype in SIK3-deficient mice due to higher rates of energy consumption despite a lower body weight. The obesity-resistant phenotype to a high-fat diet was explained by low levels of lipogenic mRNA, such as *Fasn* and *Scd1*. An impairment in ketogenesis has also been detected due to an uncoupling of glycolysis and fatty acid (FA) synthesis, shown by an upregulation of *Fgf21* and downregulation of PPARα pathways in the liver (Uebi et al., 2012). Novel treatments such as 9-cis-retinoic acid were introduced to improve lipid metabolism defects in SIK3-deficient mice.

4.1.4 Aims

Existing literature identifies the wide downstream effects of SIK3 in energy and lipid metabolism, along with recent findings in circadian and sleep regulation. Researchers highlighted the significance of post-translational regulation of SIK3. Notably, HDAC4 was identified as a key substrate of SIK3, forming the SIK3-HDAC4 axis, and is significantly implicated in sleep regulation. Whole-brain quantitative phosphoproteomics studies were subsequently conducted to explore SIK3's interactions with molecular substrates in the context of sleep regulation.

This chapter aims to extend from existing literature through the following approaches:

(1) Circadian phenotyping

From existing studies with Sik3 KO mice, the deficiency of SIK3 leads to major developmental and metabolic defects, which impose confounding effects on circadian and sleep expression. We aim to conduct a full circadian characterization using the SIK3 KI mice through wheel-running recordings under various stimulations and conditions.

(2) Sleep phenotyping

With the SIK3 KI model, we aim to characterize the sleep phenotype under the loss of SIK3 kinase activity. We aim to provide preliminary results of SIK3 KI mice under baseline LD cycle, while further investigations are ongoing.

(3) Transcriptomics and molecular substrates

Based on Sik3 gene expression profile in different brain regions, we aim to conduct tissue-specific mRNAseq to construct differential gene expression. Direct molecular substrates and phosphorylation sites of SIK3 in the cortex are identified using the optimized Pro-KALIP assay. We hypothesize that the substrates identified in the cortex could strengthen existing literature and provide a holistic understanding of SIK3's signaling architecture.

4.2 Results

4.2.1 Single-cell RNA-seq (scRNAseq) explores the distribution of SIK3 in the brain and cell types

We consulted the Allen Brain Atlas (ABC) single-cell RNAseq (scRNAseq) dataset to explore gene expression and distribution of *Sik3* in different brain regions and cell types. Looking at the scale of *Sik3* expression, there is very high gene expression of *Sik3*, ranging from approximately 63 to 510 counts per million (CPM). The bar height of the scale shows that the majority of the brain regions exhibit high levels of *Sik3* expression, resulting in high total expression (Fig. 4.1a).

In the slice containing the SCN (C57BL6:44), there is the highest expression of *Sik3* in the SCN, followed by the striatum and cortical layers, reflected in circadian, arousal and sleep phenotypes. There is relatively lower expression of *Sik3* in the hippocampus and dentate gyrus regions, marked by the light color in the respective regions in the coronal slice on the right of Fig. 4.1a. The expression in these regions is approximately around 70 to 90 CPM (Fig. 4.1a). Within the SCN, *Sik3* is most abundant in hypothalamic GABAergic cells, whereas cortical layers are predominantly composed of glutamatergic cells (Fig. 4.1b-c). In addition to neuronal cells, we also consulted the single-cell dataset for *Sik3* expression in non-neuronal cells. It is shown that *Sik3* also has high expression in oligodendrocytes, followed by astrocytes. These results suggest that *Sik3* is expressed in both neuronal and non-neuronal cells in the brain and spans across cell types (Fig. 4.1d).

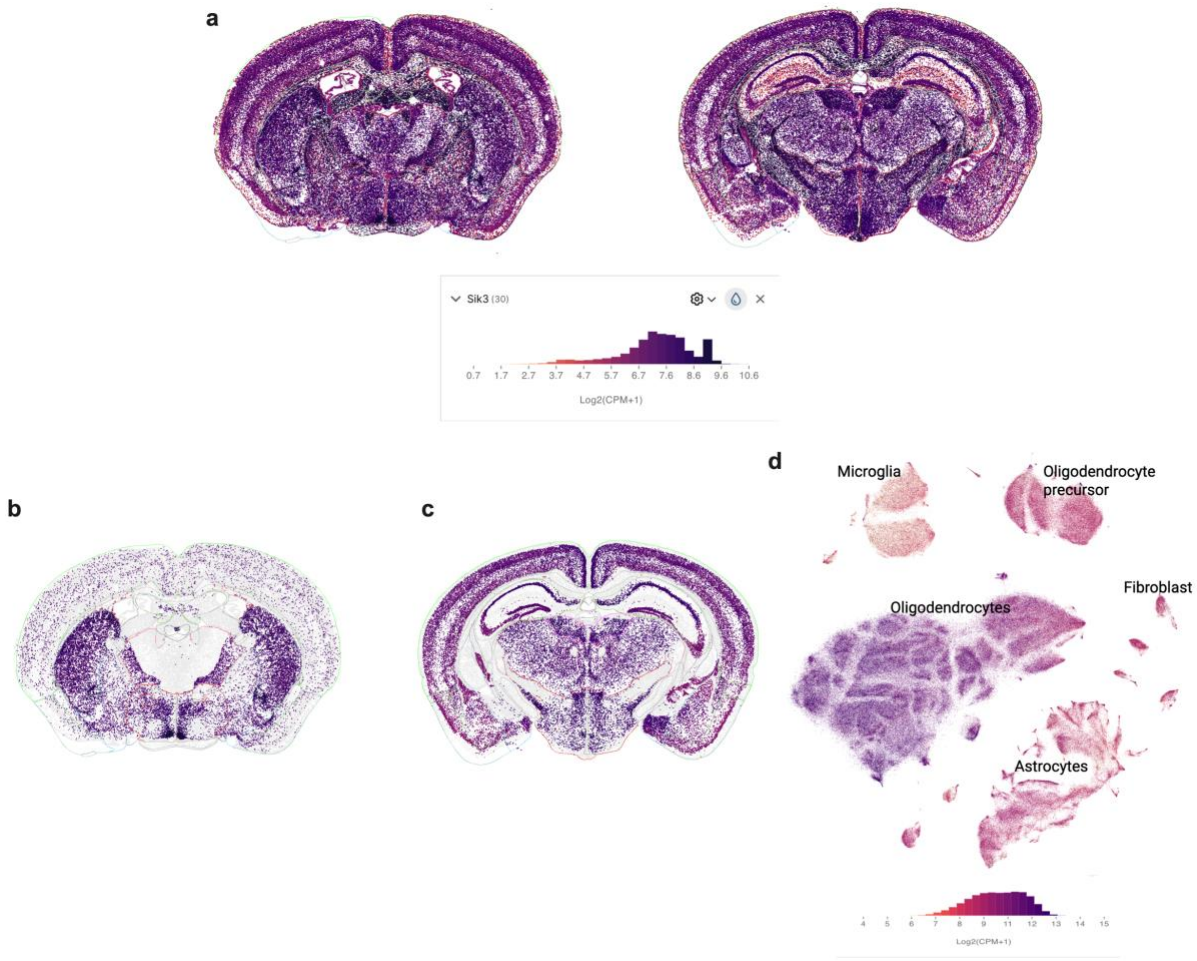

Fig. 4.1 ***Sik3* gene expression in different brain regions and cell types.** Spatial transcriptomics of *Sik3* from ABC Atlas MERFISH C57BL6J-638850 with Imputed Genes + Reconstructed Coordinates (Yao et al., 2023). (a) Coronal slices containing the SCN (left) (C57BL6J-638850.44) and hippocampus (right) (C57BL6J-638850.36) were selected. Spatial transcriptomics Allen Brain Atlas MERFISH coronal slices containing the SCN (C57BL6J-638850.44) of *Sik3* expression overlapping with 10x scRNAseq UMAP plot of (b) GABAergic neurons and (c) glutamatergic neurons. (d) Non-neuronal Cells tSNE used for Sik3 expression, labelled with regions. Gene expression measured by Log2(Counts Per Million (CPM) + 1) scale, corresponding to the darkness of bars. The height of scale bars represents the proportion of cells with that level of expression.

4.2.2 Evaluating the role of SIK3 in circadian regulation via running wheel activity

To further explore the circadian effects under inactive SIK3 kinase, we subjected age-matched WT and SIK3 KI animals to various conditions and light-dark (LD) cycle alterations for wheel-running analysis. As described in Chapter 2, the study was conducted longitudinally, with the same cohort of WT and SIK3 KI animals undergoing all conditions consecutively.

Under a baseline 12:12 LD cycle, there was no difference in circadian period between WT and SIK3 KI animals, with both averaging at around 23.8 hours (Fig. 4.2c). SIK3 KI animals had significantly lower circadian amplitude than WT animals, indicating a less robust circadian clock (Fig. 4.2d). The activity profile was also significantly different between the two genotypes. Though there was no difference in the total number of bouts, WT animals had significantly longer bouts than SIK3 KIs, which corresponded to significantly higher average counts/bouts in WT animals. SIK3 KI animals, however, had a similar number of bouts per circadian day as WT animals (Fig. 4.2e-h). These profiles indicated that SIK3 KI animals overall had lower activity than WTs, which mapped to the high sleep need phenotype (Funato et al., 2016). We also looked at non-parametric functions, interdaily stability (IS) and intradaily variability (IV) (Krafty et al., 2020). They are derived directly from linear and quadratic functions of the time series. IV quantifies the number of fragmentations throughout the day. IS is measured on a scale of 0 to 1, with higher values representing greater stability and consistency from one day to the

other. SIK3 KI animals had a significantly higher IV of 0.897 compared to 0.562 for WT animals. There was no difference in IS between the two genotypes (Fig. 4.2i-j).

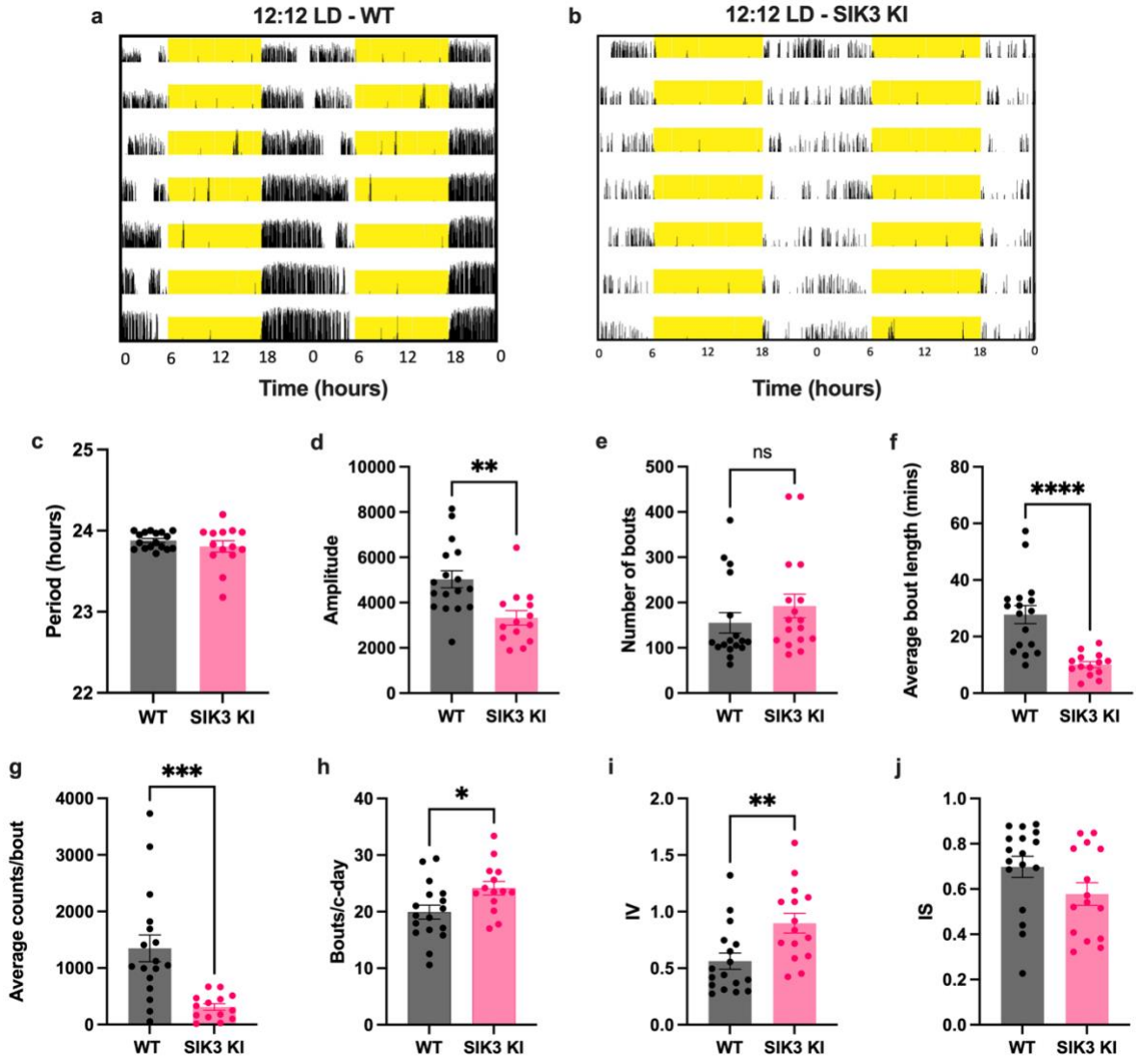

Fig 4.2 **WT and SIK3 KI animals wheelrunning activity under a 12:12 hr LD cycle.** Representative actograms from (a) WT and (b) SIK3 KI animals under a 12:12 hr LD cycle (baseline conditions). Yellow – lights on, grey – lights off, black bars – activity count bars. Lights were set at 100 lux during lights on phase. Each horizontal lines represents 24 hours double-plotted. x-axis marking circadian time in hours. Seven days of baseline 12:12 LD were taken for measurements. (c) Circadian period (hours), (d) circadian amplitude, (e) total activity bouts across time period, (f) average bout lengths (minutes), (g) activity counts per bout, (h) total bouts per circadian day, (i) intradaily variability (IV) and (j) interdaily stability (IS). ns $p>0.05$, * $p<0.05$, ** $p<0.01$, *** $p<0.001$, **** $p<0.0001$, Two-tailed unpaired t-test. Data points are mean ± SEM, n=14-16 per group.

Under constant darkness (freerunning period), SIK3 KI animals exhibited a significantly longer circadian period than WT animals, with an average of 24.8 hours compared to 23.6 hours in WT animals (Fig. 4.3c). Contrary to baseline conditions, there was no significant difference in circadian amplitude (Fig. 4.3d). Similar to 12:12 LD cycle, there was no difference in total number of bouts and bouts per circadian day between WT and SIK3 KI animals. SIK3 KI animals had significantly lower average bout length and average counts per bout. SIK3 KI animals were consistently showing low activity counts during constant darkness (Fig. 4.3e-h). There was no difference between the two groups in IV and IS (Fig. 4.3i-j).

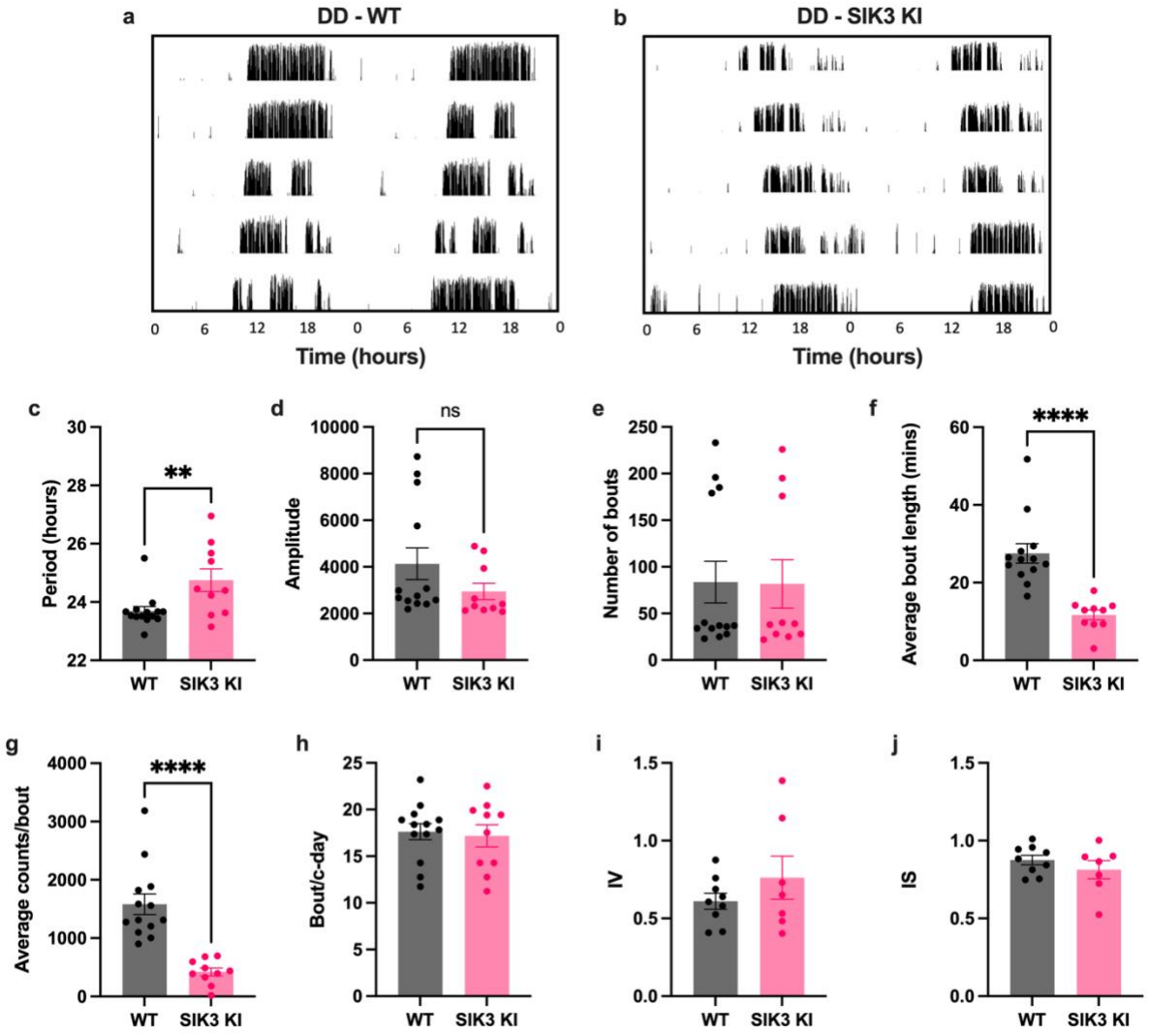

Fig 4.3 **WT and SIK3 KI animals wheelrunning activity under constant darkness (DD)**. Actograms from (a) WT and (b) SIK3 KI animals under constant darkness (DD). Grey – lights off, black bars – activity count bars. Each horizontal lines represents 24 hours double-plotted. x-axis marking circadian time in hours. Seven days of constant darkness were taken for measurements. (c) Circadian period (hours), (d) circadian amplitude, (e) total activity bouts across time period, (f) average bout lengths (minutes), (g) average counts per bout, (h) total bouts per circadian day, (i) intradaily variability (IV) and (j) interdaily stability (IS). ns $p>0.05$, * $p<0.05$, **** $p<0.0001$, Two-tailed unpaired t-test. Data points are mean ± SEM, n=14-16 per group.

Under constant light (freerunning period), there was no significant difference in circadian period between WT and SIK3 KI animals (Fig. 4.4c). There was no difference in circadian amplitude between the two groups (Fig. 4.4d). As activity was overall lower under constant light, activity counts were suppressed in both groups. There was no difference in the total number of bouts and bouts per circadian day, but SIK3 KI animals had significantly shorter average bout lengths. The difference in average counts per bout was not significant between the two groups (Fig. 4.4e-h).

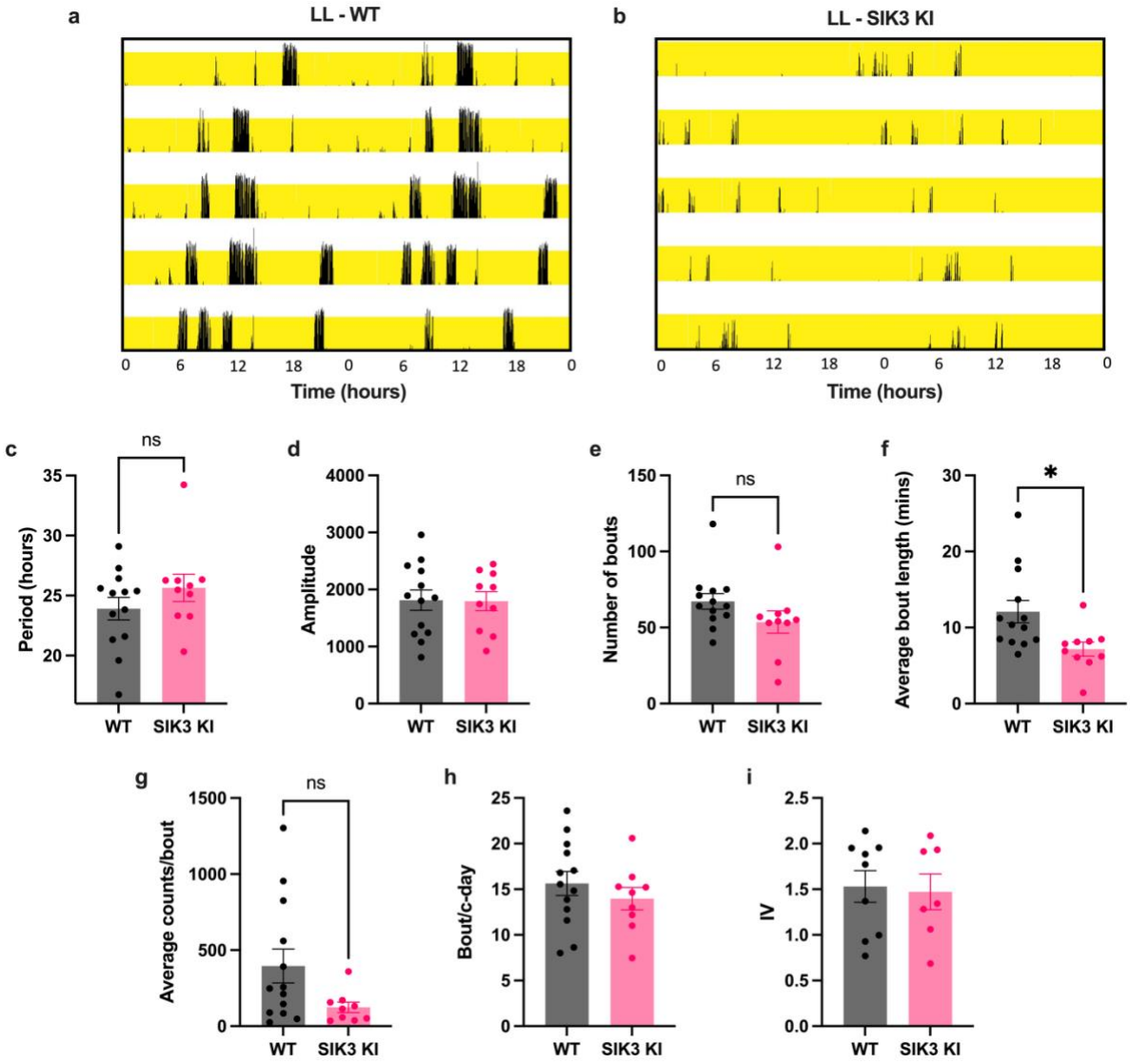

Fig 4.4 **WT and SIK3 KI animals' wheelrunning activity under constant light (LL)**. Actograms from (a) WT and (b) SIK3 KI animals under constant light (LL). Yellow – lights on, black bars – activity count bars. Each horizontal line represents 24 hours double-plotted. x-axis marking circadian time in hours. Six days of constant light activity were taken for measurements. (c) Circadian period (hours), (d) circadian amplitude, (e) total activity bouts across time period, (f) average bout lengths (minutes), (g) activity counts per bout, (h) total bouts per circadian day and (i) intradaily variability (IV). ns $p>0.05$, * $p<0.05$, Two-tailed unpaired t-test. Data points are mean ± SEM, n=14-16 per group.

To explore how SIK3 is regulated under light as a zeitgeber, we subjected SIK3 KI and WT animals to a 6hr light advance jetlag paradigm. We measured phase differences on the first, third, fifth, and seventh days after the shift. A zero-phase difference on the plot represents full entrainment to the new LD cycle, as the initial phase difference between the cycles on the first day was six. Two-way ANOVA analysis revealed significant genotype effects, suggesting a general trend of WT animals entraining faster to the new LD cycle than SIK3 KI animals ($p=0.0003$) (Fig. 4.5a-b). However, no genotype x time interaction was observed. Phase difference on day nine post-shift showed that SIK3 KI animals were still not entrained to the new LD cycle, while WT animals had a phase difference of close to zero (Fig. 4.5c).

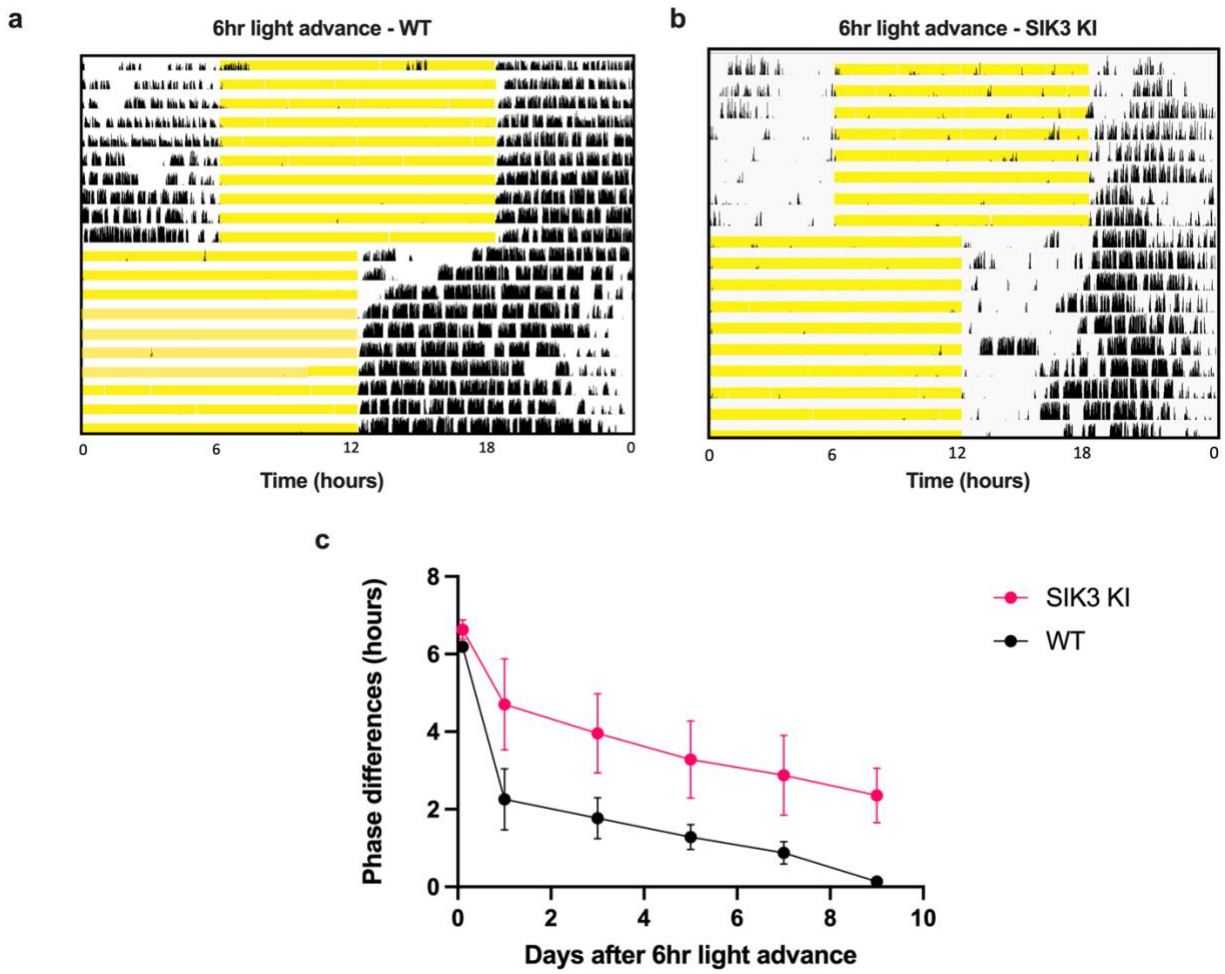

Fig 4.5 **WT and SIK3 KI animals wheel-running activity under 6-hour light advance.** WT and SIK3 KI animals were stably entrained to the 12:12 hr LD cycle and subjected to a 6-hour light advance and stable entrainment was allowed for seven days. Representative actograms of (a) WT and (b) SIK3 KI animals indicating the time of shifts. Yellow – lights on, grey – lights off, black bars – activity count bars. (c) Phase differences (hours) recorded on the day of the shift, first, third and fifth day after the shift. The slope of the curve represents entrainment speed. ns $p>0.05$, Two-way ANOVA with Geisser Greenhouse correction. Genotype and Time effects are significant. No interaction effect (Genotype x Time) was observed. Data points are mean ± SEM, n=14-16 per group.

We then released WT and SIK3 KI animals into DD and set 30-minute light pulses at various circadian times (CT) covering the entire circadian day (24 hours). The phase of onset was measured three days before and after the pulses, and the difference between them was plotted (Fig. 4.6a). As biological replicates were limited for each CT, the phase differences were binned into two-hour windows for plotting. A standard phase response curve (PRC) to light is split into different sections for interpretation. The region from CT2 to CT10 is characterized as the dead zone, where there is minimal phase response to light. CT14 is expected to have the largest phase delay and CT22 with the largest phase advance (Johnson et al 1999). The light PRC curves for WT and SIK3 KI animals showed that both genotypes responded expectedly to the light pulses, with the largest phase delays around CT14 and phase advances towards the later CTs. Two-way ANOVA analysis with genotype and circadian timepoint as factors revealed significance between individual circadian times ($p=0.0009$) as shown by the sigmoidal-like wave. No significance was found between genotypes overall ($p=0.1339$) and the genotype x circadian time interaction ($p=0.6095$), demonstrating no altered phase responses to acute photic input in SIK3 KI animals. However, area under the curve (AUC) suggested that SIK3 KI animals resulted in a flatter PRC curve. Large error bars showed that there was substantial inter-animal variability (Fig. 4.6b). Further investigations could include increasing the effect size and power.

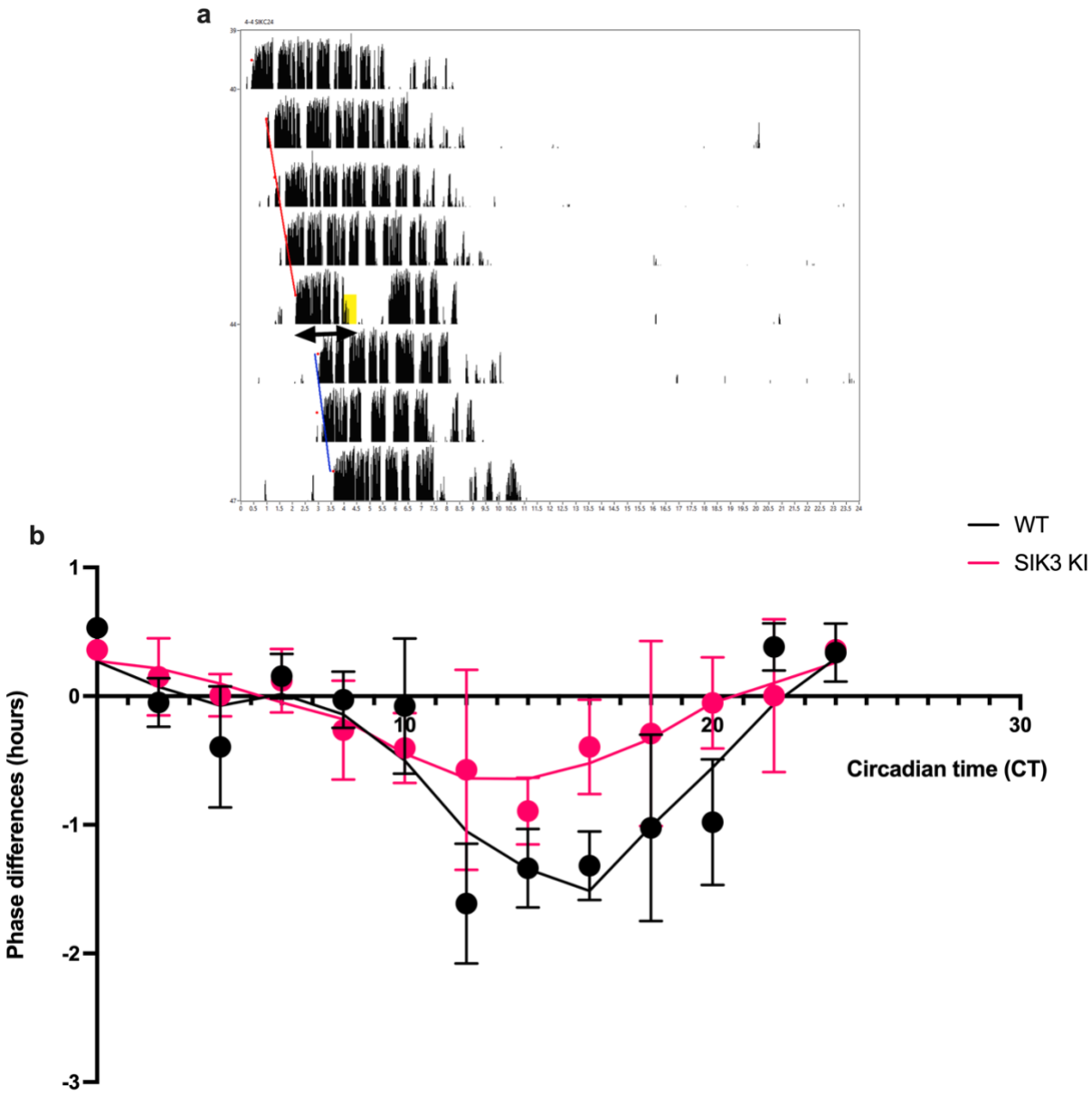

Fig 4.6 **Light Phase Response Curve (PRC) of WT and SIK3 KI animals.** WT and SIK3 KI animals were released into constant darkness (DD) and subjected to 30 min, 30 lux light pulses covering the full 24-hour phase. (a) Representative actogram showing light pulses. Phase differences were calculated as the difference between the phase of onsets (labeled with the black arrow). (b) Light pulses were allocated to the corresponding circadian time (CT) and phase differences were recorded. The phase response curve (PRC) to light was plotted in 2-hour bins. The curve was second-order smoothing with 3 neighboring points. Data points are mean ± SEM, n=1-9 per timepoint per group. Two-way ANOVA revealed no significance between Genotype and Circadian Timepoint (p=0.6095).

Previous findings showed that SIK3 KI animals exhibited weaker rhythmicity and entrainment under a baseline 12:12 LD cycle. We also showed that SIK3 KI animals had an endogenous period of close to 25 hours; therefore, we hypothesized that the phenotype could be due to internal circadian period mismatch. To test this, we adjusted the LD cycle to 25 hours (12.5 hours lights on and 12.5 hours lights off) and assessed whether clock strength and entrainment could be restored (Fig. 4.7a-b).

After stable entrainment to the new LD cycle, there was no difference in circadian period between WT and SIK3 KI animals, both showing a period of around 25 hours (Fig. 4.7c). This showed that WT and SIK3 KI animals were aligning with the period of the LD cycle normally. Consistent with baseline conditions, SIK3 KI animals had a significantly lower amplitude than WT animals, suggesting a weaker and less stable circadian clock (Fig. 4.7d). SIK3 KI animals had significantly higher total number of bouts and bouts per circadian day. This was complemented by significantly lower average bout lengths and average counts per bout (Fig. 4.7e-h). These indicated that SIK3 KI animals had less activity and more fragmented activity. SIK3 KI animals had slightly higher IV and lower IS, but these differences were not statistically significant (Fig. 4.7i-j).

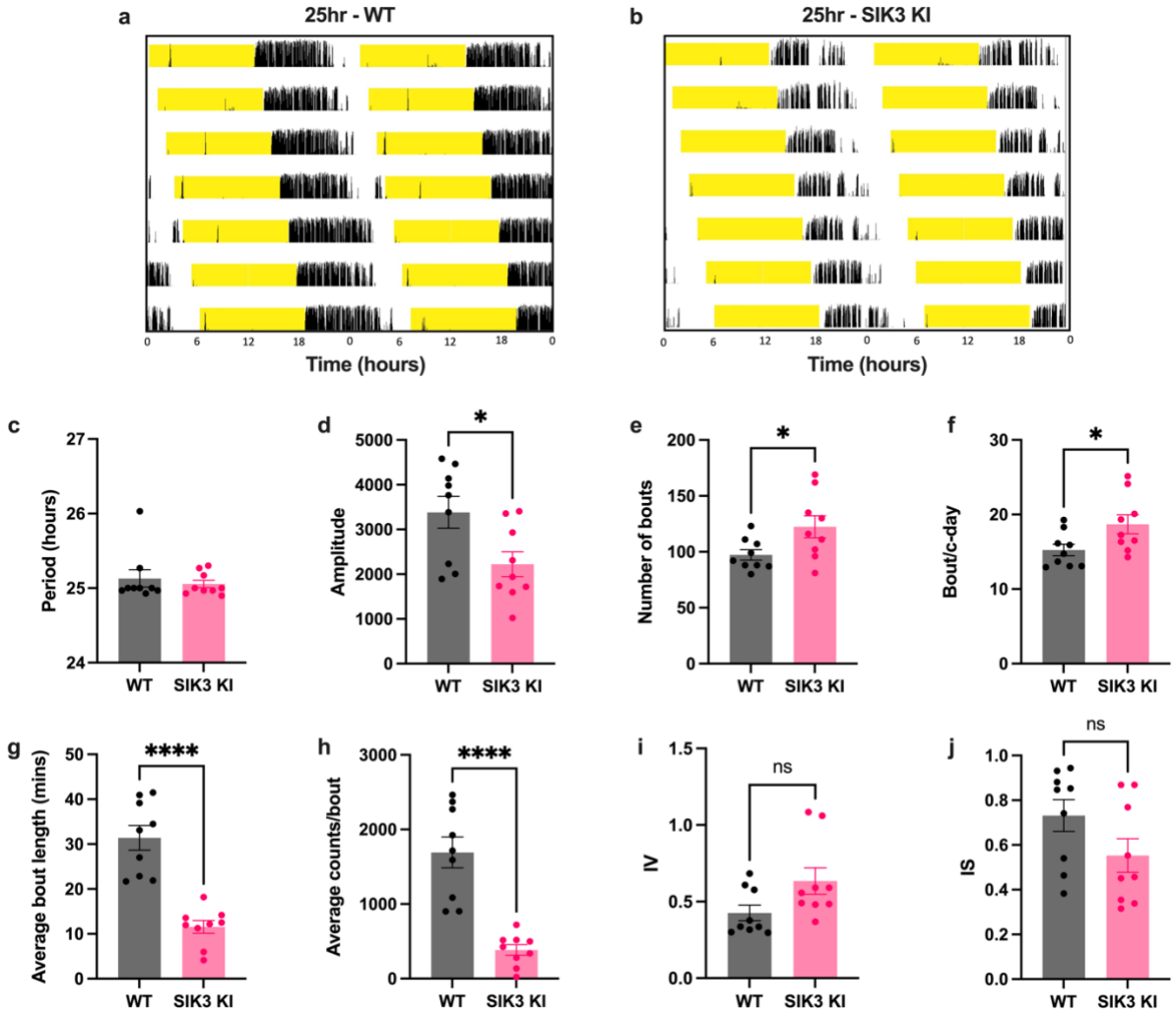

Fig 4.7 **WT and SIK3 KI animals wheelrunning activity under a 25-hr LD cycle.** Actograms from (a) WT and (b) SIK3 KI animals under a 25-hour LD cycle (12.5 hours lights on, 12.5 hours lights off). Yellow – lights on, grey – lights off, black bars – activity count bars. Lights were set at 100 lux during the lights-on phase. Each horizontal line represents 24 hours. x-axis marking circadian time in hours. Seven days of activity were taken. (c) Circadian period (hours), (d) circadian amplitude, (e) total activity bouts across time period, (f) bouts per circadian day, (g) average bout lengths (minutes), (h) average counts per bout, (i) intradaily variability (IV), and (j) interdaily stability (IS). ns $p>0.05$, * $p<0.05$, ** $p<0.01$, *** $p<0.001$, **** $p<0.0001$, Two-tailed unpaired t-test. Data points are mean ± SEM, n=14-16 per group.

We then subjected the animals to a light advance shift, in this case a 6.25-hour light advance (jetlag paradigm). Under a 24-hour LD, a light advance was shifted by a quarter, so the equivalent was applied here (Fig. 4.8a-b). We measured the phase differences on day one, three, five, and seven after the light advance. The plot showed that WT were fully entrained to the new LD cycle, on average, five days after the light advance. In contrast, SIK3 KI animals did not shift as rapidly and were not fully entrained to the new LD cycle after seven days. Two-way ANOVA analysis showed a significant genotype effect, suggesting the delayed entrainment phenotype of SIK3 KI animals (Fig. 4.8c). These results implied that the loss of SIK3 kinase activity results in altered photic entrainment responses.

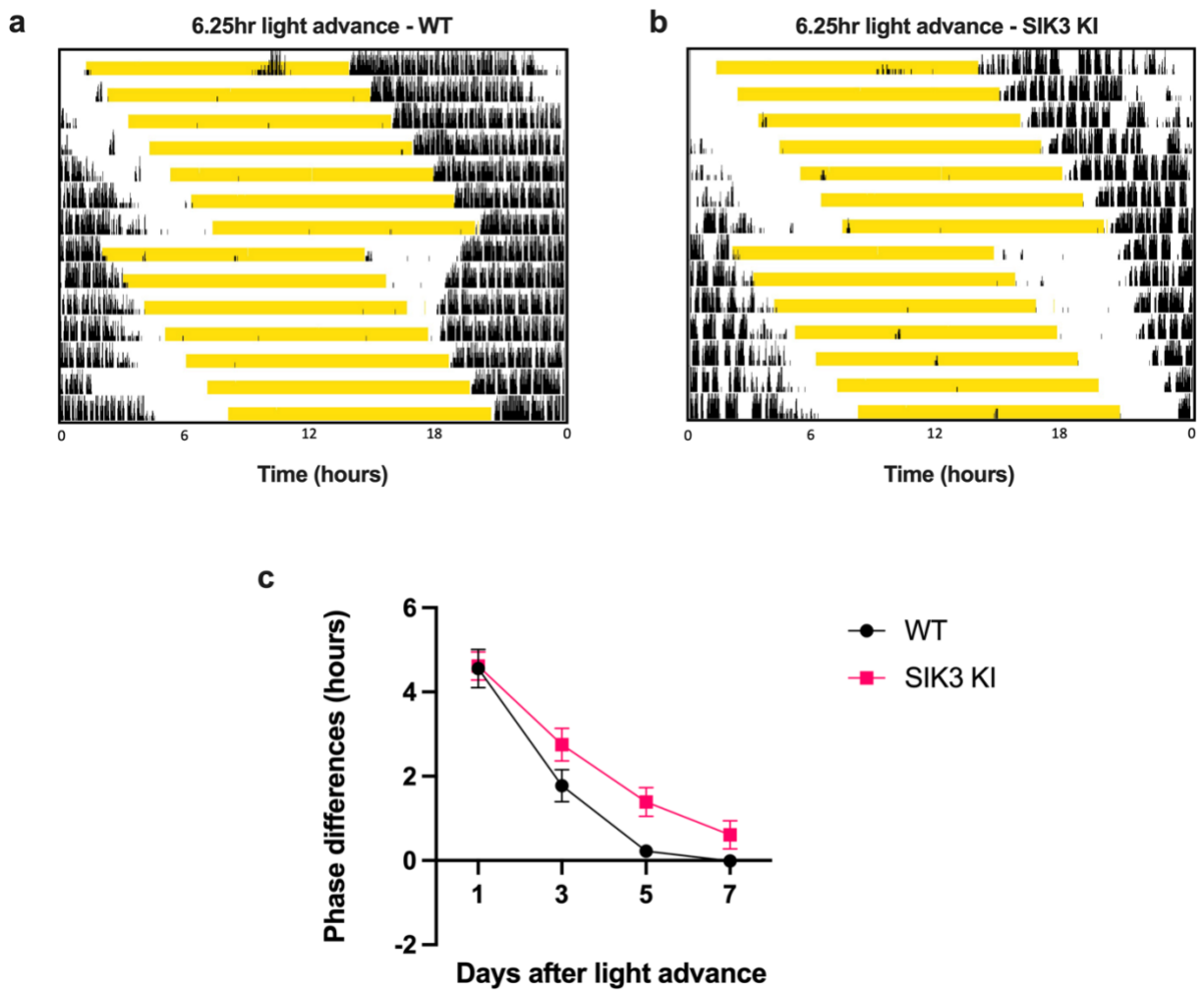

Fig 4.8 **WT and SIK3 KI animals wheelrunning activity under 6.25-hour light advance.** WT and SIK3 KI animals were stably entrained to the 25-hr LD cycle and subjected to a 6.25-hour light advance and stable entrainment was allowed for seven days. Representative actograms of (a) WT and (b) SIK3 KI animals indicating the time of shift. Yellow – lights on, grey – lights off, black bars – activity count bars. (c) Phase differences (hours) recorded for the day of the shift, first, third and fifth day after the shift. Slope of the curve represents entrainment speed. *p<0.05 Two-way ANOVA with Geisser-Greenhouse correction. Data points are mean ± SEM, n=14-16 per group.

Lastly, we subjected SIK3 KI and WT animals to a T7 cycle to explore the robustness of the endogenous circadian clock (Fig. 4.9a-b). Normally, animals would not entrain as the endogenous clock has the dominant effect (LeGates et al 2012). Results showed that SIK3 KI animals did not entrain to the cycle and maintained a circadian period of 24.95 hours (Fig. 4.9c). There was no difference in overall circadian amplitude between the two groups, suggesting that SIK3 KI animals maintained circadian rhythmicity and strength at an endogenous period of around 25 hours (Fig. 4.9d). We then analyzed Fast Fourier Transform (FFT) plots to examine activity frequencies and power under different periodicities. Under the 7-hour ultradian cycle, amplitude was significantly dampened in the SIK3 KI animals compared to WT animals, suggesting a lack of entrainment and oscillations under the imposed cycle (Fig. 4.9i). There was no difference between the number of bouts and bouts per circadian day between the two groups. SIK3 KI animals had significantly lower average bout lengths and lower average counts per bout (Fig. 4.9 e-h), showing fragmented activity and consistency with the lower activity phenotype of SIK3 deficiency. These results showed that SIK3 KI animals maintained endogenous circadian rhythms and were less plastic to environmental LD cycle alterations.

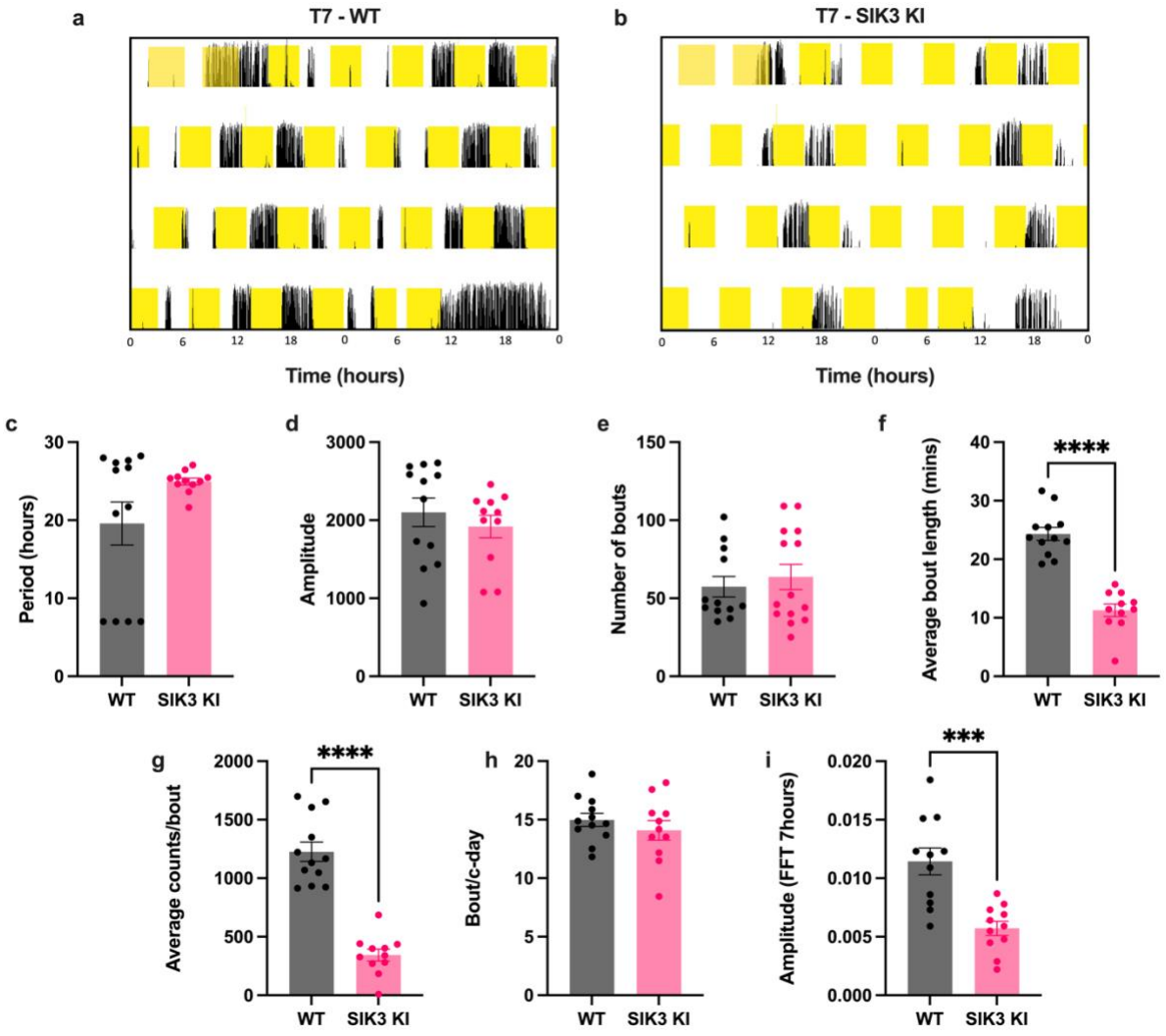

Fig 4.9 **WT and SIK3 KI animals wheelrunning activity under 3.5/3.5 hr LD cycle (T7).** WT and SIK3 KI animals were subjected to a 3.5 hr lights on / 3.5 hr lights off (T7) LD cycle for 7 days. The middle 5 days were analyzed. Representative actograms of (a) WT and (b) SIK3 KI animals under a T7 cycle. Yellow – lights on, grey – lights off, black bars – activity count bars. Lights were set at 100 lux during lights on phase. Each horizontal lines represents 24 hours. x-axis marking circadian time in hours. (c) Circadian period (hours), (d) circadian amplitude, (e) total activity bouts across five day period, (f) average bout lengths (minutes), (g) average counts per bout and (h) total bouts per circadian day. (i) FFT analysis of amplitude at 7 hours. *** p<0.001, **** p<0.0001, Two-tailed unpaired t-test. Data points are mean ± SEM, n=14-16 per group.

4.2.3 Evaluating the role of SIK3 in sleep regulation

Building on previous studies characterizing the sleep phenotype of the *Slp* mutant, we analyzed continuous EEG recordings in WT and SIK3 KI animals under a 12:12 LD cycle. These analyses represent preliminary results under baseline (n=2) and further investigations on sleep homeostatic response are ongoing.

Overall, there were no significant differences in the time spent in wakefulness and NREM sleep states. We observed a general genotype effect in REM sleep, suggesting a general trend of increased REM sleep in SIK3 KI animals compared to WT controls (Fig. 4.10a-c). No interaction between genotype and time was observed, showing that the differences were not time-specific. Similarly, a genotype effect was suggested as SIK3 KI animals had lower NREM sleep delta energy throughout the day. No difference or interaction was detected between SWA delta power and time in 2-hour bins. However, the total delta power in the range of 3-5Hz was higher in WT animals overall (Fig. 4.10d-f). Together, preliminary results implied SIK3 KI animals had prolonged REM sleep and lower NREM sleep delta power. However, as these results are underpowered, a more robust cohort is required for reliable conclusions and statistical analysis. These statistical tests remain correlative.

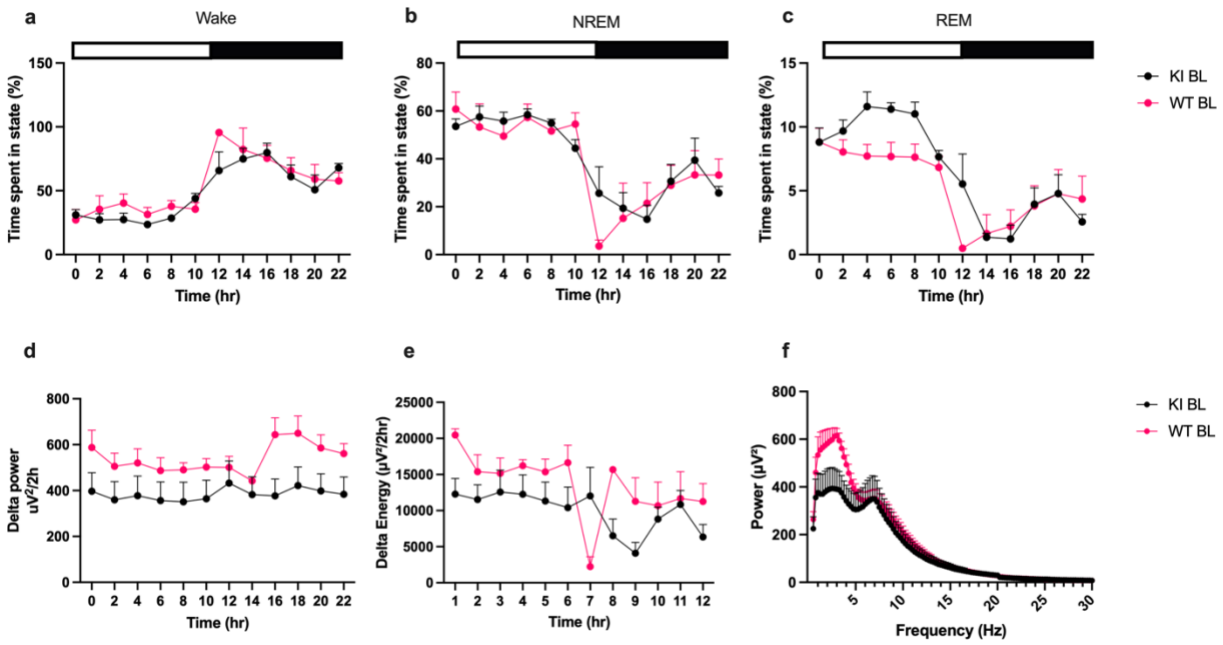

Fig. 4.10 **Preliminary EEG recording analysis of WT and SIK3 KI animals under 12:12 baseline condition**. Sleep phenotype of WT and SIK3 KI animals was characterized through EEG recordings under 12:12 hr LD cycle (baseline). Under baseline (BL), the percentage of time spent in (a) wakefulness, (b) NREM and (c) REM was recorded plotted against time in hours. The number of epochs in each vigilant state was calculated in 2-hour bins and represented as a percentage of total time in the bin. (d) NREM sleep delta power, (e) delta energy and (f) power spectrum were recorded. Hours 0-12 were light phases, indicated by hollow bars and hours 12-24 were dark phases, indicated by filled bars. Data points are mean ±SEM, n=2 per group.

4.2.4 RNA-seq transcriptomics show differential expression in the cortex in wake and sleep phases

As both existing literature and preliminary sleep phenotyping on SIK3 KI propose SIK3 as a strong candidate for sleep regulation, we performed cortex-specific transcriptomics, incorporating findings from 4.2.1. We collected 1mm^3 cortex samples from WT and SIK3 KI animals at two timepoints – end of sleep (EOS) and end of wake (EOW). The EOS phase was characterized as 2 hours before the onset of the dark phase (ZT10). The EOW phase was characterized as 2 hours before the onset of the light phase (ZT22). RNA extraction was performed on the cortex samples. A260/280 ratio from NanoDrop Spectrophotometer and Qubit BroadRange was used to measure RNA concentration in the samples. The Qubit BroadRange concentration was used for subsequent sequencing sample preparation as it is a more sensitive test for RNA (Supp. Fig. 4.1a). RNA quality was first measured by the NanoDrop and a few samples were slightly below the pure RNA A260/230 range (2-2.2). We then performed RNA TapeStation assay as a more sensitive and accurate test to acquire RNA integrity numbers (RIN). With 10 representing intact RIN, all of the samples had RIN numbers above 8.5 (Supp Fig. 4.1a).

We then had confidence to proceed to sequencing preparation. We used the kit and followed the protocol provided by the BRBseq Alithea (Alpern et al., 2019). A qPCR was performed during sample preparation as a quality control for amplification. The multi-component plot showed that the samples were amplified properly and provided appropriate cycles for subsequent steps (Supp. Fig. 4.1b). The quality of the final cDNA

sample was tested with a DNA Bioanalyzer assay. Final quality control tests were supported and performed by the Novogene sequencing facility (Supp Fig. 4.1c). The samples at EOS (ZT10) and EOW (ZT22) were sequenced, and we detected 55,492 genes (Supp. Table 4.1). We first ran a Principal Component Analysis (PCA) with the dataset to visualize variation across biological replicates (Supp Fig. 4.2). The PCA plot captured 58% of total variation across the SIK3 dataset, 33% accounted by the first principal component (PC1) and 25% by the second principal component (PC2). We saw general clustering within WT animal replicates and separation between the timepoints. Similarly, we observed a general clustering of EOW points of SIK3 KI animals towards the bottom of PC2 and the top for EOS points. Replicate 3 of WT EOS was excluded from subsequent analyses based on raw intensity values and deviation from expected clustering in the PCA plot.

We then analyzed detected genes using an interactional DEseq2 model, putting genotype and circadian timepoint (ZT10 and ZT22) as factors. Firstly, comparing WT and SIK3 KI transcriptomics at EOS ZT10, we found *Adcyap1* as significantly downregulated in the SIK3 KI animals (padj<0.05) (Fig. 4.11a; Supp. Table 4.1)). We then conducted functional analysis at the statistical cutoff to an p-value of less than 0.05 (p<0.05) and we detected 638 differentially expressed genes (DEGs). Genes with a base mean, average expression across samples, of less than 10 were excluded from functional analysis to avoid possibilities of false detection and unreliable statistical analyses.

We conducted functional analysis using GProfiler to categorize enriched pathways in the genes expressed (Fig. 4.11b; Supp. Table 4.1). In Biological Processes (BP), we detected common terms in metabolic processes and biogenesis, including *Cav2, Mkrn2, Ppard, Hnrnpd*. Caveolin-2 (Cav2) encodes a multifunctional protein that plays a significant role in cancer biology. In muscles, it could also couple with Cav1 to serve channel roles. *Ppard* is involved in lipid oxidation and homeostasis. *Mkrn2* and *Hnrnpd* are tumor suppressors that regulate p53 and bind to RNA molecules, respectively. Notably, genes regulating spermine and polyamine metabolic processes were enriched, such as *Paox, Smox, Stat2* and *Odc1*, which were generally upregulated in the SIK3 KI animals. It is implied in literature that polyamine metabolism is regulated and impacted by stress responses (Rangan et al., 2014).

There are also differentially expressed channel protein-encoding genes and transporter genes such as *Kcne1l* and *Slc1a1*. *Kcne1l* encodes for the protein part of the KCNE voltage-gated potassium channel family, which is crucial for regulating neuronal excitability. *Slc1a1* is part of the solute carrier family, which is a major glutamate transporter in the central nervous system. These genes are downregulated in the WT animals, proposing SIK3 as a negative regulator. We also detected several other members of the solute carrier family (SLC) that are important for exchange between the blood and the brain such as *Slc35f3*, the transporter of thiamine (B vitamin). Similarly, Tmem transporters such as *Tmem238* and *Tmem18* play a role in amino acid transport and energy expenditure, respectively. These changes are associated with SIK3's role in neuronal function and metabolism.

Pathway analysis also suggested that a large subset of the differentially expressed genes was located in the synapse, implicating pathways involved in synaptic strength and sleep regulation. Several genes within pathways implicated in sleep regulation were identified. *Egfr* (epidermal growth factor receptor) was significantly upregulated in WT animals. Literature has shown that EGFR signaling promotes sleep and is required for normal sleep homeostasis response after sleep deprivation (Lee et al., 2019). This indicates that SIK3 KI animals lacked EGFR signaling during the sleep phase. Notably, at ZT10, *Adcyap1* was significantly downregulated in the SIK3 KI animals (padj<0.05). *Adcyap1* encodes PACAP protein which is essential for light-induced/glutamate phase shifting in the SCN. The downregulation of the translation of PACAP in the cortex is involved in cortical excitability and wake propensity.

Similarly, we applied DEseq2 analysis to the EOW ZT22 timepoint and 51 DEGs under padj<0.05 (Fig. 4.11c; Supp. Table 4.1). By conducting functional analysis, we found enrichment in regulation of metabolic and primary metabolic processes such as *Gmpr*, *Fosb*, *Hmox1*, *Psmd1* and *Impact*. *Hspa1a* gene was also detected to be upregulated in WT animals, linking stability of the clock to stress responses (Fig. 4.11d).

Moreover, we detected a large number of ribosomal regulatory genes that are significantly upregulated in WT animals, indicating that there's a loss of ribosomal transcription under the loss of SIK3 kinase activity. We detected various genes that encode ribosomal proteins such as *Rps29*, *Rps13*, *Rps12*, *Rps26*, *Rps27* and *Rps24*, totaling 27 genes in the family. These genes also mapped to functional categories

ribosome biogenesis, ribosome assembly and rRNA metabolic process. Most importantly, these genes overlapped with terms translation at synapses, which shows that under the loss of SIK3, synaptic translation is associated with ribosomal capabilities.

Finally, we examined the interactional effects between genotype and timepoint. Though none of the genes passed the padj<0.05 cutoff, 1,046 genes were differentially expressed under p<0.05 (Fig. 4.11e; Supp. Table 4.1). By conducting functional analysis, we found that time-dependent transcriptional regulation of biogenesis and stress processes was altered in the SIK3 KI. Notably, *FosB*, an immediate early gene (IEG), showed reduced time-dependent responsiveness in the SIK3 KI, associated with desensitization to stress exposure (Perrotti et al., 2004). This was also observed in *Sdk1*, a novel retinal ganglion cell (RGC), namely the S1-RGCs (Rochon et al., 2021) and *Usp2*. There is also a variety of genes regulating metabolic processes such as *Ide*, which degrades intracellular insulin and terminates insulin activity, associated with Type 2 diabetes. Collectively, SIK3 alters circadian-dependent transcription of genes in the cortex.

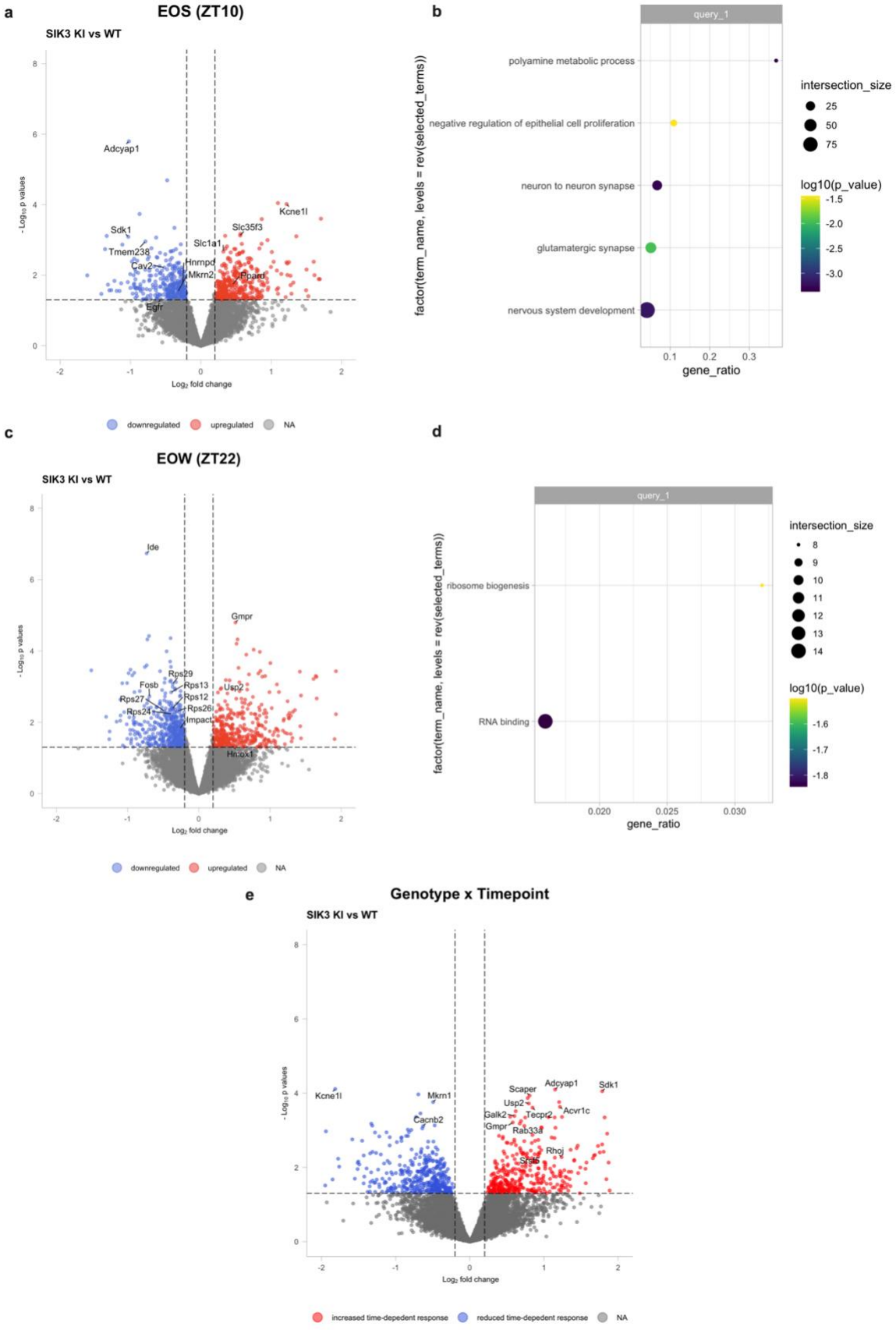
a
EOS (ZT10)
SIK3 KI vs WT
Adcyap1
Kcne1l
Sdk1
Slc35f3
Slc1a1
Tmem238
Hnrnpd
Cav2
Mkrn2
Ppard
Egfr
- Log10 p values
Log2 fold change
downregulated
upregulated
NA
b
query_1
polyamine metabolic process
negative regulation of epithelial cell proliferation
neuron to neuron synapse
glutamatergic synapse
nervous system development
factor(term_name, levels = rev(selected_terms))
gene_ratio
intersection_size
25
50
75
log10(p_value)
-1.5
-2.0
-2.5
-3.0
c
EOW (ZT22)
SIK3 KI vs WT
Ide
Gmpr
Rps29
Fosb
Rps13
Usp2
Rps27
Rps12
Rps26
Rps24
Impact
Hn1ox1
- Log10 p values
Log2 fold change
downregulated
upregulated
NA
d
query_1
ribosome biogenesis
RNA binding
factor(term_name, levels = rev(selected_terms))
gene_ratio
intersection_size
8
9
10
11
12
13
14
log10(p_value)
-1.6
-1.7
-1.8
e
Genotype x Timepoint
SIK3 KI vs WT
Kcne1l
Mkrn1
Cacnb2
Scaper
Adcyap1
Sdk1
Usp2
Acvr1c
Galk2
Tecpr2
Gmpr
Rab33a
Rhoj
Sfxn5
- Log10 p values
Log2 fold change
increased time-depedent response
reduced time-depedent response
NA

Fig. 4.11 Transcriptomics analysis of WT and SIK3 KI animals in the cortex. 1mm3 cortex punches were collected from WT and SIK3 KI animals during end of sleep phase (EOS) at ZT10 and end of wake phase (EOW) at ZT22. mRNA-seq was performed on cortex punches and differential gene analysis was conducted. (a-b) Volcano plot and functional analysis of differentially expressed genes (DEGs) between WT and SIK3 KI animals in EOS. Dotted line = log2FC (F>0.25) and uncorrected p value (p<0.05) cutoff. Blue region on the left represents downregulation in SIK3 KI animals compared to WT controls, vice versa. -log10(p-value) and overlap size/ratio were calculated and programmed in RStudio using GProfiler2 containing Biological Processes (BP), Cellular Component (CC) and Molecular Function (MF) terms. (c-d) Volcano plot and functional analysis of DEGs between SIK3 KI and WT animals in EOW. (e) Volcano plot of DEGs between SIK3 KI and WT showing significant genotype x timepoint interaction. Blue region represents negative log2C, indicating a reduced time-dependent expression in SIK3 KI compared to WT controls, vice versa. n=3-4 per genotype.

4.2.5 Explore the direct substrates of SIK3 in the cortex

Previous studies have identified global phosphorylation changes in synaptic proteins in the *Slp* mutant and in the sleep-deprived animals, characterizing them as molecular markers of sleep need. Using the previously optimized Pro-KALIP method, we aimed to delineate the direct substrates and phosphorylation sites of SIK3 in the cortex and determine whether these synaptic targets associated with sleep are directly downstream of SIK3. The cortex-specific assay will further complement the previous whole-brain phosphoproteomics. We aimed to provide a mechanistic link between SIK3 and sleep regulation and synaptic homeostasis.

Similar to Chapter 3, the activity of the purified SIK3 kinase was verified using the Kinase Glo Luminescence assay (Supp. Fig. 4.3) using dephosphorylated cortex lysate. A titration curve with a serial dilution of SIK3 kinase from 0.125nM to 40nM showed that SIK3 kinase is linear between 5nM and 40nM. The lower dilutions were unstable due to

human error and assay limitations. 20nM of SIK3 kinase was used for the *in vitro* rephosphorylation assay.

From SIK3 KALIP in the cortex, we detected 1365 phosphopeptides, mapped to 643 unique phosphoproteins and 1043 unique phosphosites (Supp. Table 4.2). Complementing existing datasets and hoping to delineate direct mechanistic targets of SIK3, we overlapped the in vitro Pro-KALIP dataset with the *Slp* vs WT *in vivo* phosphoproteome for bona fide direct substrates of SIK3 (Wang et al., 2018). The *Slp* vs WT phosphoproteomics in sum detected 21377 phosphopeptides, mapped to 4500 unique phosphoproteins and 18367 unique phosphosites. After the overlap with our SIK3 cortex KALIP data, we acquired 167 phosphoproteins and 248 phosphosites that are direct substrates of SIK3 (Fig. 4.12e).

To have confidence that the SIK3 KALIP dataset has a SIK3 (QSK) motif, we used the meta dataset from the Kinase Library that incorporates previously identified human Ser/Thr sites and maps to the mouse ortholog using FASTA sequences (Chapter 2) (Johnson et al., 2023). We used the scores and percentiles as a background and performed a contingency test. In the meta dataset, out of 89784 total sites detected, 18373 sites had a SIK3 percentile of over 80% (~20%). Since our phosphoproteomics were mouse sites, out of 248 sites, 178 mouse sites overlapped with the human sites. Out of which, 39 sites had a SIK3 percentile of over 80% (22%). The contingency test showed that the SIK3 KALIP dataset is significantly enriched for the SIK3 motif and

sites were depleted for CDK16 and GRK3 motifs (Fig. 4.12a-c). Given the interdependent relationship of SIKs and LKB1, LKB1-dependent sites were excluded. Out of the 248 phosphosites, 72 sites and 61 proteins were statistically significant between *Slp* and WT animals (padj<0.05), which were determined to be the *bona fide* direct substrates of SIK3 (Supp. Table 4.2). The signals of these sites were also shown to be SIK3-specific (Fig. 4.12d). By performing functional analysis on the direct substrates of SIK3 and raw intensity analysis, we found that they are mainly synaptic proteins (Fig. 4.12d-e). The direct substrates of SIK3 in the cortex form a strong network regulating synaptic function. For instance, multiple substrates in the synapsin family were detected. Multiple sites of synapsin-1 (SYN1) were shown as significant between *Slp* and WT, which is greatly involved in vesicle transport and neurotransmitter release (Chhabra et al., 2025). Synapsin-3 (SYN3) was also shown to perform similar roles in neurotransmitter release and synaptogenesis (Hoffmann et al., 2023). They are connected to Amphiphysin (AMPH), associated with exocytosis. SH-3 containing GRB2-like protein 3-interacting protein (SGIP1) regulates clathrin-mediated endocytosis. BIN1 is important for membrane shaping and implied as a negative regulator of endocytosis. Synaptodin (SYNPO) is involved in modulating actin-based shape and motility of dendritic spines (Zhang et al., 2013). Phosphorylated MAP1B is shown to accompany neurite extension (Nishida et al., 2023). There are also key channel proteins that are directly phosphorylated by SIK3 in the synapse. HCN2 is a potassium/sodium hyperpolarization-activated channel that contributes to native current modulation in neurons and KCNA regulates neuronal output by facilitating potassium transport in excitable membranes. There are also ABI1 and PAK2, which are key kinases involved

in cytoskeleton regulation and cell growth. ABI1 was identified as an SNIPP, correlated with sleep pressure (Wang et al., 2018). From GProfiler Biological Processes (BP), we found that the synaptic SIK3 substrates are enriched for “nervous system development” and “regulation of axonogenesis”, indicating that they are tightly associated with neurogenesis processes. We were also able to detect HDAC4 S245, which was previously validated as a key substrate of SIK3 and regulator of sleep, which gave us confidence regarding the Pro-KALIP dataset (Fig. 4.12f-g).

We then examined the direct phosphorylation sites. We detected several key phosphorylation sites of SYN1 such as S568, S605 and S553. S605 is closely related to neural plasticity and neurogenesis signaling and are downstream of CAMK2a and PKCG kinase signaling (Chhabra et al., 2025). Similarly, S568 has also been shown in literature to associated with calmodulin activity. S553 is essential for synaptic vesicle and GABAergic neurotransmitters (Qiao et al., 2014; Zhi et al., 2021). Notably, RYR2 S2807 is also associated with CAMK-dependent phosphorylation (Walweel et al., 2019) . These sites are also interconnected with channel proteins such as KCNA2. The phosphorylation site S441 on KCNA2 is shown to be upstream of SYN1.

In addition, we have identified cyclin-dependent kinases as common upstream regulators of several SIK3 direct substrates. AMPH S262 is an endogenous substrate of CDKL5 and is associated with brain and the nervous system (Katayama et al., 2020). Similarly, CDKL5 phosphorylates EFHD4, affecting calcium activity. BRSK2 S424 in humans is also downstream of CDK5 kinase. These findings show that these substrates

of SIK3 form a network that involves multiple kinases. CDKL5 itself is also significantly phosphorylated by SIK3 as a direct substrate and it was categorized as a SNIPP. CDKs are key regulators of cell cycle progression and metabolism. A set of the direct phosphosites of SIK3 is involved in metabolic regulation. For instance, ABI1 S183, FARP1 S427 and TTC3 are all implicated in insulin-related pathways. Phosphorylation of UVRAG is associated with muscle development. Overall, these findings suggested that through direct phosphorylation, SIK3 regulates and links substrates in synaptic and metabolic pathways, forming an intertwined kinase network (Fig. 4.12g).

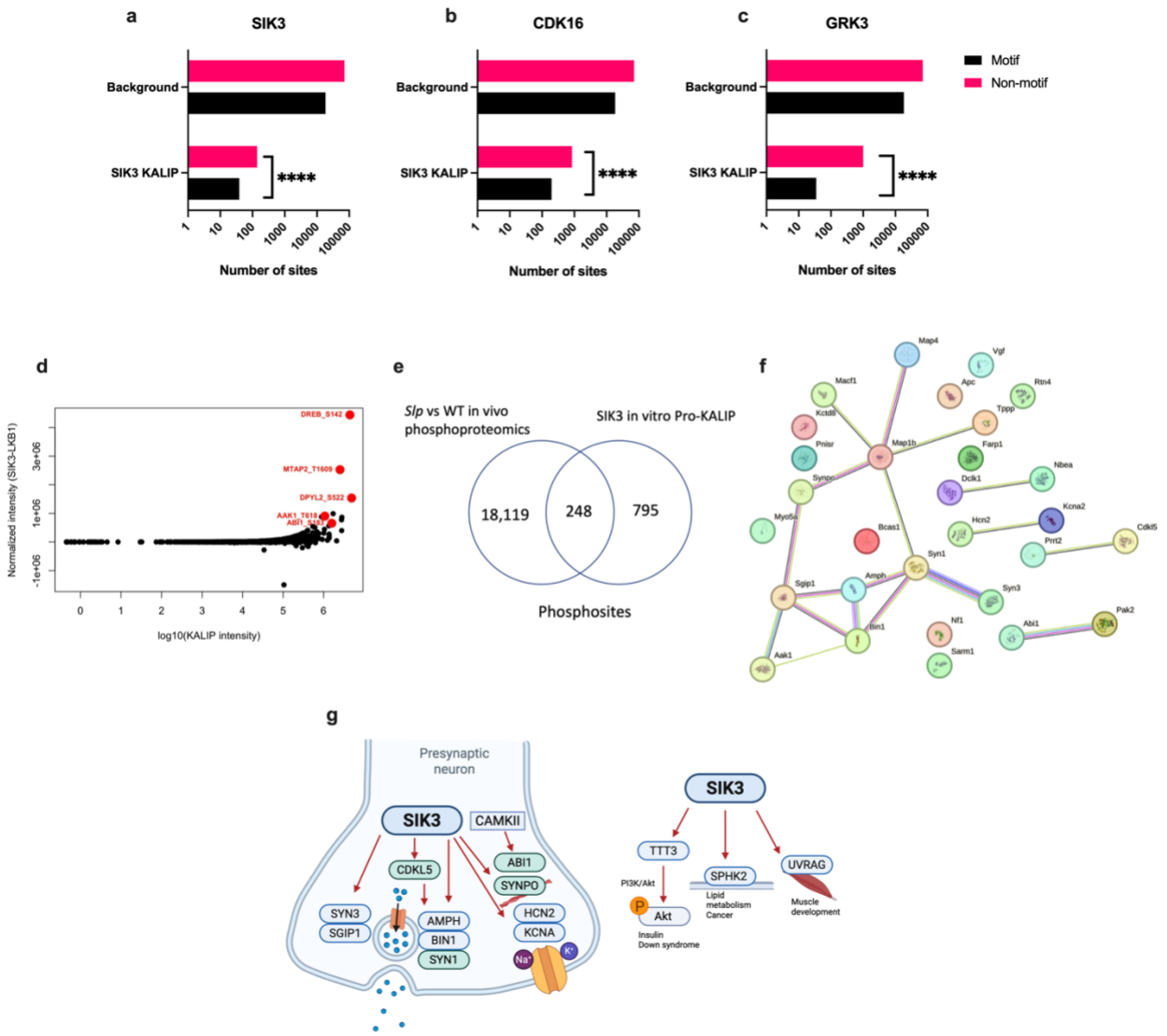

Fig. 4.12 SIK3 Cortex Pro-KALIP analysis. Motif enrichment analysis using Johnson et al as background signal for (a) SIK3, (b) CDK16, and (c) GRK3. "Motif" was defined as a site that has a motif percentile of over 80%. Number of sites was plotted for both the background and SIK3 KALIP SCN dataset comparing number of "motif" and "non-motif" sites. **** $p<0.0001$, Chi-squared test, Two-sided p-value. Odds ratio (SIK3) = 1.091; Odds ratio (CDK16) = 0.8994; Odds ratio (GRK3) = 0.1350. (d) Pro-KALIP raw intensity differences in quantity of phosphorylated peptides between the sample treated with SIK3+LKB1 trimer versus LKB1 trimer alone in the cortex, plotted against the log10-transformed intensity of peptides detected in SIK3 + LKB1 trimer. Each point represents an individual phosphosite; selected differential phosphosites are highlighted in red. (e) Venn diagram of overlapping phosphosites between SIK3 in vitro Pro-KALIP assay and in vivo Slp vs WT phosphoproteome (Wang et al 2018). (f) STRING protein-protein interaction of detected direct substrates of SIK3 in the cortex, showing the "synapse" hub. Connecting lines show interaction between proteins. (g) Schematic diagram

of SIK3-mediated substrates regulating synaptic and metabolic functions proposed in Pro-KALIP. Substrates labelled in green are SNIPPs (Wang et al., 2018).

4.3 Discussion

There is a wide range of existing evidence supporting the role of SIK in sleep regulation through a single nucleotide substitution of intron 13 in the *Sik3* gene, named *Sleepy* mutant. The GoF *Slp* mutant exhibited a significant reduction in wakefulness and an increase in total NREM sleep. Researchers have also employed whole-brain quantitative phosphoproteomics to pinpoint the molecular substrates responsible for the phenotype, establishing a kinase-substrate relationship (Wang et al., 2018). In this chapter, using the SIK3 KI model, we characterized the circadian and sleep phenotype. We implemented cortex-specific transcriptomics and Pro-KALIP to identify differential gene expression in SIK3 KI animals and direct substrates of SIK3, respectively. We hypothesized that the molecular profiling would support and contextualize the observed behavioural outputs.

Given that the behavioural circadian and sleep outputs are tightly associated with SIK3 regulation, we employed a multi-omics approach. We first consulted the ABC scRNAseq dataset to explore the distribution of *Sik3* in different brain regions and cell types. It showed that there is high gene expression of *Sik3* in the SCN and cortical layers, predominantly in GABAergic and glutamatergic cells, respectively. These findings are supported by existing studies that *Sik3* deficiency in GABAergic neurons exhibited longer circadian period and delayed phase onset (Asano et al., 2023), suggesting *Sik3* expression in GABAergic neurons is responsible for the speed and phase onsets. From

literature, *Sik3* is also expressed in AVP-expressing and neuromedin S (NMS)-expressing neurons, which co-regulate circadian period and photic responses, respectively (Asano et al., 2023). In addition, Kim et al showed that *Sik3* in cortical glutamatergic neurons regulates NREM sleep quantity and sleep need (Kim et al., 2022). Together with our findings, SIK3 plays a primary and central role in circadian and sleep output in different neuronal populations in the SCN and cortex. The relatively low expression of *Sik3* in the hippocampus suggests that SIK3 is not directly responsible for hippocampal-regulated functions such as spatial learning and memory. The expression in non-neuronal cells also suggests that molecular components and signaling pathways are acting across multiple cell types. This analysis sets the premise for tissue-specific transcriptomics and phosphoproteomics of SIK3.

4.3.1 SIK3 KI animals have longer period and less plastic clock

As SIK3 plays a significant role in energy and lipid metabolism, using our SIK3 KI model, we hope to reduce the confounding downstream effects from the developmental defects as would be expected from previous knockout (KO) models. To extend previous findings on the delayed phase and entrainment phenotype, we conducted a full circadian profiling on WT and SIK3 KI animals.

Under a 12:12hr LD cycle, baseline conditions, there was no difference in circadian period between WT and SIK3 KI animals. SIK3 KI animals had significantly lower amplitude and higher IV than WT animals, suggesting that the circadian clock was less robust and more variable within a circadian day. Higher IV also indicates that SIK3 KI

animals were having more nighttime arousals and fragmented sleep, which is shown by higher activity bouts during the light phase. Under DD, SIK3 KI animals had a significantly longer circadian period than WT animals. The differences were less pronounced as the two groups of animals behaved similarly in LL due to low activity counts. Activity profiles showed that SIK3 KI animals had significantly lower average counts per bout in all conditions. IV was similar under constant conditions for WT and SIK3 KI animals. These findings suggest that SIK3 KI animals exhibited lower stability and disrupted rhythmicity under an imposed LD cycle, while it improves during free-running. In addition, the consistent low activity in SIK3 KI mapped to the reduced wakefulness phenotype shown in *Slp* mice (Funato et al., 2016).

We then implemented various paradigms to WT and SIK3 KI animals to investigate photic entrainment. By conducting a light PRC, we showed that the loss of SIK3 kinase activity preserved phase responses to acute photic input. However, when subjected to a 6hr light advance, WT animals entrained faster than SIK3 KI animals, as SIK3 KI animals still had not yet entrained to the new LD cycle by the last day of the shift. As we found that SIK3 KI animals exhibited a longer circadian period of around 25 hours, we explored whether the lack of entrainment was due to the misalignment by analyzing core circadian parameters under a 25hr LD cycle. Similarly, SIK3 KI animals had significantly lower circadian amplitude than WT, suggesting that the lack of rhythmicity and less robustness are innate characteristics independent of the external environmental LD cycle. The animals also entrained significantly slower than WT animals, though they were shifting onsets towards the new LD cycle. We confirmed

these results by subjecting these animals to a T7 ultradian cycle and showed that SIK3 KI animals maintained an endogenous circadian period of 24.95 hours.

Together, under the loss of SIK3 kinase activity, we observed a circadian clock with lower amplitude, longer endogenous circadian period and higher variability under LD cycle. This aligns with previous studies using $Sik3^{-/-}$ animals, where similarly exhibited longer circadian period and lower amplitude due to high activity during the day (Hayasaka et al., 2017). Asano et al showed that *Sik3* deficiency in GABAergic neurons in the SCN attenuated PER2 expression, leading to lower amplitude (Asano et al., 2023). Though our study did not examine the role of SIK3 in different neuronal populations in the SCN, these findings suggest that SIK3 in these neurons exhibits various roles in circadian regulation and SCN function, leading to the observed phenotype. We have also observed higher activity during the day and lower activity during the night, leading to a greater number of activity bouts and fragmented sleep in the SIK3 KI cohort. In addition, we found that SIK3 KI animals had a less plastic clock and attenuated photoentrainment, supported by the previous knock-out model (Hayasaka et al., 2017). Interestingly, SIK3 KI animals exhibited similar phase response patterns to acute light pulses compared to WT controls. These findings imply that SIK3 is not involved in the acute light-induced pathway that involves the response to glutamate and PACAP, facilitating clock gene transcription (Sakai et al., 2004). This is contrary to the role of SIK1 in the SCN where it acts as a key mediator of CREB-mediated transcription and phase shifting, indicating isoform-dependent circadian regulation. On the other hand, photoentrainment involves the synchronization of

oscillators to the external LD cycle, depending on the coupling strength and frequencies (Jiménez et al., 2022). This suggests that SIK3 is involved in the entrainment pathway to photic cues that coordinates communication and stability between the SCN and peripheral oscillators. This is supported by *ex vivo* SCN studies that SIK3 deficiency leads to a reduction in circadian rhythmicity of oscillating cells, leading to desynchrony within the SCN (Hayasaka et al., 2017). This chapter, however, limits the response of the circadian clock to photic responses; future experiments could investigate other 'zeitgebers' on clock entrainment under the loss of SIK3 kinase activity, such as temperature and food intake.

The full circadian characterization revealed that SIK3 is involved in maintaining the periodicity and rhythmicity of the circadian clock and modulates photoentrainment pathways. Previous studies have proposed that SIK3 destabilizes PER2 protein through phosphorylation, thereby leading to desynchrony in the SCN and entrainment alterations (Hayasaka et al., 2017). Further investigations are necessary to elucidate specific mechanisms of SIK3's regulation of the circadian clock and light-input pathways in the SCN. No sex differences and effects were found in this study. The majority of conditions had good effect size and power apart from the full PRC due to data availability. As we observed lower body mass in SIK3 KI animals, the consistently lower activity counts in SIK3 KI animals observed in circadian phenotyping may be due to motivational changes. Further investigation can include infrared-based tracking and behavioral assay such as reward and choice tasks.

4.3.2 SIK3 regulates sleep

We characterized the sleep phenotype of SIK3 KI animals and analyzed preliminary results under baseline conditions. We found no differences in wakefulness and NREM sleep duration between SIK3 KI and WT animals, only a general trend of increased REM sleep. The *Slp* mutant mice were characterized to show NREM sleep-specific changes, as they exhibited increased NREM sleep and showed no changes in total REM sleep (Hayasaka et al., 2017). Further analyses are required to examine how SIK3 KI and *Slp* mutant phenotypes converge.

NREM sleep is characterized in EEG as dominating low-frequency and high-amplitude signals, marked as slow waves. SWA is the index for sleep pressure and need (Achermann & Borbély, 2003). Our preliminary findings showed a significant genotype effect as SIK3 KI animals exhibited consistent low delta energy and power in the delta range compared to WT controls. This aligns with the GoF *Slp* mutant results, where they had higher NREM sleep SWA, associated with higher sleep need (Funato et al., 2016). These reinforce SIK3 as a key molecular candidate for sleep pressure.

As *Sik3* is enriched in cortical glutamatergic neurons and has shown to be a strong candidate for sleep need and sleep pressure, we conducted transcriptomics and Pro-KALIP analysis in the cortex tissues of WT and SIK3 KI animals. As translation and proteins were shown to cycle throughout the day, aligning with the sleep-wake cycle (Brüning et al., 2019), we collected samples at EOS and EOW timepoints. RNA extractions were performed and quality-checked through Qubit and Tape Station

measurements. Transcriptomics, BRBseq, was conducted following the protocol provided by BRBseq Alithea. Sample quality were checked with in-lab tests and by the sequencing facility. A PCA analysis was performed to visualize the variation across sample replicates. Outliers and samples with large variation were excluded from subsequent differential expression analysis.

We conducted an interactional DESeq2 analysis to compare WT and SIK3 KI gene expression at the two time points. Although few genes passed the correction, functional analyses revealed enrichment in key biological themes. These include growth factor and stress signaling, translation, and metabolic regulation, which are implicated in SIK3 time-dependent regulation. While sleep analysis in SIK3 KI animals remains preliminary, the interpretations and proposed pathways are mainly from existing literature. The RNAseq and KALIP findings are exploratory and serve to open up possibilities for future investigations.

We saw a significant downregulation of epidermal growth factor receptor (*Egfr*) at ZT10 in SIK3 KI animals. Research has shown that EGFR signaling regulates sleep in Drosophila and is functionally analogous to mammals (Foltenyi et al., 2007). Lee et al extended the research and has shown that EGFR signaling leads to sleep state consolidation and is required for normal sleep levels. Using a sleep deprivation assay, EGFR was shown to be involved in maintaining sleep homeostasis through the MAPK/ERK pathway. Combined with these results, it shows that SIK3 KI animals had

reduced EGFR signaling and potentially EGFR-mediated sleep homeostasis, suggesting that SIK3 regulates sleep through EGFR signaling (Lee et al., 2019).

In addition, a downregulation of *Adcyap1*, encoding PACAP, was also detected in ZT10. Though PACAP is important for entrainment and response to nocturnal light in the SCN (Gillette & Mitchell, 2002), it is implied for mediating stress responses in the cortex (Martelle et al., 2021). Foilb et al investigated how stress peptide PACAP affects sleep and circadian rhythms and found that induction of PACAP decreased wakefulness and locomotor activity and increased slow wave sleep and REM sleep (Foilb et al., 2023). A separate study also shows that *Adcyap1*-expressing neurons are involved in sickness sleep (Darmohray et al., 2025). Moreover, in PACAP-KO cohorts, neuronal activation and vesicular transporter expression are downregulated in PACAP-expressing glutamatergic and GABAergic neurons (Zhang et al., 2021). Though the role and expression of PACAP in the cortex has not been established, these studies propose a role of SIK3 in regulating stress responses and a role in sleep and circadian rhythms. Similarly, we found a downregulation of *Hspa1a* in SIK3 KI animals, encoding for *Hsp70* and orchestrates cellular stress response (Simonova et al., 2022). Together, the downregulation of stress-associated genes implies that stress responses are altered under the loss of SIK3 kinase activity. There is a growing body of evidence that cellular stress forms a bidirectional relationship with sleep disturbances (Williams & Naidoo, 2020).

Secondly, we observed changes in genes involved in the translational machinery and metabolic processes. A large proportion of the differential genes in ZT22 encode ribosomal proteins in the synaptic terminals (both presynaptic and postsynaptic), which are essential for translation of key proteins such as *Rps13, Rps12, Rps26*. There is existing literature supporting the circadian clock control of ribosomal mRNA profiling (Jouffe et al., 2013), but these findings provide a new perspective on how ribosomal translation and local protein synthesis regulate behavioural output.

Notably, several tumor repressor genes were downregulated in SIK3 KI animals such as *Cav2*, *Fap*, *Hrnpd* and *Mkrn2.* As SIK3 is implicated in multiple tumorigenesis pathways, it was previously shown that an upregulation of SIK3 increases cell cycle progression through Akt, p21 Waf/Cip1 activity in breast and ovarian cancers. It is also modulated by the TNF/NFκB axis (Sorrentino et al., 2022). However, a lack of SIK3 shown in our transcriptomics data also leads to the downregulation of selected tumor suppressor genes, suggesting the importance of SIK3 homeostasis in cancer biology. We also observed upregulation of *Ppard,* which is heavily involved in lipid oxidation and homeostasis in SIK3 KI animals. There is growing evidence that lipid signaling is involved in synaptic plasticity and learning. Benedetti et al has shown that PPARb/d, part of the PPAR ligands, is involved in neuronal differentiation (Benedetti et al., 2016). SIK3 KI animals exhibited an increase in REM sleep and REM sleep is strongly associated with neural differentiation (McDevitt et al., 2024). This proposes a connection between metabolic markers, sleep and synaptic function coordinated by SIK3.

Lastly, the interaction between genotype and timepoint analysis revealed that SIK3 regulates time-dependent transcription. Specifically, the *Usp2*, a deubiquitinase involved in both cell cycle and tumorigenesis, was significant at both timepoints and showed increased responsiveness to timepoint shifts in SIK3 KI animals. Researchers have tested the behavioural outcome of *Usp2* KO mice and found that they showed anxiety-like behavior and a deficit in working memory (Srikanta et al., 2021). There is extensive research on the role of USP2 in the SCN as a key regulator of photic entrainment (Cermakian et al., 2013); however, there is a lack of research on the role of USP2 in sleep regulation. It was shown that other members of the USP family are associated with neurodevelopmental disorders and particularly USP14 abolishes Parkinson's Disease symptoms and is associated with sleep and circadian disturbances (downregulation ameliorates) (Favaro et al., 2024). This proposes that SIK3 modulates a family USP that play a role in both sleep/wake stages.

Collectively, these transcriptional changes suggest that the loss of SIK3 kinase activity coordinates growth factor signaling, stress responses, and metabolic processes, implying SIK3's role in cellular homeostasis. A few of the DEGs were previously characterized in the SCN and circadian regulation; these findings in the cortex propose new roles in sleep regulation.

4.3.3 SIK3 regulates sleep through a strong synaptic network

It was proposed in previous studies that global phosphorylation changes in synaptic proteins are strongly associated with sleep need and pressure, from a whole-brain quantitative phosphoproteomics study in the *Slp* mutant and sleep-deprived cohort. In this chapter, we found that Sik3 gene expression is enriched in cortical glutamatergic neurons, which are important for sleep regulation (Kim et al., 2022). Therefore, we adopted Pro-KALIP, optimized in Chapter 3, to identify the direct molecular substrates and phosphorylation sites of SIK3 in the cortex tissue. We detected 643 unique phosphoproteins and 1042 unique phosphosites. We overlapped the dataset with the *Slp* vs WT in vivo phosphoproteomics to identify whether the synaptic changes and phosphorylation patterns related to sleep regulation are directly SIK3-dependent (Wang et al., 2018).

We retrieved a 22% enrichment of SIK3 motif (>80% percentile score) in the SIK3 KALIP dataset from the human Ser/Thr dataset, giving us confidence that identified substrates were SIK3-specific. We then determined 61 proteins and 72 phosphorylation sites as bona fide SIK3 direct substrates that are statistically significant (padj<0.05) in the *Slp* vs WT *in vivo* dataset.

Of which, we observed a strong enrichment of synaptic proteins. Researchers have proposed synaptic homeostasis hypothesis (SHY), suggesting global synaptic alteration during the sleep-wake cycle (Cirelli & Tononi, 2019). Synaptic proteins and phosphorylation patterns regulate the sleep need and pressure (Brüning et al., 2019;

Noya et al., 2019). There are key proteins such as SYN1, SYN3, SGIP1, BIN1 and AMPH, that are essential players in endocytosis and exocytosis, which are crucial for neurotransmitter release and synaptic strength (Almeida et al., 2024). There are also proteins that regulate motility and shaping: SYNPO is involved in actin-based shape and motility and ABI1 and PAK2 are kinases involved in cell growth and cell-cell contacts (Zhang et al., 2013). ABI1 was also included as one of the SNIPPs identified by Slp and sleep deprivation phosphoproteomics. There are also channel proteins, such as HCN2 and KCNA, facilitating excitable neuronal output. Kv1.1 voltage-gated potassium channel a-subunits, encoded by the *Kcnal* gene, act to dampen neuronal excitability by regulating neurotransmitter release and action potential propagation. It is shown that KCNA-null mice exhibit epileptic symptoms due to hyperexcitability (Gautier & Glasscock, 2015). Hyperexcitable circuits are strongly associated with sleep fragmentation and instability (Li et al., 2022). These synaptic proteins also are enriched for “nervous system development” and “regulation of axonogenesis” in GO:BP processes such as MAP1B, accompanying neurite extension. For instance, SYN1 variant is highly associated with neurodevelopmental disorders (Ren et al., 2024). These suggest a downstream pathway of SIK3 direct substrates to neurogenesis. Together, the enrichment of synaptic proteins in direct substrates of SIK3 shows that synaptic phosphorylation changes, detected in the *Slp* dataset, associated with sleep need and pressure are mostly SIK3-dependent. These findings proposed SIK3 and its signaling pathways as strong molecular candidates for sleep regulation essential for cortical excitability and synaptic transmission. In addition, sleep-wake homeostasis is tightly associated with neuroplasticity, where wakefulness encodes new information,

increasing synaptic strength, and sleep facilitates downscaling for synaptic stabilization (Cirelli & Tononi, 2019; Tononi & Cirelli, 2006).SIK3 direct phosphorylation of synaptic proteins proposes a molecular mechanism for sleep-wake homeostasis.

4.3.4 SIK3 direct substrates share CAMK2A and CDKL5 signatures

We then examined the direct phosphorylation sites of SIK3. Notably, we identified multiple key phosphorylation sites of SYN1 such as S568, S605 and S553. The phosphorylation of S605 and S568 regulates actin polymerization and CAMKII has shown to phosphorylate the sites during calcium influx that activates PKA and CAMKII, leading to synaptic vesicle binding (Chhabra et al., 2025). Moreover, RYR2 is inhibited by calmodulin (CaM) and the human S2808 or murine S2807 site is essential for the inhibition (Fruen et al., 2003; Walweel et al., 2019), implicated significantly in cardiac biology. The CAMK signature that we are observing from these sites is implicated in sleep regulation. It is shown that knockdown of CAMK2A and CAMK2B reduces rebound sleep after deprivation, suggesting strong roles in regulating sleep homeostasis (Tone et al., 2022; Wang et al., 2024; Yang et al., 2025). As we observe a parallel CAMK signature in the SIK3 direct substrates, it is implied that SIK3 regulates key pathways in sleep homeostasis.

Moreover, we observed a strong cyclin-dependent kinase signature in the dataset and some substrates are shown in the literature to be downstream. Firstly, CDKL5, a key kinase involved in neuronal development, is phosphorylated by SIK3 at S306. Phosphorylation of CDKL5 is less studied, apart from LF2 phosphorylation, the

activation loop of CDKL5, providing function (Hou et al., 2025). However, the sleep phenotype of CDKL5 is well studied as CDKL deficiency disorder (CDD) imposes epilepsy and severe developmental delays. It is shown that children with CDD have sleep disturbances (Leonard et al., 2026) , reduced total sleep time and frequent night awakenings (Cao et al., 2025). We have also detected validated downstream substrates of CDKL5 such as AMPH S262 (Katayama et al., 2020) and EFHD2 S74. EFHD2 is a calcium-binding protein highly expressed in the central nervous system, associated with tauopathies. These results propose SIK3 as an upstream regulator of CDKL5, thereby initiating a cascade of downstream phosphorylation and new targets for sleep regulation.

4.3.5 SIK3 regulates metabolic pathways

Similar to transcriptomics, we observed an enrichment in metabolic processes in the direct substrates of SIK3.

The insulin/insulin-like growth factor-1 (IGF-1) signaling (IIS) pathway is a key process that regulates metabolic functions, proteostasis and cell growth, triggered by insulin. It activates the PI3K/Akt pathway that controls multiple transcription factors (Balaji et al., 2018). The E3 ligase TTC3 was shown to interact and phosphorylate Akt, which is related to Down Syndrome (Suizu et al., 2009).

In addition, sphingosine kinase 2 (SPHK2) was identified as a direct substrate of SIK3, which has also been shown to be involved in insulin secretion and lipid metabolism. Researchers have shown that SPHK2$^{-/-}$ mice are protected from obesity and exhibited

increased glucose tolerance, associated with the loss of SPHK2 (Ravichandran et al., 2019), which maps to the obesity-resistant phenotype of *Sik3*-deficient mice. Though the phosphorylation of SPHK2 is studied mainly in the context of cancer biology, but the metabolic effects of phosphorylated SPHK2 and the site detected S264 could be implied (Hait et al., 2007). Similarly, the expression of FARP1 is upregulated after exercise and forms a GRP81-FARP1-GLUT4 axis, coordinating glucose uptake (Niu et al., 2026). UVRAG dephosphorylation facilitates lysosomal degradation of EGFR and reduces EGFR signaling. It shows that mTORC1 phosphorylates UVRAG. SIK3 phosphorylates in parallel (Kim et al., 2015), which is implicated in mitochondrial homeostasis and skeletal muscle mass and function. UVRAG deficiency accumulates EGFR and leads to muscle dysfunction (Kim et al., 2021). This corresponds to the muscle weakness and low body weight that we observe in SIK3 KI animals (Darling et al., 2017; Sasagawa et al., 2012).

These direct substrates of SIK3 show that in addition direct effects on circadian and sleep regulation, SIK3 also facilitates peripheral cascades. These propose a mechanistic link between metabolic and sleep/circadian outcomes. Sleep-wake cycle is implied in altering metabolic outcomes such as sleep deprivation altering insulin resistance and obesity (Mesarwi et al., 2013). This links to the circadian and sleep phenotype that we observed in this chapter as secondary downstream effects from disruptions. This reinforces the central-peripheral clock interaction. It potentially proposes new roles of these identified substrates in sleep-wake regulation.

4.3.6 Conclusions

In this chapter, we aimed to build on existing literature on SIK3's role in circadian and sleep regulation using our SIK3 KI animal model. We first conducted a full circadian screening of SIK3 KI and WT animals. We showed that under the inactivity of SIK3, animals exhibited a weaker circadian clock under an imposed LD cycle and longer endogenous circadian period. They lacked photic entrainment, shown from jetlag and non-24hr LD cycle paradigms. These results showed a less plastic circadian clock. We hypothesized that the molecular substrates and pathways identified from transcriptomics and Pro-KALIP could explain the behavioural output observed. From transcriptomics in the cortex, we observed changes in genes involved in lipid metabolism, EGFR signaling and channel transport. Overlapping with *Slp* vs WT *in vivo* phosphoproteomics, we identified 61 proteins as direct substrates of SIK3. Of which, we observed an enrichment in synaptic proteins, key upstream kinases and metabolic processes. This chapter suggests that SIK3 regulates sleep homeostasis through synaptic signaling. In parallel, SIK3 also regulates metabolic processes that act in synergy. These targets could be identified as novel targets that reinforce both metabolic and sleep/circadian regulation. Future experiments could include in vitro validation assays to observe effects on both processes.

Though we observed a significant circadian phenotype under the loss of SIK3, a limitation of the study was that we did not conduct transcriptomics or Pro-KALIP in the SCN. Therefore, the changes that we observed in the cortex could not be directly applied. We could only imply the feedback to the circadian output from the cortex

targets. Given limited breeding capacity and fragility of the SIK3 KI animals due to developmental issues, we couldn't acquire an *in vivo* phosphoproteomics dataset, so there could be false direct substrates.

REFERENCES

Achermann, P., & Borbély, A. A. (2003). MATHEMATICAL MODELS OF SLEEP REGULATION. In *Frontiers in Bioscience* (Vol. 8).

Almeida, C. G., Barata, M. A., Perdigão, C., & Ramalho, J. (2024). Bin1 regulates synaptic endocytic trafficking compromised by Alzheimer's genetic risk variants. *Alzheimer's & Dementia*, *20*(S1). https://doi.org/10.1002/alz.087074

Alpern, D., Gardeux, V., Russeil, J., Mangeat, B., Meireles-Filho, A. C. A., Breysse, R., Hacker, D., & Deplancke, B. (2019). BRB-seq: ultra-affordable high-throughput transcriptomics enabled by bulk RNA barcoding and sequencing. *Genome Biology*, *20*(1), 71. https://doi.org/10.1186/s13059-019-1671-x

Asano, F., Kim, S. J., Fujiyama, T., Miyoshi, C., Hotta-Hirashima, N., Asama, N., Iwasaki, K., Kakizaki, M., Mizuno, S., Mieda, M., Sugiyama, F., Takahashi, S., Shi, S., Hirano, A., Funato, H., & Yanagisawa, M. (2023). SIK3–HDAC4 in the suprachiasmatic nucleus regulates the timing of arousal at the dark onset and circadian period in mice. *Proceedings of the National Academy of Sciences of the United States of America*, *120*(11). https://doi.org/10.1073/pnas.2218209120

Balaji, V., Pokrzywa, W., & Hoppe, T. (2018). Ubiquitylation Pathways In Insulin Signaling and Organismal Homeostasis. In *BioEssays* (Vol. 40, Number 5). John Wiley and Sons Inc. https://doi.org/10.1002/bies.201700223

Benedetti, E., Di Loreto, S., D'Angelo, B., Cristiano, L., d'angelo, M., Antonosante, A., Fidoamore, A., Golini, R., Cinque, B., Cifone, M. G., Ippoliti, R., Giordano, A., & Cimini, A. (2016). The PPARβ/δ Agonist GW0742 Induces Early Neuronal Maturation of Cortical Post-Mitotic Neurons: Role of PPARβ/δ in Neuronal Maturation. *Journal of Cellular Physiology*, *231*(3), 597–606. https://doi.org/10.1002/jcp.25103

Brüning, F., Noya, S. B., Bange, T., Koutsouli, S., Rudolph, J. D., Tyagarajan, S. K., Cox, J., Mann, M., Brown, S. A., & Robles, M. S. (2019). Sleep-wake cycles drive daily dynamics of synaptic phosphorylation. *Science*, *366*(6462). https://doi.org/10.1126/science.aav3617

Cao, L., Zhang, X., Lou, T., Ma, J., Wang, Z., Kim, S. J., Vogt, K., Hirano, A., Tanaka, T., Kikkawa, Y., Yanagisawa, M., & Liu, Q. (2025). Cdkl5 Knockout Mice Recapitulate Sleep Phenotypes of CDKL5 Deficient Disorder. *International Journal of Molecular Sciences*, *26*(8). https://doi.org/10.3390/ijms26083754

Cermakian, N., Lange, T., Golombek, D., Sarkar, D., Nakao, A., Shibata, S., & Mazzoccoli, G. (2013). Crosstalk between the circadian clock circuitry and the immune system. *Chronobiology International*, *30*(7), 870–888. https://doi.org/10.3109/07420528.2013.782315

Chhabra, A., Hoffmann, C., Aguilar Pérez, G., Korobeinikov, A. A., Rentsch, J., Hümpfer, N., Kokwaro, L., Gnidovec, L., Petrović, A., Wallace, J. N., Tromm, J. V., Román-Vendrell, C., Johnson, E. C., Ranković, B., Perego, E., Volpi, T., Fernández-Busnadiego, R., Köster, S., Rizzoli, S. O., … Milovanović, D. (2025). Condensates of synaptic vesicles and synapsin-1 mediate actin sequestering and polymerization. *EMBO Journal*, *44*(18), 5112–5148. https://doi.org/10.1038/s44318-025-00516-y

Cirelli, C., & Tononi, G. (2019). Linking the need to sleep with synaptic function. In *Science* (Vol. 366, Number 6462, pp. 189–190). American Association for the Advancement of Science. https://doi.org/10.1126/science.aay5304

Dai, X., Lin, A., Zhuang, L., Zeng, Q., Cai, L., Wei, Y., Liang, H., Gao, W., Zhang, J., & Chen, X. (2024). Targeting SIK3 to modulate hippocampal synaptic plasticity and cognitive function by regulating the transcription of HDAC4 in a mouse model of Alzheimer's disease. *Neuropsychopharmacology : Official Publication of the American College of Neuropsychopharmacology*, *49*(6), 942–952. https://doi.org/10.1038/s41386-023-01775-1

Darling, N. J., Toth, R., Arthur, J. S. C., & Clark, K. (2017). Inhibition of SIK2 and SIK3 during differentiation enhances the anti-inflammatory phenotype of macrophages. *Biochemical Journal*, *474*(4), 521–537. https://doi.org/10.1042/BCJ20160646

Darmohray, D., Sima, J., Chen, C.-H., Silverman, D., Chen, C., Xu, A., Yao, Y., & Dan, Y. (2025). Brainstem circuit for sickness-induced sleep. In *Sci. Adv* (Vol. 11). https://BioRender.com/wd76zgb.

Favaro, M., Mauri, S., Bernardo, G., Zordan, M. A., Mazzotta, G. M., & Ziviani, E. (2024). Usp14 down-regulation corrects sleep and circadian dysfunction of a Drosophila model of Parkinson's disease. *Frontiers in Neuroscience*, *18*. https://doi.org/10.3389/fnins.2024.1410139

Foilb, A. R., Taylor-Yeremeeva, E. M., Fritsch, E. L., Ravichandran, C., Lezak, K. R., Missig, G., McCullough, K. M., & Carlezon, W. A. (2023). *Differential effects of the stress peptides PACAP and CRF on sleep architecture in mice*. https://doi.org/10.1101/2023.03.22.533872

Fruen, B. R., Black, D. J., Bloomquist, R. A., Bardy, J. M., Johnson, J. D., Louis, C. F., & Balog, E. M. (2003). Regulation of the RYR1 and RYR2 Ca^{2+} Release Channel Isoforms by Ca^{2+} -Insensitive Mutants of Calmodulin. *Biochemistry*, *42*(9), 2740–2747. https://doi.org/10.1021/bi0267689

Funato, H., Miyoshi, C., Fujiyama, T., Kanda, T., Sato, M., Wang, Z., Ma, J., Nakane, S., Tomita, J., Ikkyu, A., Kakizaki, M., Hotta-Hirashima, N., Kanno, S., Komiya, H., Asano, F., Honda, T., Kim, S. J., Harano, K., Muramoto, H., … Yanagisawa, M. (2016). Forward-genetics analysis of sleep in randomly mutagenized mice. *Nature*, *539*(7629), 378–383. https://doi.org/10.1038/nature20142

Gautier, N. M., & Glasscock, E. (2015). Spontaneous seizures in Kcna1-null mice lacking voltage-gated Kv1.1 channels activate Fos expression in select limbic circuits. *Journal of Neurochemistry*, *135*(1), 157–164. https://doi.org/10.1111/jnc.13206

Gillette, M. U., & Mitchell, J. W. (2002). Signaling in the suprachiasmatic nucleus: selectively responsive and integrative. *Cell and Tissue Research*, *309*(1), 99–107. https://doi.org/10.1007/s00441-002-0576-1

Hait, N. C., Bellamy, A., Milstien, S., Kordula, T., & Spiegel, S. (2007). Sphingosine Kinase Type 2 Activation by ERK-mediated Phosphorylation. *Journal of Biological Chemistry*, *282*(16), 12058–12065. https://doi.org/10.1074/jbc.M609559200

Hayasaka, N., Hirano, A., Miyoshi, Y., Tokuda, I. T., Yoshitane, H., Matsuda, J., & Fukada, Y. (2017). Salt-inducible kinase 3 regulates the mammalian circadian clock by destabilizing PER2 protein. *ELife*, *6*. https://doi.org/10.7554/eLife.24779

Hoffmann, C., Rentsch, J., Tsunoyama, T. A., Chhabra, A., Aguilar Perez, G., Chowdhury, R., Trnka, F., Korobeinikov, A. A., Shaib, A. H., Ganzella, M., Giannone, G., Rizzoli, S. O., Kusumi, A., Ewers, H., & Milovanovic, D. (2023).

Synapsin condensation controls synaptic vesicle sequestering and dynamics. *Nature Communications*, *14*(1). https://doi.org/10.1038/s41467-023-42372-6
Honda, T., Fujiyama, T., Miyoshi, C., Ikkyu, A., Hotta-Hirashima, N., Kanno, S., Mizuno, S., Sugiyama, F., Takahashi, S., Funato, H., & Yanagisawa, M. (2018). A single phosphorylation site of SIK3 regulates daily sleep amounts and sleep need in mice. *Proceedings of the National Academy of Sciences of the United States of America*, *115*(41), 10458–10463. https://doi.org/10.1073/pnas.1810823115
Hou, Y., Omi, O. A., Stuck, M. W., Cheng, X., Walker, B., Lam, Y. W., Schmoker, A. M., Nguyen, S. N., Gonzalez-Perez, M. P., Ballif, B. A., Lechtreck, K. F., Witman, G. B., & Pazour, G. J. (2025). Activation of the ciliary kinase CDKL5 is mediated by the cyclin-dependent kinase CDK20/LF2 to control flagellar length. *PLoS Biology*, *23*(12), e3003560. https://doi.org/10.1371/journal.pbio.3003560
Jiménez, A., Lu, Y., Jambhekar, A., & Lahav, G. (2022). Principles, mechanisms and functions of entrainment in biological oscillators. In *Interface Focus* (Vol. 12, Number 3). Royal Society Publishing. https://doi.org/10.1098/rsfs.2021.0088
Johnson, J. L., Yaron, T. M., Huntsman, E. M., Kerelsky, A., Song, J., Regev, A., Lin, T. Y., Liberatore, K., Cizin, D. M., Cohen, B. M., Vasan, N., Ma, Y., Krismer, K., Robles, J. T., van de Kooij, B., van Vlimmeren, A. E., Andrée-Busch, N., Käufer, N. F., Dorovkov, M. V., … Cantley, L. C. (2023). An atlas of substrate specificities for the human serine/threonine kinome. *Nature*, *613*(7945), 759–766. https://doi.org/10.1038/s41586-022-05575-3
Jouffe, C., Cretenet, G., Symul, L., Martin, E., Atger, F., Naef, F., & Gachon, F. (2013). The Circadian Clock Coordinates Ribosome Biogenesis. *PLoS Biology*, *11*(1). https://doi.org/10.1371/journal.pbio.1001455
Katayama, S., Sueyoshi, N., Inazu, T., & Kameshita, I. (2020). Cyclin-Dependent Kinase-Like 5 (CDKL5): Possible Cellular Signalling Targets and Involvement in CDKL5 Deficiency Disorder. In *Neural Plasticity* (Vol. 2020). Hindawi Limited. https://doi.org/10.1155/2020/6970190
Katoh, Y., Takemori, H., Horike, N., Doi, J., Muraoka, M., Min, L., & Okamoto, M. (2004). Salt-inducible kinase (SIK) isoforms: Their involvement in steroidogenesis and adipogenesis. *Molecular and Cellular Endocrinology*, *217*(1–2), 109–112. https://doi.org/10.1016/j.mce.2003.10.016
Katoh, Y., Takemori, H., Lin, X. Z., Tamura, M., Muraoka, M., Satoh, T., Tsuchiya, Y., Min, L., Doi, J., Miyauchi, A., Witters, L. A., Nakamura, H., & Okamoto, M. (2006). Silencing the constitutive active transcription factor CREB by the LKB1-SIK signaling cascade. *FEBS Journal*, *273*(12), 2730–2748. https://doi.org/10.1111/j.1742-4658.2006.05291.x
Kim, M. J., Febbraro, D., Farkona, S., Gillmore, T., Son, J. E., Regeenes, R., Chang, H. H., Pollock-Tahiri, E., Yang, J., Park, Y. J., Sivasubramaniyam, T., Oh, S. J., Saraon, P., Stagljar, I., Rocheleau, J. V., Hui, C. C., Caniggia, I., Hao, Z., Mak, T. W., … Woo, M. (2021). Distinct roles of UVRAG and EGFR signaling in skeletal muscle homeostasis. *Molecular Metabolism*, *47*. https://doi.org/10.1016/j.molmet.2021.101185
Kim, S. J., Hotta-Hirashima, N., Asano, F., Kitazono, T., Iwasaki, K., Nakata, S., Komiya, H., Asama, N., Matsuoka, T., Fujiyama, T., Ikkyu, A., Kakizaki, M., Kanno, S., Choi, J., Kumar, D., Tsukamoto, T., Elhosainy, A., Mizuno, S., Miyazaki, S., … Funato, H.

(2022). Kinase signalling in excitatory neurons regulates sleep quantity and depth. *Nature*, *612*(7940), 512–518. https://doi.org/10.1038/s41586-022-05450-1

Kim, Y. M., Jung, C. H., Seo, M., Kim, E. K., Park, J. M., Bae, S. S., & Kim, D. H. (2015). MTORC1 phosphorylates UVRAG to negatively regulate autophagosome and endosome maturation. *Molecular Cell*, *57*(2), 207–218. https://doi.org/10.1016/j.molcel.2014.11.013

Krafty, R. T., Fu, H., Graves, J. L., Bruce, S. A., Hall, M. H., & Smagula, S. F. (n.d.). *Measuring Variability in Rest-Activity Rhythms from Actigraphy with Application to Characterizing Symptoms of Depression*.

Leonard, H., Szepe, E., Junaid, M., Wong, K., Saldaris, J., & Downs, J. (2026). Exploring sleep challenges in CDKL5 Deficiency Disorder. *Journal of Neurodevelopmental Disorders*, *18*(1). https://doi.org/10.1186/s11689-025-09666-w

Li, S.-B., Damonte, V. M., Chen, C., Wang, G. X., Kebschull, J. M., Yamaguchi, H., Bian, W.-J., Purmann, C., Pattni, R., Urban, A. E., Mourrain, P., Kauer, J. A., Scherrer, G., & de Lecea, L. (2022). Hyperexcitable arousal circuits drive sleep instability during aging. *Science*, *375*(6583). https://doi.org/10.1126/science.abh3021

Martelle, S. E., Cotella, E. M., Nawreen, N., Chen, C., Packard, B. A., Fitzgerald, M., & Herman, J. P. (2021). Prefrontal cortex PACAP signaling: organization and role in stress regulation. *Stress*, *24*(2), 196–205. https://doi.org/10.1080/10253890.2021.1887849

McDevitt, E. A., Kim, G., Turk-Browne, N. B., & Norman, K. A. (2024). *The role of REM sleep in neural differentiation of memories in the hippocampus*. https://doi.org/10.1101/2024.11.01.621588

Mesarwi, O., Polak, J., Jun, J., & Polotsky, V. Y. (2013). Sleep Disorders and the Development of Insulin Resistance and Obesity. In *Endocrinology and Metabolism Clinics of North America* (Vol. 42, Number 3, pp. 617–634). https://doi.org/10.1016/j.ecl.2013.05.001

Nishida, K., Matsumura, K., Tamura, M., Nakamichi, T., Shimamori, K., Kuragano, M., Kabir, A. M. R., Kakugo, A., Kotani, S., Nishishita, N., & Tokuraku, K. (2023). Effects of three microtubule-associated proteins (MAP2, MAP4, and Tau) on microtubules' physical properties and neurite morphology. *Scientific Reports*, *13*(1). https://doi.org/10.1038/s41598-023-36073-9

Niu, Y., Hu, S., Zhang, Y., Yang, J., Zhang, J., He, R., Chen, L., Xu, L., Zhao, H., Gan, B., Ren, R., Loos, R. J. F., Ye, H., Du, X., Zhao, T., Li, P., Vidal-Puig, A., & Huang, L. (2026). Lactate-activated GPR81/FARP1 signaling drives insulin-independent glucose uptake and metabolic control. *Cell Research*. https://doi.org/10.1038/s41422-025-01207-3

Noya, S. B., Colameo, D., Brüning, F., Spinnler, A., Mircsof, D., Opitz, L., Mann, M., Tyagarajan, S. K., Robles, M. S., & Brown, S. A. (2019). The forebrain synaptic transcriptome is organized by clocks but its proteome is driven by sleep. *Science*, *366*(6462). https://doi.org/10.1126/science.aav2642

Perrotti, L. I., Hadeishi, Y., Ulery, P. G., Barrot, M., Monteggia, L., Duman, R. S., & Nestler, E. J. (2004). Induction of ΔFosB in Reward-Related Brain Structures after Chronic Stress. *The Journal of Neuroscience*, *24*(47), 10594–10602. https://doi.org/10.1523/JNEUROSCI.2542-04.2004

Qiao, S., Peng, R., Yan, H., Gao, Y., Wang, C., Wang, S., Zou, Y., Xu, X., Zhao, L., Dong, J., Su, Z., Feng, X., Wang, L., & Hu, X. (2014). Reduction of Phosphorylated Synapsin I (Ser-553) Leads to Spatial Memory Impairment by Attenuating GABA Release after Microwave Exposure in Wistar Rats. *PLoS ONE*, *9*(4), e95503. https://doi.org/10.1371/journal.pone.0095503

Ravichandran, S., Finlin, B. S., Kern, P. A., & Özcan, S. (2019). Sphk2−/− mice are protected from obesity and insulin resistance. *Biochimica et Biophysica Acta - Molecular Basis of Disease*, *1865*(3), 570–576. https://doi.org/10.1016/j.bbadis.2018.12.012

Ren, B., Wu, X., Zhou, Y., Chen, L., & Jiang, J. (2024). SYN1 variant causes X-linked neurodevelopmental disorders: a case report of variable clinical phenotypes in siblings. *Frontiers in Neurology* , *15*. https://doi.org/10.3389/fneur.2024.1359287

Rochon, P. L., Theriault, C., Olguin, A. G. R., & Krishnaswamy, A. (2021). The cell adhesion molecule Sdk1 shapes assembly of a retinal circuit that detects localized edges. *ELife*, *10*. https://doi.org/10.7554/eLife.70870

Sakai, T., Tamura, T., Kitamoto, T., & Kidokoro, Y. (2004). *A clock gene, period, plays a key role in long-term memory formation in Drosophila* (Vol. 101). https://www.pnas.org

Sasagawa, S., Takemori, H., Uebi, T., Ikegami, D., Hiramatsu, K., Ikegawa, S., Yoshikawa, H., & Tsumaki, N. (2012). SIK3 is essential for chondrocyte hypertrophy during skeletal development in mice. *Development*, *139*(6), 1153–1163. https://doi.org/10.1242/dev.072652

Simonova, V. V., Guzeev, M. A., Ekimova, I. V., & Pastukhov, Y. F. (2022). Chaperone Hsp70 (HSPA1) Is Involved in the Molecular Mechanisms of Sleep Cycle Integration. *International Journal of Molecular Sciences*, *23*(8). https://doi.org/10.3390/ijms23084464

Sorrentino, A., Menevse, A. N., Michels, T., Volpin, V., Durst, F. C., Sax, J., Xydia, M., Hussein, A., Stamova, S., Spoerl, S., Heuschneider, N., Muehlbauer, J., Jeltsch, K. M., Rathinasamy, A., Werner-Klein, M., Breinig, M., Mikietyn, D., Kohler, C., Poschke, I., … Beckhove, P. (2022). Salt-inducible kinase 3 protects tumor cells from cytotoxic T-cell attack by promoting TNF-induced NF-κB activation. *Journal for Immunotherapy of Cancer*, *10*(5). https://doi.org/10.1136/jitc-2021-004258

Srikanta, S. B., Stojkovic, K., & Cermakian, N. (2021). Behavioural phenotyping of mice lacking the deubiquitinase USP2. *PLoS ONE*, *16*(2 February). https://doi.org/10.1371/journal.pone.0241403

Suizu, F., Hiramuki, Y., Okumura, F., Matsuda, M., Okumura, A. J., Hirata, N., Narita, M., Kohno, T., Yokota, J., Bohgaki, M., Obuse, C., Hatakeyama, S., Obata, T., & Noguchi, M. (2009). The E3 Ligase TTC3 Facilitates Ubiquitination and Degradation of Phosphorylated Akt. *Developmental Cell*, *17*(6), 800–810. https://doi.org/10.1016/j.devcel.2009.09.007

Tone, D., Ode, K. L., Zhang, Q., Fujishima, H., Yamada, R. G., Nagashima, Y., Matsumoto, K., Wen, Z., Yoshida, S. Y., Mitani, T. T., Arisato, Y., Ohno, R. I., Ukai-Tadenuma, M., Garçon, J. Y., Kaneko, M., Shi, S., Ukai, H., Miyamichi, K., Okada, T., … Ueda, H. R. (2022). Distinct phosphorylation states of mammalian CaMKIIβ control the induction and maintenance of sleep. *PLoS Biology*, *20*(10). https://doi.org/10.1371/journal.pbio.3001813

Tononi, G., & Cirelli, C. (2006). Sleep function and synaptic homeostasis. In *Sleep Medicine Reviews* (Vol. 10, Number 1, pp. 49–62). https://doi.org/10.1016/j.smrv.2005.05.002

Uebi, T., Itoh, Y., Hatano, O., Kumagai, A., Sanosaka, M., Sasaki, T., Sasagawa, S., Doi, J., Tatsumi, K., Mitamura, K., Morii, E., Aozasa, K., Kawamura, T., Okumura, M., Nakae, J., Takikawa, H., Fukusato, T., Koura, M., Nish, M., … Takemori, H. (2012). Involvement of SIK3 in glucose and lipid homeostasis in mice. *PLoS ONE*, *7*(5). https://doi.org/10.1371/journal.pone.0037803

Vega, R. B., Matsuda, K., Oh, J., Barbosa, A. C., Yang, X., Meadows, E., McAnally, J., Pomajzl, C., Shelton, J. M., Richardson, J. A., Karsenty, G., & Olson, E. N. (2004). Histone Deacetylase 4 Controls Chondrocyte Hypertrophy during Skeletogenesis. *Cell*, *119*(4), 555–566. https://doi.org/10.1016/j.cell.2004.10.024

Walkinshaw, D. R., Weist, R., Kim, G. W., You, L., Xiao, L., Nie, J., Li, C. S., Zhao, S., Xu, M., & Yang, X. J. (2013). The tumor suppressor kinase LKB1 activates the downstream kinases SIK2 and SIK3 to stimulate nuclear export of class IIa histone deacetylases. *Journal of Biological Chemistry*, *288*(13), 9345–9362. https://doi.org/10.1074/jbc.M113.456996

Walweel, K., Gomez-Hurtado, N., Rebbeck, R. T., Oo, Y. W., Beard, N. A., Molenaar, P., dos Remedios, C., van Helden, D. F., Cornea, R. L., Knollmann, B. C., & Laver, D. R. (2019). Calmodulin inhibition of human RyR2 channels requires phosphorylation of RyR2-S2808 or RyR2-S2814. *Journal of Molecular and Cellular Cardiology*, *130*, 96–106. https://doi.org/10.1016/j.yjmcc.2019.03.018

Wang, Y., Cao, S., Tone, D., Fujishima, H., Yamada, R. G., Ohno, R. I., Shi, S., Matsuzawa, K., Yada, S., Kaneko, M., Sakamoto, H., Onishi, T., Ukai-Tadenuma, M., Ukai, H., Hanashima, C., Hirose, K., Kiyonari, H., Sumiyama, K., Ode, K. L., & Ueda, H. R. (2024). Postsynaptic competition between calcineurin and PKA regulates mammalian sleep–wake cycles. *Nature*, *636*(8042), 412–421. https://doi.org/10.1038/s41586-024-08132-2

Wang, Z., Ma, J., Miyoshi, C., Li, Y., Sato, M., Ogawa, Y., Lou, T., Ma, C., Gao, X., Lee, C., Fujiyama, T., Yang, X., Zhou, S., Hotta-Hirashima, N., Klewe-Nebenius, D., Ikkyu, A., Kakizaki, M., Kanno, S., Cao, L., … Liu, Q. (2018). Quantitative phosphoproteomic analysis of the molecular substrates of sleep need. *Nature*, *558*(7710), 435–439. https://doi.org/10.1038/s41586-018-0218-8

Williams, J. A., & Naidoo, N. (2020). Sleep and cellular stress. In *Current Opinion in Physiology* (Vol. 15, pp. 104–110). Elsevier Ltd. https://doi.org/10.1016/j.cophys.2019.12.011

Wolber, L. E., Girotto, G., Buniello, A., Vuckovic, D., Pirastu, N., Lorente-Cánovas, B., Rudan, I., Hayward, C., Polasek, O., Ciullo, M., Mangino, M., Steves, C., Concas, M. P. ina, Cocca, M., Spector, T. D., Gasparini, P., Steel, K. P., & Williams, F. M. K. (2014). Salt-inducible kinase 3, SIK3, is a new gene associated with hearing. *Human Molecular Genetics*, *23*(23), 6407–6418. https://doi.org/10.1093/hmg/ddu346

Yang, W., Shi, J., Li, C., Yang, J., Yu, J., Huang, J., & Rao, Y. (2025). Calcium/calmodulin-dependent protein kinase II α and β differentially regulate mammalian sleep. *Communications Biology*, *8*(1). https://doi.org/10.1038/s42003-024-07449-y

Yao, Z., van Velthoven, C. T. J., Kunst, M., Zhang, M., McMillen, D., Lee, C., Jung, W., Goldy, J., Abdelhak, A., Aitken, M., Baker, K., Baker, P., Barkan, E., Bertagnolli, D., Bhandiwad, A., Bielstein, C., Bishwakarma, P., Campos, J., Carey, D., … Zeng, H. (2023). A high-resolution transcriptomic and spatial atlas of cell types in the whole mouse brain. *Nature*, *624*(7991), 317–332. https://doi.org/10.1038/s41586-023-06812-z

Zhang, X. L., Pöschel, B., Faul, C., Upreti, C., Stanton, P. K., & Mundel, P. (2013). Essential role for synaptopodin in dendritic spine plasticity of the developing hippocampus. *Journal of Neuroscience*, *33*(30), 12510–12518. https://doi.org/10.1523/JNEUROSCI.2983-12.2013

Zhang, L., Hernandez, V. S., Gerfen, C. R., Jiang, S. Z., Zavala, L., Barrio, R. A., & Eiden, L. E. (2021). Behavioral role of PACAP signaling reflects its selective distribution in glutamatergic and GABAergic neuronal subpopulations. *ELife*, *10*. https://doi.org/10.7554/eLife.61718

Zhi, W.-J., Qiao, S.-M., Zou, Y., Peng, R.-Y., Yan, H.-T., Ma, L.-Z., Dong, J., Zhao, L., Yao, B.-W., Zhao, X.-L., Feng, X.-X., Hu, X.-J., & Wang, L.-F. (2021). Low p-SYN1 (Ser-553) Expression Leads to Abnormal Neurotransmitter Release of GABA Induced by Up-Regulated Cdk5 after Microwave Exposure: Insights on Protection and Treatment of Microwave-Induced Cognitive Dysfunction. *Current Issues in Molecular Biology*, *44*(1), 206–221. https://doi.org/10.3390/cimb44010015

Zhou, R., Wang, G., Li, Q., Meng, F., Liu, C., Gan, R., Ju, D., Liao, M., Xu, J., Sang, D., Gao, X., Zhou, S., Wu, K., Sun, Q., Guo, Y., Wu, C., Chen, Z., Chen, L., Shi, B., … Liu, Q. (2022). A signalling pathway for transcriptional regulation of sleep amount in mice. *Nature*, *612*(7940), 519–527. https://doi.org/10.1038/s41586-022-05510-6

Chapter 5: Characterization of the role of SIK2

5.1 Introduction

5.1.1 Circadian, sleep, and behavioural implications of SIK2

There is limited evidence on the role of SIK2 in circadian and sleep regulation. S358 and S587 on SIK2 are PKA phosphorylation sites (Park et al., 2020), which promote the binding of 14-3-3 to SIK2 (Henriksson et al., 2012). Evidence has shown that the PKA site S551 on SIK3 is an important site for sleep need (Honda et al., 2018). Consequently, Park et al explored the SIK2 PKA site S587 and the phenotypes of the non-functional alanine S587A. Both heterozygous and homozygous SIK2 S587A mice showed an increased NREM sleep delta density, but no differences in time spent in vigilant states (Park et al., 2020), supporting the role of the SIK2-PKA axis in sleep regulation. The relationship to energy metabolism appears to be independent of proposed sleep pathways.

5.1.2 Regulation and Signalling of SIK2

Though SIK2 is less studied in the sleep and circadian context, the SIK2-CRTC2 relationship was explored in the neuronal context. It was shown that SIK2 levels are lower after ischemic injury and are accompanied by CRTC1 dephosphorylation. CRTC family dephosphorylation in response to Ca^{2+} and cAMP signals plays an important role in hippocampal long-term potentiation. It is shown that the low levels of SIK2 are essential for activation of CREB and therefore neuronal survival, which is maintained by the phosphorylation of SIK2 at T484 by CAMKI/IV kinases. It was confirmed that Sik2 knockout mice ($Sik2^{-/-}$) have enhanced neuronal survival (Sasaki et al., 2011). CRTCs

interact with CREB and are associated with behavioural and autonomic response stress-related psychiatric diseases in the paraventricular nucleus (PVN). *Sik2* mRNA is present in the PVN, and overexpression of SIK2 is linked to the inhibition of nuclear translocation of CRTC2, as it is responsible for maintaining phosphorylated CRTCs in the cytoplasm (Liu et al., 2012).

In addition, SIK2 is one of the most abundantly expressed AMPK kinases in adipocytes (Henriksson et al., 2012). *Sik2* mRNA has the highest expression in both white and brown adipose tissues, and also at lower levels in mice testes (Katoh et al., 2004a; Okamoto et al., 2004). During adipocyte differentiation, *Sik2* mRNA appeared along with *C/EBPα* mRNA, a transcription factor associated with early phase differentiation in preadipocytes. In addition, *Sik2* mRNA transcription levels correspond to transcripts associated with late response adipogenesis, such as SREBP-1, C/EBPα, PPARG and AP2, that start to appear a few days into differentiation (Okamoto et al., 2004). In human adipocytes, there is low *Sik2* mRNA in obese individuals and it is negatively correlated with insulin resistance, measured by HOMA-IR (Henriksson et al., 2014; Säll et al., 2019). It is also implicated that SIKs are involved in GLUT4 translocation and PKB/Akt phosphorylation. These studies support SIK2's role in lipid homeostasis and adipogenesis.

Literature has identified pathways and key post-translational modification (PTM) sites. It is shown that there is high SIK2 content in diabetic$^{db/db}$ mice, suggesting SIK2's role in white adipose tissue in T2D (Horike et al., 2003). Specifically, IRS proteins are

important in the insulin signaling cascade, and phosphorylation on serine residues can modulate the efficiency of insulin signaling. *In vitro*, Horike et al 2003 identified S789 in rat IRS-1 (equivalent to S794 on human IRS-1) as a substrate of SIK2 in 3T3-L1 cells. The site is also essential for CREB/CRE signaling, essential for adipocyte differentiation, accentuating SIK2's role in the initiation of adipocyte differentiation.

SIK2 S358 was identified as an essential PKA phosphorylation site and promotes the binding of 14-3-3, modulating kinase activity (Sonntag et al., 2018). It was also validated as essential for PKA-dependent phosphorylation of SIK2 in adipocytes and directly mediated S587 in response to cAMP induction, leading to relocalisation of SIK2 in the cytosolic fraction (Henriksson et al., 2012). S358 also facilitates the molecular interactions of SIK2 with CRTC2, CRTC3 and HDAC4 in adipocytes. As HDAC4 and CREB are shown to inhibit GLUT4 (Qi et al., 2009; Weems et al., 2012) and SIK2 is confirmed as an upstream kinase, knockout of SIK2 reduces 60% of GLUT4 protein levels, suggesting key roles in glucose uptake (Henriksson et al., 2014). This is further supported by studies in pancreatic beta cells. SIK2, following glucose stimulation, phosphorylates p35 at S91 and triggers ubiquitination via PJA2, establishing a SIK2-PJA2-p35 axis that contributes to insulin secretion and glucose homeostasis (Sakamaki et al., 2014).

In addition to phosphorylation sites, Lys-53 was identified as a key acetylation site targeted by p300, which, through *in vitro* ATP binding assays, was shown to suppress SIK2 kinase activity. HDAC6 also acts as the deacetylase of SIK2, which validates the counter effects of p300/CBP and HDAC6 in the acetylation of SIK2 and kinase activity,

implying SIK2's role in autophagosome progression (Yang et al., 2013). Moreover, SIK2 phosphorylates p300 and the loss of SIK2 increases ChREBP acetylation, an important mediator for glucose action in glycolysis and lipogenesis, in synergy with SREBP-1 (Bricambert et al., 2010).

5.1.2 Role of SIK2 in cancer

In multiple cancer forms, dysregulation of fatty acid metabolism was identified as a component of malignant tumor transformation. Overexpression of SIK2 is associated with significantly higher free fatty acid and triglycerides, which in turn reshapes lipid metabolism in ovarian cancer cells. There is a positive correlation between SIK2 and SREBP1c levels in ovarian cancer (OC) cells through the activation of PI3K/Akt pathway, which promotes fatty acid and cholesterol synthesis and enhances OC progression and metastasis (Zhao et al., 2020). Gao et al also found that SIK2 accentuates the Warburg effect in ovarian cancer, where cancer cells undergo aerobic glycolysis to protect and promote tumor growth. SIK2 upregulates HIF-1α by activating PI3K/Akt signaling pathway and also phosphorylates Drp1 at S616 to promote mitochondrial fission, suggesting a role of glucose metabolism in OC cells (Gao et al., 2020). In addition, Shi et al showed that SIK2 phosphorylates MYLK directly at S434, establishing a MYLK-MYL2 axis, promoting OC cell metastasis (Shi et al., 2022). As ovarian cancer metastasis occurs in the omentum, an adipocyte-rich region in the abdomen, the role of SIK2 was examined, given its strong presence in adipocytes. It was validated that SIK2 drives adipocyte-driven OC metastasis in the abdomen through the phosphorylation of p85a, a key regulatory subunit of the PI3K complex at S154,

thereby enhancing PI3K/Akt signaling (Miranda et al., 2016). In addition, Ahmed et al proposed that SIK2 is involved in mitosis and is crucial for centrosome splitting by phosphorylating C-Nap 1 at S2392. AKT phosphorylation is key to ovarian cancer growth and SIK2 presence is required for phosphorylation, as depletion of SIK2 is correlated with decreased Akt phosphorylation. Depletion of SIK2 leads to decreased resistance to paclitaxel-induced mitotic arrest as it fails to undergo centrosome separation and becomes more sensitive to paclitaxel treatment, reducing ovarian cancer tumor weight (Ahmed et al., 2010).

In prostate cancer cell lines, Bon et al has shown that loss of SIK2 leads to a delay in cell cycle, cell death initiation and increased CREB1 activity, a proto-oncogene through the SIK2/CRTC/CREB pathway. This study further supports the role of SIK2 in cell cycle regulation, providing insight into various cell type metastasis (Bon et al., 2015). In breast cancer, Zohrap et al characterized SIK2 as a tumor suppressor by inhibiting the MAPK and PI3K/Akt pathways and reducing cancer cell migration. SIK2 expression is also found to be downregulated in breast cancer cells and has a negative correlation with survival chances (Zohrap et al., 2018). Conversely, Maxfield et al found that SIK2 is crucial for triple-negative breast cancer (TNBC) tumor growth, suggesting that inhibition could suppress tumor growth (Maxfield et al., 2016).

These findings support that SIK2 plays varying roles in cancer progression in different forms of cancer.

5.1.3 Pharmacological implications of SIK2

As SIK2 is implicated in multiple disease pathologies, researchers have looked at channels to target it pharmacologically. Jiang et al found increased levels of SIK2 in the hippocampus of chronic models of depression, which reduced CRTC1 nuclear translocation and binding to CREB in the hippocampus. Overexpression of SIK2 displayed symptoms of chronic stress, shown by social behavioural tests. Knockdown of SIK2 shows significant antidepressant effects through the BDNF pathway (Jiang et al., 2019a). ARN-3236, as a selective SIK2 inhibitor, was also validated to have anti-depressant effects and has promoting effects on BDNF under baseline (Liu et al., 2021). Extending the research to ovarian cancer treatment, ARN-3261 (pan-inhibitor of SIKs) inhibited cell growth on eight ovarian cancer cell lines by inducing double-strand breaks in DNA of cancer cells. There are ongoing clinical trials on adopting ARN-3261 to ovarian cancer patients (Fan et al., 2021).

5.1.4 Aims

Previous literature has established SIK2's role in neurophysiology, lipid metabolism and cancer biology. Through small-molecule interventions, there are also ongoing efforts to target SIK2 pharmacologically. However, there is a limited understanding of SIK2 in circadian and sleep regulation, given the significance of other SIK isoforms.
This chapter aims to explore SIK2's role in the circadian and sleep context through the following approaches:

(1) Circadian and sleep phenotyping

We aim to conduct a full circadian characterization using the SIK2 KI mice through wheel-running recordings under various stimulations and conditions. Additionally, we aim to characterize the sleep phenotype under the loss of SIK2 kinase activity under baseline LD cycle and 6hr sleep deprivation (SD) for homeostatic responses.

(2) Transcriptomics and molecular substrates

Based on the Sik2 gene expression profile in different brain regions, we aim to conduct tissue-specific mRNAseq to construct differential gene expression. Direct molecular substrates and phosphorylation sites of SIK2 are identified using the optimized pro-KALIP assay. We hypothesize that the substrates identified provide a holistic understanding of SIK2's signaling architecture.

(3) Behavioural alterations

As there is a growing body of evidence linking sleep homeostasis to synaptic function, we aim to perform behavioural tests to explore memory and cognitive functions in SIK2 KI animals.

5.2 Results

5.2.1 Single-cell RNAseq (scRNAseq) explores the distribution of Sik2 in the brain and cell types

We then consulted the Allen Brain Atlas (ABC) scRNAseq dataset to examine the expression and distribution of Sik2 in the brain. Looking at the scale of *Sik2* expression, there is high variation of gene expression across the brain, ranging from approximately 0.5 to 119 counts per million (CPM). The bar height of the scale shows that the majority of the brain regions have high levels of *Sik2* expression in CPM (Fig. 5.1a).

In the slice containing the SCN, *Sik2* expression is evenly distributed across the brain regions, showing higher expression in the cortical layers. *Sik2* is shown to be predominantly expressed in GABAergic neurons in the SCN, hypothalamic and thalamic regions, and in glutamatergic neurons in the cortical layers (Fig. 5.1b). In the slice containing the hippocampus, *Sik2* is present in the dentate gyrus (DG) region. There is similarly high expression in the hypothalamus and cortical layers. There is low *Sik2* expression in dopaminergic neurons. In addition to neuronal cells, *Sik2* is also expressed highly in astrocytes and oligodendrocytes, spanning across cell types (Fig. 5.1c).

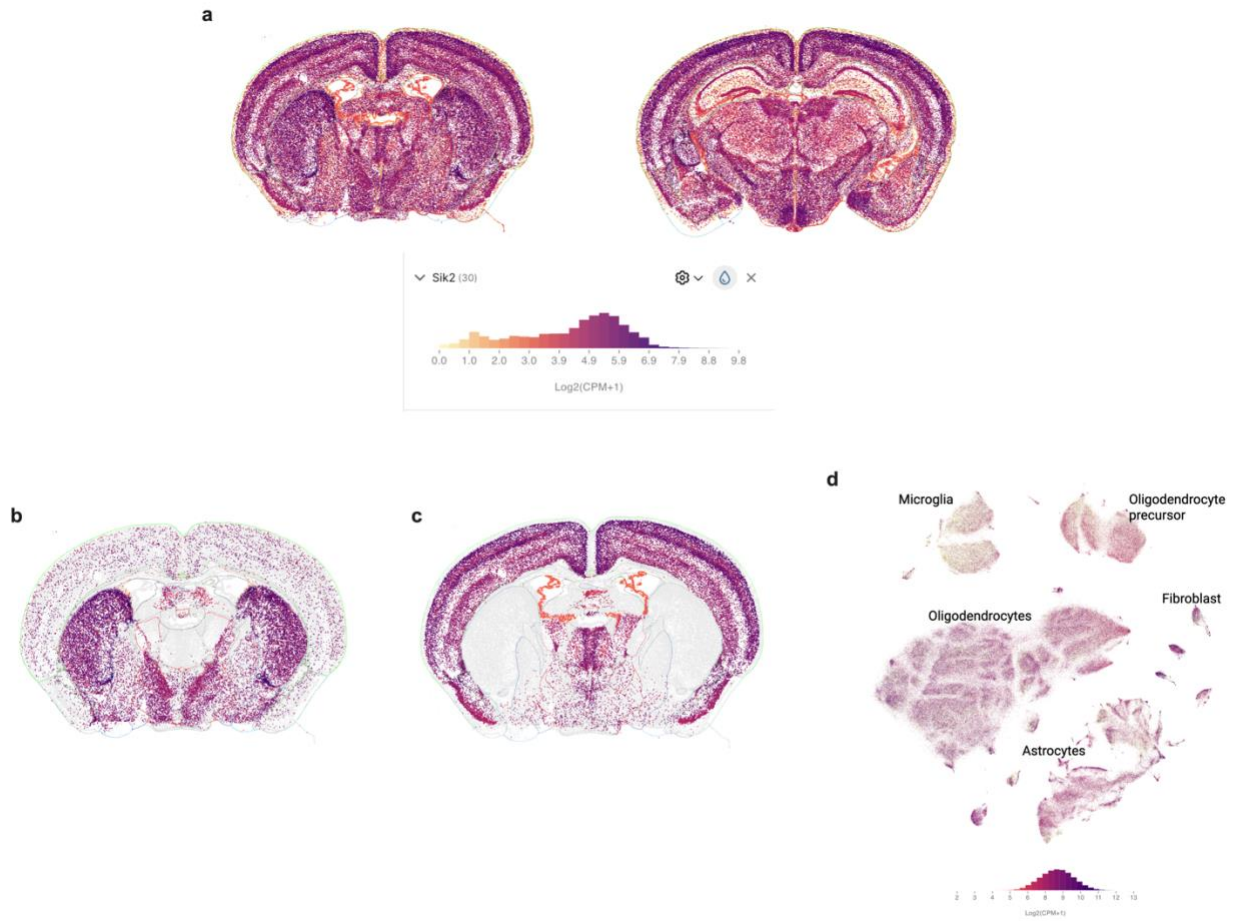

Fig. 5.1 ***Sik2* gene expression in different brain regions and cell types.** Spatial transcriptomics of Sik2 from Allen Brain Atlas MERFISH C57BL6J-638850 with Imputed Genes + Reconstructed Coordinates (Yao et al., 2023). (a) Coronal slices containing the SCN (left) (C57BL6J-638850.44) and hippocampus (right) (C57BL6J-638850.36) were selected. Spatial transcriptomics Allen Brain Atlas MERFISH coronal slices containing the SCN (C57BL6J-638850.44) of *Sik2* expression overlapping with 10x scRNAseq UMAP plot of (b) GABAergic neurons and (c) glutamatergic neurons. Non-neuronal Cells tSNE used for *Sik2* expression, labelled with regions. Gene expression measured by Log2(Counts Per Million (CPM) + 1) scale, corresponding to the darkness of bars. The height of scale bars represents the proportion of cells with that level of expression.

5.2.2 Evaluating the role of SIK2 in circadian regulation via running wheel activity

To observe the role of SIK2 in circadian regulation, we measured wheelrunning activity under various paradigms using WT and SIK2 KI animals to observe the circadian output under the loss of SIK2.

We first subjected WT and SIK2 KI animals to a 12-hour lights on/ 12-hour lights off cycle (12:12hr LD) to observe baseline parameters (Fig. 5.2a). There was no difference in circadian period between SIK2 KI and WT controls, as they both displayed a 24-hour period. WT animals had a significantly higher circadian amplitude than SIK2 KI animals ($p=0.039$). There were no significant differences in activity parameters, including bouts, average bout lengths, counts per minute and average counts per bout. We also looked at non-parametric functions, interdaily stability (IS), and intradaily variability (IV) (Krafty et al., 2020). SIK2 KI animals had significantly higher IV than WT animals, showing more circadian disturbances across days. IS measures the relative strength of the circadian rhythms, with 1 being the strongest circadian rhythm. SIK2 KI animals had a significantly lower IS of around 0.62 compared to 0.73 in the WT animals, which suggests a weaker circadian clock under the loss of SIK2 kinase activity.

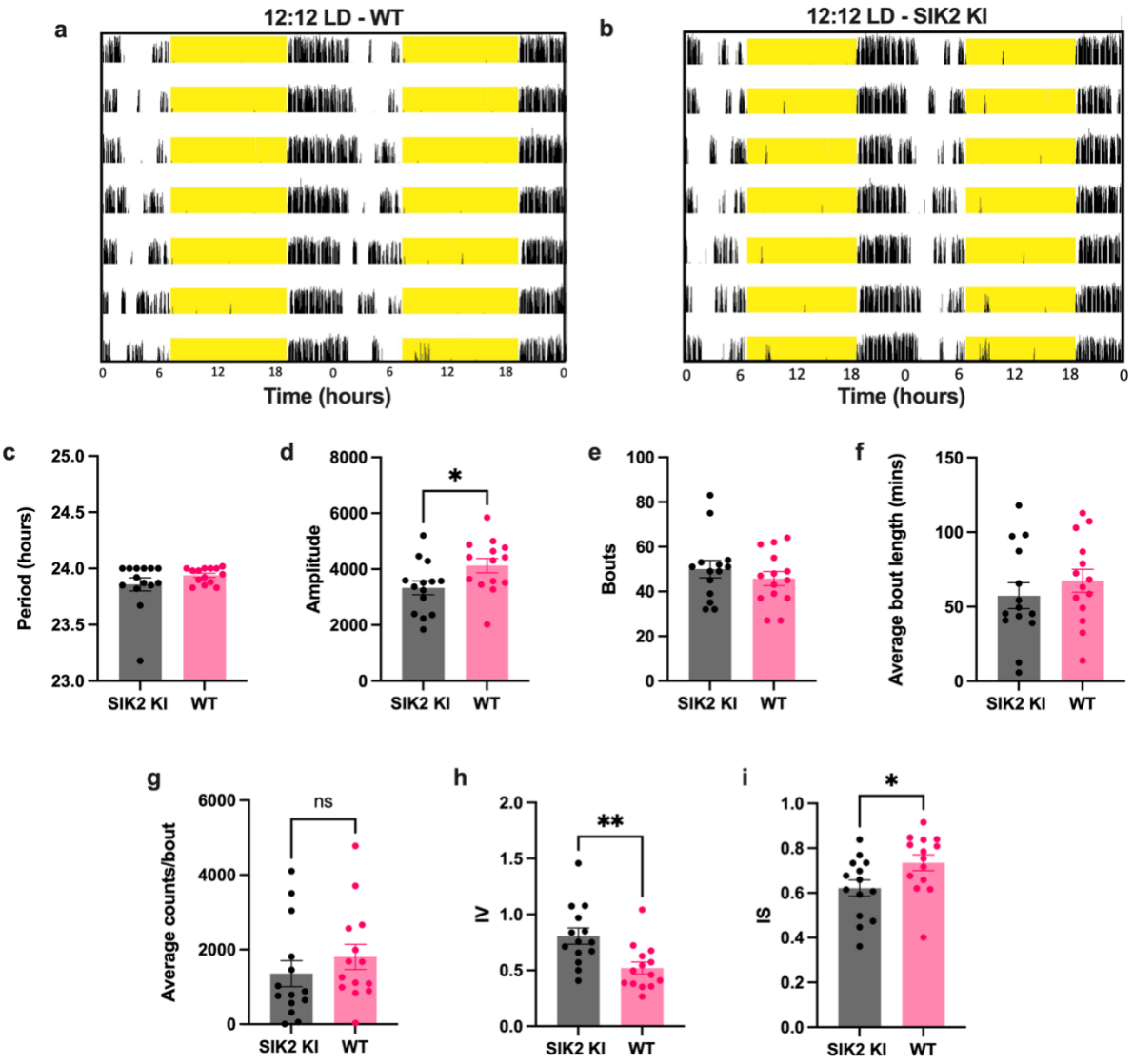

Fig 5.2 **WT and SIK2 KI animals wheelrunning activity under 12:12 hr LD cycle.** Actograms from (a) WT and (b) SIK2 KI animals under a 12:12 hr LD cycle (baseline conditions). Yellow – lights on, grey – lights off, black bars – activity count bars. Lights were set at 100 lux during lights on phase. Each horizontal line represents 24 hours double plotted. x-axis marking circadian time in hours. Seven days of baseline 12:12hr LD were taken for measurements. (c) Circadian period (hours), (d) circadian amplitude, (e) total activity bouts across time period, (f) average bout lengths (minutes), (g) activity counts per minute, (h) average counts per bout, (i) intradaily variability (IV) and (j) interdaily stability (IS). ns $p>0.05$, * $p<0.05$, Two-tailed unpaired t-test. Data points are mean ± SEM, n=14 per group.

We then released WT and SIK2 KI animals into constant conditions to observe their circadian behavior under free-running conditions. We first released them into constant darkness (DD) to observe differences in the endogenous circadian clock. There were no significant changes in core clock parameters, period and amplitude. In DD, we observed significantly lower total number of bouts in the SIK2 KI animals. However, SIK2 KI animals had significantly longer average bout lengths and higher counts per minute and per bout. This shows that SIK2 KI animals have longer and less fragmented bouts than WT animals. They also have denser activity counts within bouts than WT animals, showing that SIK2 KI animals were more active. The higher activity in SIK2 KI animals was especially prominent during the light (sleep) phase. There were no differences in IV ad IS between the genotypes (Fig. 5.3).

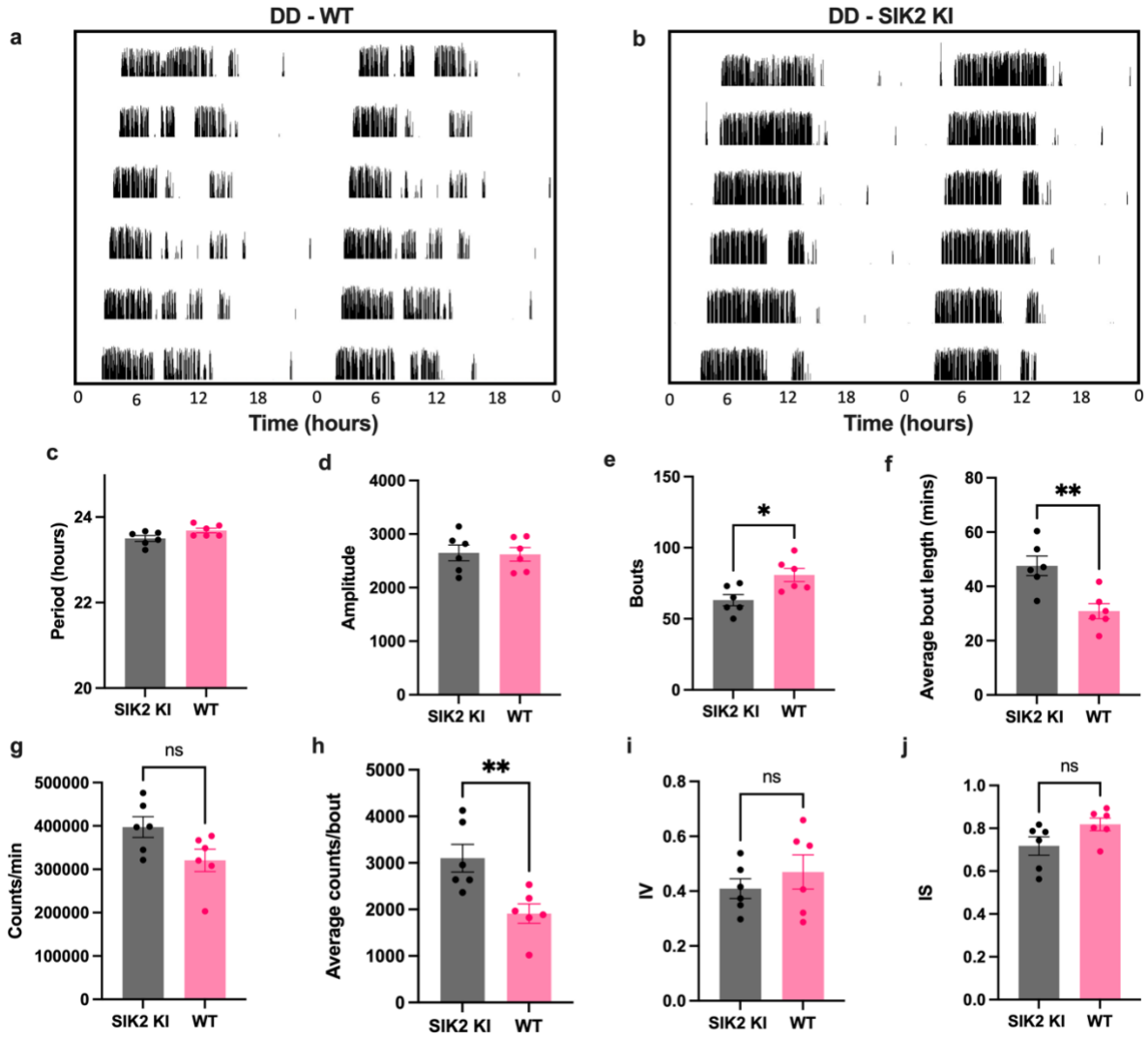

Fig 5.3 **WT and SIK2 KI animals wheelrunning activity under constant darkness (DD).** Actograms from (a) WT and (b) SIK2 KI animals under constant darkness (DD). Grey – lights off, black bars – activity count bars. Each horizontal line represents 24 hours double-plotted. x-axis marking circadian time in hours. Seven days of constant darkness were taken for measurements. (c) Circadian period (hours), (d) circadian amplitude, (e) total activity bouts across time period, (f) average bout lengths (minutes), (g) activity counts per minute, (h) average counts per bout and (i) intradaily variability (IV). ns $p>0.05$, * $p<0.05$, ** $p<0.001$ Two-tailed unpaired t-test. Data points are mean ± SEM, n=6 per group.

Subsequently, we subjected WT and SIK2 KI animals to constant light (LL). Overall, there were no differences in core circadian parameters, period and amplitude. Activity for both genotypes was suppressed in constant light conditions, resulting in lower activity measurements compared to baseline 12:12 LD or DD. There were no differences in total number of bouts, average bout lengths, total counts per minute and average counts per bout. There were also no differences in non-parametric measurements, IV and IS (Fig. 5.4).

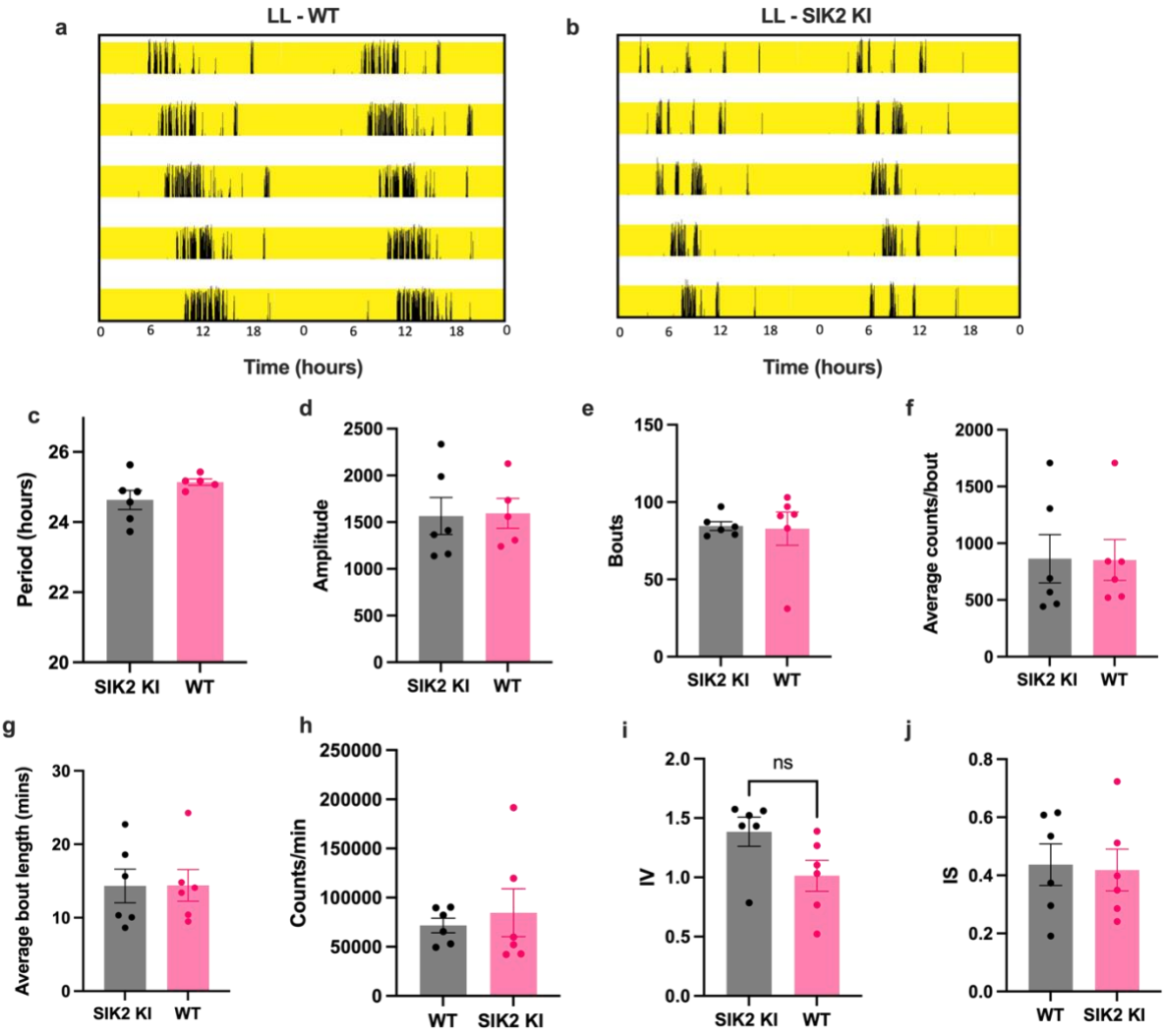

Fig 5.4 **WT and SIK2 KI animals wheelrunning activity under constant light (LL)**. Actograms from (a) WT and (b) SIK2 KI animals under constant light (LL). Yellow – lights on, black bars – activity count bars. Each horizontal line represents 24 hours double-plotted. x-axis marking circadian time in hours. Five days of constant light activity were taken for measurements. (c) Circadian period (hours), (d) circadian amplitude, (e) total activity bouts across time period, (f) average bout lengths (minutes), (g) activity counts per minute, (h) average counts per bout and (i) intradaily variability (IV). ns $p>0.05$, Two-tailed unpaired t-test. Data points are mean ± SEM, n=6 per group.

After observing effects under baseline conditions and free-running period under the loss of SIK2, we subjected WT and SIK2 KI animals to photic stimulations (Fig. 5.5). After released into DD, we imposed two 30-minute light pulses at CT14 and CT22 respective to individual animals. According to a standard light phase response curve (PRC), we expect maximum phase advance at CT22 and maximum phase delay at CT14. In both WT and SIK2 KI animals, we observed expected phase differences at corresponding timepoints. There were no significant differences in response to the light pulses between WT and SIK2 KI animals. SIK2 KI animals had a slightly greater phase difference in response to both light pulses, but it was not statistically significant. We recorded activity counts 30 minutes before and during the light pulses to analyze the circadian masking effect to light. Masking allows animals to react and respond to acute environmental changes appropriately, integrated with the internal oscillator (Rietveld et al., 1993). There were no differences in activity counts between WT and SIK2 KI animals before the light pulses, matching previous findings of no differences in activity measures. During light pulses, activity counts were significantly suppressed, suggesting similar masking behavior to WT animals. These findings suggest that SIK2 is not solely regulated in a light-dependent way.

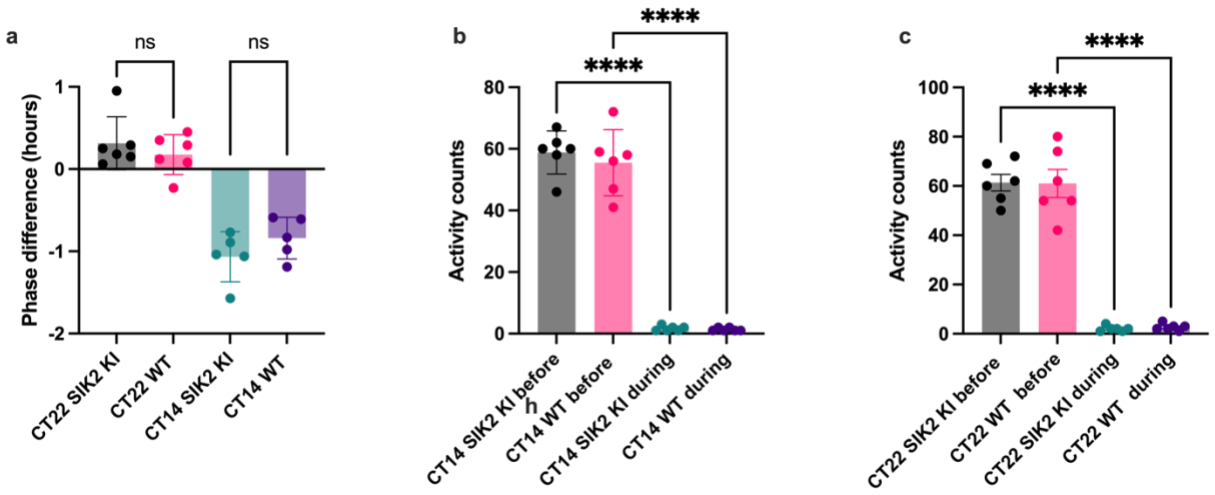

Fig 5.5 **WT and SIK2 KI animals wheelrunning activity under light pulses.** WT and SIK2 KI animals were released into constant darkness (DD) and subjected to multiple 30 min, 30 lux light pulses. (a) Representative actogram highlighting CT14 and CT22 light pulses and how phase differences are calculated. Black bars – activity count bars. (b) Phase differences (hours) measured for CT14 and CT22 light pulses. Activity counts 30 minutes before and during the (c) CT14 and (d) CT22 light pulses. ns $p>0.05$, **** $p<0.0001$, Ordinary one-way ANOVA with Šídák's multiple comparisons test. Data points are mean ± SEM, n=6 per group.

We then subjected animals to two consecutive 6hr light advances (jetlag paradigm) to observe entrainment patterns (Fig. 5.6). We recorded the progression of phase differences every other day after the light advances. Two consecutive light advances were combined and plotted as individual data points. We marked and recorded activity onsets every other day (one, three, five and seven days after the advances). Phase differences were not significant, showing no alterations in entrainment behavior under the loss of SIK2 kinase activity.

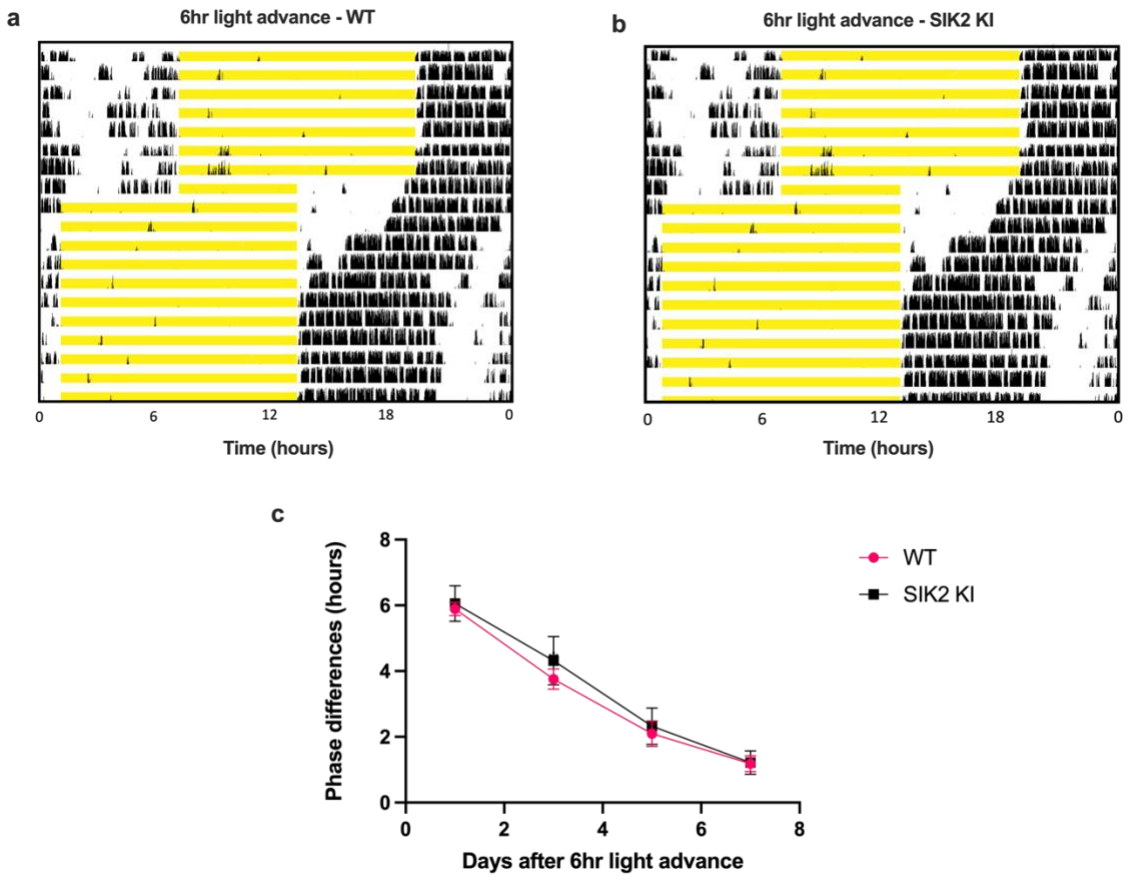

Fig 5.6 **WT and SIK2 KI animals wheelrunning activity under 6-hour light advance.** WT and SIK2 KI animals were stably entrained to the 12:12 hr LD cycle and subjected to a 6-hour light advance and stable entrainment was allowed for seven days. A consecutive 6-hour shift was imposed after stable entrainment. Representative actograms from (a) WT and (b) SIK2 KI animals indicating one of the light advances. Yellow – lights on, grey – lights off, black bars – activity count bars. (c) Phase differences (hours) calculated on the first day after the shift for both shifts. 6 hours represents full entrainment; a phase difference closer to 6 shows faster entrainment. Measurements from both 6-hour light advances were combined and treated as individual replicates. * $p<0.05$, Ordinary one-way ANOVA with Šídák's multiple comparisons test. Data points are mean ± SEM, n=14 per group.

Finally, we subjected SIK2 KI and WT animals to an ultradian light-dark cycle, which is 3.5 hours lights on and 3.5 hours lights off (T7 cycle) (Fig. 5.7). Typically, the endogenous circadian drive has an upper hand so animals do not easily entrain to non-24 hour cycles (Legates et al., 2014). This was observed with the WT animals, where they maintained a period of around 23 hours. The SIK2 KI animals, however, adjusted immediately to an average circadian period of 9.83 hours. We analyzed FFT plots to examine activity frequencies and power under different periodicities. Under the 7-hour ultradian cycle, amplitude was not significantly different but a general indication of elevated amplitude in SIK2 KI animals compared to WT controls ($p=0.11$). There were no significant changes in activity parameters. We then released the animals into DD after the T7 cycle to check for entrainment and masking. In the first three days after being released into DD, both SIK2 KI and WT animals had a period of 24 hours. This shows that SIK2 KI animals were masking to the altered LD cycle instead of entraining fully. Looking at the actograms, the onsets of activity were all after the lights turned on, so there was a lack of anticipation for the cycle. Post hoc power analysis revealed that the study had a power of around 0.73 ($n=6$, effect size = 1.64), suggesting a moderate sensitivity to detect biological effect. These results suggested that under the loss of SIK2, the endogenous circadian clock was easily adjusted in response to environmental light-dark cycle alterations as a result of a weakened circadian clock.

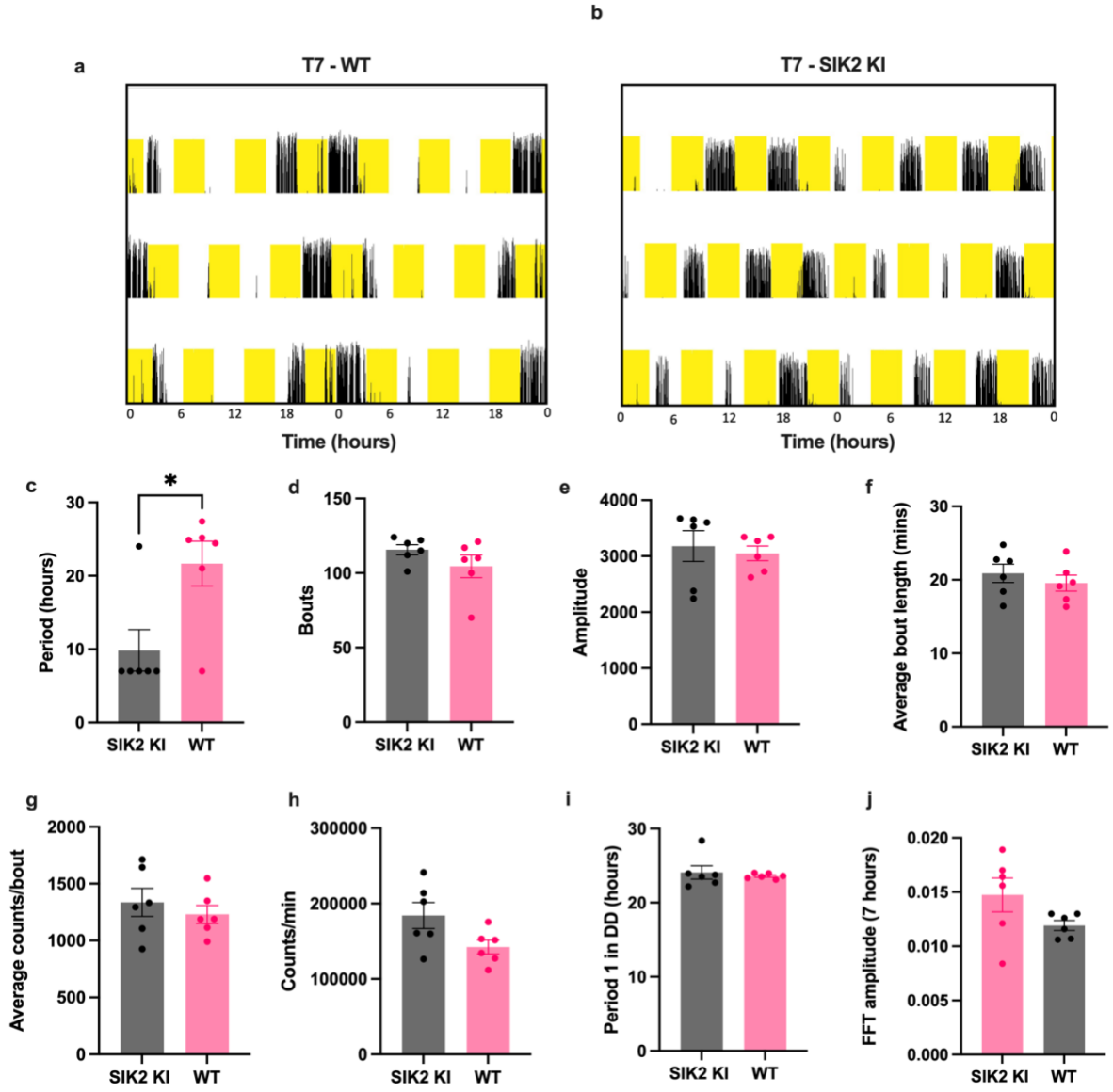

Fig 5.7 **WT and SIK2 KI animals wheelrunning activity under 3.5/3.5 hr LD cycle.** WT and SIK2 KI animals were subjected to a 3.5 hr lights on / 3.5 hr lights off (T7) LD cycle for 7 days. The middle 5 days were analyzed. Actograms from (a) WT and (b) SIK2 KI animals under a T7 cycle. Yellow – lights on, grey – lights off, black bars – activity count bars. Lights were set at 100 lux during lights on phase. Each horizontal line represents 24 hours double-plotted. x-axis marking circadian time in hours. Representative actograms only show three days of recording due to technical errors during data export. (c) Circadian period (hours), (d) circadian amplitude, (e) total activity bouts across the five-day period, (f) average bout lengths (minutes), (g) average counts per bout and (h) activity counts per minute. Animals were released into constant darkness (DD) after 7 days. (i) Circadian period acquired from periodograms across three days after release into DD. * $p<0.05$, Two-tailed unpaired t-test. Data points are mean ± SEM, n=6 per group.

5.2.3 Evaluating the role of SIK2 in sleep regulation via EEG

To explore the sleep regulation of SIK2, we first analyzed continuous EEG recordings in WT and SIK2 KI animals under a 12:12 LD cycle. Overall, no interaction between genotype and time was observed in the time spent in wakefulness and NREM sleep states. Two-way ANOVA analysis revealed genotype effects in these states, suggesting a general trend of increased wakefulness ($p=0.0177$) and reduced NREM sleep ($p=0.0088$) in SIK2 KI animals compared to WT controls (Fig. 5.8a-c). There was significant interaction between genotype and time in REM sleep state, where SIK2 KI animals had significantly lower REM sleep at ZT2, the start of sleep phase. There was no difference in SWA delta power but a significant genotype effect in delta energy ($p<0.0001$). Delta power in the range of 3 – 4.25 Hz, corresponding to NREM sleep, was significantly lower in the SIK2 KI animals (Fig. 5.8d-f).

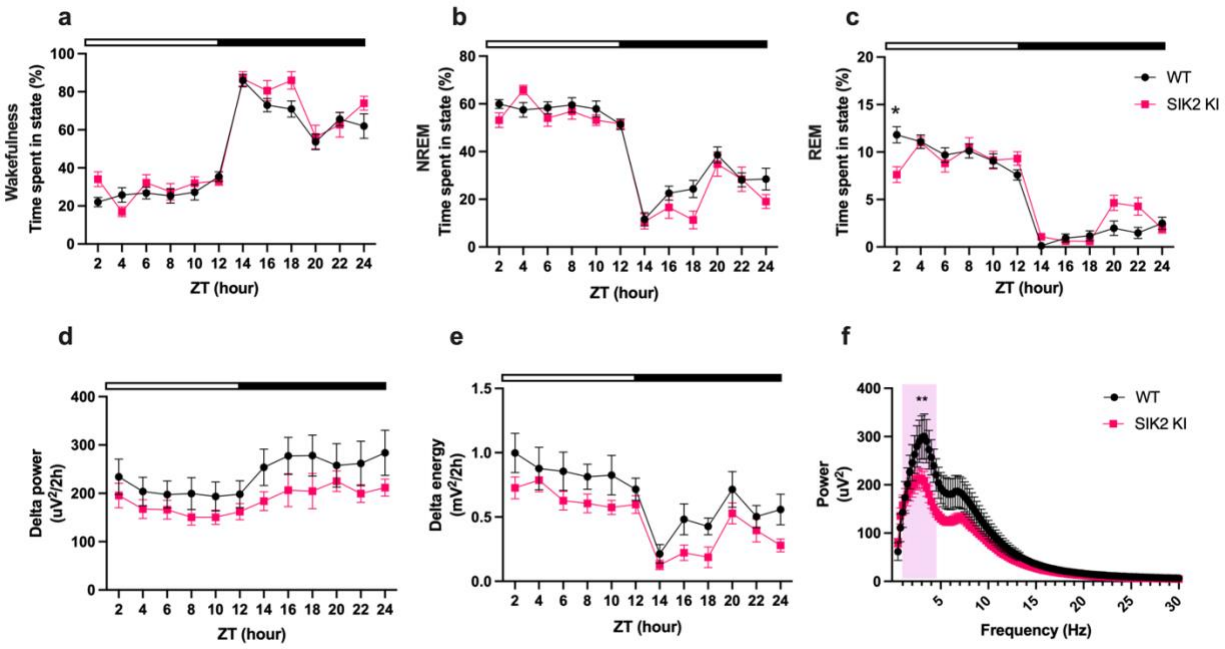

Fig. 5.8 **EEG recordings of WT and SIK2 KI animals under 12:12 hr LD cycle (baseline conditions).** Sleep phenotype of WT and SIK2 KI animals was characterized through EEG/EMG recordings under 12:12 hr LD cycle (baseline). The bar on top represents 12 hours of light (unfilled) and 12 hours of dark (filled). Under baseline, the percentage of time spent in (a) wakefulness, (b) NREM and (c) REM was recorded. (d) Delta power, (e) delta energy and (f) frequency were recorded. Two-way ANOVA with Šídák's multiple comparisons test. * $p<0.05$, ** $p<0.01$. Data points are mean ± SEM, n=3-4 per group.

We then subjected WT and SIK2 KI animals to 6 hours of sleep deprivation (SD) to explore sleep homeostatic responses. The SD was imposed at the start of the light phase, from ZT0 to ZT6, and the animals were allowed to sleep immediately after. Groups with no sleep deprivation were used as parallel controls, labelled as baseline cohorts. In WT animals, there was a significant reduction in wakefulness, an increase in NREM sleep and REM sleep at the start of the dark phase in the sleep-deprived group, showing normal rebound sleep. There was no significance in SWA and power in the delta range, but a significant genotype effect in delta energy was observed after SD ($p=0.0133$).

In SIK2 KI animals, there was no difference in time spent in wakefulness and NREM sleep following SD. The sleep-deprived group had significantly higher REM sleep at the start of the dark phase. Similarly, there was no difference in SWA, delta energy, and power. These results showed that SIK2 KI animals lacked sleep pressure buildup after the 6hr SD, suggesting altered sleep homeostatic responses (Fig. 5.9).

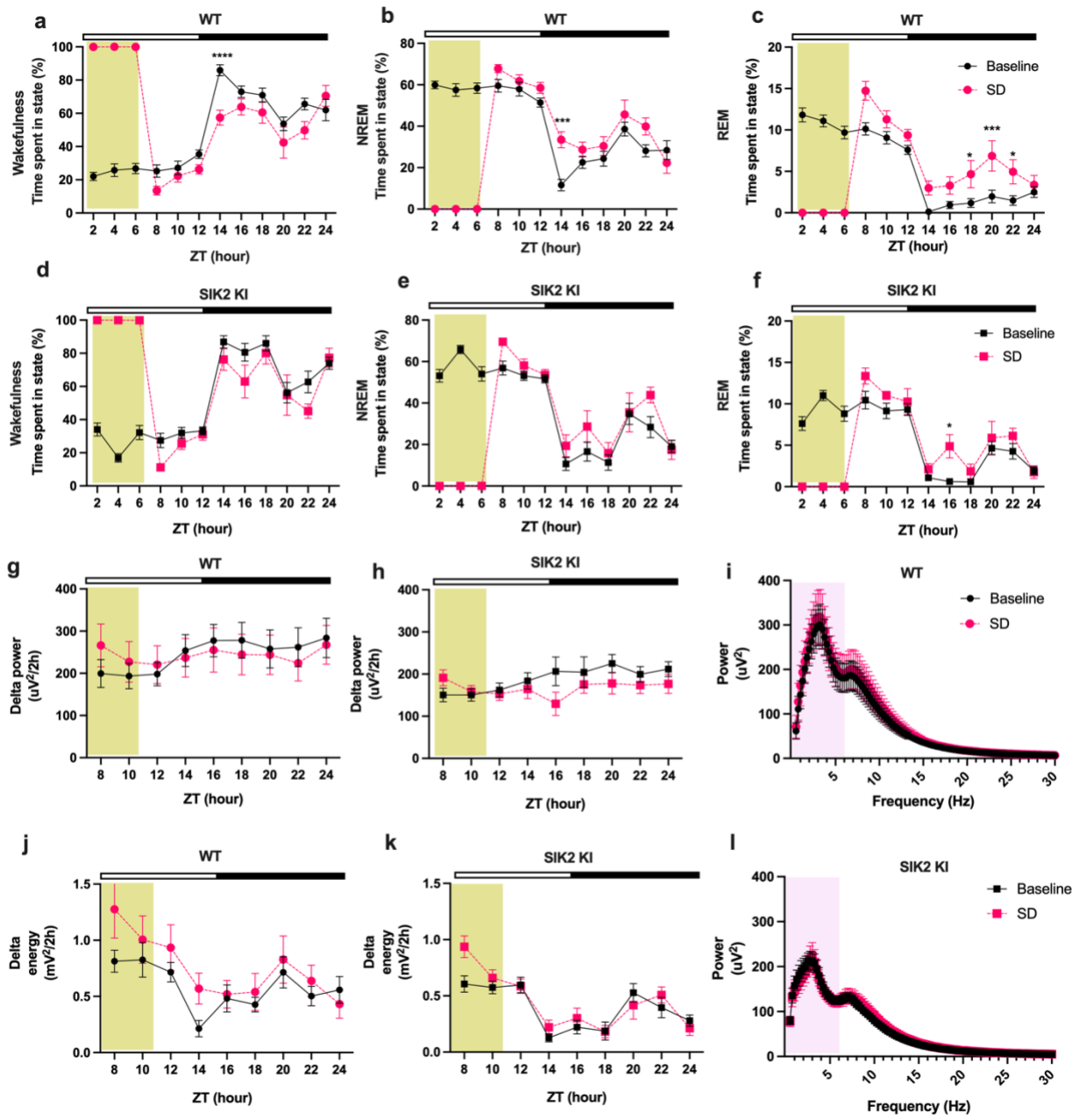

Fig. 5.9 **EEG recordings of WT and SIK2 KI animals under 6hr sleep deprivation**. Sleep phenotype of WT and SIK2 KI animals was characterized under 6hr sleep deprivation. 6hr sleep deprivation was imposed at the start of light phase (ZT0- ZT6) shown by yellow block. WT and SIK2 KI animals were recorded for percentage of time spent in (a,d) wakefulness, (b,e) NREM and (c,f) REM. (g-h) Delta power, (j-k) delta energy and (i,l) frequency were recorded. Two-way ANOVA with Šídák's multiple comparisons test. * p<0.05, **p<0.01, ***p<0.001, ****p<0.0001. Data points are mean ± SEM, n=3-4 per group.

5.2.4 RNAseq transcriptomics show differential expression in the SCN

We collected 1mm^3 SCN punches from WT and SIK2 KI animals 3 hours into the light phase during the sleep phase of the animals (ZT3). We performed mRNAseq and detected a total of 55,487 genes (Supp. Table 5.1). We first did a Principal Component Analysis (PCA) with the dataset to visualize variation between replicates and animals in the dataset. Between SIK2 KI and WT SCN samples (n=4), the replicates clustered and showed variation between genotypes (Supp Fig. 5.1). Using DEseq differential gene analysis, implementing the cutoff at padj<0.05, we detected 1112 genes that were differentially expressed between WT and SIK2 KI animals (Fig. 5.10).

By conducting G: Profiler functional analysis, we detected several hubs of terms in which the genes were enriched (Supp. Table 5.1). We detected terms “neurogenesis” and “neuron differentiation”, including genes *Ngfr, Tbx2, Efnb2, Adcy1, Septin4, Bdnf* and *Grm7*. They have known roles associated with synaptic transmission but in the meantime, overlapping with “glutamate secretion” functions, which are particularly implicated in RHT terminals in response to light. Notably, several of these are overlapping with terms relating to “circadian rhythms”, including *Ngfr, Prox1, Sik1, Usp2, Opn5, Bdnf* and *Prokr2.* Most of these genes were downregulated in the SIK2 KI animals. The overlap with synaptic regulatory genes suggests that synaptic signaling could be essential for regulating circadian rhythms. These differentially expressed genes were also shown to be localized in the GABAergic synapse in the SCN. In addition, we detected terms “glial cell differentiation” and “cell junction organization”.

These include genes such as *Nkx2-1, Cdh2, Epnb1, Abl1, Adcy1/2/3*, which are closely associated with gap junctions and astrocyte differentiation. This proposes that *Sik2* Could play a role in neuronal and non-neuronal communication in the SCN, maintaining stability and synchronization.

In molecular function, we observed enrichment in terms “neuropeptide activity” and “neuropeptide hormone activity”. These include an upregulation of *Grp, Nppc, Oxt, Npy, Avp* and *Vip.* Neuropeptide receptors, *Avpi1, Avpr1a* and *Vipr2,* were also upregulated in the SIK2 KI animals. Interestingly, there were no significant changes in core circadian clock genes such *Per1* and *Cry1* (Fig. 5.10).

5.2.5 RNAseq transcriptomics show differential expression in the cortex

Similarly, we collected 1mm^3 cortex punches from WT and SIK2 KI animals 3 hours into light phase (ZT3) and performed mRNAseq (Supp. Table 5.1). We first did a Principal Component Analysis (PCA) with the dataset to visualize variation between replicates and animals in the dataset. Between SIK2 KI and WT cortex samples (n=4), the replicates clustered and showed good variation between genotypes (Supp. Fig. 5.1). Using DEseq differential gene analysis, we detected three genes that were differentially expressed between WT and SIK2 KI animals using the cutoff padj<0.05, *Cdr1os, Lars2 and Osmr* (Fig. 5.10).

We then loosened the cutoff to p-value of less than 0.05 for volcano plots to observe differential gene expression in the cortex. Using functional analysis, similar to the SCN,

we detected enrichment in neurogenesis, some of which overlapped with differentially expressed genes in the SCN. These include *Ngfr, Serpinf1, Efnb3, Grin1, Camk1* and *Wnt3,* proposing SIK2's regulation of synaptic signaling in the cortex. We also detected genes that are associated with ion transport and channel proteins, including *Kcnn3, Cacnd2d2, Slc12a7, Slc13a3* and *Cacna2d3*. These were also implicated in calcium signaling, showing an enrichment for "regulation of calcium ion concentration" terms. A hub of differentially expressed genes was also enriched for metabolic and RNA processes such as *Ngfr, Wnt3, Gmpr, Brat* and *Grk5* (Fig. 5.10).

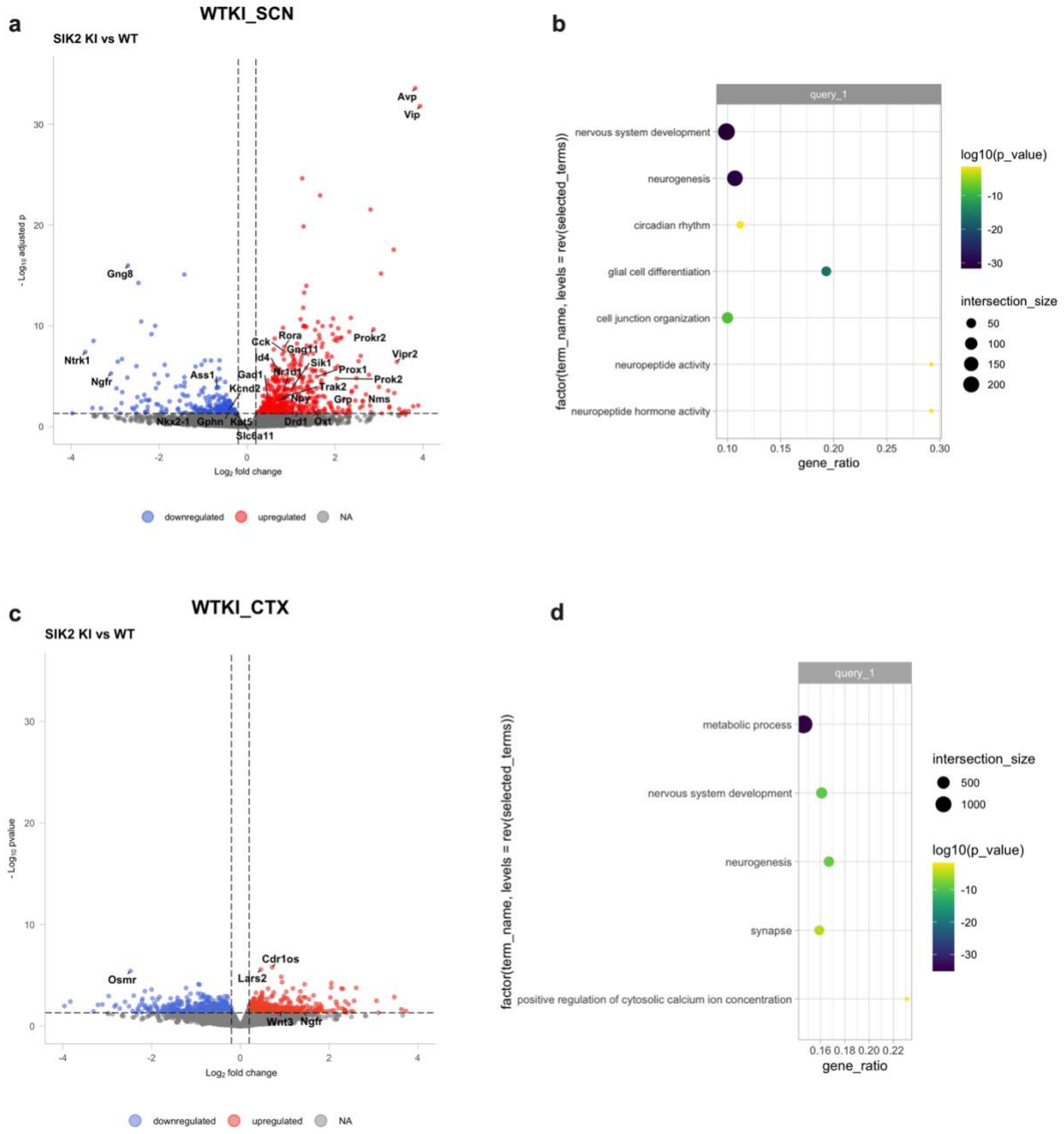

Fig. 5.10 Transcriptomics analysis of WT and SIK2 KI animals in the SCN and cortex during sleep phase. 1mm^3 SCN punches were collected from WT and SIK2 KI animals during light phase (subjective sleep phase of mice) at ZT3. mRNA-seq was performed on SCN punches and differential gene analysis was conducted. (a) Volcano plot of differentially expressed genes (DEGs) between WT and SIK2 KI animals. Dotted line = log2FC > 0.2 and p-adjusted value <0.05 cutoff. (b) GProfiler functional analysis of DEGs highlighting enriched terms. -log10(p-value) and overlap size/ratio were calculated and programmed in R studio. 1mm^3 cortex punches were collected from WT and SIK2 KI animals during light phase (subjective sleep phase of mice). mRNA-seq was performed on cortex punches and differential

gene analysis was conducted. (a) Volcano plot of differentially expressed genes (DEG) between WT and SIK2 KI animals. Dotted line= log2FC > 0.2 and uncorrected p-value <0.05 cutoff. (b) GProfiler functional analysis of DEGs highlighting enriched terms. -log10(p-value) and overlap size/ratio were calculated and programmed in RStudio. n=4 per genotype per tissue type.

5.2.6 Differential phosphorylation in the SCN in wake and sleep phases

We next performed tissue-specific phopshoproteomics to explore the molecular targets of SIK2. We collected 1mm^3 SCN punches from WT and SIK2 KI animals at end of sleep and end of wake timepoints. End of sleep (EOS) and end of wake (EOW) samples were collected two hours before the onset of activity and sleep at ZT10 and ZT22, respectively. We detected a total of 19718 phosphopeptides in the SCN (Supp. Table 5.2). To eliminate inconsistencies between samples, we normalized the phosphopeptide intensities to the corresponding total proteome. We performed a PCA analysis to look at variability and distribution across samples. Most of the samples were clustered and showed little variability between replicates. Two of the WT replicates at ZT22 behaved differently from the others. Given the larger variability in PC1, SCN16 was excluded from subsequent analysis. Comparisons between timepoints and genotypes were conducted using Limma (linear model) to explore differential phosphorylation patterns between WT and SIK2 KI animals (Supp. Fig. 5.2).

At EOS, similar changes in phosphorylation were observed, so no phosphosites passed the p-value correction. For differential analysis, the significance cutoff was set at pvalue of less than 0.05 (pvalue<0.05). Of which, 395 phosphosites were determined as significant between WT and SIK2 KI animals (Supp. Table 5.2). By conducting functional analysis, we detected significant enrichment in “synaptic signaling” and

“synapse organization”, including proteins CAMK2A, CAMK2B, DMXL2, FARP1, PCLO, PRKACA and SYN1. Within the synapse, Sik2 modulates synaptic proteins that serve various functions, for instance vesicle-mediated transport. CACNA1B, PCLO, RPH3A and CAMK2A are associated with synaptic vesicle exocytosis; ADD1, EPN2, DPYSL2 and SGIP1 are associated with endocytosis in the presynapse. Examining downstream pathways, these synaptic proteins are also strongly associated with nervous system development and neurogenesis (Fig. 5.12).

In the molecular function (MF) analysis of the phosphosites, we detected enrichment for “calmodulin binding”, including proteins CAMK2A/B/G, RYR2 and UBR4, indicating a role of SIK2 in calcium signaling. KEGG pathway analysis suggested that SIK2 molecular substrates are involved in multiple key pathways regulating physiology. The synaptic proteins and calmodulin binding proteins play significant roles in “long-term potentiation” and in the “dopaminergic synapse”, including CAMK2A/B/G, GRIN2B, PRKACA and PRKCG. According to the literature, they are also implicated in circadian entrainment. In addition, we detected enrichment for proteins involved in metabolic processes, specifically “insulin secretion” and “phosphatidylinositol signaling system”, which included ATP1A2/3, VAMP2, MTMR1/7, PLCB1 and INPP5F.

At EOW in the SCN, we detected 980 phosphosites that were significant between SIK2 KI and WT animals. Similar to EOS, we saw enrichment in synaptic functions and vesicle-mediated transport, including BSN, BAIAP3, CACNA1B, CBARP, PCLO, SYN1/2/3 and IQSEC1. Overlapping largely with the “endocytosis” KEGG pathway.

There were also proteins associated with “learning or memory” and “cognition”, including ANKRD11, GRIA1, GRIN2A, SYNGAP1, SYNPO and SHANK1/2/3. The proteins differentially phosphorylated are similarly enriched for calcium signaling pathways.

Comparing the two timepoints, 116 proteins were significantly differentially phosphorylated in both timepoints. These include a lot of the synaptic proteins, DMXL2, DPYSL2, ERMN, PCLO, RIMS1 and SYN1, which all play important roles in presynaptic vesicle transport. CAMK2A/B were also detected as significant in both timepoints, indicating the significance of calcium signaling throughout the sleep-wake cycle. There was SIK2 autophosphorylation observed at both timepoints. There were more phosphorylation changes in relation to learning and memory formation at ZT22 such as GRIA1, GRIA2 and GRIN2B, associated with more changes in proteins in the presynaptic terminal.

5.2.7 Exploring the direct substrates of SIK2

To explore the direct substrates and phosphorylation sites of SIK2, we used the pro-KALIP method optimized in Chapter 3. We optimized the SIK2 kinase concentration in vitro using Kinase Glo Luminescence assay by performing a kinase titration curve. SIK2 kinase showed a linear titration curve from 5nM to 40nM (Supp. Fig. 5.3). In addition, we tested the effect of the LKB1 trimer on SIK2 activity by loading the SCN and cortex lysate, dephosphorylated samples and rephosphorylation reaction on a pAMPK substrate motif immunoblot. Similarly, there was successful dephosphorylation with a

significant decrease in bands compared to lysate. There were also more visible and darker bands in the rephosphorylation reaction lane with SIK2 kinase and LKB1 trimer (Supp. Fig. 5.3).

From SIK2 KALIP in the SCN, we detected 9782 phosphopeptides, mapped to 2306 phosphoproteins and 7132 phosphosites (Supp. Table 5.2). We used the meta datasets with all human Ser/Thr sites as a background and performed a contingency test (Johnson et al., 2023). Using a 80% cutoff, the SIK2 KALIP dataset was significantly enriched for both the SIK2 motif. These suggested that the direct substrates of SIK2 identified from Pro-KALIP were both SIK2-specific (Supp. Fig. 5.3).

We then overlapped the Pro-KALIP dataset with the SIK2 SCN *in vivo* phosphoproteomics in 5.2.6. We detected 4664 phosphopeptides that mapped to 2901 phosphosites and 1498 phosphoproteins. We examined the ZT10 and ZT22 timepoints separately and used $p<0.05$ as the cutoff for significance. At EOS ZT10, we detected 88 phosphoproteins and 87 phosphosites that are direct substrates and phosphorylation sites of SIK2. Analyzing the direct substrates by function, we detected enrichment for activities in the synapse. DYSL2 is key for synaptic vesicle transport, GPM6A is key in neuronal differentiation, HNRNPUL2 is important for RNA splicing but also important for neurodevelopment. RAB3A is key for intracellular membrane and vesicle trafficking in the synapse. Notably, DYSL2 T509 as a direct phosphorylation site of SIK2 is important for neuroprotection. Similarly, we detected enrichment for calmodulin binding, including ADD1/3 and CAMK2/B, accentuating the role of Ca^{2+} signaling in the SCN. Specifically,

CAMK2B T287 is key for dendritic spine and synapse formation. A key hub of direct substrates, HSF1, HSP4 and UBR4 are involved in the heat shock response pathway and protein homeostasis in the SCN. HSF1 S303 has downstream effects on insulin resistance and age-related obesity. In addition to synaptic functions, these are also involved in metabolic processes. Notably, ATG2B, C2CD2L and PLPP7 are key players in phospholipid transport and insulin secretion pathways. STAMBP1 is regulated by SREBP1, which is validated in literature to be important for adipogenesis. SIK2 at T484 autophosphorylation was also detected, a PKA phosphorylation site of SIK2.

At EOW ZT22, we detected 192 phosphoproteins and 194 phosphosites that are direct substrates and phosphorylation sites. We detected a hub of structural and adaptor proteins. For instance, ADAM22, a brain-specific cell surface protein; UBXN2B; SPTBN1 and TUBB4B, modulating the stability microtubules and cytoskeleton. We also detected CXADR, which is a key cell adhesion molecule that maintains tight junctions, maintaining stability in the SCN. RAPTOR modulates cell size and mTOR protein expression. Similarly, we detected direct substrates involved in synaptic signaling, including vesicle endocytosis (EPS15D1, FBBPL1), vesicle transport (PAK1, VTI1B) and postsynaptic function (IQSEC2). Several of these are associated with downstream neurodevelopment and neural differentiation, such as SYNGAP1, DOCK10 and MEF2C. HNRNPK regulates dendritic spine density and long-term potentiation (LTP) in the hippocampus. Metabolic processes were again suggested in the direct substrates. DACT3 and DIRAS2 are both tumor suppressors through negatively regulating the Wnt/B-catenin pathway. WDR48 as a tumor suppressor acts through the Akt pathway.

RALGAP is also a prognostic marker for gastric cancer progression. In addition, several proteins are regulators of lipid transport and cholesterol homeostasis, including GRAM16 and RELCH.

DPYSL2, C2CD2L and SIK2 were identified as direct substrates in both timepoints, suggesting that they modulate pathways that are key for both sleep and wake states. Of the direct substrates, ABI, IQSEC2, SYNGAP1, CLASP1 and CAMK2B overlapped with the 80 SNIPPs identified as associated with sleep need and pressure (Wang et al 2018) (Fig. 5.11).

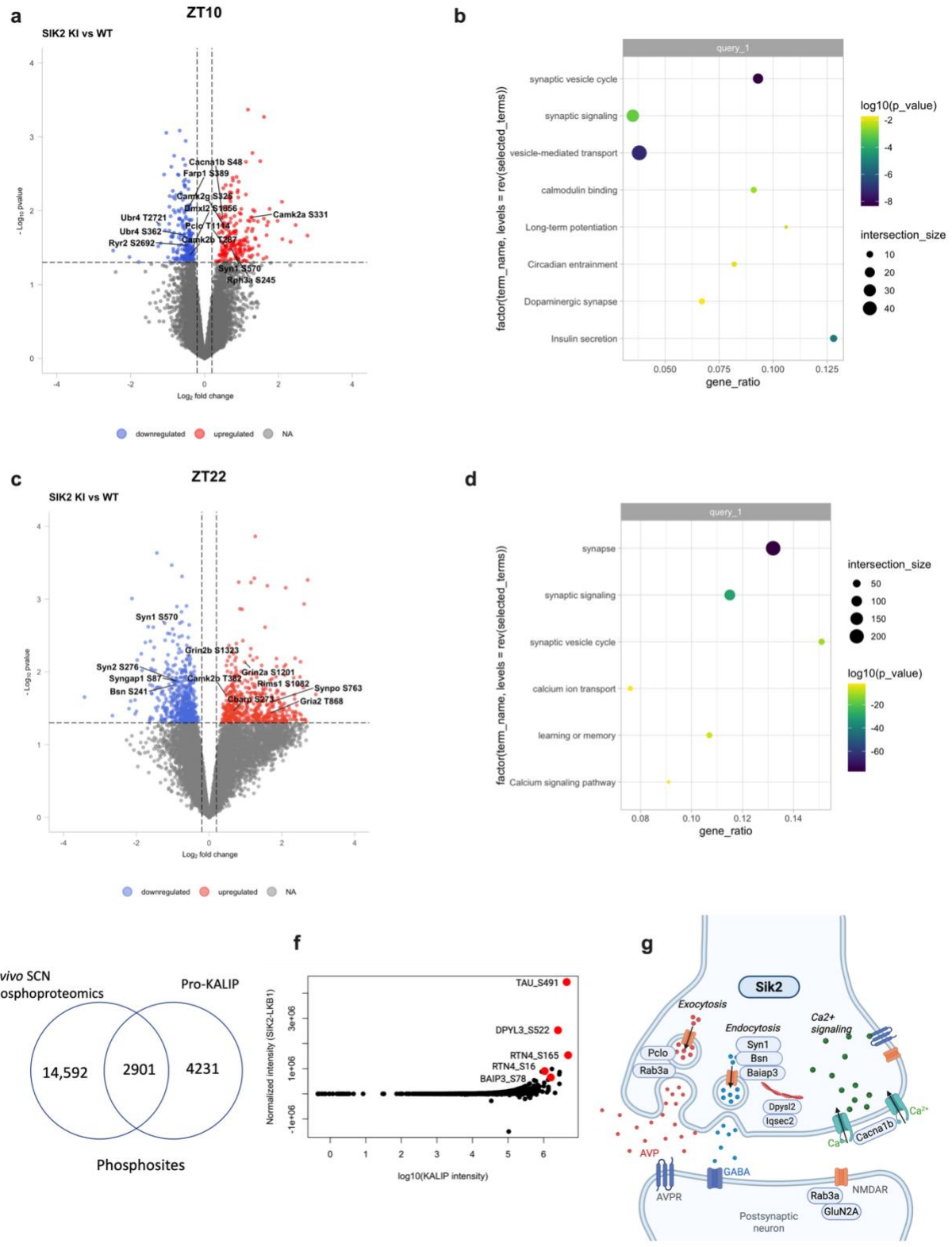
a
ZT10
SIK2 KI vs WT
Cacna1b S48
Farp1 S389
Camk2g S326
Bmxl2 S1856
Ubr4 T2721
Pclo T1144
Ubr4 S362
Camk2b T287
Ryr2 S2692
Camk2a S331
Syn1 S570
Rph3a S245
- Log10 pvalue
Log2 fold change
downregulated
upregulated
NA
b
query_1
synaptic vesicle cycle
synaptic signaling
vesicle-mediated transport
calmodulin binding
Long-term potentiation
Circadian entrainment
Dopaminergic synapse
Insulin secretion
factor(term_name, levels = rev(selected_terms))
gene_ratio
log10(p_value)
intersection_size
c
ZT22
SIK2 KI vs WT
Syn1 S570
Grin2b S1323
Syn2 S276
Syngap1 S87
Bsn S241
Camk2b T382
Grin2a S1201
Rims1 S1082
Cbarp S273
Synpo S763
Gria2 T868
- Log10 pvalue
Log2 fold change
downregulated
upregulated
NA
d
query_1
synapse
synaptic signaling
synaptic vesicle cycle
calcium ion transport
learning or memory
Calcium signaling pathway
factor(term_name, levels = rev(selected_terms))
gene_ratio
intersection_size
log10(p_value)
e
In vivo SCN phosphoproteomics
Pro-KALIP
14,592
2901
4231
Phosphosites
f
TAU_S491
DPYL3_S522
RTN4_S165
RTN4_S16
BAIP3_S78
Normalized intensity (SIK2-LKB1)
log10(KALIP intensity)
g
Sik2
Exocytosis
Endocytosis
Ca2+ signaling
Pclo
Rab3a
Syn1
Bsn
Baiap3
Dpysl2
Iqsec2
Cacna1b
Ca2+
AVP
AVPR
GABA
NMDAR
Rab3a
GluN2A
Postsynaptic neuron

Fig. 5.11 *In vivo* phopshoproteomics and Pro-KALIP in the SCN to identify direct substrates of SIK2. 1mm^3 SCN punches were collected from WT and SIK2 KI animals either 2 hours before the onset of dark phase, end of sleep phase (ZT10), or 2 hours before the onset of light phase, end of wake phase (ZT22). n=4x4 samples pooled SCN per genotype. Proteomics and phosphoproteomics enrichment were conducted. Volcano plots of phosphoproteomics changes between WT and SIK2 KI animals at (a) ZT10 and (c) ZT22. Dotted lines = log2FC>0.2 and uncorrected p-value <0.05. GProfiler functional analysis of DEGs highlighting enriched terms in (b) ZT10 and (d) ZT22. -log10(p-value) and overlap size/ratio were calculated and programmed in R studio. (e) Venn diagram of overlapping phosphosites between SIK2 in vitro KALIP assay and SIK2 in vivo phosphoproteome. (f) Pro-KALIP raw intensity differences in quantity of phosphorylated peptides between the sample treated with SIK2+LKB1 trimer versus LKB1 trimer alone in the SCN, plotted against the log10-transformed intensity of peptides detected in SIK2 + LKB1 trimer. Each point represents an individual phosphosite; selected differential phosphosites are highlighted in red. (g) Schematic diagram of SIK2-mediated substrates regulating synaptic functions proposed in Pro-KALIP.

5.2.8 Differential phosphorylation in the cortex in wake and sleep phases

In parallel, we collected 1mm^3 cortex punches from WT and SIK2 KI animals at end of sleep (EOS ZT10) and end of wake (EOW ZT22) and conducted phosphoproteomics. We detected 15780 phosphopeptides in total (Supp. Table 5.2). Similarly, we normalized the intensities of the phosphopeptides to the total proteome and performed a PCA analysis on the normalized intensities. The PCA plot captured 41.8% of total variation across the cortex samples, PC1 accounted for 27.7% and PC2 accounted for 14.1%. We saw general clustering within WT replicates and separation between timepoints. Several SIK2 KI replicates were behaving differently from others, therefore CTX4 and CTX11 were excluded from subsequent analysis (Supp. Fig. 5.2).

In EOS, WT and SIK2 KI animals showed similar phosphorylation changes so no phosphosite passed the corrected p-value significance threshold (padj<0.05). We then looked at the unadjusted p-value and detected 302 phosphosites that were significant

($p<0.05$). By conducting functional analysis, we detected significant enrichment in "synaptic signaling", including BRAF, BSN, CAMK2A, RTN4, SNAP25 and SYN2. Of which, BRAF, CAMK2A and SNAP25 are involved in exocytosis. Of these synaptic proteins, a hub of them are also key channel and transport proteins, including CACNA1A/B and SLC family (SLC12A5, SLC24A2), which regulate neurotransmitter transport and release in the synapse. Synaptic proteins showing differential phosphorylation changes in the cortex are also associated with key downstream learning and memory processes, involving ADCY1, MAP1A, MTOR and PLCB1, which are also implicated in long-term depression and potentiation. These proteins are also categorized as calmodulin binding proteins, CAMK2A, CACNA1a and RYR2, which indicates the importance of calcium signaling in the cortex, which interestingly also overlaps with "circadian entrainment" in KEGG pathways. Differential phosphorylation patterns also appeared in proteins associated with "insulin secretion" and "Type II diabetes" pathways, including ADCY1, CACNA1A/B/E, RYR2 and SNAP25.

In EOW timepoint, WT and SIK2 KI animals again showed similar phosphorylation changes, so only BAZ1B, SOX10, FAF2, MICAL3 and RRAS passed the corrected p value significance ($padj<0.05$). Of which, only BAZ1B had a significant log2FC ($logFC>0.2$). BAZ1B, a protein involved in chromatin remodelling and implicated in neurodevelopmental disorders, was significantly hypophosphorylated in SIK2 KI animals.

We then took the unadjusted p-value and detected 2821 phosphosites that were differentially phosphorylated at ZT22 ($p<0.05$). Similarly, we detected a hub of proteins involved in "synaptic signaling", including BRSK1, BSN, CAMK2A/B, CDK5, CACNA1A/C and DLGAP1/2/3, which some are also associated with vesicle transport

and neurotransmitter release. Specifically, the proteins are enriched for calcium-ion-regulated exocytosis, including the channel proteins (CACNA1A/C), CADPS, RPH3A, SNAP25, SYT1/9/11 and SYN2. These are also associated with downstream disease pathways. The differential phosphoproteins are involved in Alzheimer's disease and neurodegenerative pathways, including APC, CDK5, CSNK1E, GRIN2A/B/D, RAF1, RTN3/4 and MAPT. Similarly, a lot of them overlap with metabolic processes such as insulin secretion, notably, ADCY2/5/9. CAMK2A,B,G and SNAP25 (Fig. 5.12).

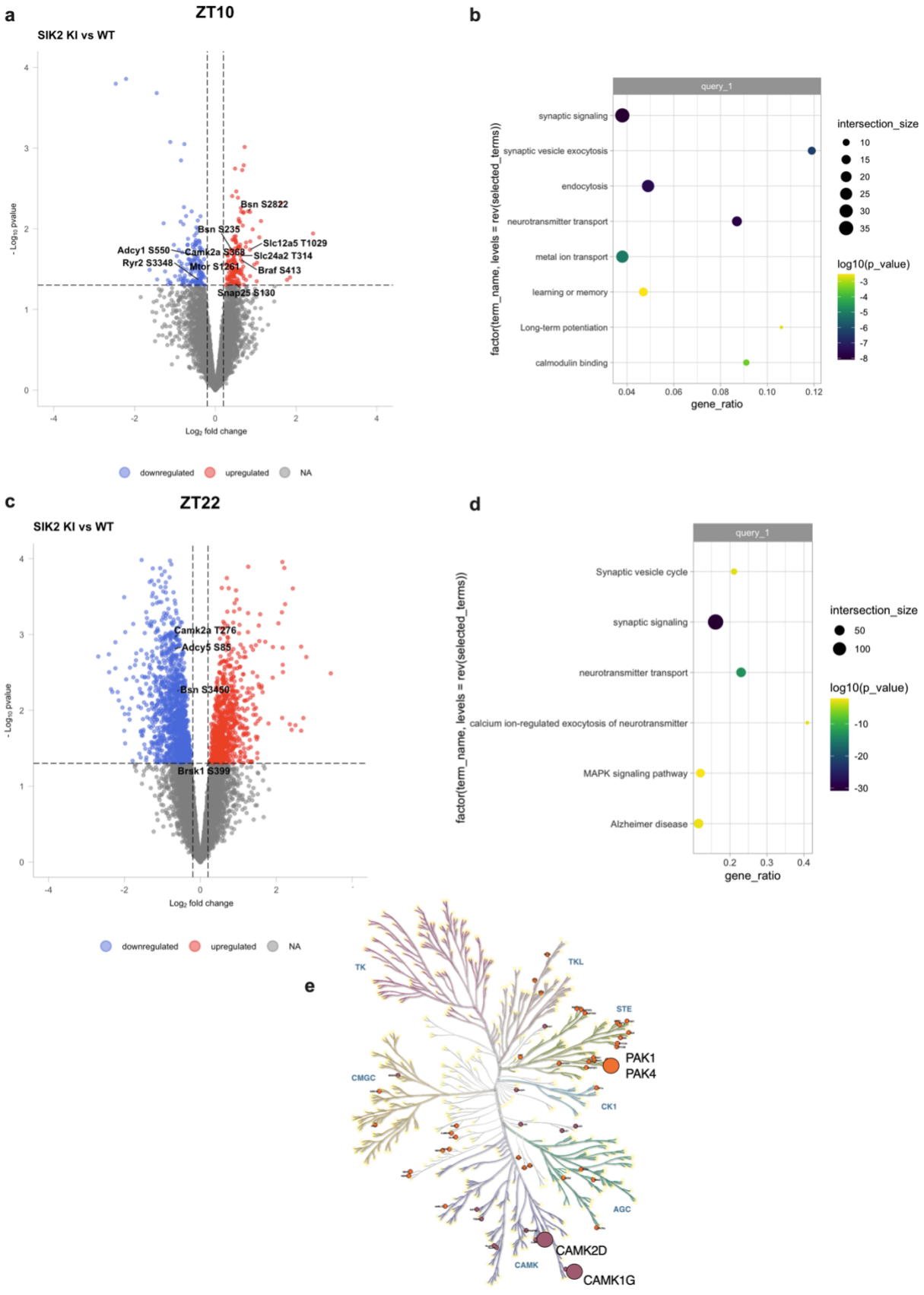
a
ZT10
SIK2 KI vs WT
- Log10 pvalue
Log2 fold change
Bsn S2822
Bsn S235
Slc12a5 T1029
Adcy1 S550
Camk2a S368
Slc24a2 T314
Ryr2 S3348
Mtor S1261
Braf S413
Snap25 S130
downregulated
upregulated
NA
b
query_1
factor(term_name, levels = rev(selected_terms))
synaptic signaling
synaptic vesicle exocytosis
endocytosis
neurotransmitter transport
metal ion transport
learning or memory
Long-term potentiation
calmodulin binding
gene_ratio
intersection_size
log10(p_value)
c
ZT22
SIK2 KI vs WT
Camk2a T276
Adcy5 S85
Bsn S3450
Brsk1 S399
d
Synaptic vesicle cycle
calcium ion-regulated exocytosis of neurotransmitter
MAPK signaling pathway
Alzheimer disease
e
TK
TKL
STE
CMGC
CK1
AGC
CAMK
PAK1
PAK4
CAMK2D
CAMK1G

Fig. 5.12 *In vivo* phopshoproteomics to identify molecular substrates of SIK2 in the cortex. 1mm3 cortex punches were collected from WT and SIK2 KI animals either 2 hours before the onset of dark phase, end of sleep phase (ZT10), or 2 hours before the onset of light phase, end of wake phase (ZT22). n=4x4 samples pooled SCN per genotype. Proteomics and phosphoproteomics enrichment were conducted. Volcano plots of phosphoproteomics changes between WT and SIK2 KI animals at (a) ZT10 and (b) ZT22. Dotted lines = log2FC>0.2 and uncorrected p-value <0.05. GProfiler functional analysis of DEGs highlighting enriched terms in (b) ZT10 and (d) ZT22. -log10(p-value) and overlap size/ratio were calculated and programmed in R studio. (e) Kinase enrichment analysis of the WT vs SIK2 KI phosphoproteome showing kinases with significantly gained activity (orange) and reduced (purple), visualised with KinMap.

5.2.9 Behavioural alterations in SIK2 KI mice

We performed novel object recognition tests to observe cognition and memory changes between WT and SIK2 KI animals at the start of the sleep phase (ZT3).

Animals were first exposed to one set of objects on the first day of the experiments (training session). One of the objects was switched for a novel object 24 hours later (testing session) (Fig. 5.13a). The training sessions were scored and analyzed to control for animals' innate biases and preferences. Total time spent on objects compared to the open space (centre) was similar between SIK2 KI and WT animals. There were also no differences in exploration time between the left and right objects. These results show that there were no significant differences in innate curiosity and position bias in the WT and SIK2 KI experimental cohorts (Supp. Fig. 5.4).

As a technical replicate, we performed the tests (training and testing) on the same cohort of animals with another set of objects, named "C" and "D". This control could ensure that the differences we observed did not arise from the choice of objects such as shape, color, or odour. However, we noticed significant object bias towards object "D" (small, yellow ping pong ball) in the WT animals, suggesting a strong innate preference

(Fig. 5.13d). The bias was not observed in SIK2 KI animals or the first set of objects “A” and “B”, suggesting a change in inclination towards specific colors and shapes under the loss of SIK2. Therefore, the replicate tests with objects “C” and “D” were subsequently excluded.

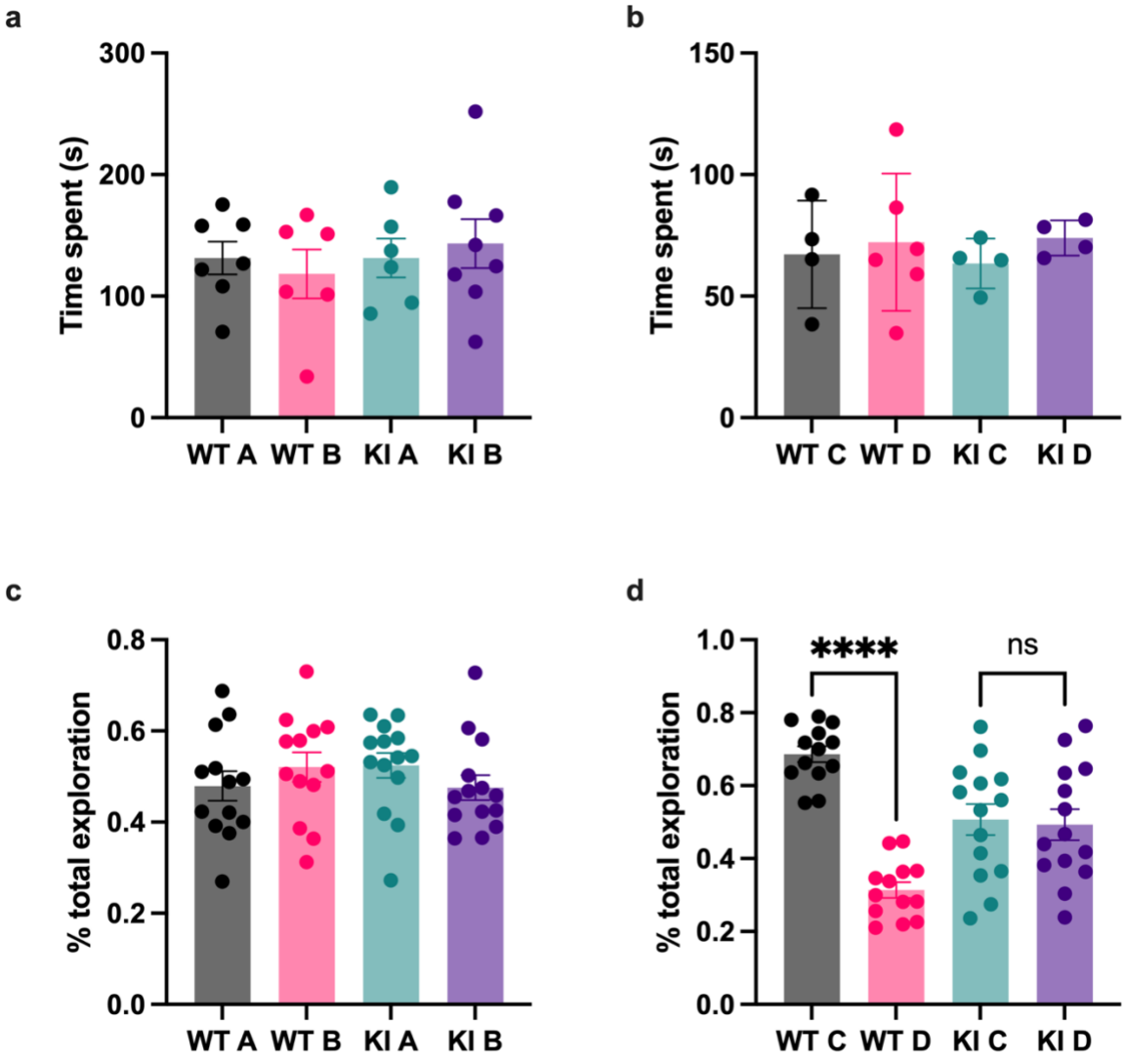

Figure 5.13 Novel Object Recognition (NOR) replicates revealed object bias in animals. The training and testing sessions were repeated twice with different sets of objects as technical replicates. (a) Images of objects used during the replicates. Objects A&B (left) were used for replicate 1 and objects C&D (right) were used for replicate 2. The training session for replicate 2 was performed one day after the first replicate was completed. Total time WT and

SIK2 KI animals spent on (b) objects A & B and (c) objects C & D during the training sessions. Fraction of total exploration time WT and SIK2 KI animals spent on (d) objects A & B and (e) objects C & D during the testing sessions. ns $p>0.05$, **** $p<0.0001$, Ordinary one-way ANOVA with Šídák's multiple comparisons test. Data points are mean ± SEM, n=13-14 per group.

During the testing session, there was no difference in total time spent on objects and left/right bias in the WT and SIK2 KI animals. These showed that the experiment was counterbalanced correctly between novel and familiar objects as they were evenly distributed across locations (Supp. Fig. 5.4). The discrimination index (DI) was calculated to determine how well the WT and SIK2 KI animals discriminate between the novel and familiar objects after 24 hours. It is the difference between the time spent on novel and familiar objects as a proportion of total time spent on objects. A positive DI represents a preference towards the novel object, whereas a negative DI represents a preference towards the familiar object. A DI of 0% means the animals explore the objects equally and have no memory or preference, representing random chance. WT animals had a positive DI of 18.12% and one sample t-test revealed that it was significantly different from chance ($p=0.0007$), suggesting that they were able to correctly differentiate between the objects and had a general curiosity towards exploring the novel. The SIK2 KI animals, on the other hand, had a significantly lower discrimination index (DI) of 3.17% ($p=0.04$) compared to WT animals. Examining the proportion of the animals, one out of thirteen WT animals had a DI under 0%, while four out of fourteen SIK2 KI animals had a DI under 0%, which had resulted in a lower DI. However, these animals did not show sex differences or bias, therefore were included in the results. One sample t-test showed that the DI of SIK2 KI animals was indistinguishable from chance, exhibiting random preference, but could be due to the

proportion of animals with negative DI (Fig. 5.14b). When the raw exploration times were split into 1-minute bins, two-way repeated measures ANOVA analysis exhibited a significant main effect of object, indicating a greater preference for the novel object than the familiar object in WT animals. SIK2 KI animals showed no differences in exploration across the 5-minute period (Fig. 5.14c-d). No object x time interaction was observed in either genotype, suggesting that preferences did not change across time.

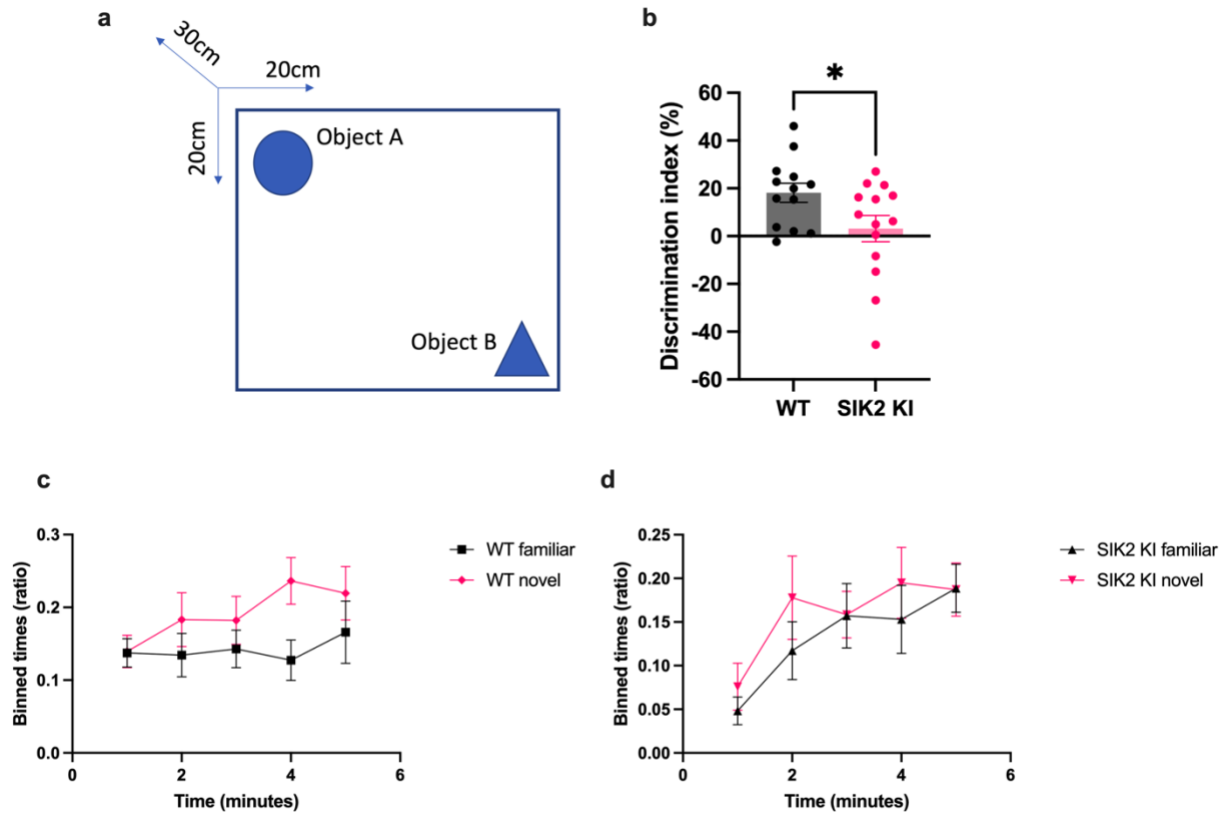

Fig. 5.14 Novel Object Recognition (NOR). WT and SIK2 KI animals were exposed to a novel object, randomized and counterbalanced for each animal and genotype. (a) Illustration of 20x20x30cm arena used. Objects were placed in opposite corners of the arena and "left" and "right" sides were determined and labelled. (b) Discrimination index (%) calculated as the difference between the time spent on the "novel" and "familiar" objects as a fraction of total exploration time on objects. Total time (c) WT and (d) SIK2 KI animals spent on each object in

seconds was split into one-minute bins and plotted as a ratio of total seconds in the bin (60 seconds) showing how preference towards novelty progressed throughout the 5-minute recording. Two-way ANOVA analysis showed a significant main effect of object in (c) ($p=0.0132$). * $p<0.05$, Two-tailed unpaired t-test. Data points are mean ± SEM, n=13-14 per group.

As *Sik2* is also expressed in the hippocampus, as shown in 5.2.4, we explored the effects of SIK2 deficiency on hippocampal-dependent spatial working memory. A Y-maze recognition test was performed at the start of the sleep phase. SIK2 KI and WT animals were first exposed to two arms where the novel arm was blocked for 5 minutes. All three arms were then exposed for 5 minutes of exploration (Fig. 5.15a). There was no retention time between the sessions. There was no significant difference between the total exploration time of the arms between WT and SIK2 KI animals. The SIK2 KI animals had slightly higher average moving speed and greater travelled distance than WT animals, but this was not statistically significant (Supp. Fig. 5.5). WT animals had a DI of 76.61% and SIK2 KI animals had a slightly lower DI of 62.49%, but failed to reach statistical significance. Both DIs were significantly different from chance (0%), as analyzed using one sample t-test, which implied that both showed a preference towards the novel arm (Fig. 5.15). Power analysis conducted in RStudio revealed that the experiment had a power of 15.8%, which is significantly underpowered. Future studies with a larger sample size would be required.

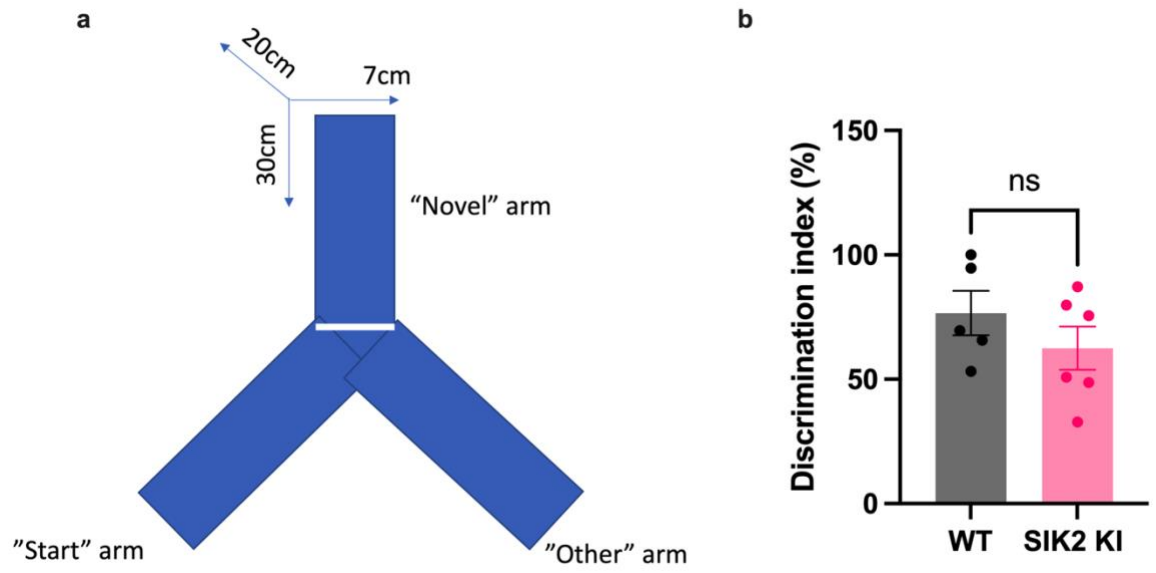

Fig. 5.15 Y-maze spatial novelty test of SIK2 KI animals. (a) Illustration of arena used. "start", "novel" and "other" arms were randomized and counterbalanced between animals and genotypes. The "novel" arm during the training session was blocked with a dark scentless plastic block, indicated by the white bar on the illustration. (b) The discrimination index (%) was calculated using the first two minutes of the recording of the testing session. It was calculated as the difference between the time spent on the "novel" and "other" arms as a fraction of the total time spent. ns = $p>0.05$, Two-tailed unpaired t-test. Data points are mean ± SEM, n=6 per group.

5.3 Discussion

Since SIK2's discovery in adipocytes, there is a growing body of studies on SIK2's role in adipogenesis, energy homeostasis and cancer biology. Following research on the SIK1 and SIK3 isoforms in circadian and sleep biology, there is limited evidence on SIK2's role in these areas. In this chapter, we conducted circadian and sleep characterizations using SIK2 KI mice. We implemented tissue-specific transcriptomics and Pro-KALIP to identify differential gene expression in SIK2 KI animals and direct substrates of SIK2, respectively. We hypothesized that the molecular profiling would support and contextualize the observed behavioural outputs.

We first consulted the publicly available ABC atlas scRNAseq dataset to pinpoint Sik2 gene expression across brain regions and cell types. Expression shows that Sik2 is abundant across various brain regions, including both the SCN and cortical layers. Sik2 is expressed predominantly in GABAergic neurons in the SCN, which are shown to maintain circadian oscillations and coupling (Ono et al., 2019). In cortical layers, Sik2 is present in glutamatergic neurons, which were implicated in sleep regulation (Allada et al., 2017). These results proposed that SIK2 is a primary regulator of circadian and sleep pathways.

5.3.1 Weak circadian clock

We first measured wheel-running activity in WT and SIK2 KI animals under baseline and LD cycle alterations. Under baseline 12:12 LD cycle, we observed no significant

differences in activity profile (counts and bouts). SIK2 KI animals had significantly lower circadian amplitude than WT controls. SIK2 KI animals also had significantly lower IS than WT animals, suggesting that endogenous circadian rhythms under the loss of SIK2 were weaker and less robust. WT and SIK2 KI animals were behaving very similarly under free-running period, DD and LL. There were no significant differences in core circadian parameters and non-parametric measures. SIK2 KI animals, under DD conditions, had fewer total activity bouts, higher counts per minute and higher total counts per bout, indicating that they were more active than WT animals. Together, these results showed that under baseline and constant conditions, the loss of SIK2 had a significant impact on circadian clock regulation.

WT and SIK2 KI animals were then subjected to photic stimulations to explore entrainment patterns. Following stable entrainment to a 12:12hr LD cycle, the animals were released into DD and exposed to two 30-minute light pulses at CT14 and CT22, expected to exhibit the largest phase shifts in response to light. There were no significant differences in phase differences between WT and SIK2 KI animals at both time points. Activity counts were also measured before and during the light pulses. Under sporadic light pulses, animals typically suppress wheel running activity and endogenous rhythms, a behavior called masking (Rietveld et al., 1993). Activity counts showed that WT and SIK2 KI animals were masking normally and similarly in response to light pulses, as they both suppressed activity. After exposing the animals to 6hr light advances, SIK2 KI and WT animals exhibited similar entrainment patterns and speeds to the new LD cycle. These findings suggested that SIK2 KI animals showed unaltered

responses to light pulses and photic cues, which confirms that SIK2 is not primarily and solely regulated through a light-dependent pathway.

Lastly, we subjected them to an ultradian cycle to further explore the robustness of the endogenous circadian clock. There were no significant differences between the activity profiles of WT and SIK2 KI animals. While the WT animals maintained an endogenous circadian period of close to 24 hours, the SIK2 KI animals adjusted their circadian period to 9.83 hours. After releasing them into DD, the circadian period of the SIK2 KI animals shifted back to the 24-hour circadian period immediately after the ultradian cycle ended. These results showed that the SIK2 KI animals were masking to the LD cycle, rather than true entrainment.

Together, under the loss of SIK2, we observed a weaker and less robust circadian clock, shown by significantly lower circadian amplitude and stability. The endogenous circadian clock was more sensitive to environmental changes, shown by the immediate masking to the ultradian cycle. The light pulses showed that SIK2 KI animals shifted phase in response to photic cues normally. Together, these suggest that SIK2 is not regulated in a light-dependent pathway.

Post-hoc power analysis revealed that the groups had small to moderate effect sizes, which may be limited statistical power. Future studies will consider these factors.

5.3.2 Altered sleep homeostasis

We then recorded continuous EEG/EMG activity in WT and SIK2 KI animals to explore the sleep regulation of SIK2. Under baseline conditions, we observed a general trend of greater wakefulness and reduced NREM sleep in SIK2 KI animals. This was accompanied by significantly lower REM sleep at the start of the sleep phase. There was also a significant, consistent trend of lower delta energy in the SIK2 KI animals compared to WT animals. Delta power (SWA) is the most recognized core measurement of sleep depth and need (Borbély, 2009; Tononi & Cirelli, 2006). It is shown that SWS declines after major sleep episodes; however, SIK2 KI animals had lower SWS despite an increased trend of greater wakefulness (Dijk, 2009). This indicated that under baseline conditions, SIK2 KI animals had disrupted sleep pressure buildup or dissipation.

We then subjected the animals to a 6hr sleep deprivation to explore sleep homeostasis. It was shown that prolonged waking after sleep deprivation increases delta power, associated with increased sleep need and recovery sleep, eliciting a compensatory mechanism to maintain homeostasis in body functions (Tononi & Cirelli, 2006). After the 6-hr sleep deprivation at the start of the light phase from ZT0 to ZT6, there was an increase in sleep need in WT animals, shown by reduced wakefulness and increased NREM sleep and REM sleep. On the contrary, there were no differences in wakefulness and sleep amounts in SIK2 KI animals following sleep deprivation, implying a lack of recovery sleep. WT animals had an increase in delta energy, whereas SIK2 KI animals showed a lack of. These together showed that there was a lack of sleep pressure and

rebound sleep buildup after sleep deprivation under the loss of SIK2, suggesting altered sleep homeostatic responses.

5.3.3 SIK2 RNAseq in the SCN and direct substrates of SIK2 explain circadian phenotype

Firstly, we conducted SCN mRNAseq at ZT3 and detected 1112 genes that are differentially expressed between WT and SIK2 KI animals. By conducting functional analysis, we found enrichment in synaptic transmission processes, which also overlap with pathways related to “circadian rhythms”, including *Ngfr, Prox1, Sik1, Opn5, Bdnf*, and *Prokr2*. Interestingly, they are also implicated in “glutamate secretion” pathways, which is the key neurotransmitter in the RHT regulating photic responses in the SCN (Hannibal, 2002). Notably, literature has shown that a handful of the DEGs are related to photoentrainment. *Ngfr* in the SCN modulates synchronicity and phase shifting to light (Bina et al). *Ngfr* upregulation was shown to be connected to stress resilience in the dark phase (Narain et al., 2024). BDNF is shown to bind to NGFR, and the downregulation of both genes in the SIK2 KI is associated with depression and synaptic plasticity (Chaudhury et al., 2015). Similarly, OPN5 (neuropsin), another photopigment expressed in the retinal ganglion cells (RGC), was downregulated in the SIK2 KI animals and it was shown to mediate local retinal and corneal photoentrainment (Buhr et al., 2015).This is supported by showing that the loss of *Opn5* results in altered and delayed circadian photoentrainment (Ota et al., 2018). Interestingly, *Sik1* was upregulated under the loss of SIK2. It has previously been shown to be induced under abnormal nocturnal light and suppress abrupt phase shifting (Jagannath et al., 2013).

However, the induction and upregulation of *Sik1* under baseline conditions and the effects on circadian clock stability are yet to be determined. *Prox1* and *Prokr2* were upregulated in the SIK2 KI. *Prox1*, together with *Bmal1* and *ERRa*, maintains core clock gene oscillations and is also significant in glucose metabolism (Dufour et al., 2011). These results suggest that under the loss of SIK2, expression of genes closely associated with photoentrainment and circadian stability in the SCN was altered, which indicates that SIK2 acts as a primary and central regulator of the transcriptional regulation of the circadian clock and response to light, while maintaining core clock genes intact. This is reflected in the alteration in circadian amplitude and instability under baseline conditions in the circadian characterization.

Notably, we observed significant upregulation of neuropeptide activity, including *Grp, Nppc, Oxt, Npy, Avp* and *Vip*. Extensive research has shown that AVP and VIP play significant roles in SCN synchronization and photoentrainment. *Avp* is suggested to be required for high circadian amplitude output, and the lack of AVP receptors V1a and V1b lead to accelerated re-entrainment of daily rhythms (Mieda et al., 2015; Yamaguchi et al., 2023). Similarly, Vipr2$^{-/-}$ *in vitro* SCN cultures were shown to significantly reduce circadian amplitude and oscillation compared to WT SCN and the ability to resist phase shifts is reduced (Hughes et al., 2011). Together, existing literature shows that an intact neuropeptide system in the SCN is essential for circadian robustness and synchrony. No changes in AVP receptors or neuropeptide activity on the protein level between SIK2 KI and WT were observed. Literature has suggested that stability and entrainment shifts depend on the phase and dose of VIP, where above 100nM of VIP reduces SCN

synchrony (An et al., 2013). These results imply that the upregulation of neuropeptides leads to overcompensation in the SCN due to altered and disrupted transcriptional circadian regulation under the loss of SIK2. Though follow-up experiments are required, gene expression profile proposes that Sik2 in involved in the transcriptional regulation of core circadian clock genes and neuropeptide signaling, influencing robustness, stability and photoentrainment.

We next examined the molecular substrates of SIK2 in the SCN at EOS and EOW by collecting SCN punches in SIK2 KI and WT animals. We found enrichment for synaptic signaling at both timepoints. It showed that SIK2 phosphorylates substrates involved in synaptic vesicle exocytosis, including PCLO and RPH3A, endocytosis (BSN, BAIAP3 and SYN1/2/3). Of which PCLO, DPYSL2, RIMS1 and SYN1 were significant in both timepoints. We detected more phosphorylation changes associated with vesicle transport and trafficking in the EOW phase, which indicates that substrates function distinctively depending on sleep-wake states. We confirmed these findings in the *in vivo* phosphoproteomics using Pro-KALIP in the SCN, including DPYSL2, SYNGAP1 and IQSEC2, identified as bona fide direct substrates of SIK2. DPYSL2 plays a significant role in mTOR signaling and modulation of schizophrenia (Pham et al., 2016).

Specifically, the site detected, S522, is implicated in Alzheimer's Disease pathology (Noguchi et al., 2025). SYNGAP1, as a negative regulator of the MAPK pathway, is regulated by the SCN clock timing and photic cues through phosphorylation at Ser1138. It was shown that SYNGAP1 heterozygous null mice had rapid entrainment to a shifted

LD cycle (Aten et al., 2021). These could map to the altered photoentrainment phenotype that we observed in SIK2 KI animals. These substrates suggest that SIK2 modulates synaptic signaling and transmission in the SCN, translating to circadian timekeeping and stability. As AVP and VIP are major neurotransmitters in synapse, the phosphorylation changes in proteins relating to synaptic vesicle transport and trafficking could link to altered neuropeptide activity and circadian output.

Notably, in both timepoints, we detected enrichment for calmodulin binding and calcium signaling pathways such as CACNA1B, CAMK2A/B, RYR2, and UBR4. Literature has shown that intracellular Ca^{2+} signaling in the SCN is essential for circadian rhythmicity and synchrony (Enoki et al., 2017). Mutations of the *Drosophila* CACANA1 subunit, *cac*, showed that CACNA1A/B are essential for maintaining circadian rhythmicity and period (Hidalgo et al., 2021). CAMK2A/B have also been identified as key sleep-promoting kinases (Tone et al., 2022). Specifically, the site CAMK2B T287 is a key autonomous site regulating synaptic and neuronal activity.

In addition, UBR4, a novel E3 ubiquitin ligase, was identified as a direct substrate of SIK2 and was hyperphosphorylated in the SIK2 KI animals. Its activity is linked to calmodulin (Grabarczyk et al., 2025). It is localized in AVP-expressing neurons and the levels of UBR4 increase following photic stimulation (Ling et al., 2014), proposing a link to the upregulation of *Avp* expression in SIK2 KI. These results suggest that SIK2 regulates circadian clock robustness and entrainment through maintaining Ca^{2+} signaling in the SCN.

Interestingly, we detected a SIK2 autophosphorylation site T484, that was hypophosphorylated at both timepoints in the SCN in the SIK2 KI. It is characterized as the PKA phosphorylation site ('gatekeeper'), which once activated, promotes binding to 14-3-3 and inhibits the activity of SIK2 (Sonntag et al., 2018). As the SIK2 T484 site normally acts as a negative feedback loop, modulating SIK2 kinase activity, the loss of the LKB1 site in the SIK2 KI model could inhibit the feedback loop, resulting in loss of phosphorylation. Literature has shown that the loss of the SIK2 PKA site S587 increases sleep need (Park et al., 2020), but the SIK2-PKA axis in the SCN and circadian regulation is understudied.

Together, combining gene expression profiling and phosphoproteomics, we found that SIK2 plays a primary role in the regulation of the circadian clock, through neuropeptide signaling and core clock components. By direct phosphorylation, SIK2 controls SCN behavioural output by maintaining synaptic and Ca^{2+} signaling. These propose a close link between transcriptional and post-translational regulation of the circadian clock by SIK2.

5.3.4 Molecular substrates in the cortex link to sleep phenotype

To understand the sleep phenotype, we conducted cortex-specific transcriptomics at ZT3 to explore differentially expressed genes (DEGs) between SIK2 KI and WT animals. We found *Cdr1os, Lars2* and *Osmr* that passed the corrected significance (padj<0.05). By conducting functional analysis, we found enrichment for synaptic regulation and neurogenesis, including *Ngfr, Serpinf1, EfnB3* and *Grin1* in the cortex. EFNB3 is a

recognized ligand of EphA4, which is a kinase associated with synaptic plasticity. EPHA4 KO mice display impaired REM SLEEP occurrence during the light phase and rhythmic expression of EPNB3 was detected in the cerebral cortex, which suggests that EPNB3 expression is implicated in sleep-wake regulation (Freyburger et al., 2016). GRIN1 variants, associated with neurodevelopmental abnormalities, also display circadian rhythm and sleep disturbances (Scala et al., 2019). These suggest that alterations in genes encode synaptic signaling.

We then conducted *in vivo* phosphoproteomics in the cortex of SIK2 and WT animals at EOS and EOW phases. Matching the gene expression profile, we similarly detected enrichment in synaptic signaling, including BRAF, BRSK1, CAMK2B, CDK5 and DLGAP1/2/3. BRAF, involved in exocytosis, is important for the CAMKII to ERK transduction cascade for synaptic transmission and plasticity (Lim et al., 2017). CDK5 downregulation promotes Ca^{2+} signaling and BDNF/CREB cascade, modulating synaptic plasticity (Posada-Duque et al., 2017; Vandael et al., 2024). The previously validated site CAMK2B T287 was not statistically significant, but was slightly hyperphosphorylated in both time points in SIK2 KI animals. Tone et al showed that T287D phospho-mimicking mice had increased sleep duration. CAMK2B T287 and CAMK2A T286 were shown to be associated with sleep need as the levels of phosphorylation are elevated after 6hr sleep deprivation (Tone et al., 2022). Researchers have also validated the significance of intracellular Ca^{2+} in sleep induction and maintenance (Y. Wang et al., 2022). SIK2 KI animals exhibited increased wakefulness and reduced NREM sleep, which would normally initiate sleep pressure

and need buildup. This aligns with the hyperphosphorylation of sleep-promoting markers such as CAMK2B phosphorylation. However, delta power was shown as consistently lower in the SIK2 KI, which suggests that SWA and sleep homeostasis are disrupted under the loss of SIK2 kinase activity.

By conducting KSEA analysis, we detected CAMK kinases, specifically CAMK2D and CAMK1G, as upstream of SIK2 substrates in the cortex. CAMK-dependent phosphosites showed reduced activity and phosphorylation. CAMKII kinases have also been studied extensively in the context of sleep regulation. It was shown that Camk2b knockout mice showed no significant rebound sleep after sleep deprivation, proposing CAMKII kinases as key regulators for sleep homeostasis (Yang et al., 2025). These studies support the altered sleep homeostasis and reduced delta energy in the sleep phenotype of SIK2 KI animals, linking CAMK activity to sleep regulation.
These results suggest that the loss of SIK2 activity disrupts the CAMK kinase system in sleep regulation, which leads to altered hemostatic responses under baseline and sleep deprivation.

5.3.5 Behavioural alterations linked to phosphorylation patterns

As we detected a handful of molecular substrates, phosphorylation changes, in the cortex associated with learning and memory in both the SCN and cortex, we next explored the downstream behavioural and cognitive changes. We performed NOR tests at ZT3 on WT and SIK2 KI animals with training and testing sessions 24 hours apart. It was shown that at a 24hr retention time, most animals will be able to discriminate

between the novel and familiar objects (Lueptow, 2017). The objects and positions were counterbalanced to avoid bias. The results showed that between WT and SIK2 KI animals, there were no differences in innate curiosity towards positions. However, WT animals had a significant bias towards object C, while interest in SIK2 KI animals remained the same between objects, suggesting a change in innate inclination towards colors or shapes. Further investigations would be necessary to draw reliable conclusions.

The DI was calculated as a percentage to determine how well animals differentiate between novel and familiar objects. One-sample t-tests were performed to test the DIs against random chance, which was set at 0%. WT animals had a positive index of 18.12% and was significantly different from random chance, showing that they effectively differentiated between the two objects and preferred novelty. This aligns with innate preferences for novelty in rodents (Lueptow, 2017). However, SIK2 KI animals, though they also had a positive DI of 3.17%, did not show significance against random chance, indicating that exploration and preference were random during the trials. However, examining the distribution and proportion of data points, the lower DI in four out of fourteen SIK2 KI animals may exist as a confound. As a result, WT animals had significantly higher DI than SIK2 KI animals, showing a greater preference towards novelty. Binned measures also revealed that while WT animals consistently preferred the novel object, SIK2 KI animals had similar levels of exploration. These findings implied that SIK2 KI animals, at a 24-hour retention, could not differentiate between

familiarity and novelty, implying a deficiency in memory. Yet, future experiments at shorter retention times would be required to draw firmer conclusions.

In previous studies, NOR tests were performed to examine learning and memory under sleep disturbances. As opposed to other behavioural exams that impose stress, fear and repetitive restrictions, NOR is based on innate preferences of rodents in response to stimuli and comparable between trials. Studies showed that sleep deprivation immediately after the training phase alters object location memory using NOR tests (Ishikawa et al., 2014), where animals were unable to discriminate. These accentuate the link between sleep and synaptic plasticity.

Consulting the molecular substrates of SIK2, we found enrichment for learning and memory processes in both the SCN and cortex, including GRIN2A/B, ADCY1, MTOR, GRIA2A, SYNPO and CAMK2B. GRIN2A and GRIN2B encode the GluN2A and GluN2B regulatory subunits of the NMDA receptors. The glutamate receptor subtypes are linked to spatial memory and plasticity. Knockout of GluN2A showed short-term memory deficits and spatial working memory deficits. It also forms a bidirectional relationship as learning and memory tasks also influence the levels of GluN2A (Bannerman, 2009; Franchini et al., 2020). Variants in GRIN2B are associated with schizophrenia, autism and neurodevelopmental disorders (Lee et al., 2021; Pan et al., 2015), affecting synaptic transmission and connectivity. Similarly, GRIA2A, an AMPA receptor, also regulates synaptic strength, influencing learning and memory over time (Kessels & Malinow, 2009). Researchers have identified GRIN2A and AMPA receptor

genes to be tightly associated with schizophrenia risk, supporting the significance of a functional glutamatergic system (Singh et al., 2022; Trubetskoy et al., 2022). These findings suggest that altered phosphorylation patterns in molecular substrates of SIK2 influence downstream memory consolidation and learning abilities. In addition, researchers showed that synaptic potentiation and depression in the cortex are associated with the sleep-wake cycle, indicated by AMPA receptors (Vyazovskiy et al., 2008). These key phosphoproteins were generally hyperphosphorylated in the wake phase and hypophosphorylated in the sleep phase in the SIK2 KI animals compared to WT controls, resulting in a larger net difference in synaptic strength. As NREM sleep is associated with synaptic depression and downscaling, the reduction in delta energy and power under the loss of SIK2 potentially disrupts synaptic potentiation during wake, leading to an overcompensatory mechanism. The changes in molecular markers, AMPARs, translate into the observed behavioural and cognitive alterations. We propose a molecular pathway connecting SIK2's role in sleep regulation and downstream effects on cognition and memory.

In addition, as consulted with ABC scRNAseq brain atlas, we have shown that there is *Sik2* gene expression in the hippocampal regions, suggesting *Sik2* could regulate hippocampal-related function. In phosphoproteomics, we also identified molecular substrates that were associated with hippocampal function. Populations of dopaminergic neurons project directly from the lateral ventral tegmental area (VTA) and substantia nigra pars compacta regions to the dorsal hippocampus (Tsetsenis et al., 2021). Long-term memory was also proposed to be linked to the dopamine circuitry

between the ventral tegmental area (VTA) and hippocampus (Rossato et al., 2009). Novelty induces the release of dopamine in the hippocampus and stabilizes memory consolidation (Duszkiewicz et al., 2019).

Specifically, we found changes in DLGAP1/3 and HRNRPK. The phosphosites of DLGAP1/3 were all hypophosphorylated in SIK2 KI in the cortex. Research has also supported that sleep deprivation and altered sleep homeostasis lead to differential gene expression related to dendritic localization and postsynaptic membrane in the hippocampus (Gaine et al., 2021) and DLGAP1 and DLGAP3 were significantly downregulated, leading to weakened synaptic plasticity. HRNRPK as a direct substrate of SIK2 in the SCN also regulates long-term potentiation (LTP) and knockdown prevents GluA1 S845 phosphorylation, a key site for AMPAR trafficking and synaptic transmission onto the hippocampus (Folci et al., 2014; Leana-Sandoval et al., 2025).

Therefore, we conducted a Y-maze recognition test to observe hippocampal-related spatial cognition in SIK2 KI and WT animals at ZT3. It was shown that SIK2 KI animals had higher average moving speed and greater travelled distance, implying that they were more active during the tests. The DI was slightly lower in SIK2 KI animals compared to WT animals, but it was not statistically significant. As previous studies have used n numbers of above 10 for Y-maze spatial tests (Viney et al., 2022), these preliminary results set the basis for future investigations, supported by power analysis. Our findings suggest novelty-induced long-term memory consolidation was altered under the loss of SIK2 kinase activity. Future experiments on spatial memory and short-

term memory would be important to pinpoint the effect of SIK2 on memory consolidation and formation. Through scRNAseq analysis, we found that loss of SIK2 does not directly alter dopaminergic systems in the hippocampus due to its absence in respective neurons. Therefore, these results propose that memory and cognition are altered as a potential downstream effect of disrupted sleep and synaptic homeostasis. This provides a perspective that, in addition to core regulation in the SCN and cortex, SIK2 also spans across other regions, impacting hippocampal-related cognitive functions.

5.3.6 SIK2 and the Two Process Model

We then overlapped the molecular substrates of SIK2 in the SCN and cortex at the two timepoints. We found 51 substrates that were both significant at ZT10 EOS including key synaptic proteins relating to synaptic vesicles such as DPYSL2, PCLO and DMXL2. Similarly, we detected 356 proteins at ZT22, mostly synaptic processes and more proteins related to Ca^{2+} signaling such as IQSEC1/2, UBR4, BSN and CACNG2/3/8. This suggests that there is more synaptic activity during wakefulness than sleep, more synaptic potentiation (Vyazovskiy et al., 2008). Furthermore, we detected 27 substrates that are significant in both the SCN and cortex and at both timepoints. For instance, in the SCN, significant CAMK2A sites, S275 and T306, are mostly hyperphosphorylated in the SIK2 KI. Whereas in the cortex, significant CAMK2A sites T276 and S404 were hypophosphorylated in the cortex at ZT22. This indicates that CAMK2A as a key substrate of SIK2 regulates both circadian and sleep processes by phosphorylating different sites and at corresponding times of the sleep-wake cycle. The substrates in the SCN predominantly regulate SCN stability and the circadian clock, mapping to Process

C, whereas the substrates in the cortex are sleep-associated, relating to Process S. Therefore, we propose that the overlapping substrates in both the SCN and cortex are key molecular substrates for the Two Process Model, proposing SIK2 as the master regulator.

5.3.7 Conclusion

In this chapter, we aimed to explore the role of SIK2 in circadian and sleep regulation. We first conducted a full circadian characterization using SIK2 KI and WT animals under baseline conditions and various light-dark cycle alterations. We found that under the inactivity of SIK2, the circadian clock is weaker with lower circadian amplitude and lower stability. It is also accompanied rapid masking to the ultradian LD cycle. Using RNAseq, phosphoproteomics and Pro-KALIP to examine differential gene expression of SIK2 in the SCN. We detected a significant upregulation of neuropeptide activity, *Avp* and *Vip,* and downregulation of genes related to circadian rhythms under the loss of Sik2, which maps to the weaker circadian clock. The direct substrates of SIK2 in the SCN show that SIK2 regulates synaptic proteins and calcium signaling through direct phosphorylation which stabilizes and synchronizes the SCN. We then conducted a full sleep characterization and found that under the loss of SIK2, NREM delta energy was consistently lower and sleep homeostasis was disrupted after 6hr sleep deprivation. Similarly, we conducted RNAseq and phosphoproteomics and found that SIK2 similarly regulates synaptic proteins, regulating sleep need and pressure. We found these phosphorylation changes to be overlapping in the SCN and cortex, regulating both Process C and Process S, providing a molecular link for the Two Process Model. We

have also shown that SIk2 regulates metabolic processes, lipid and energy homeostasis, suggesting a wider role in whole body physiology through direct phosphorylation.

Moreover, learning and memory pathways were found to be altered under the loss of SIK2 through phosphorylation changes and targets. We performed memory tests, novel object recognition (NOR) and the short-term spatial recognition test, Y-maze. Findings suggested that SIK2 KI animals have altered long-term novelty-induced memory, potentially associated with disrupted sleep and synaptic homeostasis.

REFERENCES

Ahmed, A. A., Lu, Z., Jennings, N. B., Etemadmoghadam, D., Capalbo, L., Jacamo, R. O., Barbosa-Morais, N., Le, X. F., Vivas-Mejia, P., Lopez-Berestein, G., Grandjean, G., Bartholomeusz, G., Liao, W., Andreeff, M., Bowtell, D., Glover, D. M., Sood, A. K., & Bast, R. C. (2010). SIK2 Is a Centrosome Kinase Required for Bipolar Mitotic Spindle Formation that Provides a Potential Target for Therapy in Ovarian Cancer. *Cancer Cell*, *18*(2), 109–121. https://doi.org/10.1016/j.ccr.2010.06.018

Allada, R., Cirelli, C., & Sehgal, A. (2017). Molecular mechanisms of sleep homeostasis in flies and mammals. *Cold Spring Harbor Perspectives in Biology*, *9*(8). https://doi.org/10.1101/cshperspect.a027730

An, S., Harang, R., Meeker, K., Granados-Fuentes, D., Tsai, C. A., Mazuski, C., Kim, J., Doyle, F. J., Petzold, L. R., & Herzog, E. D. (2013). A neuropeptide speeds circadian entrainment by reducing intercellular synchrony. *Proceedings of the National Academy of Sciences*, *110*(46). https://doi.org/10.1073/pnas.1307088110

Aten, S., Kalidindi, A., Yoon, H., Rumbaugh, G., Hoyt, K. R., & Obrietan, K. (2021). SynGAP is expressed in the murine suprachiasmatic nucleus and regulates circadian-gated locomotor activity and light-entrainment capacity. *European Journal of Neuroscience*, *53*(3), 732–749. https://doi.org/10.1111/ejn.15043

Bannerman, D. M. (2009). Fractionating spatial memory with glutamate receptor subunit-knockout mice. *Biochemical Society Transactions*, *37*(6), 1323–1327. https://doi.org/10.1042/BST0371323

Bon, H., Wadhwa, K., Schreiner, A., Osborne, M., Carroll, T., Ramos-Montoya, A., Ross-Adams, H., Visser, M., Hoffmann, R., Ahmed, A. A., Neal, D. E., & Mills, I. G. (2015). Salt-inducible kinase 2 regulates mitotic progression and transcription in prostate cancer. *Molecular Cancer Research*, *13*(4), 620–635. https://doi.org/10.1158/1541-7786.MCR-13-0182-T

Borbély, A. A. (2009). Refining sleep homeostasis in the two-process model: Editorial. In *Journal of Sleep Research* (Vol. 18, Number 1, pp. 1–2). https://doi.org/10.1111/j.1365-2869.2009.00750.x

Bricambert, J., Miranda, J., Benhamed, F., Girard, J., Postic, C., & Dentin, R. (2010). Salt-inducible kinase 2 links transcriptional coactivator p300 phosphorylation to the prevention of ChREBP-dependent hepatic steatosis in mice. *Journal of Clinical Investigation*, *120*(12), 4316–4331. https://doi.org/10.1172/JCI41624

Buhr, E. D., Yue, W. W. S., Ren, X., Jiang, Z., Liao, H.-W. R., Mei, X., Vemaraju, S., Nguyen, M.-T., Reed, R. R., Lang, R. A., Yau, K.-W., & Van Gelder, R. N. (2015). Neuropsin (OPN5)-mediated photoentrainment of local circadian oscillators in mammalian retina and cornea. *Proceedings of the National Academy of Sciences*, *112*(42), 13093–13098. https://doi.org/10.1073/pnas.1516259112

Chaudhury, D., Liu, H., & Han, M. H. (2015). Neuronal correlates of depression. In *Cellular and Molecular Life Sciences* (Vol. 72, Number 24, pp. 4825–4848). Birkhauser Verlag AG. https://doi.org/10.1007/s00018-015-2044-6

Dijk, D.-J. (2009). Regulation and functional correlates of slow wave sleep. *Journal of Clinical Sleep Medicine : JCSM : Official Publication of the American Academy of Sleep Medicine*, *5*(2 Suppl), S6-15.

Dufour, C. R., Levasseur, M. P., Pham, N. H. H., Eichner, L. J., Wilson, B. J., Charest-Marcotte, A., Duguay, D., Poirier-Héon, J. F., Cermakian, N., & Giguère, V. (2011). Genomic convergence among ERRα, PROX1, and BMAL1 in the control of metabolic clock outputs. *PLoS Genetics*, *7*(6). https://doi.org/10.1371/journal.pgen.1002143

Duszkiewicz, A. J., McNamara, C. G., Takeuchi, T., & Genzel, L. (2019). Novelty and Dopaminergic Modulation of Memory Persistence: A Tale of Two Systems. In *Trends in Neurosciences* (Vol. 42, Number 2, pp. 102–114). Elsevier Ltd. https://doi.org/10.1016/j.tins.2018.10.002

Enoki, R., Ono, D., Kuroda, S., Honma, S., & Honma, K. I. (2017). Dual origins of the intracellular circadian calcium rhythm in the suprachiasmatic nucleus. *Scientific Reports*, *7*. https://doi.org/10.1038/srep41733

Fan, D., Yang, H., Mao, W., Rask, P. J., Pang, L., Xu, C., Vankayalapat, H., Ahmed, A. A., Bast, R. C., & Lu, Z. (2021). A novel salt inducible kinase 2 inhibitor, ARN-3261, sensitizes ovarian cancer cell lines and xenografts to carboplatin. *Cancers*, *13*(3), 1–15. https://doi.org/10.3390/cancers13030446

Folci, A., Mapelli, L., Sassone, J., Prestori, F., D'Angelo, E., Bassani, S., & Passafaro, M. (2014). Loss of hnRNP K Impairs Synaptic Plasticity in Hippocampal Neurons. *Journal of Neuroscience*, *34*(27), 9088–9095. https://doi.org/10.1523/JNEUROSCI.0303-14.2014

Franchini, L., Carrano, N., Di Luca, M., & Gardoni, F. (2020). Synaptic gluN2A-containing NMDA receptors: From physiology to pathological synaptic plasticity. *International Journal of Molecular Sciences*, *21*(4). https://doi.org/10.3390/ijms21041538

Freyburger, M., Pierre, A., Paquette, G., Bélanger-Nelson, E., Bedont, J., Gaudreault, P.-O., Drolet, G., Laforest, S., Blackshaw, S., Cermakian, N., Doucet, G., & Mongrain, V. (2016). EphA4 is Involved in Sleep Regulation but Not in the Electrophysiological Response to Sleep Deprivation. *Sleep*, *39*(3), 613–624. https://doi.org/10.5665/sleep.5538

Gaine, M. E., Bahl, E., Chatterjee, S., Michaelson, J. J., Abel, T., & Lyons, L. C. (2021). Altered hippocampal transcriptome dynamics following sleep deprivation. *Molecular Brain*, *14*(1). https://doi.org/10.1186/s13041-021-00835-1

Gao, T., Zhang, X., Zhao, J., Zhou, F., Wang, Y., Zhao, Z., Xing, J., Chen, B., Li, J., & Liu, S. (2020). SIK2 promotes reprogramming of glucose metabolism through PI3K/AKT/HIF-1α pathway and Drp1-mediated mitochondrial fission in ovarian cancer. *Cancer Letters*, *469*, 89–101. https://doi.org/10.1016/j.canlet.2019.10.029

Grabarczyk, D. B., Ehrmann, J. F., Murphy, P., Yang, W. S., Kurzbauer, R., Bell, L. E., Deszcz, L., Neuhold, J., Schleiffer, A., Shulkina, A., Lee, J., Shin, J. S., Meinhart, A., Versteeg, G. A., Zavodszky, E., Song, H. K., Hegde, R. S., & Clausen, T. (2025). Architecture of the UBR4 complex, a giant E4 ligase central to eukaryotic protein quality control. *Science*, *389*(6763), 909–914. https://doi.org/10.1126/science.adv9309

Hannibal, J. (2002). Neurotransmitters of the retino-hypothalamic tract. In *Cell and Tissue Research* (Vol. 309, Number 1, pp. 73–88). https://doi.org/10.1007/s00441-002-0574-3

Henriksson, E., Jones, H. A., Patel, K., Peggie, M., Morrice, N., Sakamoto, K., & Göransson, O. (2012). The AMPK-related kinase SIK2 is regulated by cAMP via phosphorylation at Ser 358 in adipocytes. *Biochemical Journal*, *444*(3), 503–514. https://doi.org/10.1042/BJ20111932

Henriksson, E., Säll, J., Gormand, A., Wasserstrom, S., Morrice, N. A., Fritzen, A. M., Foretz, M., Campbell, D. G., Sakamoto, K., Ekelund, M., Degerman, E., Stenkula, K. G., & Göransson, O. (2014). Salt-inducible kinase 2 regulates CRTCs, HDAC4 and glucose uptake in adipocytes. *Journal of Cell Science*. https://doi.org/10.1242/jcs.153932

Hidalgo, S., Campusano, J. M., & Hodge, J. J. L. (2021). The Drosophila ortholog of the schizophrenia-associated CACNA1A and CACNA1B voltage-gated calcium channels regulate memory, sleep and circadian rhythms. *Neurobiology of Disease*, *155*. https://doi.org/10.1016/j.nbd.2021.105394

Honda, T., Fujiyama, T., Miyoshi, C., Ikkyu, A., Hotta-Hirashima, N., Kanno, S., Mizuno, S., Sugiyama, F., Takahashi, S., Funato, H., & Yanagisawa, M. (2018). A single phosphorylation site of SIK3 regulates daily sleep amounts and sleep need in mice. *Proceedings of the National Academy of Sciences of the United States of America*, *115*(41), 10458–10463. https://doi.org/10.1073/pnas.1810823115

Horike, N., Takemori, H., Katoh, Y., Doi, J., Min, L., Asano, T., Sun, X. J., Yamamoto, H., Kasayama, S., Muraoka, M., Nonaka, Y., & Okamoto, M. (2003). Adipose-specific expression, phosphorylation of Ser794 in insulin receptor substrate-1, and activation in diabetic animals of salt-inducible kinase-2. *Journal of Biological Chemistry*, *278*(20), 18440–18447. https://doi.org/10.1074/jbc.M211770200

Hughes, A. T. L., Guilding, C., & Piggins, H. D. (2011). Neuropeptide Signaling Differentially Affects Phase Maintenance and Rhythm Generation in SCN and Extra-SCN Circadian Oscillators. *PLoS ONE*, *6*(4), e18926. https://doi.org/10.1371/journal.pone.0018926

Ishikawa, H., Yamada, K., Pavlides, C., & Ichitani, Y. (2014). Sleep deprivation impairs spontaneous object-place but not novel-object recognition in rats. *Neuroscience Letters*, *580*, 114–118. https://doi.org/10.1016/j.neulet.2014.08.004

Jagannath, A., Butler, R., Godinho, S. I. H., Couch, Y., Brown, L. A., Vasudevan, S. R., Flanagan, K. C., Anthony, D., Churchill, G. C., Wood, M. J. A., Steiner, G., Ebeling, M., Hossbach, M., Wettstein, J. G., Duffield, G. E., Gatti, S., Hankins, M. W., Foster, R. G., & Peirson, S. N. (2013). The CRTC1-SIK1 pathway regulates entrainment of the circadian clock. *Cell*, *154*(5). https://doi.org/10.1016/j.cell.2013.08.004

Jiang, B., Wang, H., Wang, J. L., Wang, Y. J., Zhu, Q., Wang, C. N., Song, L., Gao, T. T., Wang, Y., Meng, G. L., Wu, F., Ling, Y., Zhang, W., & Li, J. X. (2019). Hippocampal Salt-Inducible Kinase 2 Plays a Role in Depression via the CREB-Regulated Transcription Coactivator 1–cAMP Response Element Binding–Brain-Derived Neurotrophic Factor Pathway. *Biological Psychiatry*, *85*(8), 650–666. https://doi.org/10.1016/j.biopsych.2018.10.004

Johnson, J. L., Yaron, T. M., Huntsman, E. M., Kerelsky, A., Song, J., Regev, A., Lin, T. Y., Liberatore, K., Cizin, D. M., Cohen, B. M., Vasan, N., Ma, Y., Krismer, K., Robles, J. T., van de Kooij, B., van Vlimmeren, A. E., Andrée-Busch, N., Käufer, N. F., Dorovkov, M. V., … Cantley, L. C. (2023). An atlas of substrate specificities for the human serine/threonine kinome. *Nature*, *613*(7945), 759–766. https://doi.org/10.1038/s41586-022-05575-3

Katoh, Y., Takemori, H., Horike, N., Doi, J., Muraoka, M., Min, L., & Okamoto, M. (2004). Salt-inducible kinase (SIK) isoforms: Their involvement in steroidogenesis and adipogenesis. *Molecular and Cellular Endocrinology*, *217*(1–2), 109–112. https://doi.org/10.1016/j.mce.2003.10.016

Kessels, H. W., & Malinow, R. (2009). Synaptic AMPA Receptor Plasticity and Behavior. In *Neuron* (Vol. 61, Number 3, pp. 340–350). https://doi.org/10.1016/j.neuron.2009.01.015

Krafty, R. T., Fu, H., Graves, J. L., Bruce, S. A., Hall, M. H., & Smagula, S. F. (n.d.). *Measuring Variability in Rest-Activity Rhythms from Actigraphy with Application to Characterizing Symptoms of Depression*.

Leana-Sandoval, G., Madrid, A., Kolli, A. V., Chinn, C. A., Sandoval, M. A., Lo, I., Alizo Vera, V., Simms, J., Wood, M. A., & Díaz-Alonso, J. (2025). The GluA1 cytoplasmic tail regulates intracellular AMPA receptor trafficking and synaptic transmission onto dentate gyrus GABAergic interneurons, gating response to novelty. *Molecular Psychiatry*. https://doi.org/10.1038/s41380-025-03328-y

Lee, G. S., Zhang, J., Wu, Y., & Zhou, Y. (2021). 14-3-3 proteins promote synaptic localization of N-methyl d-aspartate receptors (NMDARs) in mouse hippocampal and cortical neurons. *PLOS ONE*, *16*(12), e0261791. https://doi.org/10.1371/journal.pone.0261791

Legates, T. A., Fernandez, D. C., & Hattar, S. (2014). Light as a central modulator of circadian rhythms, sleep and affect. In *Nature Reviews Neuroscience* (Vol. 15, Number 7, pp. 443–454). Nature Publishing Group. https://doi.org/10.1038/nrn3743

Lim, C.-S., Kang, X., Mirabella, V., Zhang, H., Bu, Q., Araki, Y., Hoang, E. T., Wang, S., Shen, Y., Choi, S., Kaang, B.-K., Chang, Q., Pang, Z. P., Huganir, R. L., & Zhu, J. J. (2017). *BRaf signaling principles unveiled by large-scale human mutation analysis with a rapid lentivirus-based gene replacement method*. https://doi.org/10.1101/gad.294413

Ling, H. H., Beaulé, C., Chiang, C. K., Tian, R., Figeys, D., & Cheng, H. Y. M. (2014). Time-of-day- and light-dependent expression of ubiquitin protein ligase E3 component N-recognin 4 (UBR4) in the suprachiasmatic nucleus circadian clock. *PLoS ONE*, *9*(8). https://doi.org/10.1371/journal.pone.0103103

Liu, Y., Poon, V., Sanchez-Watts, G., Watts, A. G., Takemori, H., & Aguilera, G. (2012). Salt-Inducible Kinase Is Involved in the Regulation of Corticotropin-Releasing Hormone Transcription in Hypothalamic Neurons in Rats. *Endocrinology*, *153*(1), 223–233. https://doi.org/10.1210/en.2011-1404

Liu, Y., Tang, W., Ji, C., Gu, J., Chen, Y., Huang, J., Zhao, X., Sun, Y., Wang, C., Guan, W., Liu, J., & Jiang, B. (2021). The Selective SIK2 Inhibitor ARN-3236 Produces Strong Antidepressant-Like Efficacy in Mice via the Hippocampal CRTC1-CREB-BDNF Pathway. *Frontiers in Pharmacology*, *11*. https://doi.org/10.3389/fphar.2020.624429

Lueptow, L. M. (2017). Novel object recognition test for the investigation of learning and memory in mice. *Journal of Visualized Experiments*, *2017*(126). https://doi.org/10.3791/55718

Maxfield, K. E., Macion, J., Vankayalapati, H., & Whitehurst, A. W. (2016). SIK2 Restricts Autophagic Flux To Support Triple-Negative Breast Cancer Survival. *Molecular and Cellular Biology*, *36*(24), 3048–3057. https://doi.org/10.1128/MCB.00380-16

Mieda, M., Ono, D., Hasegawa, E., Okamoto, H., Honma, K. ichi, Honma, S., & Sakurai, T. (2015). Cellular clocks in AVP neurons of the scn are critical for interneuronal coupling regulating circadian behavior rhythm. *Neuron*, *85*(5), 1103–1116. https://doi.org/10.1016/j.neuron.2015.02.005

Miranda, F., Mannion, D., Liu, S., Zheng, Y., Mangala, L. S., Redondo, C., Herrero-Gonzalez, S., Xu, R., Taylor, C., Chedom, D. F., Karaminejadranjbar, M., Albukhari, A., Jiang, D., Pradeep, S., Rodriguez-Aguayo, C., Lopez-Berestein, G., Salah, E., Abdul Azeez, K. R.,

Elkins, J. M., … Ahmed, A. A. (2016). Salt-Inducible Kinase 2 Couples Ovarian Cancer Cell Metabolism with Survival at the Adipocyte-Rich Metastatic Niche. *Cancer Cell*, *30*(2), 273–289. https://doi.org/10.1016/j.ccell.2016.06.020

Narain, P., Petković, A., Šušić, M., Haniffa, S., Anwar, M., Arnoux, M., Drou, N., Antonio-Saldi, G., & Chaudhury, D. (2024). Nighttime-specific differential gene expression in suprachiasmatic nucleus and habenula is associated with resilience to chronic social stress. *Translational Psychiatry*, *14*(1). https://doi.org/10.1038/s41398-024-03100-w

Noguchi, D., Watamura, N., Nikkuni, M., Saido, T. C., Goshima, Y., & Ohshima, T. (2025). Involvement of CRMP2 Phosphorylation in Amyloid Beta-induced Tau Phosphorylation of Hippocampal Neurons in Alzheimer's Disease Mouse Model. *Molecular Neurobiology*, *62*(6), 7413–7420. https://doi.org/10.1007/s12035-025-04721-y

Okamoto, M., Takemori, H., & Katoh, Y. (2004). Salt-inducible kinase in steroidogenesis and adipogenesis. In *Trends in Endocrinology and Metabolism* (Vol. 15, Number 1, pp. 21–26). Elsevier Inc. https://doi.org/10.1016/j.tem.2003.11.002

Ono, D., Honma, K. ichi, Yanagawa, Y., Yamanaka, A., & Honma, S. (2019). GABA in the suprachiasmatic nucleus refines circadian output rhythms in mice. *Communications Biology*, *2*(1). https://doi.org/10.1038/s42003-019-0483-6

Ota, W., Nakane, Y., Hattar, S., & Yoshimura, T. (2018). Impaired Circadian Photoentrainment in Opn5-Null Mice. *IScience*, *6*, 299–305. https://doi.org/10.1016/j.isci.2018.08.010

Pan, Y., Chen, J., Guo, H., Ou, J., Peng, Y., Liu, Q., Shen, Y., Shi, L., Liu, Y., Xiong, Z., Zhu, T., Luo, S., Hu, Z., Zhao, J., & Xia, K. (2015). Association of genetic variants of GRIN2B with autism. *Scientific Reports*, *5*. https://doi.org/10.1038/srep08296

Park, M., Miyoshi, C., Fujiyama, T., Kakizaki, M., Ikkyu, A., Honda, T., Choi, J., Asano, F., Mizuno, S., Takahashi, S., Yanagisawa, M., & Funato, H. (2020). Loss of the conserved PKA sites of SIK1 and SIK2 increases sleep need. *Scientific Reports*, *10*(1). https://doi.org/10.1038/s41598-020-65647-0

Pham, X., Song, G., Lao, S., Goff, L., Zhu, H., Valle, D., & Avramopoulos, D. (2016). The DPYSL2 gene connects mTOR and schizophrenia. *Translational Psychiatry*, *6*(11). https://doi.org/10.1038/tp.2016.204

Posada-Duque, R. A., Ramirez, O., Härtel, S., Inestrosa, N. C., Bodaleo, F., González-Billault, C., Kirkwood, A., & Cardona-Gómez, G. P. (2017). CDK5 downregulation enhances synaptic plasticity. *Cellular and Molecular Life Sciences*, *74*(1), 153–172. https://doi.org/10.1007/s00018-016-2333-8

Qi, L., Saberi, M., Zmuda, E., Wang, Y., Altarejos, J., Zhang, X., Dentin, R., Hedrick, S., Bandyopadhyay, G., Hai, T., Olefsky, J., & Montminy, M. (2009). Adipocyte CREB Promotes Insulin Resistance in Obesity. *Cell Metabolism*, *9*(3), 277–286. https://doi.org/10.1016/j.cmet.2009.01.006

Rietveld, W. J., Minors, D. S., & Waterhouse, J. M. (1993). Circadian Rhythms and Masking: An Overview. *Chronobiology International*, *10*(4), 306–312. https://doi.org/10.1080/07420529309059713

Rossato, J. I., Bevilaqua, L. R. M., Izquierdo, I., Medina, J. H., & Cammarota, M. (2009). Dopamine Controls Persistence of Long-Term Memory Storage. *Science*, *325*(5943), 1017–1020. https://doi.org/10.1126/science.1172545

Sakamaki, J. I., Fu, A., Reeks, C., Baird, S., Depatie, C., Al Azzabi, M., Bardeesy, N., Gingras, A. C., Yee, S. P., & Screaton, R. A. (2014). Role of the SIK2-p35-PJA2

complex in pancreatic β-cell functional compensation. *Nature Cell Biology*, *16*(3), 234–244. https://doi.org/10.1038/ncb2919
Säll, J., Negoita, F., Hansson, B., Kopietz, F., Linder, W., Pettersson, A. M. L., Ekelund, M., Laurencikiene, J., Degerman, E., Stenkula, K. G., & Göransson, O. (2019). Insulin induces Thr484 phosphorylation and stabilization of SIK2 in adipocytes. *Cellular Signalling*, *55*, 73–80. https://doi.org/10.1016/j.cellsig.2018.12.011
Sasaki, T., Takemori, H., Yagita, Y., Terasaki, Y., Uebi, T., Horike, N., Takagi, H., Susumu, T., Teraoka, H., Kusano, K. ichi, Hatano, O., Oyama, N., Sugiyama, Y., Sakoda, S., & Kitagawa, K. (2011). SIK2 Is a Key Regulator for Neuronal Survival after Ischemia via TORC1-CREB. *Neuron*, *69*(1), 106–119. https://doi.org/10.1016/j.neuron.2010.12.004
Scala, M., Amadori, E., Fusco, L., Marchese, F., Capra, V., Minetti, C., Vari, M. S., & Striano, P. (2019). Abnormal circadian rhythm in patients with GRIN1-related developmental epileptic encephalopathy. *European Journal of Paediatric Neurology*, *23*(4), 657–661. https://doi.org/10.1016/j.ejpn.2019.05.011
Shi, X., Yu, X., Wang, J., Bian, S., Li, Q., Fu, F., Zou, X., Zhang, L., Bast, R. C., Lu, Z., Guo, L., Chen, Y., & Zhou, J. (2022). SIK2 promotes ovarian cancer cell motility and metastasis by phosphorylating MYLK. *Molecular Oncology*, *16*(13), 2558–2574. https://doi.org/10.1002/1878-0261.13208
Singh, T., Poterba, T., Curtis, D., Akil, H., Al Eissa, M., Barchas, J. D., Bass, N., Bigdeli, T. B., Breen, G., Bromet, E. J., Buckley, P. F., Bunney, W. E., Bybjerg-Grauholm, J., Byerley, W. F., Chapman, S. B., Chen, W. J., Churchhouse, C., Craddock, N., Cusick, C. M., … Daly, M. J. (2022). Rare coding variants in ten genes confer substantial risk for schizophrenia. *Nature*, *604*(7906), 509–516. https://doi.org/10.1038/s41586-022-04556-w
Sonntag, T., Vaughan, J. M., & Montminy, M. (2018). 14-3-3 proteins mediate inhibitory effects of cAMP on salt-inducible kinases (SIKs). In *FEBS Journal* (Vol. 285, Number 3, pp. 467–480). Blackwell Publishing Ltd. https://doi.org/10.1111/febs.14351
Tsetsenis, T., Badyna, J. K., Wilson, J. A., Zhang, X., Krizman, E. N., Subramaniyan, M., Yang, K., Thomas, S. A., & Dani, J. A. (2021). Midbrain dopaminergic innervation of the hippocampus is sufficient to modulate formation of aversive memories. *Proceedings of the National Academy of Sciences*, *118*(40). https://doi.org/10.1073/pnas.2111069118
Tone, D., Ode, K. L., Zhang, Q., Fujishima, H., Yamada, R. G., Nagashima, Y., Matsumoto, K., Wen, Z., Yoshida, S. Y., Mitani, T. T., Arisato, Y., Ohno, R. I., Ukai-Tadenuma, M., Garçon, J. Y., Kaneko, M., Shi, S., Ukai, H., Miyamichi, K., Okada, T., … Ueda, H. R. (2022). Distinct phosphorylation states of mammalian CaMKIIβ control the induction and maintenance of sleep. *PLoS Biology*, *20*(10). https://doi.org/10.1371/journal.pbio.3001813
Tononi, G., & Cirelli, C. (2006). Sleep function and synaptic homeostasis. In *Sleep Medicine Reviews* (Vol. 10, Number 1, pp. 49–62). https://doi.org/10.1016/j.smrv.2005.05.002
Trubetskoy, V., Pardiñas, A. F., Qi, T., Panagiotaropoulou, G., Awasthi, S., Bigdeli, T. B., Bryois, J., Chen, C.-Y., Dennison, C. A., Hall, L. S., Lam, M., Watanabe, K., Frei, O., Ge, T., Harwood, J. C., Koopmans, F., Magnusson, S., Richards, A. L., Sidorenko, J., … van Os, J. (2022). Mapping genomic loci implicates genes and synaptic biology in schizophrenia. *Nature*, *604*(7906), 502–508. https://doi.org/10.1038/s41586-022-04434-5

Vandael, D., Vints, K., Baatsen, P., Śliwińska, M. A., Gabarre, S., De Groef, L., Moons, L., Rybakin, V., & Gounko, N. V. (2024). Cdk5-dependent rapid formation and stabilization of dendritic spines by corticotropin-releasing factor. *Translational Psychiatry*, *14*(1). https://doi.org/10.1038/s41398-024-02749-7

Viney, T. J., Sarkany, B., Ozdemir, A. T., Hartwich, K., Schweimer, J., Bannerman, D., & Somogyi, P. (2022). Spread of pathological human Tau from neurons to oligodendrocytes and loss of high-firing pyramidal neurons in aging mice. *Cell Reports*, *41*(7), 111646. https://doi.org/10.1016/j.celrep.2022.111646

Vyazovskiy, V. V., Cirelli, C., Pfister-Genskow, M., Faraguna, U., & Tononi, G. (2008). Molecular and electrophysiological evidence for net synaptic potentiation in wake and depression in sleep. *Nature Neuroscience*, *11*(2), 200–208. https://doi.org/10.1038/nn2035

Wang, Y., Minami, Y., Ode, K. L., & Ueda, H. R. (2022). The role of calcium and CaMKII in sleep. *Frontiers in Systems Neuroscience*, *16*. https://doi.org/10.3389/fnsys.2022.1059421

Weems, J. C., Griesel, B. A., & Olson, A. L. (2012). Class II Histone Deacetylases Downregulate *GLUT4* Transcription in Response to Increased cAMP Signaling in Cultured Adipocytes and Fasting Mice. *Diabetes*, *61*(6), 1404–1414. https://doi.org/10.2337/db11-0737

Yamaguchi, Y., Maekawa, Y., Kabashima, K., Mizuno, T., Tainaka, M., Suzuki, T., Dojo, K., Tominaga, T., Kuroiwa, S., Masubuchi, S., Doi, M., Tominaga, K., Kobayashi, K., Yamagata, S., Itoi, K., Abe, M., Schwartz, W. J., Sakimura, K., & Okamura, H. (2023). An intact pituitary vasopressin system is critical for building a robust circadian clock in the suprachiasmatic nucleus. *Proceedings of the National Academy of Sciences of the United States of America*, *120*(43). https://doi.org/10.1073/pnas.2308489120

Yamaguchi, Y., Suzuki, T., Mizoro, Y., Kori, H., Okada, K., Chen, Y., Fustin, J.-M., Yamazaki, F., Mizuguchi, N., Zhang, J., Dong, X., Tsujimoto, G., Okuno, Y., Doi, M., & Okamura, H. (n.d.). *Mice Genetically Deficient in Vasopressin V1a and V1b Receptors Are Resistant to Jet Lag*. Retrieved https://www.science.org

Yang, F. C., Tan, B. C. M., Chen, W. H., Lin, Y. H., Huang, J. Y., Chang, H. Y., Sun, H. Y., Hsu, P. H., Liou, G. G., Shen, J., Chang, C. J., Han, C. C., Tsai, M. D., & Lee, S. C. (2013). Reversible acetylation regulates salt-inducible kinase (SIK2) and its function in autophagy. *Journal of Biological Chemistry*, *288*(9), 6227–6237. https://doi.org/10.1074/jbc.M112.431239

Yang, W., Shi, J., Li, C., Yang, J., Yu, J., Huang, J., & Rao, Y. (2025). Calcium/calmodulin-dependent protein kinase II α and β differentially regulate mammalian sleep. *Communications Biology*, *8*(1). https://doi.org/10.1038/s42003-024-07449-y

Yao, Z., van Velthoven, C. T. J., Kunst, M., Zhang, M., McMillen, D., Lee, C., Jung, W., Goldy, J., Abdelhak, A., Aitken, M., Baker, K., Baker, P., Barkan, E., Bertagnolli, D., Bhandiwad, A., Bielstein, C., Bishwakarma, P., Campos, J., Carey, D., … Zeng, H. (2023). A high-resolution transcriptomic and spatial atlas of cell types in the whole mouse brain. *Nature*, *624*(7991), 317–332. https://doi.org/10.1038/s41586-023-06812-z

Zhao, J., Zhang, X., Gao, T., Wang, S., Hou, Y., Yuan, P., Yang, Y., Yang, T., Xing, J., Li, J., & Liu, S. (2020). SIK2 enhances synthesis of fatty acid and cholesterol in ovarian cancer cells and tumor growth through PI3K/Akt signaling pathway. *Cell Death and Disease*, *11*(1). https://doi.org/10.1038/s41419-019-2221-x

Zohrap, N., Saatci, Ö., Ozes, B., Coban, I., Atay, H. M., Battaloglu, E., Şahin, Ö., & Bugra, K. (2018). *SIK2 attenuates proliferation and survival of breast cancer cells with simultaneous perturbation of MAPK and PI3K/Akt pathways*. Retrieved www.oncotarget.com

Chapter 6:

General Discussion

Increasing efforts were directed toward understanding the molecular components of sleep and circadian rhythms, and kinases and phosphorylation were highlighted as key players. SIKs, implicated in multiple physiological processes, were proposed as regulators of sleep and circadian rhythms. This thesis builds on existing literature and explores the roles of SIKs in sleep and circadian regulation using behavioural and multi-omics approaches. Using the SIK KI animal model, we conducted comprehensive circadian and sleep characterizations by analyzing wheel running and EEG/EMG recordings, respectively. We subsequently conducted SCN- and cortex-specific transcriptomics and phosphoproteomics to explore SIK-dependent differential gene expression and phosphorylation changes. We supported the datasets by optimizing tissue-specific Pro-KALIP and effectively identified the direct substrates and phosphorylation sites of SIKs. We consolidated isoform-specific expression, roles in circadian and sleep regulation, the Two Process Model and implications to whole-body physiology.

6.1 SIKs gene expression and functions

By consulting the Allen Brain Cell (ABC) Atlas scRNAseq, we examined SIK gene expression across brain regions and cell types. The dataset indicates that SIK3 has the most abundant expression across the whole mouse brain, followed by SIK2, while SIK1 shows the lowest expression. Early studies have primarily focused on SIKs' roles in whole body physiology, specifically in lipid and energy metabolism. Northern blot experiments showed that *Sik1* and *Sik2* mRNA are enriched in the adrenal cortex and adipose tissues, respectively, whereas *Sik3* mRNA is ubiquitous across murine tissues

(Katoh et al., 2004a). This suggests that *Sik1* and *Sik2* expression are more specific, and *Sik3* is everywhere in the body, regulating a wide variety of pathways, which corresponds to and translates into the high expression in the brain.

As we aimed to explore the role of SIKs in circadian and sleep regulation, we shifted to individual slices containing the SCN, the master pacemaker of the circadian clock. We observed salient expression of all three SIKs in the SCN region. Interestingly, *Sik1* is expressed exclusively in the SCN, which corresponds to previous studies regarding SIK1's light-dependent regulation of entrainment (Jagannath et al., 2013). In addition, SIKs' expression in the SCN is predominantly in GABAergic neurons. Moore et al. have established GABA as a primary circadian neurotransmitter, since most of the neurons are GABA-producing in the SCN, and it co-localizes with neuropeptides AVP and VIP (Moore & Speh, 1993). Ono et al followed-up the findings by using mice lacking the GABA receptor VGAT in fetal SCN and found that GABA refines SCN firing rhythms, impacting output signals (Ono et al., 2021b, 2021c). It was also shown that GABA neurotransmission plays a role in photic entrainment (Ralph & Menaker, 1989). Our findings showed that SIKs, along with other key neurotransmitters, co-localize in GABA-producing neurons in the SCN, accentuating that they may be regulators of circadian functions and SCN synchrony.

In addition, we found that *Sik2* and *Sik3* are expressed in the cortical layers, mainly in glutamatergic neurons. There is abundant evidence that cortical circuitry is involved in sleep and vigilant control. Krone et al showed that the inhibition of neocortical layer 5 pyramidal cells significantly increased wakefulness and reduced rebound sleep,

implying that cortical layers regulate sleep vigilance and homeostasis (Krone et al., 2021). There is also literature demonstrating the role of cortical glutamatergic neurons in sleep-wake regulation. The cortex is an interconnected system that interacts with the basal forebrain, brainstem and hypothalamus. It utilizes the prefrontal cortex as a central node, projecting both top-down through innervation and receiving bottom-up signals to regulate cortical arousal. Glutamatergic neurons are key to this transmission (Henny & Jones, 2008; Luo et al., 2025). As regions and layers of the cortex play distinct roles, the localization of *Sik2* and *Sik3* need further investigation. *Sik2* and *Sik3* expression were also present in the hippocampus and dentate gyrus regions. There is evidence showing that models of depression increase hippocampal *Sik2* levels, and the SIK2-CRTC1 pathway in the hippocampus was implicated in antidepressant effects (Jiang et al., 2019a). Yet, the molecular components are understudied. Our findings imply that SIK2 and SIK3 may play roles in hippocampal-related pathways and functions.

Moreover, SIK expression spans across non-neuronal cell types. scRNAseq study on SIK1 KI and WT animals showed that there are large transcriptional changes in astrocytes, regulating SCN rhythms (Appendix 1). We also detected expression of *Sik2* and *Sik3* in non-neuronal cells, including astrocytes and oligodendrocytes.

Together, from consulting the scRNAseq data, we explored isoform-specific gene expression of SIKs. Overall, Sik1 is exclusively in the SCN, which shows that it may be a regulator of Process C. While SIK2 and SIK3 are in both the SCN and cortex, placing

them as potential regulators of both sleep and circadian function. These findings set the premise for our circadian and sleep characterization of SIK KI animals.

6.2 SIKs and Circadian Activity

We conducted circadian characterizations on SIK KI animals to compare phenotype differences between isoforms. SIK KI cohorts, along with matching WT controls, were subjected to various LD cycle alterations and photic stimulations.

Under baseline conditions, SIK1 KI animals behaved similarly to WT, showing that the loss of SIK1 kinase activity does not disrupt core circadian parameters. Circadian amplitude and stability were significantly dampened under the loss of SIK2 and SIK3, supporting that the endogenous circadian clocks are weaker. We proposed that SIK2 and SIK3 are involved in regulating the robustness and strength of the circadian clock. In addition, the circadian period in the free-running period is longer under the loss of SIK3, implying that SIK3 also plays a role in facilitating periodicity.

SIK1 has a very distinct photic entrainment phenotype, which aligns with previous literature (Jagannath et al., 2013), regulating CRTC1/CREB-mediated transcription of clock genes in response to glutamate and PACAP. Under the loss of SIK1, there is rapid entrainment to 6hr light advance (Appendix 1). This phenotype is mediated in a light-dependent manner, supported by larger phase shifts in response to acute light pulses (Appendix 1). On the other hand, SIK3 is not involved in the response to acute photic stimulation, as the loss of SIK3 had similar phase shifts to WT controls.

However, animals showed a significantly delayed entrainment phenotype, implying a role in photoentrainment and synchronicity between oscillators in the body. These findings indicate that SIK1 and SIK3 are involved in regulating the plasticity of the circadian clock in response to photic cues, but with opposing effects. SIK1 acts as a buffering mechanism in response to acute nocturnal light with control of initial wake signals and entrainment (Appendix 1; (Wakaf et al., 2026)). While SIK3 mediates coupling between the clock and external LD cycles. Under the loss of SIK2, photoentrainment and light-regulated pathways are intact, as SIK1 and SIK3 were present in the model. Rapid masking to the ultradian cycle was observed, but it was likely due to the weakened core clock, leading to instability.

These results show that SIKs regulate aspects of the circadian clock in specific ways, contributing to distinct pathways. These findings show that the isoforms' roles are non-redundant in circadian regulation, and the presence of the other two isoforms cannot fully compensate for the loss. This shows that they work in coordination and in distinct pathways to maintain an intact circadian clock.

6.3 SIKs and Sleep Activity

As SIK1 expression was not characterized in the cortical layers, we hypothesized that SIK1 is mainly involved in Process C-mediated activity. Notably, our recent study showed that the loss of SIK1 kinase activity does not disrupt sleep under baseline conditions. Following the 6hr light advance, where SIK1 KI animals exhibited a prominent circadian phenotype and early initiation of wakefulness, recordings indicate

no change in sleep induction or sleep homeostasis. These findings validate that the phenotype is circadian-initiated with alterations to Process S, supporting that SIK1 is predominantly a regulator of Process C (Appendix 1).

Preliminary sleep characterizations of SIK2 and SIK3 in this thesis proposed them as potential key molecular candidates for sleep pressure. Both SIK2 KI and SIK3 KI animals had trends in reduced NREM sleep delta power and energy, suggesting lower SWS and sleep pressure. This aligns with the previously characterized GoF *Slp* mutant with higher NREM sleep delta power and sleep need (Funato et al., 2016). Following 6hr sleep deprivation, SIK2 KI animals also had a lack of sleep and SWA buildup. These findings suggest that SIK2 regulates sleep homeostatic responses. Further investigations are required to fully examine the sleep phenotypes of SIK2 and SIK3 and how they converge.

6.4 Pro-KALIP method to identify direct molecular substrates

A common challenge of quantitative phosphoproteomics is separating the downstream effects of targets, intertwining relationships and direct targets. This is particularly crucial for studying SIKs, one of the 13 AMPK kinases, as they impact multiple levels of physiology and are involved in interconnected regulatory pathways (Jagannath et al., 2023).

We optimized the Pro-KALIP method that was first proposed by Xue et al and adapted it to our SCN- and cortex-specific model in Chapter 3 (Xue et al., 2016.). This provides a

way to delineate direct pathways from developmental compensations and downstream signaling.

In particular, we incorporated the LKB1:STRADα:MO25α trimer into the rephosphorylation reaction, upstream regulator of the SIK family, to increase kinase activity. The steps were validated via immunoblot and *in vitro* Kinase Luminescence assays. The trimer was introduced as an essential upstream activator of SIKs and could increase SIK activity by 20- to 50-fold in *E.coli*-purified kinases (Lizcano et al., 2004). However, it is an activator for all AMPK kinases and will activate multiple pathways. Therefore, we prepared separate samples and runs that were LKB1 trimer only in the SCN and cortex as background signals to eliminate further false positives. This helps us eliminate LKB1-specific substrates. We validated the authenticity of the assay by detecting SIK motifs in the dataset, proving that they were SIK-specific sites.

Despite the strengths of Pro-KALIP, false positives could arise in the dataset. In Chapters 3 and 5, our findings from pAMPK substrate motif immunoblot have shown that complete dephosphorylation was not achieved. When conducting a motif analysis, though SIKs were solely enriched, false positives were detected due to residual endogenous kinase activity and incomplete dephosphorylation. Therefore, we have only included substrates that are SIK-specific as direct substrates in subsequent analysis, as consulted from Phosphosite Plus (Johnson et al., 2023). We have also overlapped the dataset with *in vivo* phosphoproteomes to obtain *bona fide* direct substrates. In addition, as Pro-KALIP is an *in vitro* phosphoproteomics by adding an exogenous purified kinase, the substrates detected were those that were only phosphorylated in the presence of a

kinase. Therefore, it only provides insight into directly activating phosphosites rather than inhibitory ones. Additional assays, such as site-directed mutagenesis, are recommended to validate specific sites on kinase function and direct interactions.

6.5 SIKs in the SCN

Given the strong presence of SIKs in the SCN and prominent circadian phenotypes, we conducted SCN-specific transcriptomics, phosphoproteomics and Pro-KALIP.

Research by our group supported that SIK1 KI animals do not have behavioural changes and differential gene expression under baseline conditions. However, it is only induced under nocturnal light or a shifted LD cycle (Jagannath et al., 2013; Wakaf et al., 2026). It is established that SIK1 is involved in the phosphorylation of CRTC1 and the negative transcriptional feedback loop of clock genes. Surprisingly, the early initiation of wakefulness following the 6hr light advance was not accompanied by changes in core clock genes such as *Per1* and *Cry1*, only changes in activity markers (Appendix 1). We then identified the direct substrates of SIK1 by SCN-specific quantitative phosphoproteomics and Pro-KALIP to examine post-transcriptional changes.
We found hubs of synaptic proteins and phosphosites involved in calcium regulation (Appendix 1). It is shown that SIK1 regulates presynaptic synaptic transmission and Ca^{2+} signaling to maintain SCN synchrony through phosphorylation, which is reflected in behavioural circadian outputs.

Similarly, core clock genes such as *Per1* and *Cry1* were not significantly altered in SIK2 KI animals. In turn, we observed differential gene expression in circadian rhythms- and glutamate secretion- related genes such as *Ngfr*, *Opn5* and *Sik1* that are tightly associated with photoentrainment. In addition, *Avp* and *Vip,* primary neuropeptides that synchronize 24h rhythmic cycles in the SCN, were significantly altered.
Previously, Bruning et al. have established that synaptic
protein phosphorylation shows cycling patterns corresponding to the sleep-wake cycle (Brüning et al., 2019b). Therefore, we conducted SCN-specific phosphoproteomics and Pro-KALIP to identify the direct substrates of SIK2 in two different timepoints (EOS and EOW). Similarly, we found molecular substrates enriched for synaptic signaling and transport. We found that a lot of them are related to synaptic trafficking, which is related to *Avp* neurotransmitter release and activity. Interestingly, *Avp* appeared to be significantly upregulated post-shift in the SIK1 KI animals. While it was likely due to an activity-led change in neurotransmitter output (Appendix 1), SIK2 exhibited a non-redundant function in regulating AVP and VIP neuropeptide signaling.

Together, previous circadian characterizations suggested that SIK1 and SIK2 play regulatory roles in circadian function and SCN synchrony. SIK1 is involved in photoentrainment, while SIK2 modulates the robustness of the core clock. Given the established SIK-CRTC axis, it is commonly hypothesized that regulation would be transcriptional and through changes in the TTFL. However, our datasets revealed no changes in core clock genes, accentuating the significance of post-transcriptional regulation, notably phosphorylation. We showed that both SIK1 and SIK2 regulate synaptic signaling in the SCN. SIK1 regulates presynaptic Ca2+ signaling through

validated targets such as PKCy, while SIK2 regulates proteins involved in vesicle trafficking and neurotransmitter release that impact neuropeptide signaling.

We then overlapped the SIK1 and SIK2 datasets to examine the common transcriptional and molecular substrates. We identified ANK2 (regulates dendritic excitability, synaptic stability and also implied in autism) (Yang et al., 2019; Yoon & Penzes, 2025); DMXL2 (presynaptic endocytosis and recycling) (Peng et al., 2024); SRRM2 (implicated in nuclear speckle formation and neurodevelopmental disorders (Chang et al., 2025; Xu et al., 2022); WDR7 (vesicle transport and synaptic transmission); DPYSL2 (modifying membrane localization of ion channels and controlling currents to regulate synaptic function) (Pham et al., 2016) (Supp. Table 6.1).

These overlapping phosphoproteins showed a strong enrichment in synaptic signaling and neurotransmission in the SCN, regulated by SIK1 and SIK2. Notably, only two direct phosphosites – SRRM2 S1810 and DPYSL2 S540 – were common between SIK1 and SIK2, and both were detected in the sleep phases. Though the functional relevance of these sites in the sleep-wake cycle requires further validation, these findings suggest that SIK isoforms may regulate a shared phosphorylation network of synaptic proteins in a time-of-day-dependent manner.

6.6 SIKs in the cortex

We then performed cortex-specific transcriptomics, phosphoproteomics and Pro-KALIP for SIKs to contextualize sleep phenotypes.

We first observed a unified CAMK signature across the molecular substrates of SIKs in the cortex. After 6hr light advance, where we observed the early initiation of wakefulness, SIK1 KI phosphoproteomics revealed significant changes in CAMKII pre- and post-synaptic targets such as SYNGAP1, SYN1 and RIMS2. These changes reveal elevated cortical excitation in the SIK1 KI animals, which are shown to be responses to wakefulness signals from the circadian drive in the SCN rather than sleep homeostatic alterations (Appendix 1). In SIK3, we detected a CAMKIIA signature in the molecular substrates such as SYN1 and RYR2. Similarly, key sites of CAMKIIB and CAMKIIA were hyperphosphorylated under the loss of SIK2 activity. Previous studies have established CAMKII kinases as sleep-promoting kinases and key molecular markers for sleep pressure (Wang et al., 2022). Preliminary sleep phenotyping suggested that the loss of SIK2 and SIK3 is accompanied by reduced sleep pressure and altered homeostasis, implying the role of CAMKII signalling.

As SIK1 does not have a strong presence in the cortex and is predominantly characterized as a regulator of Process C, we overlapped SIK2 and SIK3 molecular substrates in the cortex and identified 33 phosphoproteins that are involved in both regulatory pathways. Of these, we identified ABI1 and SYNPO that were previously characterized as SNIPPs (Wang et al., 2018). Given that SIK2 KI and SIK3 KI animals showed altered sleep homeostasis along with the *Slp* mutant, this further confirms that

these phosphoproteins are associated with sleep homeostatic regulation. Notably, Wang et al applied adeno-associated virus (AAV)-based adult brain chimeric (ABC) expression/knockout (KO) screening of ABI1 and SYNPO and found no prominent sleep phenotypes (Wang et al., 2021). As sites were differentially detected on these SNIPPs in SIK2 and SIK3, individual phosphosites could exhibit different phenotypes and regulatory pathways. For instance, a single site on HDAC S245 was shown to be responsible for sleep need (Asano et al., 2023), which accentuates the significance of site-directed validation assays.

Overlapping SIK2 and SIK3, we detected a hub of synaptic proteins in the cortex, proposed to be involved in sleep regulation (Supp. Table 6.1). There is a growing body of evidence that sleep need is associated with synaptic function (Cirelli & Tononi, 2019; Tononi & Cirelli, 2006). For instance, AAAK1 is a key regulator for synaptic transmission (Taoufiq et al., 2020), which is also implicated in synucleinopathy in Parkinson's disease (PD) (Vargas et al., 2020). The Abelson helper integration site 1 (AHI1) is also implicated in neurodevelopment and cognitive function, which are diseases associated with early brain development (Yang et al., 2022). In particular, we detected SYN1 (synapsin-1), which is essential for synaptic vesicle sequestering (Hoffmann et al., 2023), and the key sites S568 and S605 were detected as direct phosphorylation sites of SIK3 in the cortex. In existing literature, they are sites that are phosphorylated by CAMKII. During neuronal stimulation, Ca^{2+} signals lead to the phosphorylation of S568 and S605 by CAMKII, which reduces the binding of SYN1 to synaptic vesicles, prohibiting condensation. SYN1 condensation is shown to be key for actin polymerization. This suggests that phosphorylation of SYN1 is key for neurotransmitter

release (Chhabra et al., 2025). As neurotransmitters such as glutamate and GABA in the synapse are central for the sleep-wake cycle, maintenance of synaptic transmission is essential.

Interestingly, we detected SIK3 as an intriguing target. Previous literature has shown that the kinase inhibitor staurosporine (STS) of SIKs enhanced SIK1 and SIK2 LKB1-phosphorylated Thr sites but not SIK3. An autophosphorylation site of SIK1 in the activation loop was also identified, and similar mechanisms were implicated for SIK2. Combining these results, due to different regulatory and structural mechanisms, researchers did not detect autophosphorylation sites for SIK3 (Hashimoto et al., 2008; Katoh et al., 2006).Here, though we detected SIK3 T71 as an autophosphorylation site, it has a low site percentile for SIK3 (Johnson et al., 2023), indicating that it is not SIK3-specific, which aligns with current literature that SIK3 does not have autophosphorylation. The detection could be a result of cross-reactivity or endogenous kinase activation from the KALIP assay. In the SIK2 phosphoproteomics, we detected SIK3 T221 as a direct phosphorylation site of SIK2. Existing literature showed with in vitro assays that T221 is essential for SIK3's catalytic activity and protein stability, as levels of the non-phosphorylatable alanine mutant (T221A) showed a significant reduction in protein levels following inhibition of protein synthesis. As SIK3 was proposed to be a sleep-promoting kinase, EEG/EMG recordings suggest that the T221A mutant exhibited a reduction in sleep pressure. It was shown that delta power at all points over the 24-hour period in NREM was lower than WT mice, suggesting that T221 is essential for sleep need (Li et al., 2021).SIK3 T221 was only significant in the dark phase (ZT22) and was hyperphosphorylated in the SIK2 KI. From our data, it seems

that the hyperphosphorylation also leads to the reduction of delta power similar to the non-functional mutant, indicating an overcompensation. Further studies would be required to draw conclusions. The finding of SIK3 as a direct substrate in the cortex further validates SIK3 as an important kinase in sleep regulation, in accordance with previous literature (Funato et al., 2016). It also proposes that SIK2 and SIK3 form an intertwining kinase-substrate network.

These results suggest that SIK2 and SIK3 regulate and coordinate a hub of synaptic proteins through phosphorylation in the cortex. It suggests that a coherent network is required for maintaining and regulating sleep homeostasis, connecting to the synaptic homeostasis theory.

6.7 Astrocytic communication and structural dynamics

From existing literature and our findings, neuronal targets of SIKs were studied in regulating pathways in the SCN and cortex. In our recent study on SIK1, we conducted a single-cell transcriptomics (scRNAseq) on SIK1 KI and WT animals and found significant enrichment in astrocytes (Appendix 1). Consulting the Allen Brain Cell (ABC) Atlas scRNAseq data, we found in Chapters 4 and 5 that there is high expression of *Sik2* and *Sik3* in non-neuronal cells, including astrocytes and oligodendrocytes. This proposes that SIKs' role spans across non-neuronal cell types.

Notably, in Chapter 3, through Pro-KALIP of SIK1 in the SCN, we identified CX43 (GJA1) S373 as a direct substrate. We validated the relationship and function

by establishing an *in vitro* C6 glioma reporter cell line. We validated that the non-phosphorylatable mutation S373A abolishes Ca^{2+}-induced hemichannel opening and SIK1 is a direct activator of CX43-mediated hemichannel opening through phosphorylation at S373. As Ca^{2+} is key for the SCN to modulate the circadian clock and sleep (Wang et al., 2022), research has also shown that astrocytes respond to Ca^{2+}-induced glutamate release, which is involved in the sleep circuitry in the cortex (Poskanzer & Yuste, 2016). Brancaccio et al showed that, through $[Ca^{2+}]$ imaging in SCN slices, astrocytic circadian oscillations of intracellular calcium ($[Ca^{2+}]_i$) are anti-phase to neuronal ones, and that dorsal SCN may be a key mediator site for astrocyte-neuronal communication (Brancaccio et al., 2017). As we applied extracellular ATP release as a marker for hemichannel opening and function, there is evidence showing that cultured astrocytes exhibit daily oscillation of ATP release, proposing that ATP is a circadian output. Therefore, astrocytes display oscillations in terms of ATP release dependent on clock genes (Marpegan et al., 2011). Tso et al supported that abolishing *Bmal1* clock gene expression in SCN astrocytes lengthens circadian period, suggesting that astrocyte-neuron communication is key for circadian rhythmicity and output (Tso et al., 2017). Circling back, it was shown that neuronal populations become asynchronous following the inhibition of CX43 by Gap26 *in vitro*. This suggests that intracellular communication between astrocytes facilitated by CX43 is important for coordinating neuronal circadian clock rhythms (Giantomasi et al., 2023). However, there is still a gap in molecular mechanisms. Our findings through SIK1 propose a new molecular target that regulates circadian rhythmicity in astrocytes. This suggests a coherent neuronal-astrocytic network modulated by SIK1 in the SCN.

While we detected CX43 as a direct substrate of SIK1 in the SCN, it was not detected as a direct molecular pathway in other SIKs. However, we observed enrichment in cytoskeleton organization and cellular junctions across SIK2 and SIK3 in the cortex. We observed several channel proteins, including HCN and KCNA2. Hyperpolarization-activated cyclic nucleotide-gated (HCN) channels are permeable to K^+ and Na^+, which allows faster potential kinetics and ESPS-spike coupling. It was shown that rodent pv interneurons, HCN channels are expressed at the axon and regulate firing and neurotransmitter release in the hippocampus and cerebellar basket cells, as well as human neocortex (Elgueta et al., 2015; Roth & Hu, 2020; Southan et al., 2000; Szegedi et al., 2023). They are suggested to modulate excitability in Layer2/3 pyramidal cells, which are key for cortical information transfer (Oláh et al., 2023). KCNA is the Kv1.2 voltage-gated potassium channel and is similarly shown to regulate neurotransmitter release, endocytosis, vesicle trafficking and neuronal excitability (Alam et al., 2023; Lai & Jan, 2006; Sheng et al., 1993). Chia et al, through statistical modeling, found that excitability is associated with degrees of sleepiness and that both excitatory and inhibitory neurons are involved (Chia et al., 2021). As wakefulness is also related to hyperactivity, along with synaptic potentiation (Cirelli & Tononi, 2019), these channel proteins, crucial for cortical excitability, may play a role in sleep regulation.

In addition, cytoskeletal proteins converged as common substrates of SIK2 and SIK3, including MACF1, MAP4 and MAP6, which are major microtubule proteins (Nishida et al., 2023). Microtubules are cylindrically shaped tubulins that are major components of the cytoskeleton and serve structural and regulatory functions (Salem & Fecek, 2023). Literature has shown that phosphorylated MACF1 by GSK3β inhibits the migration of

neurons and axon outgrowth (Ka & Kim, 2016). There is limited evidence on the link between the sleep-wake cycle and microtubules. Jarzynka et al proposed that microtubule depolymerization in the SCN enhances the efficacy of melatonin to induce phase-shifts (Jarzynka et al., 2009). Melatonin, acting as an antioxidant, also could reduce cytoskeleton damage and therefore neuronal complications (Reiter & Benitez–King, 1977). These propose a bidirectional relationship between melatonin, an element in the sleep-wake cycle, and cytoskeleton maintenance. In addition, phosphorylation of cortactin, a cytoskeletal protein, in the hippocampus was shown to alter REM sleep (Davis et al., 2006). These establish a link between cytoskeletal maintenance and sleep-wake regulation.

Together, this thesis proposes a novel SIK1-CX43 kinase-substrate relationship and SIKs' potential regulation across non-neuronal cell types. They also regulate channel and structural proteins to maintain synaptic integrity, which could be a mechanism linking to sleep-wake.

6.8 SIKs and the Two Process Model

Circling back to the central aim of this project, this work seeks to elucidate the role of salt-inducible kinases (SIKs) in sleep and circadian regulation, with the broader goal of identifying molecular components underlying the Two Process Model.

To address this, we performed a comparative analysis of SIK substrates identified in the SCN and the cortex. Proteins shared between these regions represent candidates that

may contribute to both circadian (Process C) and homeostatic (Process S) regulation. This overlap therefore provides a framework to identify molecular pathways through which SIKs could coordinate interactions between these two processes.

Overlapping both the SCN and the cortex, it appears that SRRM2 is the protein that overlaps between all three SIKs and is involved in both the SCN and the cortex. SRRM2 was discovered to be localized in nuclear speckles (NS) along with SON, forming the core of NS. The depletion of SRRM2 leads to the near-dissolution of NS. It is unclear what the exact biological functions are of NS, but they are membraneless organelles that store splicing factors and are implicated in viral responses, linking to diseases such as Huntington's disease (Ilık et al., 2020). Using *in vitro* models, researchers showed that SRRM2 organizes NS and facilitates alternative splicing, acting as a splicing factor. Deficiency in SRRM2 could lead to disruptions in immunity and cell homeostasis (Xu et al., 2022). Recently, emerging research has proposed the role of SRRM2 in multiple disease pathways. Yan et al showed that SRRM2 activates the mTOR-S6K axis through alternative splicing on S6K2 expression and promotes colorectal cancer growth (Yan et al., 2025). It is also implicated in Alzheimer's Disease (AD) pathology. SRRM2 is shown to be mislocalised from the NS to the soma, which is accompanied by increasing tau deposition in the cytoplasm, a biomarker of AD (Lester et al., 2021; McMillan et al., 2021), indicating that AD is associated with nuclear speckle composition disruption. The site SRRM2 S1068, detected as a direct phosphorylation site of SIK1 in the SCN from Pro-KALIP in Chapter 3, is observed in the brains of early-phase AD mouse models. The site is associated with the translocation of SRRM2 to the cytoplasm, which destabilizes splicesome component PQBP1, significantly affecting RNA splicing of

synaptic genes, leading to cognitive impairment. The validated upstream kinases are ERK1/2 and MAPK3/1; here, we propose SIK1 as a new regulator (Tanaka et al., 2018). Variants in SRRM2 are also associated with patients with mild developmental delay and other metabolic defects (Cuinat et al., 2022).

There is insufficient research on SRRM2 or nuclear speckles in sleep and circadian regulation. However, there is limited evidence on alternative splicing and temperature-regulated clock function. As alternative splicing is an important transcriptional process that enables large and diverse mRNA transcription from a limited number of genes. It was shown to be important for circadian regulation under abiotic responses in plants. Notably, Splicesomal Timekeeper Locus1 (STIPL1), a core component of the splicesome, could affect the circadian period of *A.thaliana*. Furthermore, PRMT5, a protein arginine methyl transferase, also regulates the alternative splicing of core clock genes in *A.thaliana* and is observed in *D.melanogaster* as well (Fan et al., 2022). Though further investigation is required, these studies propose a potential link between alternative splicing and circadian regulation.

Together, these results suggest that SRRM2 is involved in multiple regulatory pathways, from neurodevelopmental to cancer biology. In this thesis, we identified SRRM2 as a common substrate of all three isoforms of SIKs in both the SCN and cortex. This suggests that it is involved in both the circadian and sleep regulatory mechanisms. It is proposed as a molecular link between Process C and Process S, placing SIKs as the central regulators. We were able to detect multiple and distinct sites of SRRM2 phosphorylated by each of the SIKs. All in all, we propose that SIKs phosphorylate

SRRM2 at different sites at different timepoints in the SCN and cortex to coordinate the sleep-wake cycle in a coherent fashion. This is also carried over to downstream effects on whole-body physiology. Future experiments could include *in vitro* knockdown, site-directed mutagenesis and *in vivo* experiments to validate functions.

6.9 SIKs and Memory/Cognition

There is evidence that calcium signalling plays a role in dendritic growth and synaptic function, mediated through CAMK kinases and CREB in cortical neurons. Koizumi et al suggested that elevated intracellular calcium levels could influence dendritic structure and stabilization(Koizumi et al., 1999). Other researchers supported that SIK targets could already play a role in memory formation, such as CREB. It was shown that the dephosphorylation of CREB S133 is related to long-term depression (LTD) (Mauna et al., 2011).The SIK-CRTC axis has also been implicated in memory formation and synaptic plasticity in the hippocampus. It is shown that genetic overexpression of SIK2 in the hippocampus is associated with depressive behaviors, suggesting a kinase-substrate relationship in the pathogenesis of neurophysiology (Jiang et al., 2019a).

In SIK1 and SIK2 gene expression profiles, we observed a downregulation of *Shisa6* under the loss of SIK1 and SIK2. Research has shown that *Shisa6* is an auxiliary subunit of AMPARs, which mediates excitatory synaptic transmission, and it keeps AMPARs activated in the postsynapse, inhibiting full synaptic depression (Klaassen et al., 2016). Synaptic depression is associated with memory and cognitive defects (Duman & Aghajanian, 2012). There is also evidence that activation of AMPARs in the

SCN during early subjective night can phase delay the rhythm (Mizoro et al., 2010), important for the transmission of photic cues.

It was shown that SIK2 and SIK3 phosphorylate SYNPO in the cortex; multiple sites were hypophosphorylated, specifically the overlapping SYNPO S567 in both SIK2 and SIK3. It was previously established that SYNPO is an SNIPP, strongly associated with sleep need and pressure (Wang et al., 2018). Though specific pathways and mechanisms are understudied, existing literature has established a connection between SYNPO and downstream synaptic alterations. It was shown that, in SYNPO KO 15 and 21-day-old mice, PKA-dependent hippocampal long-term potentiation (LTP) is significantly impaired. It suggests that SYNPO regulates PKA-dependent dendritic spine expansion, which is essential for long-term memory storage (Zhang et al., 2013). This shows that SIK regulation in downstream cognitive effects spans across different brain regions. This is supported by the scRNAseq brain atlas, where we observed expression of *Sik2* and *Sik3* in the hippocampus.

In addition, we saw significant hypophosphorylation of glutamate receptors GluN2A/B and AMPA receptors, GRIA2A, which have both been shown to play key roles in synaptic strength, learning and memory formation. As synaptic potentiation and depression are strongly associated with an intact sleep-wake cycle, the synaptic network is disrupted in the cortex under the loss of SIK kinase activity. We further validated the downstream effects in NOR and preliminary Y-maze spatial recognition tests and found that SIK2 KI animals had alterations in novel object differentiation, linking to long-term memory consolidation. Our findings further support

that the loss of SIK2 disrupts sleep and synaptic homeostasis, reflected in downstream cognitive and neuronal functions. Further investigations of SIK1 and SIK3 are ongoing to explore the phenotypes.

6.10 SIKs and Metabolic Processes

SIKs from existing literature show that they are involved in metabolic processes such as lipid and energy metabolism and insulin uptake. Overlapping the SIK1 and SIK2 RNAseq datasets, we discovered several genes that are involved in metabolic processes such as *Cpne4* (Ca^{2+}-dependent lipid), *Xkr4* (phospholipid) and *Hecw2* (E3 ubiquitin ligase Akt/mTOR colorectal cancer). Most of them are Ca^{2+} regulated, which could indicate that the SIKs regulate Ca^{2+} dynamics to regulate circadian rhythms and metabolic functions. These show that SIKs modulate clock-controlled genes, which also regulate downstream metabolic functions. Similarly, we identified C2CD2L in the SCN, a common substrate of both SIK1 and SIK2. It is a Ca^{2+} regulated component that transfers phosphatidylinositol from the ER to the plasma membrane and interacts with insulin (Sun et al., 2019).

In the cortex, we detected common substrates between SIK2 and SIK3, such as UVRAG, BCAS1, DCLK1, PAK2 and TPPP. For instance, BCAS1 (breast-carcinoma amplified sequence 1) is expressed in the oligodendroglial subpopulation in the brain and is implicated in multiple sclerosis (Fard et al., 2017). In parallel, it is also amplified in multiple tumor pathways.

It was shown extensively in literature that SIK2 is involved in lipid metabolism and insulin resistance. We also detected enrichment for metabolic processes in the molecular substrates of SIK2. For instance, STAMBPL1 is a direct substrate of SIK2 in the SCN and was hyperphosphorylated at both timepoints in the SIK2 KI mice compared to WT controls, showing that SIK2 is a negative regulator of STAMBPL1 phosphorylation. It activates the Wnt/ β-catenin pathway and enhances expression of cancer-promoting genes. It is also transcriptionally regulated by SREBP1 (Jin et al., 2024). Previous literature has supported that SIK2 is correlated with SREBP1-related adipogenesis and OC cell progression (Okamoto et al., 2004). This proposes a molecular link between core circadian control in the SCN and downstream metabolic pathways.

Notably, there is evidence that sleep and circadian disruption lead to higher risks of cardiovascular diseases and cancer, providing a bidirectional link (Jouret, 2013; Lloyd et al., 2025). Transcriptomics on blood samples following insufficient sleep showed changes in gene expression associated with immune and stress responses (Möller-Levet et al., 2013). It was also further supported that sleep disorders disrupt lipid metabolism, increasing the risk of type 2 diabetes mellitus (T2DM) (Li et al., 2025).

One of the limitations of this analysis is that it is difficult to distinguish whether the changes in phosphorylation states are due to the innate developmental defects or other confounding factors, as we observed and supported by literature, than the loss of SIK3 results in deficiencies in lipid metabolism and bone development. As the phosphoproteomics studies were not conducted after sleep/circadian disruptions

such as sleep deprivation or jetlag, we cannot conclude that the substrates are sleep-wake dependent. However, this study proposes new perspectives on the link between sleep/circadian regulation and metabolic pathways, suggesting that SIKs play central roles in modulating both processes. The direct substrates are novel molecular links between the two processes.

6.11 Limitations and Future Directions

Several overarching limitations of this thesis are consolidated here, beyond the technical caveats mentioned in individual chapters.

The KI mouse model used in this thesis is a constitutive kinase loss-of-function model throughout development. As developmental defects were observed in previous studies, compensatory mechanisms could arise. Core kinases, such as other AMPK kinases, may facilitate downstream pathways and activity, which could obscure the extent of the phenotype. Conditional KI models or rescue experiments would be helpful to understand these relationships and networks.

The multi-omics approach used is exploratory and correlative. The optimized Pro-KALIP method provides strong evidence of strong direct phosphorylation, and the integration with quantitative *in vivo* phosphoproteomics elevates confidence. However, due to the challenges of reproducibility, depth, and inherent noise in omics technology, substrate-specific validation assays are required. This thesis is limited to CX43 S373 in Chapter 3,

but the remaining substrates of SIKs are yet to be validated before drawing reliable pathways and causations. Future experiments should prioritise high-confidence candidates, particularly ones with known circadian and sleep phenotypes.

The scale of the thesis limits sleep phenotyping across SIK2 and SIK3 to small cohorts. The conclusions must be treated as hypothesis-generating until fully powered studies are complete. Baseline sleep and homeostatic responses after sleep deprivation recordings are ongoing.

6.12 Concluding Remarks / Implications

Together, through the multi-omics approach, we propose that SIKs modulate a hub of substrates that are involved in multiple levels of physiology. We have proposed substrates that are involved in circadian and sleep regulatory pathways. In addition, parallel with existing literature, we identified substrates that are involved in neural and metabolic pathways. This study establishes a set of substrates that provide a molecular link between sleep/circadian regulation and other physiological conditions.

This thesis has proposed a post-transcriptional regulatory pathway via SIKs, specifically phosphorylation. According to the literature, there are various overlaps between gene expression and upstream regulators such as LKB1 and PKA. However,
we observed the behavioural differences in circadian and sleep phenotype that are non-redundant between isoforms. By pinpointing the precise molecular targets, we propose that SIKs are involved in various signaling pathways by phosphorylating unique

substrates and at unique sites. Analysis of SIK consensus motifs revealed differences in preferences for residue frequencies and positions between isoforms, which supports isoform-specific phosphorylation patterns.

This study opens up theories to understand the Two Process Model on a molecular level by adopting a multi-omics approach. We have identified SIKs as important markers for sleep and circadian regulation, involved in important diseases such as sleep and circadian disruptions. There are emerging small-molecular inhibitors of SIKs in the market, introduced in Chapter 1, as pharmacological avenues for these diseases. The inhibitors currently available are primarily targeted at ovarian cancer and autoimmune and inflammatory diseases (Valdés-Albuernes et al., 2025; J. Zhou et al., 2017b). However, as SIKs are major kinases, as shown in this thesis and existing research, affecting multiple aspects of physiology, a SIK inhibitor would not be sufficient and specific for particular diseases. For instance, it was shown that ARN-3236 attenuates ovarian cancer cell progression through the proposed AKT pathway. However, the confounding effects of SIK inhibitors are understudied, where they might affect other metabolic processes, neurodevelopment and circadian/sleep pathways. Therefore, by identifying the direct substrates of SIKs through Pro-KALIP, we propose that it will separate them from downstream pathways and could be used as pharmacological avenues instead. These small substrates downstream of SIK could be used as effective solutions for sleep and circadian disruptions and physiological conditions.

REFERENCES

Alam, K. A., Svalastoga, P., Martinez, A., Glennon, J. C., & Haavik, J. (2023). Potassium channels in behavioural brain disorders. Molecular mechanisms and therapeutic potential: A narrative review. In *Neuroscience and Biobehavioural Reviews* (Vol. 152). Elsevier Ltd. https://doi.org/10.1016/j.neubiorev.2023.105301

Asano, F., Kim, S. J., Fujiyama, T., Miyoshi, C., Hotta-Hirashima, N., Asama, N., Iwasaki, K., Kakizaki, M., Mizuno, S., Mieda, M., Sugiyama, F., Takahashi, S., Shi, S., Hirano, A., Funato, H., & Yanagisawa, M. (2023). SIK3–HDAC4 in the suprachiasmatic nucleus regulates the timing of arousal at the dark onset and circadian period in mice. *Proceedings of the National Academy of Sciences of the United States of America*, *120*(11). https://doi.org/10.1073/pnas.2218209120

Brancaccio, M., Patton, A. P., Chesham, J. E., Maywood, E. S., & Hastings, M. H. (2017). Astrocytes Control Circadian Timekeeping in the Suprachiasmatic Nucleus via Glutamatergic Signaling. *Neuron*, *93*(6), 1420-1435.e5. https://doi.org/10.1016/j.neuron.2017.02.030

Brüning, F., Noya, S. B., Bange, T., Koutsouli, S., Rudolph, J. D., Tyagarajan, S. K., Cox, J., Mann, M., Brown, S. A., & Robles, M. S. (2019). Sleep-wake cycles drive daily dynamics of synaptic phosphorylation. *Science*, *366*(6462). https://doi.org/10.1126/science.aav3617

Chang, S. H., Wang, X., Jin, J. Y., Wang, Q., & Wu, L. P. (2025). Rare SRRM2 mutation in neurodevelopmental disorders involving hyperphagia triggering severe obesity and other complication. *Frontiers in Medicine*, *12*. https://doi.org/10.3389/fmed.2025.1492851

Chhabra, A., Hoffmann, C., Aguilar Pérez, G., Korobeinikov, A. A., Rentsch, J., Hümpfer, N., Kokwaro, L., Gnidovec, L., Petrović, A., Wallace, J. N., Tromm, J. V., Román-Vendrell, C., Johnson, E. C., Ranković, B., Perego, E., Volpi, T., Fernández-Busnadiego, R., Köster, S., Rizzoli, S. O., … Milovanović, D. (2025). Condensates of synaptic vesicles and synapsin-1 mediate actin sequestering and polymerization. *EMBO Journal*, *44*(18), 5112–5148. https://doi.org/10.1038/s44318-025-00516-y

Chia, C.-H., Tang, X.-W., Cao, Y., Cao, H.-T., Zhang, W., Wu, J.-F., Zhu, Y.-L., Chen, Y., Lin, Y., Wu, Y., Zhang, Z., Yuan, T.-F., & Hu, R.-P. (2021). *Cortical excitability signatures for the degree of sleepiness in human*. *10*, 65099. https://doi.org/10.7554/eLife

Cirelli, C., & Tononi, G. (2019). Linking the need to sleep with synaptic function. In *Science* (Vol. 366, Number 6462, pp. 189–190). American Association for the Advancement of Science. https://doi.org/10.1126/science.aay5304

Cuinat, S., Nizon, M., Isidor, B., Stegmann, A., van Jaarsveld, R. H., van Gassen, K. L., van der Smagt, J. J., Volker-Touw, C. M. L., Holwerda, S. J. B., Terhal, P. A., Schuhmann, S., Vasileiou, G., Khalifa, M., Nugud, A. A., Yasaei, H., Ousager, L. B., Brasch-Andersen, C., Deb, W., Besnard, T., … Cogné, B. (2022). Loss-of-function variants in SRRM2 cause a neurodevelopmental disorder. *Genetics in Medicine*, *24*(8), 1774–1780. https://doi.org/10.1016/j.gim.2022.04.011

Davis, C. J., Meighan, P. C., Taishi, P., Krueger, J. M., Harding, J. W., & Wright, J. W. (2006). REM sleep deprivation attenuates actin-binding protein cortactin: A link

between sleep and hippocampal plasticity. *Neuroscience Letters*, *400*(3), 191–196. https://doi.org/10.1016/j.neulet.2006.02.046
Duman, R. S., & Aghajanian, G. K. (2012). Synaptic Dysfunction in Depression: Potential Therapeutic Targets. *Science*, *338*(6103), 68–72. https://doi.org/10.1126/science.1222939
Elgueta, C., Köhler, J., & Bartos, M. (2015). Persistent discharges in dentate gyrus perisoma-inhibiting interneurons require hyperpolarization-activated cyclic nucleotide-gated channel activation. *Journal of Neuroscience*, *35*(10), 4131–4139. https://doi.org/10.1523/JNEUROSCI.3671-14.2015
Fan, T., Aslam, M. M., Zhou, J. L., Chen, M. X., Zhang, J., Du, S., Zhang, K. L., & Chen, Y. S. (2022). A crosstalk of circadian clock and alternative splicing under abiotic stresses in the plants. In *Frontiers in Plant Science* (Vol. 13). Frontiers Media S.A. https://doi.org/10.3389/fpls.2022.976807
Fard, M. K., van der Meer, F., Sánchez, P., Cantuti-Castelvetri, L., Mandad, S., Jäkel, S., Fornasiero, E. F., Schmitt, S., Ehrlich, M., Starost, L., Kuhlmann, T., Sergiou, C., Schultz, V., Wrzos, C., Brück, W., Urlaub, H., Dimou, L., Stadelmann, C., & Simons, M. (2017). BCAS1 expression defines a population of early myelinating oligodendrocytes in multiple sclerosis lesions. *Science Translational Medicine*, *9*(419). https://doi.org/10.1126/scitranslmed.aam7816
Funato, H., Miyoshi, C., Fujiyama, T., Kanda, T., Sato, M., Wang, Z., Ma, J., Nakane, S., Tomita, J., Ikkyu, A., Kakizaki, M., Hotta-Hirashima, N., Kanno, S., Komiya, H., Asano, F., Honda, T., Kim, S. J., Harano, K., Muramoto, H., … Yanagisawa, M. (2016). Forward-genetics analysis of sleep in randomly mutagenized mice. *Nature*, *539*(7629), 378–383. https://doi.org/10.1038/nature20142
Giantomasi, L., Ribeiro, J. F., Barca-Mayo, O., Malerba, M., Miele, E., De Pietri Tonelli, D., & Berdondini, L. (2023). Astrocytes actively support long-range molecular clock synchronization of segregated neuronal populations. *Scientific Reports*, *13*(1). https://doi.org/10.1038/s41598-023-31966-1
Hashimoto, Y. K., Satoh, T., Okamoto, M., & Takemori, H. (2008). Importance of autophosphorylation at Ser186 in the a-loop of salt inducible kinase 1 for its sustained kinase activity. *Journal of Cellular Biochemistry*, *104*(5), 1724–1739. https://doi.org/10.1002/jcb.21737
Henny, P., & Jones, B. E. (2008). Projections from basal forebrain to prefrontal cortex comprise cholinergic, GABAergic and glutamatergic inputs to pyramidal cells or interneurons. *European Journal of Neuroscience*, *27*(3), 654–670. https://doi.org/10.1111/j.1460-9568.2008.06029.x
Hoffmann, C., Rentsch, J., Tsunoyama, T. A., Chhabra, A., Aguilar Perez, G., Chowdhury, R., Trnka, F., Korobeinikov, A. A., Shaib, A. H., Ganzella, M., Giannone, G., Rizzoli, S. O., Kusumi, A., Ewers, H., & Milovanovic, D. (2023). Synapsin condensation controls synaptic vesicle sequestering and dynamics. *Nature Communications*, *14*(1). https://doi.org/10.1038/s41467-023-42372-6
Ilık, İ. A., Malszycki, M., Lübke, A. K., Schade, C., Meierhofer, D., & Aktaş, T. (2020). Son and srrm2 are essential for nuclear speckle formation. *ELife*, *9*, 1–48. https://doi.org/10.7554/eLife.60579
Jagannath, A., Butler, R., Godinho, S. I. H., Couch, Y., Brown, L. A., Vasudevan, S. R., Flanagan, K. C., Anthony, D., Churchill, G. C., Wood, M. J. A., Steiner, G., Ebeling,

M., Hossbach, M., Wettstein, J. G., Duffield, G. E., Gatti, S., Hankins, M. W., Foster, R. G., & Peirson, S. N. (2013). The CRTC1-SIK1 pathway regulates entrainment of the circadian clock. *Cell*, *154*(5). https://doi.org/10.1016/j.cell.2013.08.004

Jagannath, A., Taylor, L., Ru, Y., Wakaf, Z., Akpobaro, K., Vasudevan, S., & Foster, R. G. (2023). THE MULTIPLE ROLES OF SALT-INDUCIBLE KINASES IN REGULATING PHYSIOLOGY. In *Physiological Reviews* (Vol. 103, Number 3, pp. 2231–2269). American Physiological Society. https://doi.org/10.1152/physrev.00023.2022

Jarzynka, M. J., Passey, D. K., Johnson, D. A., Konduru, N. V., Fitz, N. F., Radio, N. M., Rasenick, M., Benloucif, S., Melan, M. A., & Witt-Enderby, P. A. (2009). Microtubules modulate melatonin receptors involved in phase-shifting circadian activity rhythms: in vitro and in vivo evidence. *Journal of Pineal Research*, *46*(2), 161–171. https://doi.org/10.1111/j.1600-079X.2008.00644.x

Jiang, B., Wang, H., Wang, J. L., Wang, Y. J., Zhu, Q., Wang, C. N., Song, L., Gao, T. T., Wang, Y., Meng, G. L., Wu, F., Ling, Y., Zhang, W., & Li, J. X. (2019). Hippocampal Salt-Inducible Kinase 2 Plays a Role in Depression via the CREB-Regulated Transcription Coactivator 1–cAMP Response Element Binding–Brain-Derived Neurotrophic Factor Pathway. *Biological Psychiatry*, *85*(8), 650–666. https://doi.org/10.1016/j.biopsych.2018.10.004

Jin, J., Wang, Y., & Hu, Y. (2024). STAMBPL1, transcriptionally regulated by SREBP1, promotes malignant behaviors of hepatocellular carcinoma cells via Wnt/β-catenin signaling pathway. *Molecular Carcinogenesis*, *63*(11), 2158–2173. https://doi.org/10.1002/mc.23801

Johnson, J. L., Yaron, T. M., Huntsman, E. M., Kerelsky, A., Song, J., Regev, A., Lin, T. Y., Liberatore, K., Cizin, D. M., Cohen, B. M., Vasan, N., Ma, Y., Krismer, K., Robles, J. T., van de Kooij, B., van Vlimmeren, A. E., Andrée-Busch, N., Käufer, N. F., Dorovkov, M. V., … Cantley, L. C. (2023). An atlas of substrate specificities for the human serine/threonine kinome. *Nature*, *613*(7945), 759–766. https://doi.org/10.1038/s41586-022-05575-3

Jouret, J. (2013). Interlinks between sleep and metabolism. In *The Lancet Diabetes and Endocrinology* (Vol. 1, Number 1, pp. 16–17). Lancet Publishing Group. https://doi.org/10.1016/S2213-8587(13)70018-4

Ka, M., & Kim, W. Y. (2016). Microtubule-Actin Crosslinking Factor 1 Is Required for Dendritic Arborization and Axon Outgrowth in the Developing Brain. *Molecular Neurobiology*, *53*(9), 6018–6032. https://doi.org/10.1007/s12035-015-9508-4

Katoh, Y., Takemori, H., Horike, N., Doi, J., Muraoka, M., Min, L., & Okamoto, M. (2004). Salt-inducible kinase (SIK) isoforms: Their involvement in steroidogenesis and adipogenesis. *Molecular and Cellular Endocrinology*, *217*(1–2), 109–112. https://doi.org/10.1016/j.mce.2003.10.016

Katoh, Y., Takemori, H., Lin, X. Z., Tamura, M., Muraoka, M., Satoh, T., Tsuchiya, Y., Min, L., Doi, J., Miyauchi, A., Witters, L. A., Nakamura, H., & Okamoto, M. (2006). Silencing the constitutive active transcription factor CREB by the LKB1-SIK signaling cascade. *FEBS Journal*, *273*(12), 2730–2748. https://doi.org/10.1111/j.1742-4658.2006.05291.x

Klaassen, R. V., Stroeder, J., Coussen, F., Hafner, A. S., Petersen, J. D., Renancio, C., Schmitz, L. J. M., Normand, E., Lodder, J. C., Rotaru, D. C., Rao-Ruiz, P., Spijker,

S., Mansvelder, H. D., Choquet, D., & Smit, A. B. (2016). Shisa6 traps AMPA receptors at postsynaptic sites and prevents their desensitization during synaptic activity. *Nature Communications*, *7*. https://doi.org/10.1038/ncomms10682

Koizumi, S., Bootman, M. D., Bobanovic, L. K., Schell, M. J., Berridge, M. J., & Lipp, P. (1999). Characterization of Elementary Ca 2 Release Signals in NGF-Differentiated PC12 Cells and Hippocampal Neurons. In *Neuron* (Vol. 22).

Krone, L. B., Yamagata, T., Blanco-Duque, C., Guillaumin, M. C. C., Kahn, M. C., van der Vinne, V., McKillop, L. E., Tam, S. K. E., Peirson, S. N., Akerman, C. J., Hoerder-Suabedissen, A., Molnár, Z., & Vyazovskiy, V. V. (2021). A role for the cortex in sleep–wake regulation. *Nature Neuroscience*, *24*(9), 1210–1215. https://doi.org/10.1038/s41593-021-00894-6

Lai, H. C., & Jan, L. Y. (2006). The distribution and targeting of neuronal voltage-gated ion channels. *Nature Reviews Neuroscience*, *7*(7), 548–562. https://doi.org/10.1038/nrn1938

Lester, E., Ooi, F. K., Bakkar, N., Ayers, J., Woerman, A. L., Wheeler, J., Bowser, R., Carlson, G. A., Prusiner, S. B., & Parker, R. (2021). Tau aggregates are RNA-protein assemblies that mislocalize multiple nuclear speckle components. *Neuron*, *109*(10), 1675-1691.e9. https://doi.org/10.1016/j.neuron.2021.03.026

Li, W., Zhao, Q., Chen, Y., Zhao, G., & Fu, C. (2025). The impact of sleep status on lipid profiles and incident type 2 diabetes mellitus: a mediation analysis in a Chinese population cohort. *Diabetes Research and Clinical Practice*, *229*. https://doi.org/10.1016/j.diabres.2025.112475

Li, Y., Zhou, E., Liu, Y., Yu, J., Yang, J., Li, C., Cui, Y., Wang, T., Li, C., Liu, Z., & Rao, Y. (2021). *Sleep Need, the Key Regulator of Sleep Homeostasis, Is Indicated and Controlled by Phosphorylation of Threonine 221 in Salt Inducible Kinase 3*. https://doi.org/10.1101/2021.11.06.467421

Lizcano, J. M., Göransson, O., Toth, R., Deak, M., Morrice, N. A., Boudeau, J., Hawley, S. A., Udd, L., Mäkelä, T. P., Hardie, D. G., & Alessi, D. R. (2004). LKB1 is a master kinase that activates 13 kinases of the AMPK subfamily, including MARK/PAR-1. *EMBO Journal*, *23*(4), 833–843. https://doi.org/10.1038/sj.emboj.7600110

Lloyd, M., Prakash, B. A., Zhao, L., Ni, G., Ru, Y., & Vasudevan, S. R. (2025). Circadian rhythms in metabolism and mental health: a reciprocal regulatory network with implications for metabolic and neuropsychiatric disorders. *Current Opinion in Physiology*, *45*, 100836. https://doi.org/10.1016/j.cophys.2025.100836

Luo, W., Duan, M., Liang, E., Wang, S., & Yuan, J. (2025). The regulation of glutamatergic nervous system in sleep-wake states and general anesthesia. In *Brain Research Bulletin* (Vol. 221). Elsevier Inc. https://doi.org/10.1016/j.brainresbull.2025.111220

Marpegan, L., Swanstrom, A. E., Chung, K., Simon, T., Haydon, P. G., Khan, S. K., Liu, A. C., Herzog, E. D., & Beaule, C. (2011). Circadian Regulation of ATP Release in Astrocytes. *Journal of Neuroscience*, *31*(23), 8342–8350. https://doi.org/10.1523/JNEUROSCI.6537-10.2011

Mauna, J. C., Miyamae, T., Pulli, B., & Thiels, E. (2011). Protein phosphatases 1 and 2A are both required for long-term depression and associated dephosphorylation of

cAMP response element binding protein in hippocampal area CA1 *in vivo*. *Hippocampus*, *21*(10), 1093–1104. https://doi.org/10.1002/hipo.20823
McMillan, P. J., Strovas, T. J., Baum, M., Mitchell, B. K., Eck, R. J., Hendricks, N., Wheeler, J. M., Latimer, C. S., Keene, C. D., & Kraemer, B. C. (2021). Pathological tau drives ectopic nuclear speckle scaffold protein SRRM2 accumulation in neuron cytoplasm in Alzheimer's disease. *Acta Neuropathologica Communications*, *9*(1), 117. https://doi.org/10.1186/s40478-021-01219-1
Mizoro, Y., Yamaguchi, Y., Kitazawa, R., Yamada, H., Matsuo, M., Fustin, J. M., Doi, M., & Okamura, H. (2010). Activation of AMPA receptors in the suprachiasmatic nucleus phase-shifts the mouse circadian clock in vivo and in vitro. *PLoS ONE*, *5*(6). https://doi.org/10.1371/journal.pone.0010951
Möller-Levet, C. S., Archer, S. N., Bucca, G., Laing, E. E., Slak, A., Kabiljo, R., Lo, J. C. Y., Santhi, N., Von Schantz, M., Smith, C. P., & Dijk, D. J. (2013). Effects of insufficient sleep on circadian rhythmicity and expression amplitude of the human blood transcriptome. *Proceedings of the National Academy of Sciences of the United States of America*, *110*(12). https://doi.org/10.1073/pnas.1217154110
Moore, R. Y., & Speh, J. C. (n.d.). *GABA is the principal neurotransmitter of the circadian system*.
Nishida, K., Matsumura, K., Tamura, M., Nakamichi, T., Shimamori, K., Kuragano, M., Kabir, A. M. R., Kakugo, A., Kotani, S., Nishishita, N., & Tokuraku, K. (2023). Effects of three microtubule-associated proteins (MAP2, MAP4, and Tau) on microtubules' physical properties and neurite morphology. *Scientific Reports*, *13*(1). https://doi.org/10.1038/s41598-023-36073-9
Okamoto, M., Takemori, H., & Katoh, Y. (2004). Salt-inducible kinase in steroidogenesis and adipogenesis. In *Trends in Endocrinology and Metabolism* (Vol. 15, Number 1, pp. 21–26). Elsevier Inc. https://doi.org/10.1016/j.tem.2003.11.002
Oláh, V. J., Wu, J., Kaczmarek, L. K., & Rowan, M. J. (2023). *Input-specific gating of NMDA amplification via HCN channels in mouse L2/3 pyramidal neurons*. https://doi.org/10.1101/2023.09.25.559198
Ono, D., Honma, K. I., & Honma, S. (2021a). Roles of Neuropeptides, VIP and AVP, in the Mammalian Central Circadian Clock. In *Frontiers in Neuroscience* (Vol. 15). Frontiers Media S.A. https://doi.org/10.3389/fnins.2021.650154
Ono, D., Honma, K. ichi, & Honma, S. (2021b). GABAergic mechanisms in the suprachiasmatic nucleus that influence circadian rhythm. In *Journal of Neurochemistry* (Vol. 157, Number 1, pp. 31–41). Blackwell Publishing Ltd. https://doi.org/10.1111/jnc.15012
Peng, H., Wang, L., Gao, Y., Liu, H., Lin, G., Kong, Y., Xu, P., Liu, H., Yuan, Q., Liu, H., Song, L., Yang, T., & Wu, H. (2024). DMXL2 Is Required for Endocytosis and Recycling of Synaptic Vesicles in Auditory Hair Cells. *Journal of Neuroscience*, *44*(38). https://doi.org/10.1523/JNEUROSCI.1405-23.2024
Pham, X., Song, G., Lao, S., Goff, L., Zhu, H., Valle, D., & Avramopoulos, D. (2016). The DPYSL2 gene connects mTOR and schizophrenia. *Translational Psychiatry*, *6*(11). https://doi.org/10.1038/tp.2016.204
Poskanzer, K. E., & Yuste, R. (2016). Astrocytes regulate cortical state switching in vivo. *Proceedings of the National Academy of Sciences*, *113*(19). https://doi.org/10.1073/pnas.1520759113

Ralph, M. R., & Menaker, M. (1989). GABA Regulation of Circadian Responses to Light. I. Involvement of GABA,-Benzodiazepine and GABA, Receptors. In *The Journal of Neuroscience* (Number 8).

Reiter, R. J., & Benitez–King, G. (1977). *Melatonin reduces neuronal loss and cytoskeletal deterioration: implications for Psychiatry*.

Roth, F. C., & Hu, H. (2020). An axon-specific expression of HCN channels catalyzes fast action potential signaling in GABAergic interneurons. *Nature Communications*, *11*(1). https://doi.org/10.1038/s41467-020-15791-y

Salem, D., & Fecek, R. J. (2023). Role of microtubule actin crosslinking factor 1 (MACF1) in bipolar disorder pathophysiology and potential in lithium therapeutic mechanism. In *Translational Psychiatry* (Vol. 13, Number 1). Springer Nature. https://doi.org/10.1038/s41398-023-02483-6

Sheng, M., Liao, Y. J., Jan, Y. N., & Jan, L. Y. (1993). Presynaptic A-current based on heteromultimeric K+ channels detected in vivo. *Nature*, *365*(6441), 72–75. https://doi.org/10.1038/365072a0

Southan, A. P., Morris, N. P., Stephens, G. J., & Robertson, B. (2000). Hyperpolarization-activated currents in presynaptic terminals of mouse cerebellar basket cells. *The Journal of Physiology*, *526*(1), 91–97. https://doi.org/10.1111/j.1469-7793.2000.t01-1-00091.x

Sun, E. W., Guillén-Samander, A., Bian, X., Wu, Y., Cai, Y., Messa, M., & De Camilli, P. (2019). Lipid transporter TMEM24/C2CD2L is a Ca $^{2+}$ -regulated component of ER–plasma membrane contacts in mammalian neurons. *Proceedings of the National Academy of Sciences*, *116*(12), 5775–5784. https://doi.org/10.1073/pnas.1820156116

Szegedi, V., Bakos, E., Furdan, S., Kovács, B. H., Varga, D., Erdélyi, M., Barzó, P., Szücs, A., Tamás, G., & Lamsa, K. (2023). HCN channels at the cell soma ensure the rapid electrical reactivity of fast-spiking interneurons in human neocortex. *PLoS Biology*, *21*(2). https://doi.org/10.1371/journal.pbio.3002001

Tanaka, H., Kondo, K., Chen, X., Homma, H., Tagawa, K., Kerever, A., Aoki, S., Saito, T., Saido, T., Muramatsu, S. ichi, Fujita, K., & Okazawa, H. (2018). The intellectual disability gene PQBP1 rescues Alzheimer's disease pathology. *Molecular Psychiatry*, *23*(10), 2090–2110. https://doi.org/10.1038/s41380-018-0253-8

Taoufiq, Z., Ninov, M., Villar-Briones, A., Wang, H.-Y., Sasaki, T., Roy, M. C., Beauchain, F., Mori, Y., Yoshida, T., Takamori, S., Jahn, R., & Takahashi, T. (2020). Hidden proteome of synaptic vesicles in the mammalian brain. *Proceedings of the National Academy of Sciences*, *117*(52), 33586–33596. https://doi.org/10.1073/pnas.2011870117

Tononi, G., & Cirelli, C. (2006). Sleep function and synaptic homeostasis. In *Sleep Medicine Reviews* (Vol. 10, Number 1, pp. 49–62). https://doi.org/10.1016/j.smrv.2005.05.002

Tso, C. F., Simon, T., Greenlaw, A. C., Puri, T., Mieda, M., & Herzog, E. D. (2017). Astrocytes Regulate Daily Rhythms in the Suprachiasmatic Nucleus and Behavior. *Current Biology*, *27*(7), 1055–1061. https://doi.org/10.1016/j.cub.2017.02.037

Valdés-Albuernes, J. L., Díaz-Pico, E., Alfaro, S., & Caballero, J. (2025). Advanced modeling of salt-inducible kinase (SIK) inhibitors incorporating protein flexibility

through molecular dynamics and cross-docking. *Scientific Reports*, *15*(1). https://doi.org/10.1038/s41598-025-03699-w

Vargas, K. J., Colosi, P. L., Girardi, E., Park, J.-M., & Chandra, S. S. (2020). *α-Synuclein facilitates clathrin assembly in synaptic vesicle endocytosis*. https://doi.org/10.1101/2020.04.29.069344

Wakaf, Z., Ru, Y., Taylor, L., Ferrari, M., Dang, Q., Li, S., Hasan, S., Clark, K., Cohen, P., Vyazovskiy, V., Kauko, O., Brancaccio, M., Vasudevan, S., & Foster, R. (2026). *A SIK1-led presynaptic phosphorylation network gates the circadian control of sleep-wake timing*.

Wang, G., Li, Q., Xu, J., Zhao, S., Zhou, R., Chen, Z., Jiang, W., Gao, X., Zhou, S., Chen, Z., Sun, Q., Ma, C., Chen, L., Shi, B., Guo, Y., Wang, H., Wang, X., Li, H., Cai, T., … Liu, Q. (2021). *Somatic genetics analysis of sleep in adult mice*. https://doi.org/10.1101/2021.05.05.442860

Wang, Y., Minami, Y., Ode, K. L., & Ueda, H. R. (2022). The role of calcium and CaMKII in sleep. *Frontiers in Systems Neuroscience*, *16*. https://doi.org/10.3389/fnsys.2022.1059421

Wang, Z., Ma, J., Miyoshi, C., Li, Y., Sato, M., Ogawa, Y., Lou, T., Ma, C., Gao, X., Lee, C., Fujiyama, T., Yang, X., Zhou, S., Hotta-Hirashima, N., Klewe-Nebenius, D., Ikkyu, A., Kakizaki, M., Kanno, S., Cao, L., … Liu, Q. (2018). Quantitative phosphoproteomic analysis of the molecular substrates of sleep need. *Nature*, *558*(7710), 435–439. https://doi.org/10.1038/s41586-018-0218-8

Xu, S., Lai, S. K., Sim, D. Y., Ang, W. S. L., Li, H. Y., & Roca, X. (2022). SRRM2 organizes splicing condensates to regulate alternative splicing. *Nucleic Acids Research*, *50*(15), 8599–8614. https://doi.org/10.1093/nar/gkac669

Xue, L., Wang, W.-H., Iliuk, A., Hu, L., Galan, J. A., Yu, S., Hans, M., Geahlen, R. L., & Tao, W. A. (n.d.). *Sensitive kinase assay linked with phosphoproteomics for identifying direct kinase substrates*. https://doi.org/10.1073/pnas.1119418109/-/DCSupplemental

Yan, Z., He, L., Yuan, J., Niu, Y., Shuai, S., Luo, S., Du, C., & Rao, H. (2025). The splicing factor SRRM2 modulates two S6K kinases to promote colorectal cancer growth. *Oncogene*, *44*(18), 1284–1299. https://doi.org/10.1038/s41388-025-03307-1

Yang, R., Walder-Christensen, K. K., Kim, N., Wu, D., Lorenzo, D. N., Badea, A., Jiang, Y. H., Yin, H. H., Wetsel, W. C., & Bennett, V. (2019). ANK2 autism mutation targeting giant ankyrin-B promotes axon branching and ectopic connectivity. *Proceedings of the National Academy of Sciences of the United States of America*, *116*(30), 15262–15271. https://doi.org/10.1073/pnas.1904348116

Yang, W., Li, S., & Li, X. J. (2022). AHI1: linking depression and impaired antiviral immune response. In *Cell Research* (Vol. 32, Number 10, pp. 869–870). Springer Nature. https://doi.org/10.1038/s41422-022-00702-1

Yoon, S., & Penzes, P. (2025). Roles of ANK2/ankyrin-B in neurodevelopmental disorders: Isoform functions and implications for autism spectrum disorder and epilepsy. In *Current Opinion in Neurobiology* (Vol. 90). Elsevier Ltd. https://doi.org/10.1016/j.conb.2024.102938

Zhang, X. L., Pöschel, B., Faul, C., Upreti, C., Stanton, P. K., & Mundel, P. (2013). Essential role for synaptopodin in dendritic spine plasticity of the developing

hippocampus. *Journal of Neuroscience*, *33*(30), 12510–12518. https://doi.org/10.1523/JNEUROSCI.2983-12.2013

Zhou, J., Alfraidi, A., Zhang, S., Santiago-O'Farrill, J. M., Reddy, V. K. Y., Alsaadi, A., Ahmed, A. A., Yang, H., Liu, J., Mao, W., Wang, Y., Takemori, H., Vankayalapati, H., Lu, Z., & Bast, R. C. (2017). A novel compound ARN-3236 inhibits salt-inducible kinase 2 and sensitizes ovarian cancer cell lines and xenografts to paclitaxel. *Clinical Cancer Research*, *23*(8), 1945–1954. https://doi.org/10.1158/1078-0432.CCR-16-1562